MODELLING AND ANALYSIS OF CHATTER MITIGATION STRATEGIES IN MILLING

by

Khaled Saleh

Submitted in fulfilment of the degree of Doctor of Philosophy

June 2013

Department of Mechanical Engineering

Sheffield, UK

Supervisor: Dr N. D. Sims

ABSTRACT

Machining stability plays a major role in improving machine tool performance and product quality. Uncontrolled chatter phenomenon causes too many defects and problems in manufacturing industry such as increased surface roughness, tool wear and even machine breakdown.

In this subject area, great effort has been focused on developing different mechanisms and techniques in an attempt to reduce and control the machining vibrations. Spindle speed variation is one of the common approaches that has received attention recently. Non-uniform tool geometry is an alternative method that could be used for regenerative chatter suppression. Basically these two methods focus on breaking up the regeneration of surface waves.

A phenomenon known a process damping also has a vital effect on the stability improvement, particularly at low cutting speeds. Process damping is believed to be influenced by the interference of the relief face of the cutting tool with the waveform traced on the arc surface. An alternative explanation for process damping is known with the short regenerative effect. This concept is based on the distribution of forces along the tool flank face.

In the present research, a new approach based upon energy analysis is developed for more detailed interpretation of the stability of these different chatter mitigation mechanisms. Moreover, a comprehensive time domain model is developed to allow multiple effects such as variable spindle speed, process damping, loss of contact, variable helix tool and energy to be considered. Meanwhile performance of this milling model has been further benchmarked along with these effects to enable the numerical prediction to be computed more quickly with an acceptable numerical accuracy.

ACKNOWLEDGEMENTS

Praises to Allah and peace be upon the beloved final Prophet Muhammad. Thanks to Allah to be always with me to give guidance and mercy along my life, for his help and blesses to give me strength and patience to complete the thesis.

I would like to express my deepest appreciation to the people who have given their time and support to contribute towards completion of the work. Dr Neil Sims, my supervisor, is on the top of the list, which in fact I can not find enough words to express my respect and appreciation for him. He was very supportive, strong encouragement, insightful guidance with patience towards complete my PhD study. Neil's advice and experience with his high standard of developing the ideas creates a meaningful working experience.

I would like also thank my officemates and departmental staff, for their support and good friendship.

I offer my deepest thanks to my parents and my parents-in-law in Libya, who always pray sincerely for my success in study and life. Not to forget, this space and credit to my dearest wife, Dr. S. Abuzwida, and my two lovely children, Ayub and Ariam, for the moral support which has made me feel stronger and inspired. There is no greater support and encouragement besides all of you.

TABLE OF CONTENTS

LIST OF FIGURES

LIST OF TABLES

NOMENCLATURE AND ABBREVIATION

A_{sl}	Average angular acceleration
b	Depth of cut
dl	Layer thickness
f_t	Feed per tooth
F_c	Cutting force
F_s	Structural damping force
F_{idl}	Idealised force
F_{loc}	Loss of contact force
F_{pd}	Process damping force
F_{rc}	Cutting force in the radial direction
F_{tc}	Cutting force in the radial tangential
F_{rclN_t}	Radial cutting force that acting at each layer and tooth
F_{tclN_t}	Tangential cutting force that acting at each layer and tooth
F_{fpd}	Frictional process damping force
F_{npd}	Normal process damping force at
F_{fplN_t}	Frictional process damping force at each layer and tooth
F_{nplN_t}	Normal process damping force at each layer and tooth
$G_{h(s)}$	Delay chip function
G_{h_con}	Constant transfer function
G_{h_exp}	Exponential transfer function
G_{h_lin}	Linear transfer function
$iters$	Total number of iterations per revelation
h	Instantaneous chip thickness
h_c	Chip thickness with positive values
$h_{d,max}$	Maximum uncut chip thickness for dynamic system
$h_{s,max}$	Maximum uncut chip thickness for static system
h_{loc}	Loss of contact chip thickness
K_b	Specific cutting pressure
K_{np}	Normal indentation coefficient
K_r	The radial specific cutting pressure
K_t	The tangential specific cutting pressure
K_{re}	The edge force coefficients
K_{te}	The rubbing force coefficients
l	Current arc surface layer
l_{-1}	Previous arc surface layer
l_c	Chip contact length

l_f	Total flank length
$log(\|Xse\|)$	Natural-logarithmic for the maximum amplitude per frame
l_{ft}	Current flank contact length
L_{01}	The distance between the two closest points (S_{a0}, S_{a1})
n	Speed in rev/sec
n_l	Total number of discretised layers
N_t	Number cutter flutes
r_i	Radial immersion
r_p	Arc surface dimension
r_s	Intercept segment radius
r_t	Tool radius
r_0	Distance of the intercept segment point S_{a0} relative to the tool centre
r_1	Distance of the intercept segment point S_{a1} relative to the tool centre
RVA	Amplitude ratio
RVF	Frequency ratio
S_{ty}	Coordinates of the point that is located on the tool clearance face
S_{a0}, S_{a1}	The closest points on the previous arc surface S_{a-1}
S_{ax}, S_{ay}	Coordinates of the current arc surface points relative to the workpiece
S_{ax0}, S_{ay0}	The Cartesian components of the point S_{a0} on the S_{a-1} arc surface
S_{ax1}, S_{ay1}	The Cartesian components of the point S_{a1} on the S_{a-1} arc surface
(S_{atx}, S_{aty})	Global coordinates of the current tool position
(S_{fx}, S_{fy})	Local coordinates located on the tool centre
T	Tooth passing frequency
t_1	Start cutting time
t_2	Exit cutting time
v_s	Chip surface speed
V	Indentation volume
V_i	Segment indentation volume
W_s	Structural damping energy in Joules
W_{rs}	Structural damping energy in Joules per revolution
W_{idl}	Idealised energy in Joules
W_{loc}	Loss of contact energy in Joules
W_{pd}	Process damping energy in Joules
W_{ridl}	Idealised energy in Joules per revolution
W_{rloc}	Loss of contact energy in Joules per revolution
W_{rpd}	Process damping energy in Joules per revolution
X_{se}	Maximum amplitude per frame

(x, y)	Global coordinates based on the feed direction
α	Slope angle of the dimension r_0 relative to the dimension
α_{01}	Slope angle of the dimension l_f relative to the tool coordinate (S_{fy})
β	Slope angle of the dimension r_1 relative to the dimension
δ	Logarithmic decrement
ε	Phase shift
η_h	A non-dimensional chatter coefficient
γ	Tool flank relief angle
λ	Helix angle
λ_c	Process damping wave length
λ_g	Eigenvalues
λ_r	Chip compression ratio
θ_{ex}	Exit cutting angle
θ_f	Flank angle
θ_p	Arc surface inclination angle
θ_{st}	Start cutting angle
θ_t	Angular position
Θ_u	Tool angular position
τ	Periodicity of the spindle speed signal
τ_t	Number of revolutions
ω	Spindle speed (rpm)
ω_A	Variation amplitude (rpm)
ω_c	Chatter frequency (Hz)
ω_m	Mean spindle speed(rpm)
$w(\tau)$	Weighting function

CHAPTER 1 INTRODUCTION

1.1 Background

Milling is one of the most well-known material removal techniques, where material is removed from a workpiece using a rotating cutter. The rotating cutter can be a single or multi flute tool to produce chips in one tool cycle. In the milling process, usually milling cutter is mounted on a rotating spindle to remove the material by the free end from the workpiece which usually is clamped on the table is linearly moved towards the cutter, as shown in Figure 1.1. The process can be categorised as down-milling or up-milling depending on the direction of the cutter rotation with respect to the feed direction.

Milling is considered a critical process not only because it can remove the unwanted part of materials efficiently, but also because it can create almost all kinds of contoured surface smoothly. However, milling is a very complicated machining process. It is a discontinuous cutting process with varying chip load and forces. Moreover, the tool geometry in milling is complex. Along the milling tool edges, the rake and clearance angles vary with respect to the distance from the milling tool tip. In addition, for the helical end mills, chip thickness and the cutting forces are varying along the flute axis as the helix and pitch angles are changed. Therefore, the analysis of milling process and milling tool performance is always a big challenge.

In general, during the cutting processes, three different mechanical vibrations can occur due to the lack of dynamic stiffness of one or several elements of the system composed by the machine tool, the tool holder, the cutting tool and the workpiece material. These three types of vibrations are known as free vibrations, forced vibrations and self-excited vibrations. Free vibrations occur when the mechanical system is displaced from its equilibrium and is allowed to vibrate freely. Forced vibrations appear due to external excitations. The principal source of forced vibrations in milling processes is when each cutting tooth enters and exits the workpiece. Free and forced vibrations can be avoided or reduced when the cause of the vibration is identified. However, self-excited

vibrations (or regenerative chatter) extract energy from the interaction between the cutting tool and the workpiece during the machining process. This phenomenon is a result of an unstable interaction between the machining forces and the structural deflections. The forces generated when the cutting tool and part come into contact produce significant structural deflections. These structural deflections modulate the chip thickness that, in turn, changes the machining forces. For certain cutting conditions, this closed-loop, self-excited system becomes unstable and regenerative chatter occurs. Regenerative chatter may result in excessive machining forces and tool wear, tool failure, and scrap parts due to unacceptable surface finish, thus severely decreasing operation productivity and part quality [1].

When chatter occurs, the vibration amplitude will increase continuously until the relative displacement between the cutter and workpiece is so large that the cutter will leave the workpiece for part of the time. This becomes a nonlinear behaviour, which limits the vibration amplitude to a finite value. The magnitude of vibration depends on the cutting force characteristics, such as the magnitude and direction of the cutting forces, and the tooth passing frequency at which a cutting flute comes in contact with the workpiece. The dynamic characteristics of the entire machining system in terms of the natural frequencies the damping coefficients and the stiffness of the machine tool structure, also affect the vibration magnitude.

The cutting forces characteristics of the milling process are much more complex than that of turning. Milling operation is characterised by a multi-tooth cutter, and the cutting process itself is interrupted (the cutter flute was not in contact with the workpiece all the time). In addition, the direction of the cutting forces generated by each tooth does not remain constant with respect to machine tool structure as for turning operations, rather it changes direction as function of cutter position. This makes determining the stability limit of the milling process much more complex. In addition, the interrupted behaviour and discontinuity of milling process will result in large cutting variation and hence vibrations are unavoidable in the milling operations.

Chatter avoidance techniques aim to prevent chatter from occurring during the machining process, by selecting spindle speed and axial depth of cut based on a stability chart, the so-called stability lobe diagram, as shown in Figure 1.2. This was first introduced by Tobias and Fishwick [2] . If the process parameters are above the stability borderline, chatter will occur, however, if the process parameters are below the stability borderline, chatter will not occur. The critical stability borderline is the depth-of-cut below which stable machining is guaranteed regardless of the spindle speed. The lobed behaviour of the stability borderline allows stable lobe-regions to form; thus, at specific ranges of spindle speeds, the depth-of-cut may be substantially increased beyond the critical stability limit. These lobe-regions become smaller as the spindle speed decreases. However, stability is increased at low spindle speeds due to the process damping phenomenon [2].

In general, mitigation of chatter refers to a method to improve the stability margin in the cutting process. Various methods for chatter control have been proposed such as damping, spindle speed manipulation or variation, and vibration absorbers. Vibration absorption method refers to adding an additional mass to the structure to passively absorb the unwanted vibration energy [3-6], whereas active control requires external power to counteract the unwanted vibration [7-10].

Energy dissipation mechanisms have been recognised as a vital technique for chatter mitigation. Besides the damping produced from the structure of machine tools, the machining process itself can add damping to the system through a phenomenon known as process damping. This phenomenon is recognized as tool/workpiece interference [2, 11-20], or the short regenerative effect [21-23].

Disruption of the regenerative effect is also proposed to improve the machining stability. For example, the use of a non-uniform cutting tool, i.e. with variable pitch and variable helix milling tools has been proposed to increase the stable limit [20, 24-28]. Another popular technique is using spindle speed variation, by considering nominal spindle speed and frequency continuous to vary the spindle speed is the other method to disrupt regenerative effects [29-38].

1.2 **Aims and Objectives**

The aim of this research is to perform a model based investigation of chatter mitigation in milling. The main objectives of this study are to:

- Develop an existing milling model (which was used for constant speed machining) to consider variable speed machining.
- Extend the self- excited damping ratio technique to investigate the stability of variable speed machining.
- Develop an energy balance method as a new technique for investigating the basic underlying cause of regenerative chatter, including the effect of non-linearity due to the loss of contact and process damping.
- Apply the energy analysis to the case of variable helix tools under process damped conditions.
- Apply the energy analysis for process damping based upon the concept known as the short regenerative effect.
- To measure model performance by benchmarking different applications of chatter detection and mitigation techniques.

1.3 **Thesis outline**

The structure of the thesis is organised as follows. The layout of thesis is presented in the schematically in Figure 1.3.

The next chapter presents and reviews the literature, which begins by reviewing types of the mechanical vibrations, followed by previous research on the theory and the mechanism of the regenerative chatter. The prediction, detection and control of machine tool chatter are described. Due to the abovementioned focus in terms of the variable speed machining, process damping, variable helix tool, and regenerative effects, literature review pays special attention to these mechanisms.

In Chapter 3 the Simulink model used to simulate the vibration motion of the cutting tool and the workpiece is discussed. The model formulation is briefly described. Milling

kinematics for uncut chip thickness calculation and tool-workpiece interference volume computation, and milling forces (shear and process damping forces) are explained.

In Chapter 4 a variable spindle speed in time domain milling model is presented. A mechanism for modelling spindle speed variation is explained. The so-called peak to peak method [39] for chatter stability analysis is applied. However this method did not offer a formal interpretation of the stability behaviour. Consequently, the self-excitation damping ratio concept [40] is applied for variable spindle milling. The proposed chatter stability criterion and signal processing mechanism are discussed, and the stability analysis for linear and triangular speed variations are presented. However, even the self-excited damping ratio did not provide a comprehensive interpretation of the stability behaviour, particularly for stable cases. Therefore, a new approach used upon energy analysis is developed.

Chapter 5 focuses on developing an energy balance approach for chatter analysis. Application of the energy balance for chatter detection is performed for simple single tooth cutting and multi-teeth cutting. Energy balance approach is applied for the stability analysis is illustrated and the importance of the different energy dissipation mechanisms are investigated and quantified.

In Chapter 6, for the milling operation, process damping effects for chatter suppression are presented. The amount of dissipated energy by the process damping mechanism and loss of contact behaviour are measured and illustrated. Influences of several cutting parameters including tool geometry on the process damping behaviour are quantifiably investigated. Since the energy analysis approach has offered a realistic investigation in measuring process damping effects, consequently application of this approach is extended to consider different effects.

Chapter 7 presents the influence of the variable helix tools on system stability through the energy balance analysis. Modelling the energy behaviour in multiple degree of freedom systems is explained. The interaction between the variable helix tools and process damping is then explored.

Chapter 8 focuses on investigating the effects of process damping based on the short regenerative effect. The energy analysis approach is used to quantifiably demonstrate the influence of the tool-workpiece interference mechanism and the theory of the short regenerative effect using the numerical model. Rates of the energy dissipation by the short regenerative effects are measured and compared to that dissipated by the tool flank interference mechanism.

Finally Chapter 9 presents the conclusion of this research and some suggestions for further work.

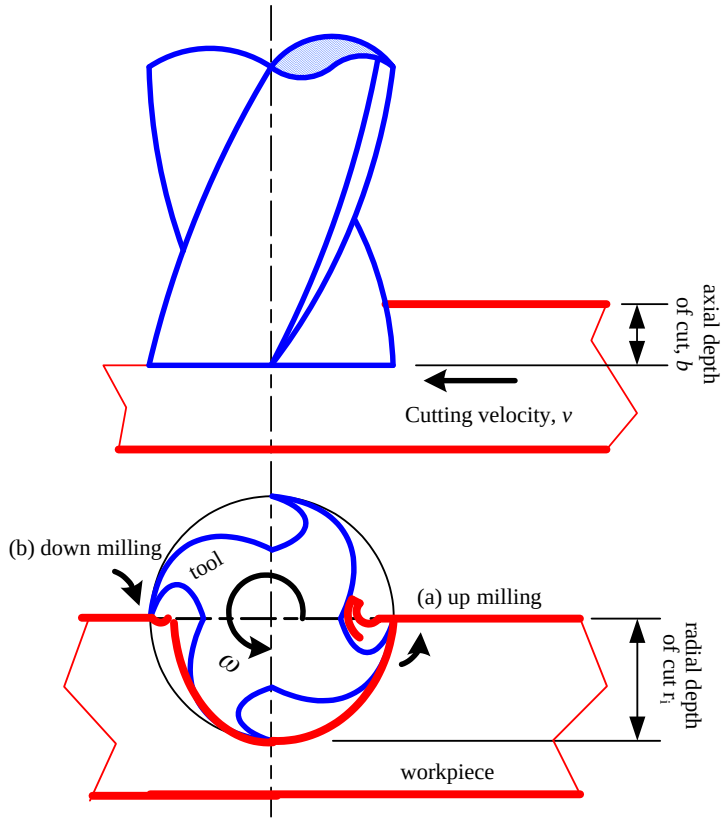

Figure 1.1 Cutting tool process parameters and type of milling operation

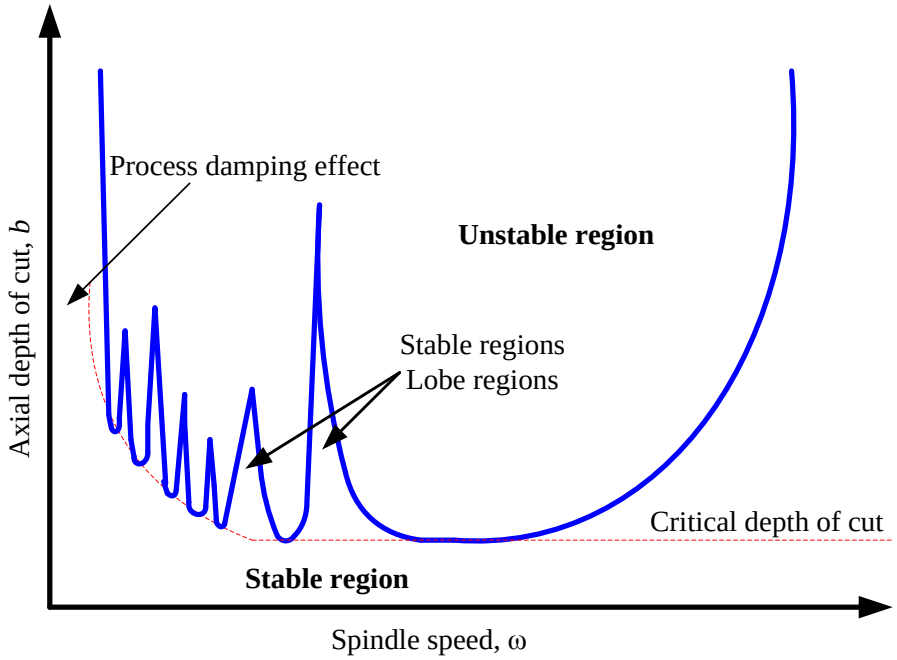

Figure 1.2 Stability lobes diagram

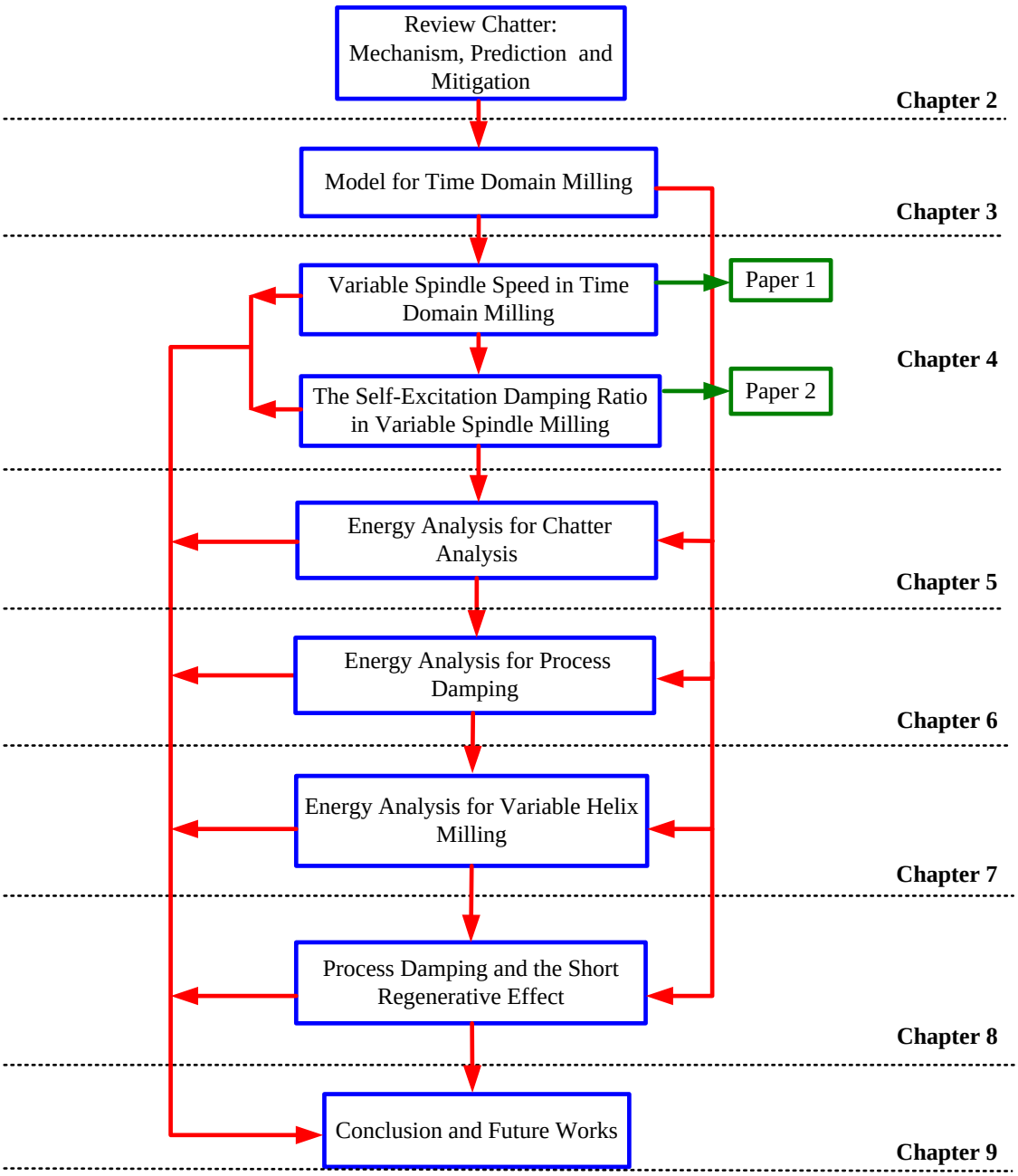

Figure 1.3 Overview of thesis

CHAPTER 2 LITERATURE REVIEW

2.1 Generalities

In recent decades, machining technologies have been developed very rapidly, and the advanced machines in particular have experienced significant changes such as the incorporation of numerical control systems. Every year it is possible to observe at fairs, conferences and of course, in the market, how production capabilities have increased. The accuracy and productivity are being enhanced constantly with innovative solutions to achieve market demands or even raise them to higher quality levels. For several years, analysis of machine tool vibrations and instability issues has received significant attention in order to improve the metal removal process. However, despite these enhancements in the manufacturing sector, there are still some limitations and challenges that arise.

Chatter vibration has been, for the last sixty years or more, a limitation of improving productivity and part quality in metal removal processes. This phenomenon has been a common issue for academic and industrial research. It should be noted that most of the machines and structures are not rigid bodies, but rather systems consisting of elastic components that respond to external or internal forces with finite deformations. In 1907, Taylor [41] stated that chatter is the "most obscure and delicate of all problems facing the machinist". Several years later, Tobias [42] stated in the preface of his book: "Machine tool development in recent decades has created an increasing number of vibration problems. Machine tool designers in early development phases are worried about vibration characteristics; production engineers know that vibrations diminish tool life, generate unacceptable surface finishes on the parts and reduce productivity". Nowadays, authors still refer to vibrations as a limiting factor, one of the most important machining challenges and, of course, an aspect to be improved [1].

2.2 Mechanical Vibrations in Metal Cut

Metal cutting processes can involve all three types of mechanical vibrations, which can be attributed to the lack of dynamic stiffness of one or several elements of the system

comprising the machine tool, the tool holder, the cutting tool and the workpiece material. These three types of vibrations are known as free vibrations, forced vibrations and self-excited vibrations [1].This classification is based on the external energy sources which are briefly defined in the next sections.

1- **Free vibrations**: When any external energy source is applied to initiate vibrations and is then removed, the consequential vibrations are known as free vibrations. In the absence of non-conservative forces, free vibrations sustain themselves and are periodic. The structure will vibrate in its natural modes until the damping causes the motion to die out [43].
2- **Forced vibrations:** Forced vibrations occur due to external harmonic excitations. The principle source of forced vibrations in milling processes is when the cutting edge enters and exits the workpiece. However, forced vibrations are also associated, for example, with unbalanced bearings or cutting tools, or it can be transmitted by other machine tools through the workshop floor. Free and forced vibrations can be avoided or reduced if the causes of the vibration are identified. In this field, a variety of methods and techniques have been developed to mitigate and reduce their occurrence [44].
3- **Self-excited vibration:** Self-excited vibration in milling is also known as chatter. Chatter extracts energy to start grows continuously, as a result of the interaction between the cutting tool and the workpiece during the machining process. Chatter is further classified into regenerative chatter and non-regenerative chatter. The regenerative effect is caused by the undulation of successive cuts, where the tool removes a wavy surface generated in the previous pass. Non regenerative vibration is maintained by the cutting force fluctuations that are induced by the tool-workpiece relative displacement of a periodic nature [45] .

In this chapter, the theory and the mechanism of chatter during machining are introduced. This chapter also discusses the previous work of other researchers in chatter suppression techniques.

2.3 **Chatter Vibrations in Machining**

Chatter is a form of unstable self-excited vibration in dynamic metal cutting. It has been and is still considered a challenging task for manufacturing research. This can be attributed to two principle factors: first the complexity of the phenomenon makes its study and understanding nontrivial. Second, the negative effects of chatter stimulate interest in solving the problem [1]. With regard to the first factor, chatter is a highly complex phenomenon due to the diversity of elements that can be composed of the dynamic system and its behaviour: the cutting tool, the tool holder, the workpiece material, the machine tool structure and the cutting parameters. Predicting its occurrence is still the subject of much research, even though the regenerative effect, the main cause of chatter, was identified and studied very early on [2, 46]. Moreover, chatter can occur in different metal removal processes, including milling [46-52] and turning [29, 31, 47, 53-63]. Regarding the second factor, chatter occurrence has several negative effects [1]:

- Poor surface quality.
- Unacceptable inaccuracy.
- Excessive noise.
- Disproportionate tool wear.
- Machine tool damage.
- Reduced material removal rate.
- Increased costs in terms of production time.
- Waste of materials.
- Waste of energy.
- Environmental impact in terms of materials and energy.
- Costs of recycling.

For these reasons, chatter avoidance is an issue of enormous interest. In workshops, machine tool operators often select conservative cutting parameters to avoid chatter, and consequently production is reduced. In some cases, additional manual operations are required to clean chatter marks left on the part's surface.

2.4 **Chatter Mechanism**

Many factors including cutting conditions, tool geometry, material properties, and structural characteristics have played a major role in defining whether or not chatter will occur. The theory of chatter in metal cutting has been well developed since the 1950's.

It is well documented that the fundamental cause of chatter under most machining conditions is the regeneration effect [39, 64]. Even when forced vibrations are extremely small, the slightest marks left on the cutting surface causes vibrations in the chip thickness for the following tooth. This regenerative effect is the most important cause of chatter. For this reason it has become a convention that "chatter" only refers to regenerative chatter. It is possible to distinguish between frictional chatter, mode coupling chatter and regenerative chatter based on the mechanism that causes the vibration. Frictional chatter occurs when rubbing on the clearance face excites vibration in the direction of the tangential force and limits in the radial force direction. Mode coupling chatter exists as the vibration in the radial direction generates vibration in the tangential direction and vice versa. This results in simultaneous vibration in the tangential and radial force directions. This can be caused by a number of sources such as friction on the rake and clearance surfaces, chip thickness variation, shear angle oscillations and the regeneration effect [1].

Regenerative chatter often occurs because most cutting operations involve overlapping cuts which can be a source of vibration amplification. Considering the machining operation in Figure 2.1, the combination of the waviness on the surface left by the previous tooth and vibration of the currently cutting tooth creates the periodically changing chip thickness. In other words, tool vibrations leave a wavy surface and when the cutting tooth is in the cut, it encounters this wavy surface and generates a new wavy surface. The chip thickness and, hence, the forces on the cutting tool vary due to the phase difference between the wave left by the previous tooth and the wave left by the current one. This phenomenon can greatly amplify vibrations, and therefore instability.

Figure 2.2 shows how the chip thickness variation depends on the phase shift ε between the undulations of successive cutting teeth paths. Figure 2.2(a) shows that a zero phase shift produces a constant chip thickness despite the disturbances in the system. Figure 2.2(b) and (c) present the chip load with a phase shift π/2 and the extreme case of a π phase shift, both of which can lead to unstable conditions [65, 66]. This oscillating chip thickness causes varying forces, which in turn adds more vibrations into the system. This feedback in the process is the regeneration effect which may cause instability.

The phase shift, ε radians, can be calculated as a function of tooth period, T, and chatter frequency, ω_c [65, 66]:

$$k + \frac{\varepsilon}{2\pi} = T\omega_c \tag{2.1}$$

where k is the number of complete wave marks on the surface during each tooth period and $\frac{\varepsilon}{2\pi}$ is the remaining fraction of a cycle between subsequent tooth passes.

It can be seen that the most stable condition, as far as the regenerative effect is concerned, is when the tooth passing frequency is an integer fraction of the chatter frequency, which results in a zero phase shift. This corresponds to spindle speed ω (rpm) [65] of:

$$\omega = \frac{60k\omega_c}{2\pi} \quad , k = 1,2,3 \ldots .. \tag{2.2}$$

2.5 **Chatter Prediction**

A number of modelling mechanisms have been developed for better investigation of the machining dynamics and chatter. For example, Tobias and Fishwick [2] presented a graphical method of stability analysis using the Nyquist plot of the transfer function *G(s)* for the flexible system. Chatter was also investigated analytically by Tlusty [67, 68] and Tobias [42] who developed the stability lobe diagram that describes the relationship between the depth of cut and spindle speed. The analytical prediction was then reproduced based on control system theory.

The dynamics of the cutting process and chatter were analysed and modelled in the frequency domain or in the time domain. The frequency domain analysis leads to the identification of chatter-free cutting conditions such as spindle speed, axial and radial depth of cut. Merritt [69] presented an elegant stability theory using a system theory terminology and derived a comprehensive stability criterion. A detailed theoretical analysis of the milling process has been developed by Sridhar et al. [37]. Opitz *et al* [70] developed a general closed-loop representation of a dynamic machining operation that can be applied to both turning and milling. Minis *et al.* [52, 60] redeveloped the analysis by applying the theory of periodic differential equations to the milling dynamic equations. This method was applied to a theoretical milling system to predict the critical depth of cut for chatter-free milling under various rotational speeds. Shi and Tobias [71] proposed a theory of finite amplitude machine tool instability to consider the effects of the two non-linear phenomena caused by: the tool leaving the workpiece material, and a non-linear characteristic of the cutting force. The former arises in all cutting processes when the vibration amplitudes are sufficiently large. The latter is specific and depends on the workpiece material and other factors, such as tool geometry. Altintas and Budak [72] presented an alternative method for the analytical prediction of stability lobes in milling. The stability analysis of the dynamic milling system leads to analytical relations for the chatter limits which can be used to generate the stability diagrams.

Most of the previous analytical modelling and analysis of chatter in machining are usually based on a number of simplifying assumptions, such as an average direction of the cutting force, or an infinitely large cutter diameter [73]. However, chatter is in fact always a nonlinear process. It is well known that when chatter starts, it does not grow indefinitely but stabilises at limited amplitude of vibration. Tlusty and Ismail [74] pointed out that once the vibration is large enough, the tool jumps out of the cut for a part of its vibratory period. During this time, the force is no longer proportional to chip thickness but it is simply zero. In an effort to improve on the accuracy of the prediction and to gain more insight into the cutting operation, and with the advancement of computing technology, time domain simulation models were developed. This method is quite powerful since it allows various tool geometries and nonlinearities such as the

variation in chip thickness, the changing orientation of the cutting force, the possibility that the tool may lose contact with the workpiece, and others.

Time domain models are used to predict cutting forces, torque, power, dimensional surface finish and the amplitudes and frequency of vibration [75]. Tlusty and Ismail [74, 76] used the time domain digital simulations to describe the dynamic behaviour of milling and investigated the boundary region between the stable and the unstable conditions. Tlusty *et al.* [39, 77] also investigated the dynamics of high-speed milling using the time domain simulation. Lee *et al*. [59] examined the effects of workpiece dynamics on the cutting process.

However when using time domain simulations to predict the borderline of stability in milling, it is often difficult to distinguish between cases of vibrations due to instability and cases of excessive vibrations due to large periodic forces. Using predicted vibrations or cutting forces may not properly isolate chatter from stable forced vibration. The model developed by Altintas and Lee [78] used differences in peak-to-peak force between simulations of a rigid versus flexible workpiece/cutter system. The simulation provided good results for half and full immersion cuts, but has difficulties detecting chatter at small radial immersions, particularly with large static deflections [79]. In addition the peak-to-peak technique was also used in [19, 39, 60] to identify the stability boundary during the constant speed machining cases.

Campomanes and Altintas [79] proposed a chatter criteria based on predicted uncut chip thickness. A non-dimensional chatter coefficient, η_h, was defined as:

$$\eta_h = \frac{h_{d,max}}{h_{s,max}}$$

where $h_{d,max}$ is the maximum uncut chip thickness during a dynamic time domain simulation, and $h_{s,max}$ is the maximum uncut chip thickness during a time domain simulation in which the workpiece and tool are rigid. The margin of stability behaviour was assumed at $\eta_h = 1.25$; an unstable chatter condition is triggered when $\eta_h > 1.25$.

In addition Li *et al* [80] employed a numerical method to solve the differential equations governing the dynamics of the milling system. They proposed that the ratio of the predicted maximum dynamic cutting force to the predicted maximum static cutting force was used as a criterion for the chatter stability. More recently, Sims [40] developed a new method called the self-excitation damping ratio for analysing the chatter stability of time-domain milling. The method relies on signal processing of the predicted vibrations.

The once-per-revolution sampling method was also used for evaluating the milling stability [81]. This notion is based on Poincare mapping techniques; the stability can be evaluated by plotting the x direction versus y direction tool motions and identifying the once-per-revolution sampled data points. For stable cuts, the synchronously sampled points approach a fixed point on the Poincare map and thus provide a tight distribution. Physically, this means that the forced vibrations repeat once per tooth pass. In other words, the tool motions are synchronous with the spindle rotation and the tool returns to approximately the same position in each revolution under steady state conditions. In contrast, tool motions during the chatter vibrations are not synchronous with spindle rotation; instead, they occur near the natural frequency corresponding to the most flexible system mode due to the nature of self-excited vibrations. For these unstable behaviours, the tool does not return to the same position each revolution. Rather, the once-per-revolution sampled distribution can tend toward an elliptical shape due to the quasi-periodic nature of chatter [81].

2.6 **Existing Chatter Mitigation Strategies**

Merrit [69] demonstrated that regenerative chatter occurs when there is an interaction between the structural dynamics of a machine tool and the dynamics of the cutting process. A closed loop feedback diagram was also introduced to represent regenerative chatter in a control perspective, as shown in Figure 2.3. Due to the detrimental nature of chatter, great efforts are still focusing on investigating what is the most effective approach which can be used for avoiding or suppressing this kind of vibration.

Now some of these approaches which are considered in this research are listed below:

- Spindle speed control
- Process damping phenomenon of tool flank interference
- Non-uniform tool geometry method
- The process damping phenomenon known as the short regenerative effect

These methods are now briefly reviewed.

2.6.1 **Spindle Speed Control**

Spindle speed selection or modulations are very common approaches that have been used to avoid or reduce chatter during the machining process. Spindle speed selection is an offline approach where information about the dynamic system or previous cutting data is used to improve machining stability by tuning the spindle speed. However spindle speed modulation manipulates the spindle speed or cutting conditions, (i.e. axial or radial depth of cut) during machining.

Tlusty [77] proposed that changing the spindle speed can stabilise an unstable machining process in the stability lobe diagram, particularly by use of the lobbing effect at high cutting speed. Kurdi *et al.*[82] applied Temporal Finite Element Analysis as an analytical approach to select optimum operating conditions, (spindle speed and depth of cut) when optimising material removal rate and surface location error simultaneously in order to search for a stable cutting operation. Tarng and Lee [83] considered the relationships between spindle speed and phase angle difference. They assumed a 90 degree phase angle for the largest machining stability. Spindle speed selection is sometimes considered unsuccessful way due to the power, torque, and speed limitations of the machine.

A spindle speed modulation procedure is an on-line method used for chatter suppression. This method controls cutting speed or reduces radial or axial depth of cut when chatter is detected. Delio *et al.* [84] for instance, detected the dominant chatter frequency by sensing the sound with a microphone, then analysed its frequency. The speed was regulated to search for a stable process after an audio signal detected the loud noise of

an unstable machining process. Sim *et al.* [85] used a similar approach to detect chatter, integrated with a knowledge based system of the machine tools, cutting tools and machinability data. Then spindle speed and feed rate were modified when chatter was detected.

Another common online technique that has received some attention is the use of continuously varying spindle speed during the milling process. This technique is based on varying the spindle speed around the mean value. Lin *et al* [33] for example considered a nominal spindle speed, amplitude ratio and the frequency ratio for controlling the speed variation in face milling. Altintas and Chan [30] proposed a digital dynamic milling simulation model to investigate the influence of various cutting and tool conditions as well as structural parameters on the stability of milling. It has been shown that when the spindle speed is sufficiently oscillated, the wave regeneration mechanism in dynamic milling can be disturbed and chatter vibrations can be suppressed. For example, in Liao and Young's [32] experiment, the variable spindle speed approach was used to reduce chatter by maintaining the phase angle at 90 degrees. Furthermore, Sastry *et al*. [86] proposed a solution technique based on a discrete time approach to the stability problem for the variable spindle speed face-milling process. A finite difference scheme is used to discretised the system and model it as a linear time varying (LTV) system with multiple time delays. Tsao *et al's* [38] presented an analytical method for chatter stability analysis of the variable speed face-milling process. By using tool position rather than time as the independent variable, the time varying time delay in the system equations is converted to a constant delay in the angle domain.

Ismail *et al* [31] employed spindle speed modulation for real-time control of chatter in peripheral milling. Yilmaz *et al.*[87], presented a new method of multi-level random spindle speed variation. Sri and Beddini [36], and Pakdemirli and Ulsoy [88], considered the mechanism of spindle speed variation for chatter suppression using the delay differential equations with periodically perturbed delays. Al-Regib *et al.*[29], introduced the concept of programming the spindle speed variation for minimum energy input by the cutting process. More recently, Seguy *et al*.[89] studied the effect of

spindle speed variation in a high speed domain using a semi-discretisation method for computing the optimal amplitudes and frequencies of the speed modulations.

2.6.2 **Non-Uniform Tool Geometry Method**

Variable helix and/or pitch tools are an alternative method that focuses on disrupting the regenerative effect to increase the stable region of the stability lobe diagram for milling problems. In the case of variable helix/pitch cutters, the phase between two subsequent waves is not constant for all teeth, thus disturbing the regeneration mechanism. This can reduce the modulation in chip thickness and disrupt vibrations, which consequently increases the stability of the process. As an example, the uniform and variable helix/ pitch tool's effectiveness in disrupting the regenerative waviness can be visualized in Figure 2.4. For the uniform tool (Figure 2.4(a)), the variation in phase delay between any subsequent waves is regular and relatively severe, and this could result in more forcing functions that impart energy into the system, such that the effect is self-exciting. Under the variable helix/pitch tool (Figure 2.4(b)), however, the variation in the phase delay is not as severe and the resulting irregular force may not be sufficient to create a self-exciting effect. In other words, by disrupting the time delay, the system will not be able to sustain the same phase between subsequent surface undulations, or equally, the same vibration frequency to cause chatter.

The effectiveness of variable pitch cutters in suppressing chatter vibrations during milling was first demonstrated by Slavicek [27]. He proposed a rectilinear tool motion for the cutting teeth and applied the orthogonal stability theory for non-uniform tooth pitch. By assuming an alternating pitch variation, he obtained a stability limit expression as a function of the variation in the pitch. Non uniform tool geometry can be used with variable helix angles or with non-constant pitch angles. Altintas *et al*. [24] presented an analytical model used to analyse the stability with variable pitch cutters. For a given process and a desired spindle speed, they optimised the tooth pitch by plotting the axial depth of a cut as a function of the first and second pitch angle, which led to a stabilisation of the process. Based on this model, Turner *et al* [90] investigated the variation of the variable helix and variable pitch angles to increase stability. They

proposed a nonlinear condition or process damping disturbed stable phase between subsequent teeth. Budak [25] used a similar method for designing the variable pitch to maximize the stability limit. The analytical method is only suitable for variable pitch tools at high radial immersion. Recently, Sims *et al*. [26] investigated the stability of variable pitch and variable helix end mills by adopting the semi-discretisation method. Yusoff and Sims [28] optimized variable helix tools, combining the semi-discretisation method with differential evolution.

2.6.3 **Process Damping Phenomenon**

Besides the damping produced from the structure of machine tools, the machining process itself can add damping to the system through a phenomenon known as process damping. Tobias and Fishwick [2] proposed that such a force occurs when the tool flank face rubs against the wavy workpiece surface at low spindle speeds. Tlusty [68] demonstrated the process damping mechanism schematically as shown in Figure 2.5. Here at the low cutting speeds, vibration marks imprinted on the surface become narrower and hence the tool flank rubs against it. This causes an additional forces act against the vibration velocity to produce a damping. Process damping forces have a fundamental effect when the tool travels from point A to C compared with when it travels from C to D. This means that while the velocity of the vibratory moment is acting downwards from A to C it encounters a greater reactive force than when it rises from C to D. The variation in the thrust force is in opposite phase to the velocity and acts as damping [68].

Lee *et al*. [16] and Fontaine *et al.* [14] proved experimentally that incorporating process damping forces can have a vital effect in increasing machining stability, particularly at low cutting speeds, which allows higher depths of cut to be used, thereby increasing material removal rates. Therefore process damping due to the tool/workpiece interference is considered as another successful strategy which can be involved in chatter mitigation at lower surface speeds.

However, even to date, there are limited modelling studies that include process damping forces. This is possibly due to the complexity of the fundamental mechanism of the

process damping forces, or because these forces depend principally on both the tool geometry and the cutting condition at the instantaneous interference region. Recently studying process damping in milling operations has received significant interest, using simulation or experimental methods (or both). For example, Montgomery and Altintas [17] used a model-based approach to investigate ploughing forces. Delio *et al.* [12] considered the wavelength of chatter vibration and the loss of process damping behaviour at higher spindle speeds. Elbestawi *et al*. [13] modelled process damping effects when cutting aluminium and showed that the model could produce additional damping forces due to the tool flank/workpiece interference. Ranganath *et al*. [18] also developed a time-domain model of process damped milling and compared the results to experimental data from an aluminium alloy workpiece. Huang and Wang [15] proposed a model that considered the consequences of chatter vibration on the effective rake and relief angles. They included additional empirical parameters in their model so that the cutting stiffness became a function of these effective angles and thereby produced a process damping effect.

Recently, Budak and Tunc [11] developed a method for identification and simulation of process damping. Process damping coefficients are obtained from chatter tests. The method is generalized by determining the indentation force coefficient responsible for the process damping through the energy analysis. This coefficient is then used for process damping and the stability limit prediction in different cases. These predictions are verified by time domain simulations and experimental results.

Yusuff *et al*. [20] performed milling experiments to evaluate the performance of process damping under different tool geometries (edge radius, rake and relief angles and variable helix/pitch). The results clearly indicated that variable helix/pitch angles most significantly increase process damping performance. Additionally, increased cutting edge radius moderately improved process damping performance, while rake and relief angles have a smaller and closely coupled effect. More recently, Sims [19] developed a model to investigate the influence of feed rate on process damping in milling. A qualitative agreement is found between experimental behaviour and the numerical model. In particular, the model predicts a strong relationship between the workpiece

feed rate (expressed as a feed per tooth), and the acceptable chatter stability defined by the process damping wavelength.

In a cutting test conducted by Budak and Tunc [11], a phenomenon known as a limit cycle was observed in some cases. Authors attributed this to the existence of process damping. It was proposed that limit cycle behaviour could be caused by the nonlinear variation of the damping forces with the vibration amplitudes [11]. When the stability limit is exceeded, the vibration amplitudes are expected to grow when process damping effects are not considered. However, with the presence of process damping as the vibration amplitude starts increasing, the process damping also increases, providing more stability effects. As a consequence, vibrations will be inhibited at a particular limit where the system behaves as marginally stable. However a disturbance to the system by increasing or decreasing the vibration amplitudes will cause process damping effects to increase or decrease as well. In this case, limit cycle behaviour could be reached again. Therefore it can be said that vibration amplitudes, and thus process damping effects are proportional to the cutting depth, and the vibrations may stabilise at different limit cycles for different cutting depths of cut for a given cutting speed. However, at a particular depth, the increase in the process damping becomes insufficient to stabilise the process. Consequently, there will be two different stability limits for a cutting speed. The first one is the cutting depth at which the limit cycle behaviour starts (i.e., the minimum stability limit), whereas the second is the cutting depth at which the limit cycle behaviour diminishes and the vibration amplitudes are starting to grow increasingly (i.e., the maximum stability limit for the same speed) [11].

It should be stated that most of the previously published work considered the stability limit based on the minimum limit, whereas analysing the limit cycle behaviour under the process damping effect has not been considered yet.

2.6.4 **The Short Regenerative Effect**

It is well known that increased stability behaviour is commonly observed at low speed machining. In the past, this improved stability is attributed to the energy dissipated due to the interference between the tool relief face and the work surface as described above. However, an alternative representation known as a short regenerative effect has recently been introduced for stability improvement particularly at lower turning speeds [21-23, 91]. Stepan was the first to propose that instead of modelling the cutting forces as a single point force, at the tool tip [91], these forces (see Figure 2.6) could be assumed to have a distribution per unit length with varying magnitudes along the tool chip interface. In addition Khasawneh, *et al*. [21] investigated the influence of the distributed force model on the stability behaviour of continuous and interrupted turning. They described an approach to transform the distributed-delay equations into a discrete-delay system. Theoretical stability investigations are performed using a state-space Temporal Finite Element Analysis technique. More recently, Taylor, *et al* [23] employed a frequency domain approach for solving the short regenerative model in turning. The short regenerative effect was investigated based on an estimation of the chip contact time on the tool rake face, along with knowledge of a weighting function that distributes the cutting force along the tool rake face as a function of the chip thickness along the rake face. It has been shown that none of these weighting functions can provide sufficient increases in stability for the model to match experimentally observed data.

2.7 **Time Domain Modelling**

In recent years, time domain modelling has been used extensively since it provides realistic information regarding the chatter stability and the qualitative evaluation of the chatter severity as well as the arc surface behaviour. In addition there are some other advantages of time domain techniques over other methods of stability analysis of chatter.

For example, time domain simulations provide more insight into the dynamics of the milling operation. Some early simplistic models ignored the dynamics of the tool and workpiece system and the changing directions of the milling forces were developed for more advanced models. Tlusty was the pioneer in this field, and he used time domain

modelling to consider the changes in the cutting force's directions due to a rotating cutter and the helical flutes [64]. A comparison done by Tlusty [92] between the stability limits obtained by the improved formulation of the dynamic cutting forces and from the previous simplified models showed significant differences.

Time domain modelling has also been used for some physical and qualitative analyses of chatter instability. For instance, observations of the relationship between machining stability and structural flexibility are made in [76]. While the stability lobe diagram approximates the maximum allowable depth of cut for a chosen spindle speed as the quantitative aspect of chatter, while the qualitative aspect of the severity of chatter can be understood from the amplitudes of cutting forces, chip thickness and displacements. Normally this information is not available from the stability lobe diagram.

Time domain modelling offers a better illustration about the basic non-linearity in the chatter phenomenon which is the jumping of the tool out of the cut, due to excessive vibrations. Kline and DeVor [93] considered time domain modelling to study the effects of run-out on milling forces. However, the regeneration effect of chatter was not considered, validating the model only for the case of static milling. In addition, Ranganath *et al*. [18] developed an improved model, which considers effects of cutter deflection, and the damping effect of flank face contact with the workpiece, while the force's dynamics are modelled, but it does not study regeneration and chatter.

Time doming modelling allows multiple effects to be considered and their relative contribution on the stability behaviour to be assessed. Turner et al [90] used the time domain chatter recognition and analytical models to explore the effect of the variable helix and variable pitch angles on increasing stability, simulation outputs was tested against the experimental results. They proposed process damping and a disturbed stable phase between subsequent teeth, to inhibit the onset of chatter. This argument was quite difficult to be tested experimentally. Budak and Tunc [11] used a new analytical approach for identification of the indentation force coefficient responsible for process damping through energy analysis. This coefficient is then used for process damping and

stability limit predictions in different cases and predictions are verified by time domain simulations and experimental results.

In addition, during the machining process, chatter can be predicted by the experience of the operator, due to the sound produced during the cut or the characteristics of the machined surface. However, in order to avoid the possibility of human error, and to increase productivity, researchers have been motivated to develop advanced chatter detection techniques. Following this trend, a number of techniques have been developed for rapid chatter detection and analysis. The more common approaches are: once-per revolution, peak-to-peak, the chip thickness ratio and more advanced self-excited damping ratio which were briefly reviewed in the Section 2.5. However, at this point, the performance of these techniques will be briefly evaluated: As the once per revolution sampling and the chip thickness variance have almost the same behaviour, here the chatter threshold must be chosen to be slightly higher than the stable value, but not so high as to give a stable depth prediction that is too high. For the peak-to-peak method, there is no evident value for the chatter threshold, but the value does not start to increase more sharply after the onset of instability. The self-excitation damping ratio has a physical stability margin value (zero), but it requires more signal processing steps than the other methods and may not be appropriate for variable pitch tools [44].

2.8 **Summary**

This chapter has reviewed some types of mechanical vibration. The theory and the mechanism of self-excited vibration are discussed including some early and recent research concerning chatter prediction. Next, a number of the existing chatter mitigation techniques were reviewed such as: varying the spindle speed, a process damping mechanism due to the tool/workpiece interference, non uniform tool geometry and short regenerative effect.

It is clear that comprehensive time domain models can offer a useful insight into the machine behaviour. They are able to predict cutting forces, power, machined surface amplitudes and frequency of vibration so that detailed investigations of chatter

mitigation methods can be performed. These effects are often difficult to measure by other means for instance: loss of contact and process damping are difficult to measure experimentally, tool geometry cannot be precisely controlled, and the poor signal to noise ratio during the actual machining process makes it difficult to interpret observed behaviour. Consequently, time domain modelling can serve a useful purpose in providing more insight into complex chatter mitigation techniques.

As a result, this thesis will focus on developing a comprehensive time domain model, along with a novel energy-based analysis method. These two tools will then be used to explore typical chatter mitigation methods in a simulation environment. This numerical method does not offer any scope within this thesis for experimental validation of the model. To overcome this, the model assumptions were matched to those found in the common literature, and where possible the numerical predictions were compared to experimental results from existing literature.

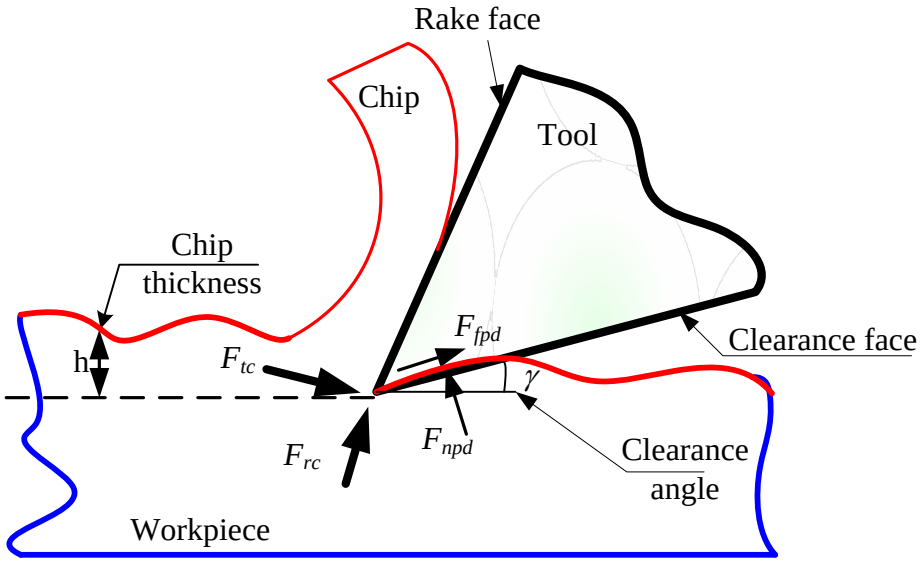

Figure 2.1 Model of metal cutting

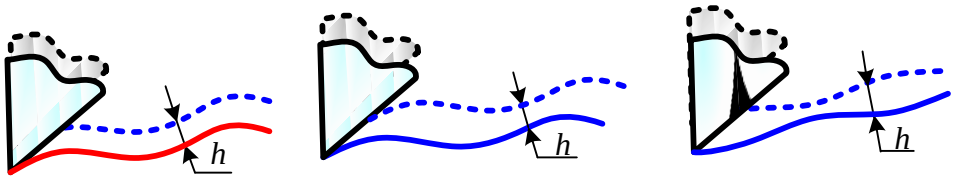

(a) ε=0 (rad) (b) ε=π/2 (rad) (c) ε=π (rad)

Figure 2.2 Regeneration process during and phase influence on chip thickness

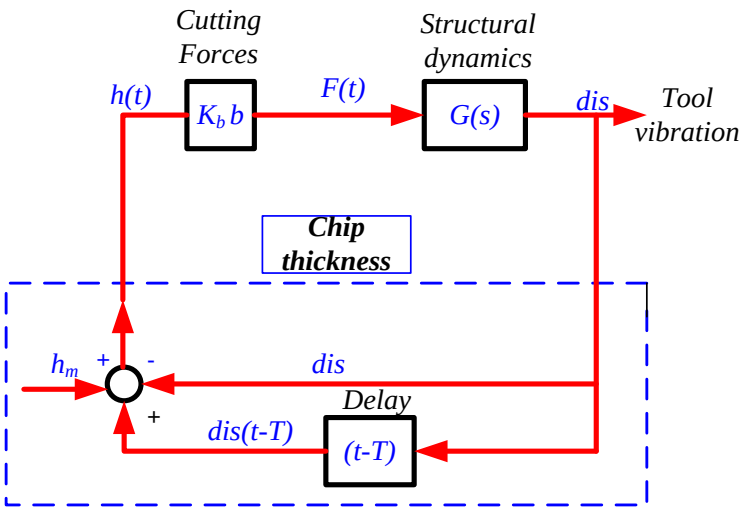

Figure 2.3 Chatter as a closed loop system by Merritt [69, 94]

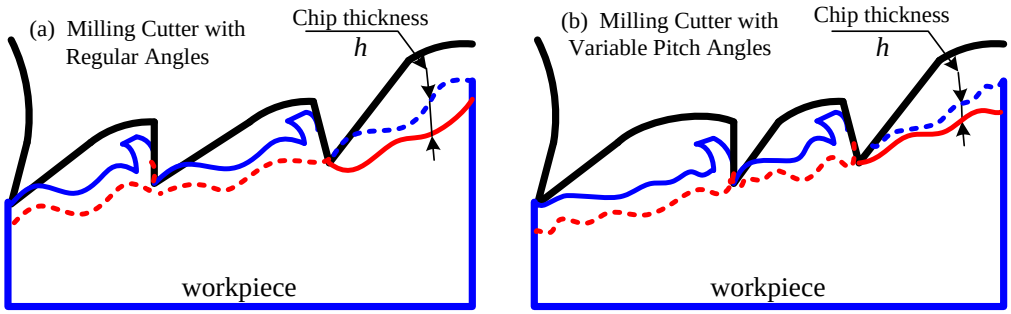

Figure 2.4 Regenerative waviness behaviour

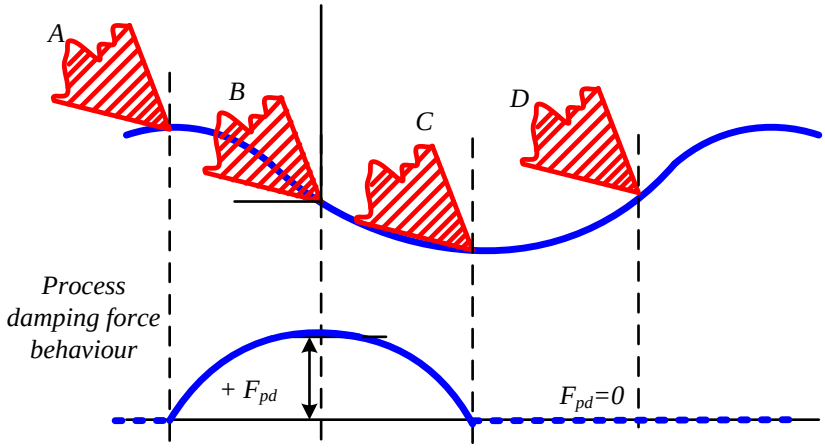

Figure 2.5 Process damping mechanism

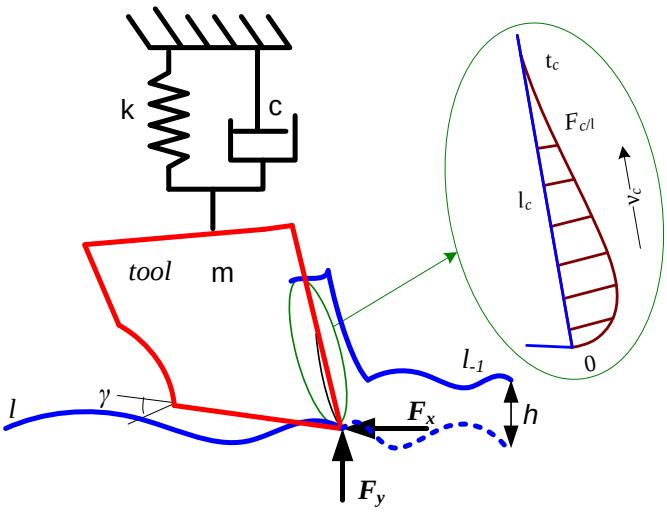

Figure 2.6 Schematic diagram of a distributed force model uses a stress distribution over the tool rake face and applies a finite time for the chip to travel along the tool-chip interface.

CHAPTER 3 MODEL FOR TIME DOMAIN MILLING

3.1 Introduction

A number of time-domain models have been developed to better understand the milling process. There are certain advantages of time domain techniques over other methods of stability analysis of chatter. The time domain method provides a realistic simulation of the cutting process and chatter instability, since the number of assumptions involved is minimised. The combination of the feed and the relative oscillations between the tool and the workpiece can be incorporated. A qualitative evaluation in terms of severity of the chatter and accuracy of surface finish can be achieved. A comprehensive time-domain simulation can predict the time-history of vibrations during the machining process. Nonlinearity behaviour such as loss of contact and process damping can be easily included. It provides more insight into the dynamics of the milling operation [95]. However, the only drawback of time domain simulations is the extreme computational cost that is required, and the difficulty of clearly interpreting the system stability from the predicted response.

In the present research, the model proposed by Sims [19, 40] is developed to be used in this research. It should be noted that the aim in this Chapter is not to create a new model of milling, but instead use Sheffield's existing time domain model, whose performance has been tested in several published applications. For instance, chatter stability detection [40], and investigation feed rate effects on process damping behaviour [19] have been previously explored along the constant spindle speeds. However during this research this model will be developed to consider the variable spindle speed and the cutting energy computation.

The Simulink milling model shown in Figure 3.1 has been designed based on the same concept of the chatter loop diagram (Figure 2.3).The model consists of three main blocks: milling kinematics, milling forces and system dynamics. The milling kinematics systems are where the C-program is coded for the chip thickness and the indentation contact computation. This block is connected with the milling forces block which

contains on other subsystems blocks as shown in Figure 3.2. These simple Simulink blocks are associated with milling forces (shear and process damping forces) calculations. The output of the milling forces block will be fed to the system dynamics block where the system relative displacements and the velocities are computed. Finally the output of this block in terms of the system relative displacement is combined with the appropriate feed rate to feed the milling kinematics block, thereby the loop is closed.

The main model program is coded in the C-programming language which can be interfaced with the Matlab/Simulink software. Here the simulation is executed through fixed time intervals, moreover the concept of discretising the tool/workpiece model is adopted to compute the chip thickness, the interference contact volume and cutting forces at each step time. In addition computational effort was reduced by compiling the model as a C-program executable. This enables multiple simulation runs to be performed on a cluster of desktop computers [96].

In this research, the model assumptions are similar to those found in common literature for example in [79, 97]:

- The tool stiffness and cutting force coefficient are assumed constant.
- The cutting forces are evaluated using the linear-edge force model.
- The cutting geometry is modelled using a discretised kinematics algorithm. This provides a realistic representation of how the cutter and the workpiece interact during vibratory milling.

The inputs and outputs simulation data of this model are stored in the Matlab m-files.

1- **The main model inputs are:**
    i. **Dynamic parameters***:* natural frequency, stiffness and damping ratio or the equivalent (mass, stiffness and damping coefficient) for each mode of vibration.
    ii. **Tool geometry parameters***:* number of teeth, tool radius, helix angle and flank clearance angle and length.

iii. **Cutting parameters***:* spindle speed, feed per tooth, depth of cut, cutting stiffness coefficient, radial immersion, cutting mode, process damping normal forces coefficient and process damping friction coefficient.

iv. **Simulation parameters***:* number of cycles, iterations per cycle and number of axial layers.

2- The main model outputs are:

The main outputs which can be considered from this model are cutting forces (shear and process damping forces), system relative displacement and velocity, chip thickness, tool rotational angle, the interference contact (area or volume), tool rotation angle and possibly the arc surfaced trajectory.

Now, having defined all the simulation inputs, the simulation is performed according to the flow chart shown in Figure 3.3 for the milling kinematics simulation. The simulation is executed for each step time. At every step time, the angular position of cutting tooth is determined, then for each tooth that is engaged in the cut region, the instantaneous of the chip thickness and the flank interference contact are calculated. These results are used for calculating the components of the cutting forces (cutting and process damping forces). These cutting forces are resolved in the x and y direction (as appropriate) using the predictive milling force model as will be described in later sections.

Having computed the total cutting forces, the instantaneous system displacements and velocities in x and y direction can be determined by solving the differential equations of the system using the Runge-Kutta 4^{th} order numerical method, as implemented by the Simulink.

The model formulation will be presented in more details in the next section.

3.2 Model Formulation

With reference to Figure 3.4 the kinematics model begins by dividing the tool into n_l discrete axial slices (layers) to model the tool /workpiece geometry within each slice. Two coordinate systems are used: a local coordinate (S_{fx} , S_{fy}) based upon the centre of

the tool with angles taken relative to the feed direction, and a global coordinate system (x, y) based upon the workpiece feed direction. The relative displacements of the workpiece and tool (accounting for feed rate and vibration effects) are provided as input for the chip thickness calculation. The basis of the computation is the manipulation of a set of arrays of Cartesian coordinates (one array for each tooth on each axial slice), that define the surface of the workpiece that was produced by that tooth. The array length represents a complete revolution of the tooth, therefore with each tooth revolution the array values are overwritten, or updated. For each time step in the simulation, the following calculations are repeated for each tooth on each axial slice [40]:

1. The position of the tooth is calculated based upon the current simulation time, and the spindle speed.
2. The workpiece surface array for the present tooth is updated.
3. The instantaneous chip thickness for the present tooth is calculated, based upon the current tooth position, and the surface array for the preceding tooth.
4. The geometrical interference between the tool flank and just-cut surface is calculated.

The Simulink model shown in Figure 3.1 adopts the state space formulation which can be used to represent even the coupled dynamics between the x and y directions for multi degree milling system. In addition, the cutting forces (Figure 3.2) were expressed with subsystems of standard Simulink blocks, whereas the more complex kinematics model was performed in a c-program that interfaces with Simulink via the s-function/mex-file [98]. Now the model aspects will be descried in more details.

3.3 **Milling Kinematics**

Milling is an intermittent multi-point operation which involves feeding the workpiece into a rotating cutter. The milling operation can generally be divided into two categories: peripheral and face milling. In peripheral milling, the cut surface is parallel to the axis of the cutting tool. In face milling, the working surface is perpendicular to the cutting tool. In addition, milling can also be classified into two main orientations as shown in

Figure 3.5. Milling in which the cutter rotates in direction against the feed of the workpiece is known up-milling or conventional milling (Figure 3.5(a)): here the chip thickness starts at zero thickness and increases up to the maximum. The orientation in which the workpiece is fed in the direction of the cutter rotation (Figure 3.5(b)) is known as down-milling or climb milling: here each tooth engages the material at a definite point, and the width of the cut starts at the maximum and decreases to zero.

In addition the instantaneous chip thickness for the milling is described with reference to Figure 3.6, at any instantaneous point in time, the chip thickness h can be calculated based upon the current tooth position and the workpiece surface coordinates representing the surface from the previous tooth pass. Moreover the flank contact or the interference region (area or volume) between just the cut-surface and the current position of the tool is then determined based upon the relief angle $\boldsymbol{\gamma}$ and the maximum allowable interference contact length (flank length) l_f. This interference contact (area or volume) is then used to calculate the normal forces that arise due to process damping mechanism. The workpiece material that has been penetrated by the flank surface is assumed to plastically deform so that it follows the flank surface.

Details of calculating the milling chip thickness and interference contact volume are now explained.

3.3.1 **Chip Thickness Calculation in Time Domain Milling**

In milling process, calculating the instantaneous uncut chip thickness h accurately is very essential step for estimating the radial and tangential cutting forces on the cutter at each cutting point. This section discusses the method that incorporates simultaneously the cutter/workpiece relationships and the immersion angle variation into the calculation. It should be noted that, chip thickness simulation of this model is following similar procedure that developed by Sims [40], Campomanes and Altintas [79] and Peigne *et al* [99] which now is summarised.

In general by considering the regeneration model, the calculation is determined based on the relative positions between the current tooth tip and the workpiece surface layer

generated by the preceding tooth pass. The engagement/separation of the cutter from the workpiece is instantaneously identified. It should be known that during the chip thickness simulation, centre of the tool is used as a reference for all the computed dimensions.

The milling kinematics model begins by discretising the tool/workpiece contact geometry to n_l number of axial slices (layers) as shown in Figure 3.4(a), each layer consisting of an array of x, y data points. At each instantaneous point of time, the chip thickness is calculated upon the current tooth position and the workpiece surface coordinates representing the surface from the previous tooth pass. This is demonstrated in Figure 3.6(b), which shows an example for simulating the chip thickness using a tool with uniform teeth. Here the data points stored in the workpiece surface arrays for each tooth. The instantaneous chip thickness h is calculated using a circular interpolation method between the two closest points, S_{a0} and S_{a1} left by the preceding tooth N_{t-1} on the previous arc surface l_{-1}, and the N_t current cutting tooth tip position S_{at} at the current arc surface l. The close-up Figure 3.6(b) shows how the chip thickness h is calculated based upon the intersection of two lines. One line is the line from the present tooth's position to the tool centre, and the other is the line of the segment of the workpiece surface array for the previous tooth.

However, during the milling process the tooth can lose contact with the workpiece surface due to the rotation outside of the cut, or the excessive vibrations between the tool and workpiece. The latter case is illustrated in Figure 3.6(d), where the tooth tip does not intersect the surface array l_{-1} generated by the preceding tooth. In this case, the surface array l for the current tooth is updated by interpolation between the data points on the layer surface l_{-1}. In physical terms this is equivalent to the workpiece surface being unchanged, since the tooth is not cutting. In this situation, the value of the instantaneous chip thickness becomes negative $(-h)$. These values of the chip thickness are called loss of contact chip thickness h_{loc}which in Chapter 5 will be used to measure what is called loss of contact energy. The procedure of calculating the chip thickness is now demonstrated in more detail:

1- Identifying the Current Tooth Position:

For each step time the instantaneous tooth position at the current axial layer is identified. Figure 3.7 shows an example of the geometry of the chip thickness during the milling process. Here coordinates of the current cutting tooth (S_{atx}, S_{aty}) are determined by the means of the tool radius r_t and its angular position Θ_u along the cutting region. The mathematical relationship of defining the angular position Θ_u of each tooth including the constant helix angle and the instantaneous coordinate (S_{atx}, S_{aty}) is expressed as follows:

$$\Theta_u = \theta_t + \varphi - \frac{(1+l) * b}{n_l} \frac{tan(\lambda)}{r_t} \tag{3.1}$$

$$\begin{aligned} S_{atx} &= r_t \cos(\Theta_u) \\ S_{aty} &= r_t \sin(\Theta_u) \end{aligned} \tag{3.2}$$

where θ_t is the angular position of the cutting tool, calculated from its angular velocity, ω and the time, t, $(\theta_t = \omega t)$, φ is the angular position of each tooth *i* relative to the reference tooth, λ is the regular helix angle, r_t is the radius of the cutter, and n_l is the total number of axial discretisation layers.

2- Defining the Workpiece Arc Surface Points:

At each step time the workpiece surface is digitised by a number of points, each data point is defined in global coordinates stored in an array. Along the segment geometry the two closest arc surface points S_{a0} and S_{a1} on the previous arc surface l_{-1} at the points *A* and *B* respectively (Figure 3.7) are defined using c-program codes. These points are defined in the global coordinates (S_{ax0}, S_{ay0}) and (S_{ax1}, S_{ay1}) with angular positions θ_{a0} and θ_{a1} respectively. These slope angles are calculated based on the global coordinates using the four-quadrant inverse tangent function as follows:

$$\begin{aligned} \theta_{a0} &= atan2(S_{ay0}, S_{ax0}) \\ \theta_{a1} &= atan2(S_{ay1}, S_{ax1}) \end{aligned} \tag{3.3}$$

3- Calculate Dimensions of the Intercept Segment Geometry

For each step time the dimensions of this segment are calculated and updated. Here with reference to Figure 3.7 dimensions r_0 and r_1 are measured as the distance from the tool centre position O to the defined arc surface points S_{a0} (A) and S_{a1} (B) on the previous arc surface respectively. These dimensions r_0 and r_1 with the slope angles θ_0 and θ_1 respectively are calculated as follows:

$$r_0 = \sqrt{(S_{ax0})^2 + \left(S_{ay0}\right)^2}$$
$$r_1 = \sqrt{(S_{ax1})^2 + \left(S_{ay1}\right)^2} \tag{3.4}$$

$$\theta_0 = \theta_u - \theta_{a0} \tag{3.5}$$
$$\theta_1 = \theta_{a1} - \theta_u$$

Angles θ_0 and θ_1 are defining the angular position of the arc surface points S_{a0} and S_{a1} relative to the current tooth radius position. Then the intersection angles θ_{01} , β, α and dimension L_{01} can be found:

$$\theta_{01} = \theta_0 + \theta_1$$
$$L_{01} = \sqrt{r_0^2 + r_1^2 - 2r_0 r_1 cos(\theta_{01})}$$
$$\beta = \sin^{-1}\frac{(r_0 sin(\theta_{01}))}{L_{01}} \tag{3.6}$$
$$\alpha = \sin^{-1}\frac{(r_1 sin(\theta_{01}))}{L_{01}}$$

Now the intercept segment radius r_s is calculated which is equal to the distance from the current tool centre O to the point O' (Figure 3.7). When the angle θ_0 is equal to zero the radius of intercept segment r_s is equal to the dimension r_0, $(r_s = r_0)$ according to the triangle ($\Delta AOO'$) (Figure 3.7). However, if the angle θ_1 ($\Delta BOO'$) equals zero then the radius r_s will equal the dimension r_1, $(r_s = r_1)$.

$$r_s = \begin{cases} r_0 & \text{when} \quad \theta_0 = 0 \text{ and } \theta_1 > 0 \\ r_1 & \text{when} \quad \theta_1 = 0 \text{ and } \theta_0 > 0 \end{cases} \tag{3.7}$$

In addition when the angle β ($\Delta OBO'$) is not found or equals zero, then the intercept segment radius r_s is calculated based on the ($\Delta OAO'$) triangle relationship. However

when the angle α ($\Delta OAO'$) equals zero then the radius of the intercept segment r_s can be found from the triangle ($\Delta OBO'$).

$$r_s = \begin{cases} \dfrac{r_0 sin\ \alpha}{sin\ (\pi - \alpha - \theta_0)} & \text{when} \quad \beta = 0 \text{ and } \alpha > 0 \\ \dfrac{r_1 sin\ \beta}{sin\ (\pi - \beta - \theta_1)} & \text{when} \quad \alpha = 0 \text{ and } \beta > 0 \end{cases} \tag{3.8}$$

If the all dimensions of the cutting segment are found and computed. The intercept segment radius r_s will be calculated along the both triangles ($\Delta AOO'$) and ($\Delta BOO'$) geometries and select the highest value as shown in Figure 3.7.

$$\begin{aligned} r_{sA} &= \frac{r_0 sin\alpha}{sin(\pi - \alpha - \theta_0)} && \text{from} \quad \Delta AOO' \\ r_{sB} &= \frac{r_1 sin\beta}{sin(\pi - \beta - \theta_1)} && \text{from} \quad \Delta BOO' \\ r_s &= r_{sA} && if\ r_{sA} > r_{sB} \\ r_s &= r_{sB} && if\ r_{sB} > r_{sA} \end{aligned} \tag{3.9}$$

Now with reference to Figure 3.7, the instantaneous uncut chip thickness h is measured as the distance between the current tooth edge (S_{atx}, S_{aty}) at point C and the intersection point O' that is crossing the intersect segment dimension L_{01}. In other words, the instantaneous uncut chip thickness h is equal to the current tooth radius r_t minus the radius of the intercept segment r_s:

$$h = r_t - r_s \tag{3.10}$$

4- Update the Intercept Segment Radius

During the milling process the workpiece is fed into the cutter at the rate f_t (mm/tooth). Therefore radius of the intercept segment r_s needs to be updated for each step time. Since in this model the cutting tooth is assumed to be sharp-edged then the intercept segment radius is updated based on the current tooth radius and position as follows:

During the simulation at each step time the value of the intercept segment radius r_s is checked to determine whether the tooth is in the cut or not. If the current value is not

found, this means the tooth is rotating outside the cut (due to the vibration or rotating outside the cutting segment), in this case the intercept segment radius r_s is updated to be set equals to the current tool radius r_t,($r_s = r_t$). Then the radius of the intercept segment r_s is recalculated for each new surface layer as previously explained. Furthermore, coordinates of the current tool point (S_{atx}, S_{aty}) on the current layer are updated by using the current updated tool radius and converted to global coordinates as follows:

$$\begin{aligned} S_{atx} &= r_t \ cos\,\Theta_u \\ S_{aty} &= r_t \ \ sin\,\Theta_u \end{aligned} \tag{3.11}$$

Finally values of the dynamic chip thickness h for each tooth N_t and each layer l are stored in arrays to be input data for the cutting force calculation.

3.3.2 **Modelling Tool/Workpiece Interference Contact Region**

It is well known that during the metal cut the tooth edge is not perfectly sharp, and that even a very carefully treated tool edge can not retain its original sharpness after engaging a cut. It is also believed that material that moves in front of the tool edge is severely retarded [100] due to the friction between material layers. As a result, the separation of material around the tool tip may effectively occur along the segment of a circular arc with a finite radius [101, 102], as shown in Figure 3.8. The size of this effective radius depends on the tool geometry and work materials , as well as the cutting conditions, for example , cutting at either a low cutting speed or a small uncut chip thickness usually creates a large effective radius [103]. With reference to the same figure, due to the finite effective radius, the material approaching the tool cutting edge may be deformed in one of two ways. In the upper segment, the material is deformed and removed as a part of the chip. In the lower part, due to an effective large negative rake angle, the material can not move up ward to become part of the chip but instead is extruded and pressed under the tool [104, 105]. This extruded material flows under the tool tip and eventually departs from under the tool flank face. During this extrusion process, the material is displaced down ward different distances according to the shape of the contact surface. The maximum surface displacement here is called the depth of tool penetration, which refers to the penetration of the tool into the workpiece. The total volume of the material displaced at any given instant is dependent

not only on the sharpness of the tool tip but also on the instantaneous cutting conditions [103]. In addition, in dynamic milling, the volume of material displaced by the flank face of the cutting tool through the penetration mechanism is varying as the tool vibrates and changes the instantaneous cutting direction. The relationship between the volume and the tool position for this model which considers a sharp tool is described below.

With reference to the close up view in Figure 3.6(c) shows a scenario of how the tool flank/workpiece interference is occurred. As described in [19], the current relief contact length l_{ft} is calculated from the intersection of two lines. One line represents the flank face of the tool, and the other line is the relevant segment of the workpiece surface array for the present tooth. If the workpiece is assumed to plastically deform, then any workpiece surface array elements within the interference zone are moved radially outwards as shown by the arrow. The most straightforward physical mechanism for the flank forces is to consider the total penetration length multiplied by the thickness of each slice to give the effective contact area between the tool flank and workpiece (for each slice) [19]. This method was applied by a small number of researchers for instance Montgomery and Altintas [17], Budak and Tunc [11] and Ahmadi and Ismail [106]. However this method is not utilising all of the information that is available concerning the flank/workpiece penetration. For example, what if the penetration is much deeper but confined to the same contact length? A more complex contact model would account for this issue, but at the expense of the computation efforts required. An alternative is to consider the flank normal force to be proportional to penetration volume of material that is pressed by the tooth flank face.

The interference volume is defined as the material forced below the cutting tool's flank face. This material is displaced beneath the radial cutting edge and the clearance face. For example Ranganath *et al* [18, 107] and Wu [108] used this method for modelling process damping forces. They proposed calculating the instantaneous interface volume by considering the region of the work surface from the tool tip extending backwards along the flank face of the tool. The cutting tool is assumed to have a zero edge radius. It should be noted that, the arc surface points are calculated after considering the effects

of cutter deflection, run out and the actual feed of the tool. Therefore the model does not impose any restrictions on the machined surfaces. The arc surface is traced out by these points which are then used to calculate the volume of the interference.

The question arises here as to whether the workpiece material that penetrates the flank undergoes a permanent deformation, thereby changing the geometry of the just-cut surface. Two extremes are fully elastic deformation (where the workpiece surface in unaffected), and fully plastic deformation. In the latter case, the material penetrating the tool flank will be removed and the workpiece surface redefined to align with the flank surface.

In the most recent studies such as [11, 13, 16, 18, 47, 107-109] process damping forces were modelled based on the volume interference between the tooth flank face and the wavy surface of the workpiece. The interference geometry is discretised into a number of segments. The volumes of these segments are calculated and added to each other to represent the total interference volume that is pressed beneath the tool flank face. Figure 3.9 shows a scenario of the interference mechanism during the milling. Here the cutting tool is assumed to be a sharp edge with a nominal clearance angle $\boldsymbol{\gamma}$. During the interference mechanism, the following contact points on the flank face and the arc surface are defined:

- (S_{atx}, S_{aty}) Coordinates of the contact point generated by the leading edge of the sharp tool at a tooth engagement angle θ_u .
- $\left(S_{fx}, S_{fy}\right)$ Coordinates of the contact point generated by the leading edge on the machined workpiece surface.
- (S_{fx}, S_{ty}) Coordinates of the contact point on the flank face and corresponds to the point on the workpiece arc surface (S_{fx}, S_{fy}).

1- Penetration of the Tool Flank Face

Data points of the workpiece arc surface that are penetrating the tooth relief face are defined as follows:

- With reference to Figure 3.9 the flank region of the cutting tooth is firstly defined. The flank angle Θ_f is calculated based on the global coordinates using the trigonometry relationships as follows:

$$\Theta_f = \Theta_u - sin^{-1} \frac{L_f \cos \gamma}{\sqrt{r_t^2 + L_f^2 - 2\, r_t\, L_f \sin \gamma}} \tag{3.12}$$

- Coordinates of the current tooth position point (S_{atx}, S_{aty}) is defined on the current arc surface l using the tooth radius and the engagement angle Θ_u at the current time step Δt_i:

$$\begin{aligned} S_{atx} &= r_t \cos \Theta_u \\ S_{aty} &= r_t \sin \Theta_u \end{aligned} \tag{3.13}$$

- Then the coordinates of the previous point $(S_{ax(t-1)}, S_{ay(t-1)})$ is determined by performing the C-program codes, this point is defined on the arc surface l (Figure 3.10) that was generated at the time step (Δt_{i-1}).

$$\begin{aligned} S_{ax(t-1)} &= S_{ax(t-1)} = (r_t \cos \Theta_u)_{t-1} \\ S_{ay(t-1)} &= S_{ay(t-1)} = (r_t \sin \Theta_u)_{t-1} \end{aligned} \tag{3.14}$$

Determine the position of this point relative to the position of the current tool tip (Figure 3.10). This can be achieved by calculating the dimension L_{01} and the slope angle α_{01}. Using results of the Equation (3.14) of the defined arc surface points relative to current tooth edge.

$$\begin{aligned} L_{01} &= \sqrt{(S_{ax(t-1)} - S_{atx})^2 + (S_{ay(t-1)} - S_{aty})^2} \\ \alpha_{01} &= tan^{-1} \frac{(S_{ay(t-1)} - S_{aty})}{(S_{ax(t-1)} - S_{atx})} - (\Theta_u + \frac{\pi}{2}) \end{aligned} \tag{3.15}$$

- Convert the dimension L_{01} into the tool coordinates (S_{fx}, S_{fy}):

$$S_{fx} = L_{01}\, cos\, \alpha_{01} \qquad (3.16)$$
$$S_{fy} = L_{01}\, sin\, \alpha_{01}$$

- Assuming the tooth geometry is sharp (tool wear is not considered), the coordinate S_{ty} of the point that is located on the tool clearance face and corresponding with its coordinate S_{fx} is calculated as follows.

$$S_{ty} = S_{fx} \tan(\gamma) \qquad (3.17)$$

- In this model plastic deformation mechanism is considered during the metal cutting. Therefore the arc surface points that are penetrating the tool flank face are calculated. As can be seen in Figure 3.10 when the coordinates S_{fy} of these points are greater than the flank face coordinates S_{ty}, then the position of each point is calculated (dimension L_{01} and slope α_{01}) are calculated based on the coordinates S_{ty} of the tool clearance face as follows:

$$L_{01} = \sqrt{{S_{fx}}^2 + {S_{ty}}^2} \qquad (3.18)$$
$$\alpha_{01} = tan^{-1}(\frac{S_{ty}}{S_{fx}}) - (\Theta_u + \frac{\pi}{2})$$

- Convert the dimension L_{01} into the tool coordinates (S_{fx}, S_{fy}):

$$S_{fx} = L_{01} \times cos\, \alpha_{01} \qquad (3.19)$$
$$S_{fy} = L_{01} \times sin\, \alpha_{01}$$

2- Modify the Interference Contact Region

Calculating an accurate interference contact volume is very essential step for accurate process damping forces. In some cases, the calculated points are possibly laid in the flank region but are not interfacing with the flank face as shown in Figure 3.11. In this situation, these points should be modified. The first case can be assumed as when the point is located at the beginning of the interference region is not interfacing with the tool flank face (case1 in Figure 3.11). This occurs only when the coordinate S_{fy1} of this point is less than its coordinate S_{ty1}, this means that the dimension y_{n1} is negative, whereas the coordinate S_{fy2} of the second point is greater than its coordinate S_{ty2}, and

its dimension value y_{n2} is greater than zero. Therefore, to find the starting point of the front interference contact, the first point should be moved backwards to be located on the tool flank face using the follow expression:

$$x'_{n1} = -y_{n1} . \frac{x_{n2} - x_{n1}}{y_{n2} - y_{n1}} + x_{n1} \quad \text{when } y_{n1} < 0 \text{ and } y_{n2} > 0 \qquad (3.20)$$
$$y_{n1} = 0$$

However, for the case 2 in Figure 3.11, the point here is located at the end of contact region which possibly is not interfering with the tool flank face. This occurs only when the coordinate S_{fy2} of this point is less than its coordinate S_{ty2}, this means that its dimension y_{n2} is less than zero. Whereas the coordinate S_{fy1} of the first point is greater than its coordinate S_{ty1}, thereby its dimension y_{n1} is greater than zero. Therefore, to find the point that defines the end of the interference contact, the second point should be moved inwards to be located on the tool flank face as follows:

$$x'_{n2} = y_{n2} . \frac{x_{n1} - x_{n2}}{y_{n1} - y_{n2}} + x_{n2} \quad \text{when } y_{n2} < 0 \text{ and } y_{n1} > 0 \qquad (3.21)$$
$$y_{n2} = 0$$

3. Calculating the Interference Volume

In order to calculate the interference volume accurately, the contact region is sliced into number of segments. Volumes of these segments are numerically calculated and added to each other to estimate the total volume of the interference region that is pressed by the tool flank face. Figure 3.12 shows a close-up view of the modelled interference contact region at certain step time. The interference volume of each segment is expressed as follows:

$$V_i = A_i . dz \qquad (3.22)$$

The volume of each segment V_i is calculated by multiplying the slice thickness dz by each computed segment area A_i which is calculated by using the trapezoid method. Having calculated all the segment volumes ($V_{i(N_t)}$) for each tooth N_t then a numerical

integration is used to calculate the total volume of the interference region V. The total interference contact volume is given as follows:

$$V = \sum_{1}^{N_t} \sum_{i=1}^{V_v} (V_{i(N_t)}) \tag{3.23}$$

The output values of the interference contact volume are stored in arrays and sent to the milling forces block as an input data to calculate the process damping forces.

3.4 **Milling Forces**

3.4.1 **Modelling Cutting Forces**

It is well known that cutting forces are directly proportional to the chip area behaviour [68, 110, 111]. A simplified orthogonal cutting force has been introduced in [68] to model dynamics of the forces in the cutting process. The cutting forces that are expressed in equation (3.24) composed of the tangential cutting force F_t which is directly proportional to the chip area, and the radial cutting force F_r which is orthogonal and proportional to the tangential force. The chip area is determined by product of the chip thickness h and the depth of cut b.

$$\begin{aligned} F_t &= K_t . b . h \\ F_r &= K_r . F_t = K_r . K_t . b . h \end{aligned} \tag{3.24}$$

where K_t and K_r are the tangential and radial specific cutting pressure respectively, and $(b.h)$ is the chip area. This model is corresponding to a straight tooth cutter [68]. However, in practice most of the milling tools may have a uniform or variable helical flute, so each flute penetrates into the workpiece depending on the angular position along the helix angle as shown in Figure 3.4. The geometry of the chip formation and the milling force components are also illustrated in the same figure.

Now, by considering the cutting geometry shown in Figure 3.4 both the tool and workpiece are discretised into a number of layers n_l along the axial depth of the cut b. For the end-mill each layer has a disk shape with thickness $dl = \frac{b}{n_l}$ (Figure 3.4 (b)). As with many previous publications [18, 40, 49, 79], at each axial layer the cutting force of

each tooth is calculated by product of the instantaneous cross-sectional area of uncut chip and the cutting pressure coefficient. At any step time the cutting forces due to the mechanics of chip generation are given by:

$$\begin{aligned} F_{rclN_t} &= \frac{b}{n_l}(K_{rc}h + K_{re}) \\ F_{tclN_t} &= \frac{b}{n_l}(K_{tc}h + K_{te}) \end{aligned} \tag{3.25}$$

where F_{rclt}, is the cutting force that acting in the radial direction of the tooth for layer l and tooth N_t. Likewise, F_{tclt} is the cutting force due to the chip mechanics acting in the tangential direction of the tooth N_t and layer l. Subscripts (rc & tc) are referring to the radial and tangential cutting respectively. Whereas coefficients K_{rc} and K_{tc} are widely used cutting forces coefficients that must be empirically obtained for a particular workpiece and (often) a particular tool. The edge or rubbing force coefficients K_{re} and K_{te} can be also included in the model formulation, but in this thesis for simplicity they are initially assumed to be zero.

Then these forces are transformed to the global coordinates based on the immersion angle θ_u as shown in Figure 3.4(c) the cutting forces are resolved into components F_{xlt} and F_{ylt} and summed up in the x and y directions respectively.

$$\begin{aligned} F_{xclN_t} &= F_{tclN_t} cos\left(\theta_u - \frac{\pi}{2}\right) + F_{rclN_t} cos\,(\theta_u + \pi) \\ F_{yclN_t} &= F_{tclN_t} sin\left(\theta_u - \frac{\pi}{2}\right) + F_{rclN_t} sin\,(\theta_u + \pi) \end{aligned} \tag{3.26}$$

$$\begin{aligned} F_{xc} &= \sum_{l=1}^{n_l}\sum_{t=1}^{N_t} F_{xlN_t} \\ F_{yc} &= \sum_{l=1}^{n_l}\sum_{t=1}^{N_t} F_{ylN_t} \end{aligned} \tag{3.27}$$

3.4.2 **Process Damping Forces**

It is believed that the process damping phenomenon exists due to the variation on the actual clearance or relief angle of the tool whilst cutting a wavy surface and its relation to the thrust on the cutter [112]. When the tool or workpiece vibrates during cutting, waves are generated on the workpiece surface as a result. Process damping occurs where the edge and flank of the cutting tool interfere with these waves. This interference causes a force out of phase with the vibration motion, which has a damping effect [113]. Some researchers assumed that process damping forces can be a result from the surface contact between the tool and workpiece [114], however the prevalent definition was expressed by Wu [103] is that process damping occurs due to ploughing, i.e. deformation of the workpiece by the tool.

In addition, experimental research has shown that the flank relief angle ($\boldsymbol{\gamma}$) of the cutting tool has a strong damping effect on the cutting process. This effect is attributed to the actual contact between the workpiece and the tool relief face which includes the tool cutting edge and its adjacent flank face [115].

Having calculated the workpiece/flank contact volume, the process damping forces are then calculated as follows:

$$\begin{aligned} F_{nplN_t} &= K_{np} V_{N_{t_t}} \\ F_{fplN_t} &= \mu_p F_{npN_t} = \mu_p K_{np} V_{N_t} \end{aligned} \tag{3.28}$$

With reference to Figure 3.4(c), F_{nplN_t} is the cutting force due to process damping acting in the direction normal to the flank face, for layer l and tooth N_t. Meanwhile, $F_{fplN_t}$is the frictional force acting on the direction of the flank face. Equation (3.28) has introduced two new variables: the process damping normal force coefficient K_{np}, and a corresponding coefficient of friction μ_p.

In addition the ploughing forces (process damping forces) can be resolved into components F_{xN_t} and F_{yN_t} acting in the x and y directions respectively:

$$F_{xplN_t} = F_{fplN_t} cos\left(\theta_u + \frac{\pi}{2} - \gamma\right) + F_{nplN_t} cos\,(\theta_u + \pi - \gamma) \tag{3.29}$$

$$F_{yplN_t} = F_{fplN_t} sin\left(\theta_u + \frac{\pi}{2} - \gamma\right) + F_{nplN_t}\, sin(\theta_u + \pi - \gamma)$$

$$F_{xp} = \sum_{l=1}^{n_l} \sum_{t=1}^{N_t} F_{xpN_t} \tag{3.30}$$

$$F_{yp} = \sum_{l=1}^{n_l} \sum_{t=1}^{N_t} F_{ypN_t}$$

where N_t is the number of teeth on the tool and n_l is the number of axial layers.

3.4.3 **Total Cutting Forces**

The total forces acting on the tool in the global $\boldsymbol{x}$ and $\boldsymbol{y}$ directions then are determined as follows:

$$F_x = F_{xc} + F_{xp}$$
$$F_y = F_{yc} + F_{yp} \tag{3.31}$$

These forces are then sent to the machining dynamics model where the system vibration is computed.

3.5 **Model System Dynamics**

Having calculated the total cutting forces that are acting on the tool, the corresponding system displacements can be obtained by modelling the structural dynamics of the flexible tool/workpiece. Figure 3.13 shows an example of the vibratory model used for machining dynamics modelling of milling. The cutter is considered to be a one-degree-of-freedom spring-damper vibratory system in the two commonly orthogonal directions x and y. The cutting forces exciting the system in the feed (x) and normal (y) directions are causing dynamic displacements *x* and *y*, respectively. These displacements are then fed back to the milling kinematics model. The dynamics of this milling system can be represented by the differential equations of motion as follows:

$$m_x\, \ddot{x} + c_x \dot{x} + k_x x = F_x(t) \tag{3.32}$$
$$m_y\, \ddot{y} + c_y \dot{y} + k_y y = F_y(t)$$

where m_x and m_y, are the masses, c_x and c_y are the damping coefficients, k_x and k_y are the stiffness of the machine tool structure in directions *x* and *y*, respectively, and $F_x(t)$ and $F_y(t)$ are the components of the cutting force that are applied on the tool in the directions of x and y respectively. The dynamic characteristics of the machine tool structure, including the masses, damping coefficient, and stiffness, or in another form of the dynamic stiffness, natural frequency, and the damping ratio, can be obtained from the modal testing.

Most of the available time domain simulations for chatter in machining use the 4th Runge–Kutta method to solve the differential equations because of the accuracy. Here the continuous time variable t is replaced by the discrete variable t_i, and the differential equations are solved progressively in constant time increment Δt, starting from known initial conditions. In general, better accuracy is obtained by choosing a smaller time step, but the number of computations will then increase [73].

For the Simulink model used in this research, the governing equations (3.32) are solved by considering the fourth order Runge-Kutta method at fixed time steps. The time step is defined by ($\Delta t = \frac{60}{iters \times \omega}$), where *iters* is number of the samples or steps per tool revolution and ω is the spindle speed in revolution per minute. In general, this model performs well along this time step selection. As an example for implementing the 4th Runge-Kutta to solve the differential equation (3.32) is presented in Appendix B [73].

With reference to this model shown in Figure 3.1, the equations of motion are solved in the time domain using relevant Simulink blocks to calculate the vibrations of the system. These vibrations are then fed back to calculate the instantaneous dynamic chip thickness. Once the instantaneous chip thickness is determined, the cutting force components can be predicted from the predictive force model as described in the previous section. It is assumed that the dynamic cutting forces in milling react instantaneously to the changes in undeformed chip geometry that are occurring due to the dynamic regenerative effects.

3.6 **Summary**

In this chapter, the formulation of the Simulink model has been illustrated. In addition the model's aspects have been described: milling kinematics, milling forces, and system dynamics. The milling kinematics calculates the chip thickness and tool/ workpiece interference contact volume. The milling forces calculate the shear cutting forces that are proportional with the chip thickness, and process damping forces that are proportional with the tool/workpiece contact volume.

Cutting process can become nonlinear for various reasons. In some cases, a nonlinear relationship between the cutting forces and the chip thickness can be observed. Excessive vibrations can lead to the tool leaving the cut so that the cutting force becomes zero. The advantage of a time-domain model is that these issues can be directly included in the model. Nevertheless, a linear model can still give a first approximation to the chatter stability. It should be noted that the techniques developed here are equally applicable to models with nonlinear components. Finally modelling system dynamics with an example of two degree of freedom are described to show how the system displacement can be modelled in x or y directions.

In the following chapters, the Simulink model will be used to consider different effects of the chatter mitigation mechanisms. In next the Chapter 4, the effects of the variable spindle speed will be explored. The model will then be extended to consider energy calculations, to explore process damping effects, variable helix tool and short regenerative effects.

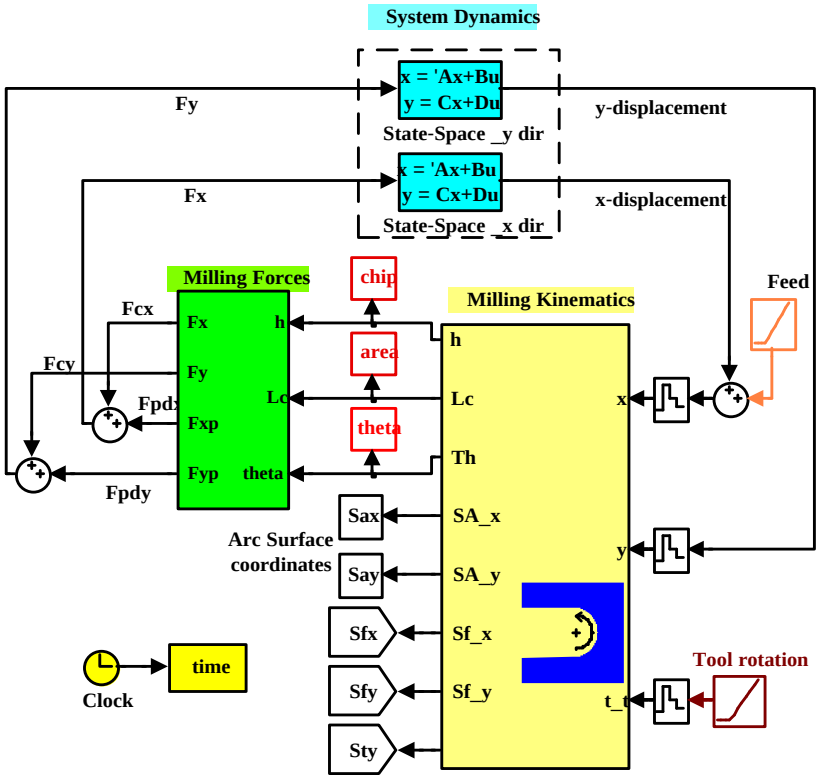

Figure 3.1 Main Simulink model with process damped milling.

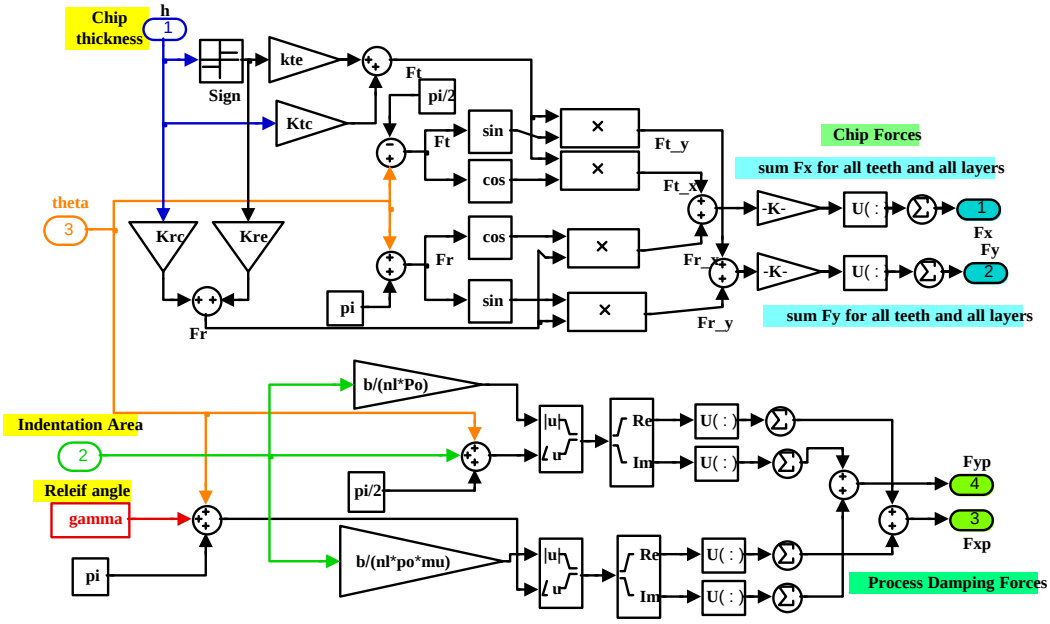

Figure 3.2 Cutting forces calculation in Simulink subsystem.

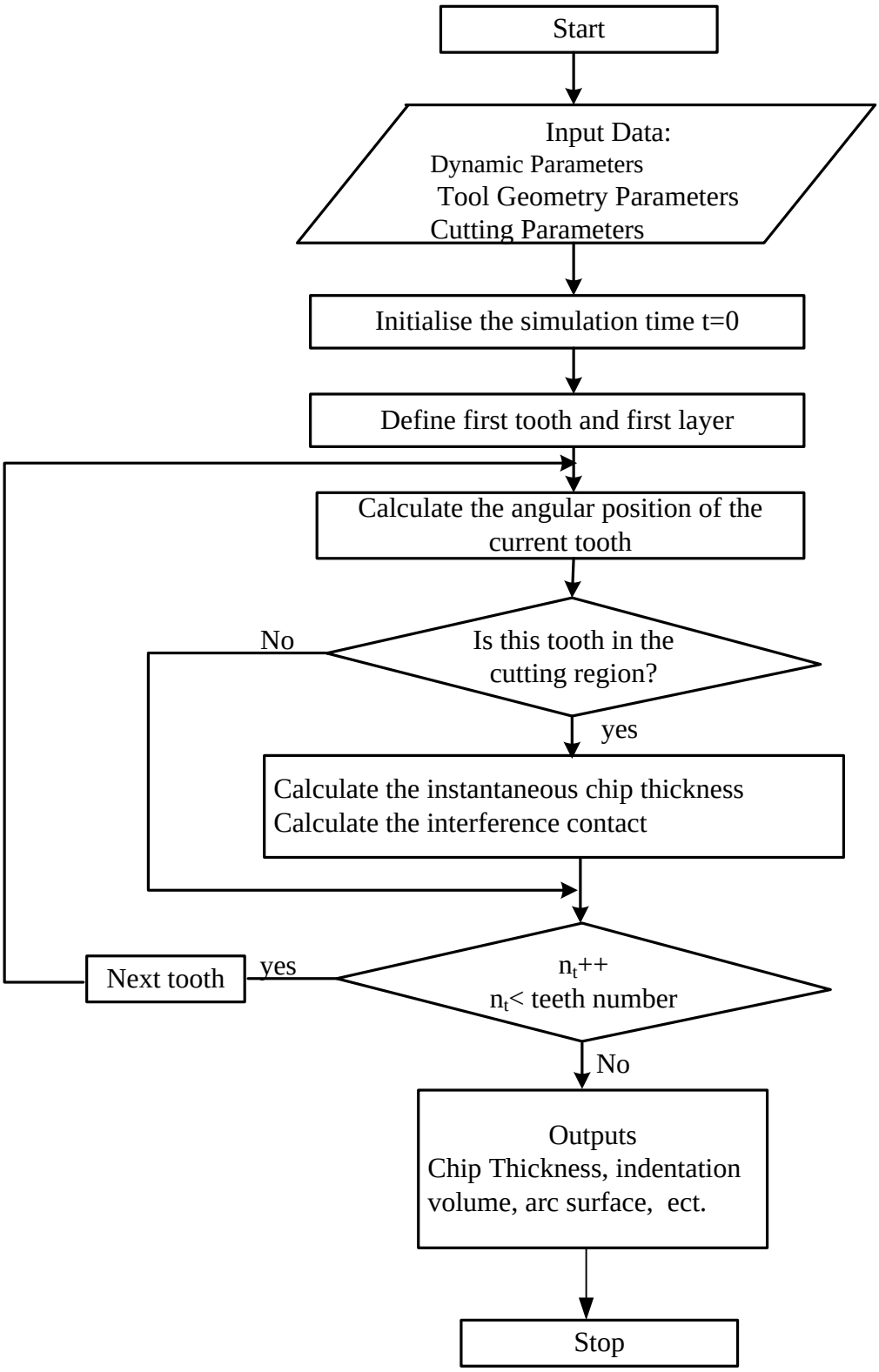

Figure 3.3 Flowchart of the Simulation

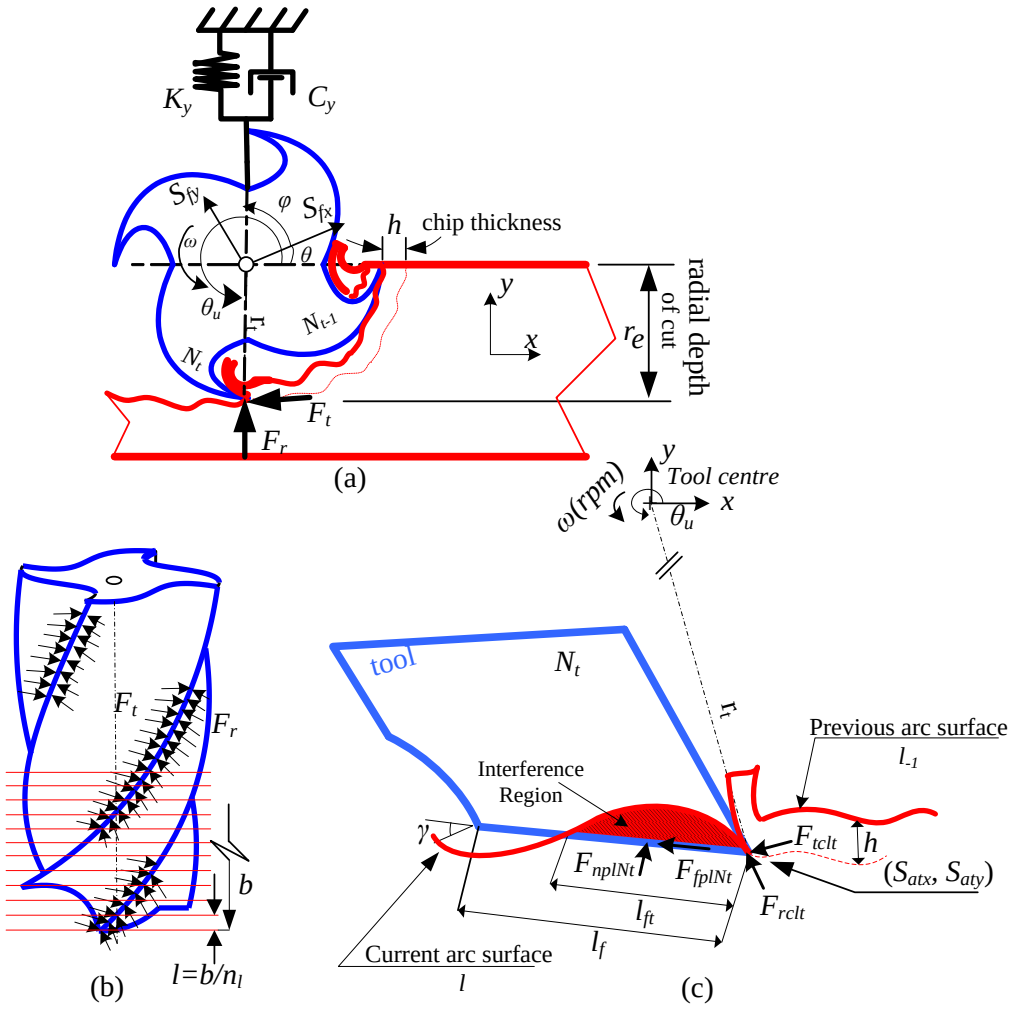

Figure 3.4 Milling dynamic model, giving the relative position between the cutting tool and the workpiece at each axial ‘‘layer’’

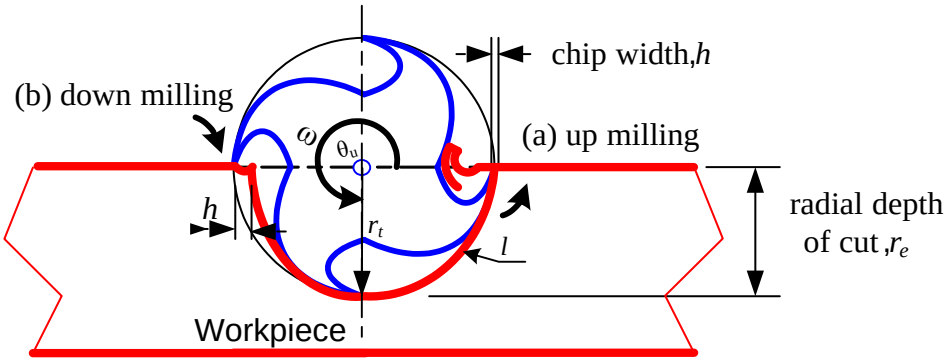

Figure 3.5 Tool and Workpiece Geometry during up and down milling

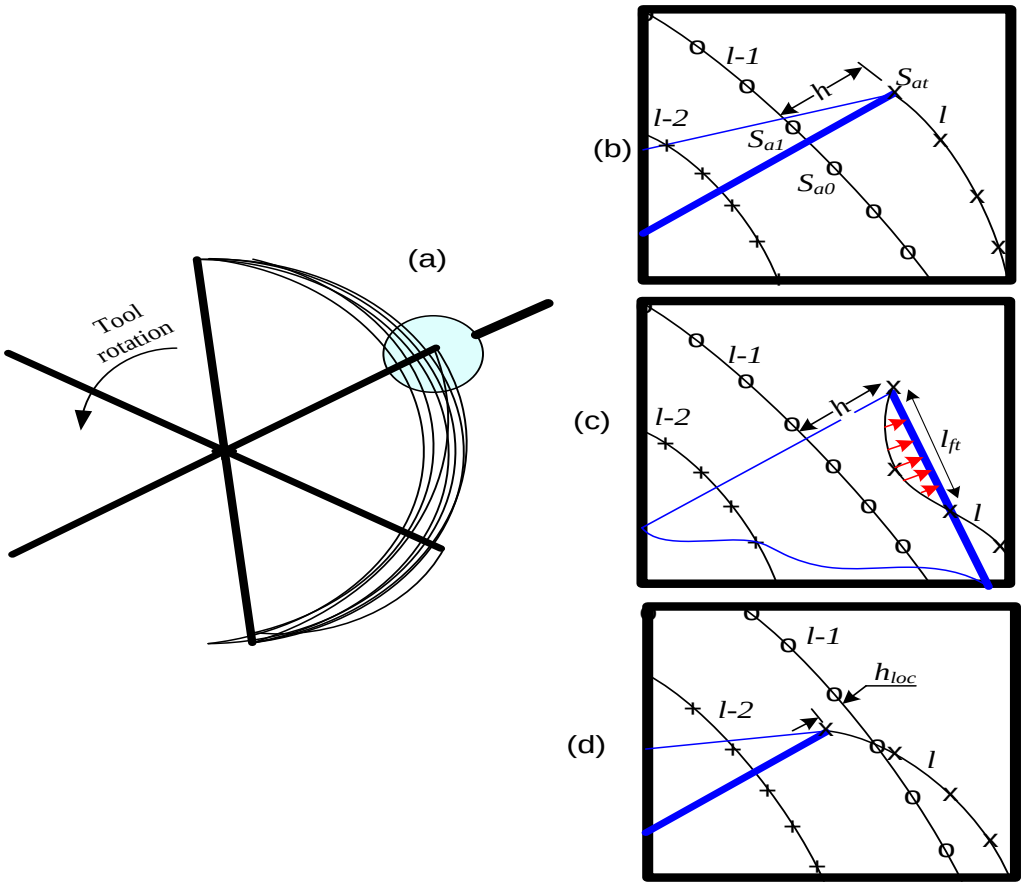

Figure 3.6 Simulation of the instantaneous chip thickness for a tool with 6 teeth[19].

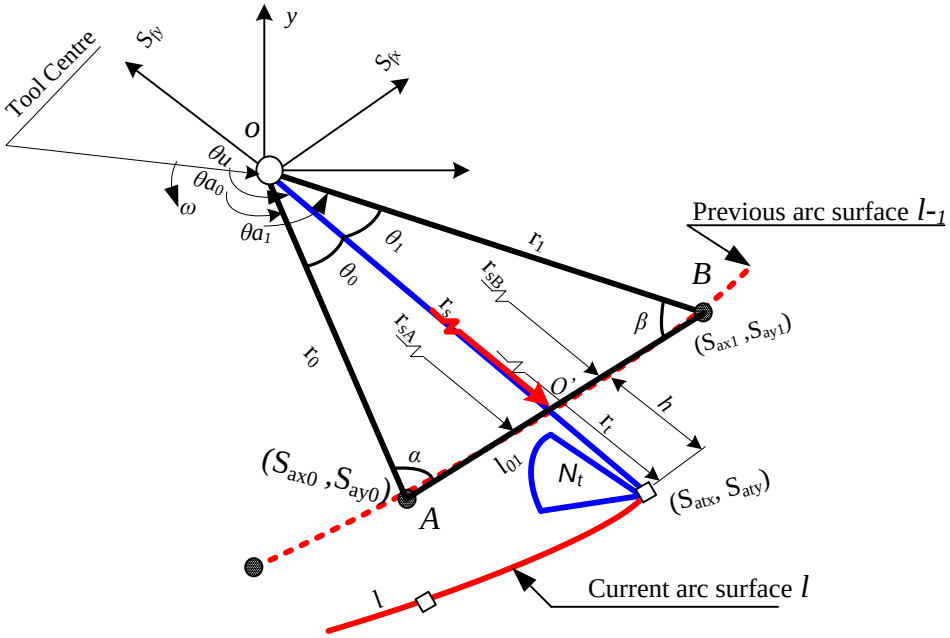

Figure 3.7 geometry of the chip thickness during the milling process

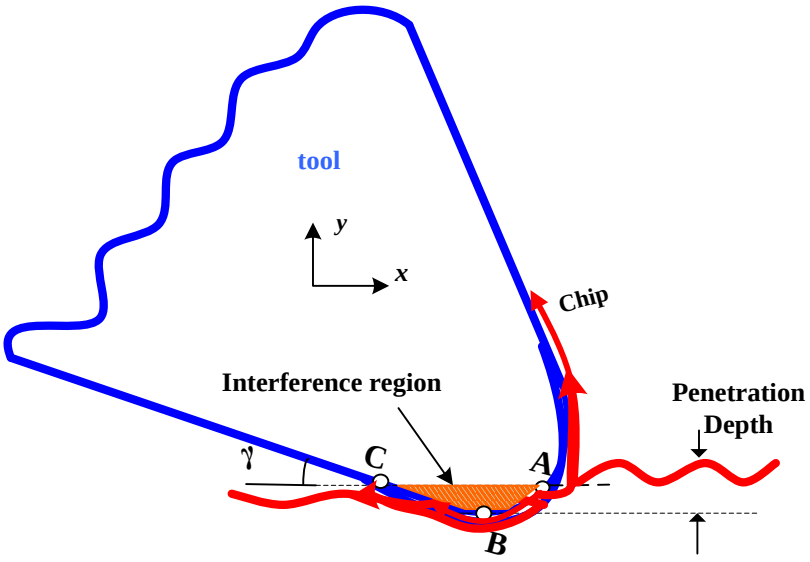

Figure 3.8 the ploughing mechanism

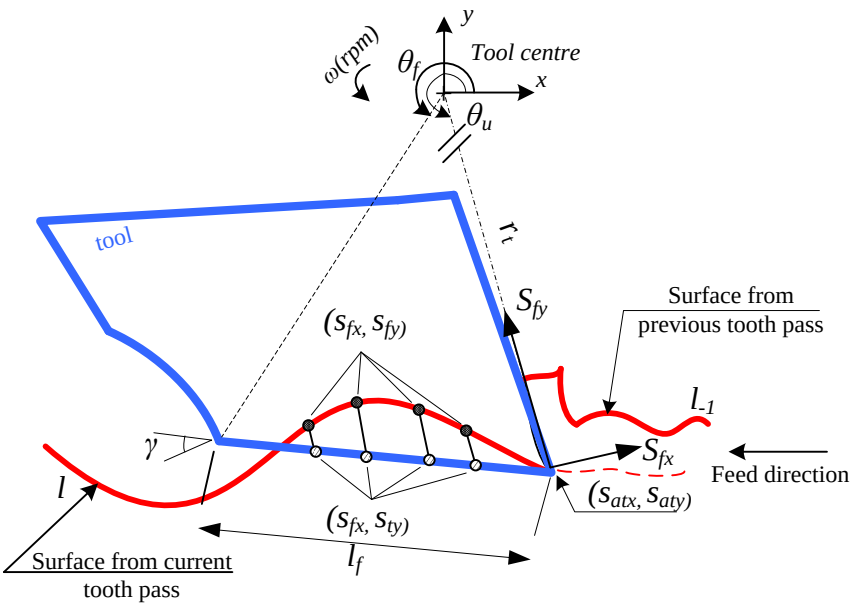

Figure 3.9 Tooth Flank Interference Geometry

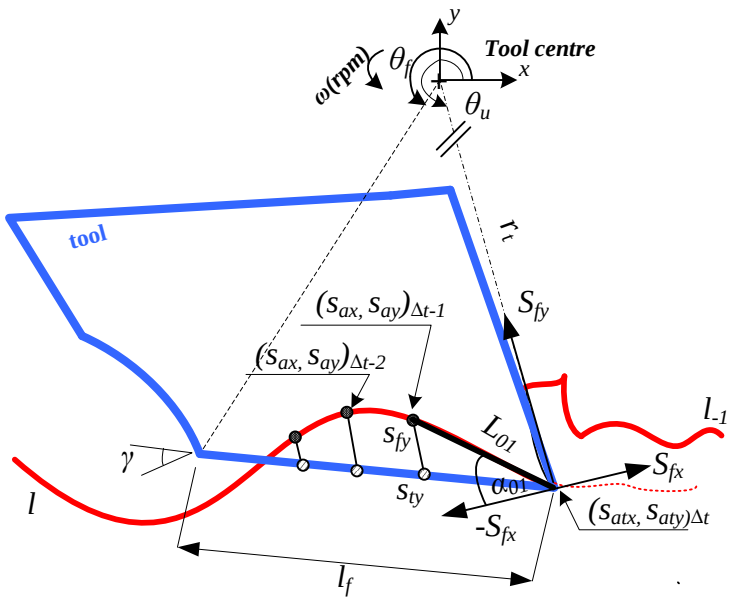

Figure 3.10 modelling points that penetrate the tool flank face

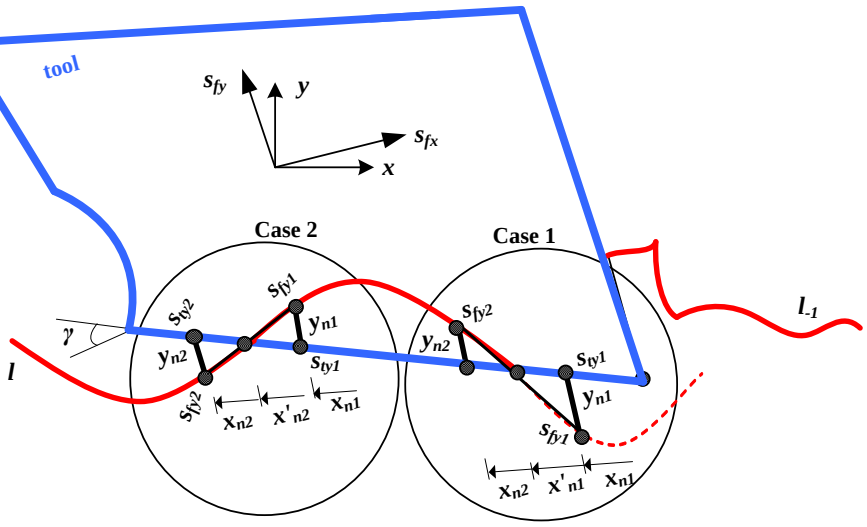

Figure 3.11 Modifying the Penetration Region

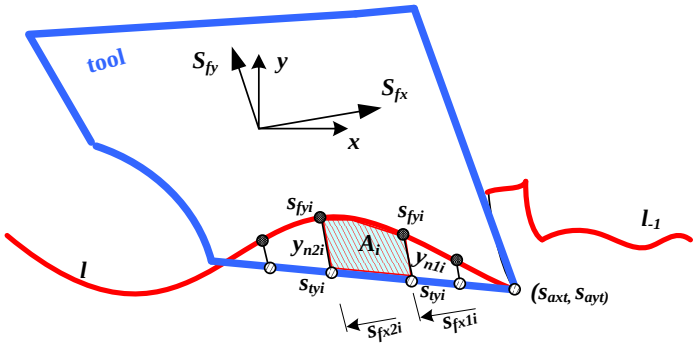

Figure 3.12 Modelling of the interference Contact Region

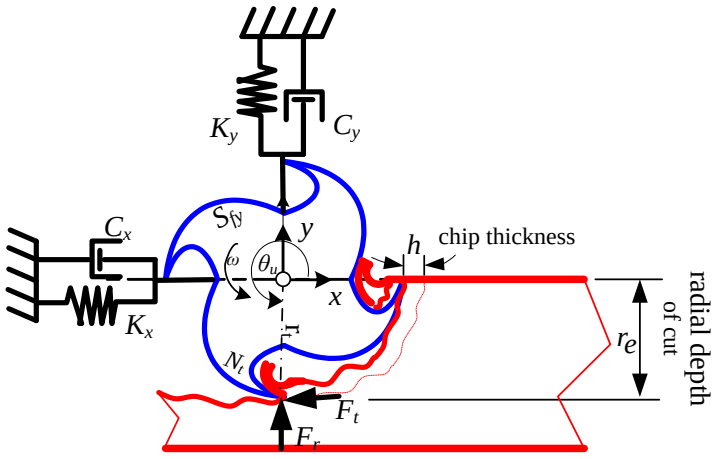

Figure 3.13 Two modes of the spring damper vibratory model of milling operation

CHAPTER 4 VARIABLE SPINDLE SPEED IN TIME DOMAIN MILLING

4.1 Introduction

Machining instability was traditionally overcome by selecting conservative cutting conditions, such as reducing feed rate or depth of cut [38]. More recent work has proposed continuously varying spindle speeds during milling. This is suggested as an effective technique to suppress regenerative chatter, which has become the focus of interest for many studies. Ismail *et al*.[31], for example employed the spindle speed modulation for real-time control of chatter in peripheral milling. Yilmaz *et al*.[87], presented a new method of multi-level random spindle speed variation. Sri and Beddini [36] and Pakdemirli and Ulsoy [88] considered the mechanism of spindle speed variation for chatter suppression using the delay differential equations with periodically perturbed delays. Seguy *et al.* [116] studied the effect of spindle speed variation in the high-speed domain using a semi-discretisation method for computing the optimal amplitudes and frequencies of the speed modulations. In addition Al-Regib *et al.* [29] considered the concept of programming the spindle speed variation for minimum energy input by the cutting process.

In general, models designed for determining and analysing machining stability of Constant Speed Machining (CSM) are not directly applicable to Variable Speed Machining (VSM) due to the presence of the time varying delay in the differential equations[117]. Therefore special mathematical techniques are used for analysing machining stability, since the corresponding mathematical model is a delayed-differential equation with a time varying delay term. Insperger and Stepan [118] for example considered the semi-discretisation method to study numerically a single degree of freedom model with time varying delayed equation. Jayaram *et al.* [117] analysed the system by considering a special combination of Fourier expansion and Bessel functions. Tsao *et al* [38] presented an angle domain analytical method for chatter stability analysis of variable speed milling. In this method, the system equations were transformed to the angle domain, using the spindle angular position instead of the time as the independent variable. The time varying delay in the system equations is converted

to a constant delay in the angle domain. However, the analysis presented in their study was for the simplified situation of continuous cutting with only single tooth in cut at any point of time.

However, the techniques and the procedures that are used in the current model as will be described in this chapter allow the above limitations to be overcome. This approach can be also applied to systems with multiple modes of vibration, and involving interrupted cutting with multiple teeth engaged in the cut simultaneously. It is also straightforward to include a nonlinear relationship between cutting force and chip thickness, and the periodic excitation force is inherently modelled. Consequently, the present chapter will describe a modification of the existing model so that it can be used for variable speed machining.

This chapter formed a two conference papers, abstracts are given in Appendix A1 and A2.

4.2 **Mechanism of the Spindle Speed Variation**

Periodic spindle speed variation is considered in the form:

$$\omega(\tau) = \omega_m + \omega_A S(\tau) \tag{4.1}$$

where ω_m is the mean spindle speed, ω_A is the amplitude of the speed variation and $S(\tau) = S(\tau + \boldsymbol{\tau_v})$ is a periodic shape function that varies between -1 and 1[116]. In the literature, mostly sinusoidal, triangular or square-wave modulations are considered. In this chapter a triangular speed variation shown in Figure 4.1will be considered. It is assumed that the spindle speed variation is periodic at period τ_v with a mean value ω_m, frequency ratio RVF and speed amplitude ratio RVA. According to the general notation in the corresponding previous studies, the amplitude and the frequency of the speed variation is normalized by the mean spindle speed ω_m, as:

$$RVA = \frac{\omega_A}{\omega_m}$$
$$RVF = \frac{60}{\omega_m \tau_v} \tag{4.2}$$

In practical applications, the maximum value for RVA is about 0.3 [116]. This represents a variation of 30% of the spindle speed and results in a variation of 30% of the feed by tooth due to the constant feed velocity. RVF is the ratio between the variation frequency f_r and the average spindle frequency $\frac{\omega_m}{60}$. The variation frequency f_r is typically about 1-2 Hz [116].

In this work, by using the normalized parameters introduced above, the triangular milling speed trajectory can be approximated. Sample of the Matlab codes in Appendix (D1) show how this speed trajectory are can be calculated based on the average spindle speed periodicity τ_v. However, the speed periodicity was determined based on the ratio of the speed variation frequency RVF and the mean value of the spindle speed ω_m as follows:

$$\tau_v = \frac{60}{(\omega_m RVF)} \tag{4.3}$$

In addition, amplitude ratio RVA is used to define the limits of this speed trajectory, here as shown in the Figure 4.1 the limits of the speed at points (1, 3, … odd numbers) are greater than the nominal value ω_m with value $(\omega_m RVA)$ whereas the limits at points (2,4,…. even numbers) are less than the nominal value ω_m with amount $(\omega_m RVA)$.

$$\omega(\tau_i) = \begin{cases} \omega_m(1 + RVA) & \text{for} \quad \tau_i = (1{:}\,2{:}\,\text{length}(\tau_t)) \\ \omega_m(1 - RVA) & \text{for} \quad \tau_i = (2{:}\,2{:}\,\text{length}(\tau_t)) \end{cases} \tag{4.4}$$

Then the spindle speed trajectory is stored in array in terms of the instantaneous number of revolutions τ_t versus the instantaneous spindle speed value ω.

4.3 **Milling Time Domain Simulation**

4.3.1 **Constant Speed Machining (CSM)**

Consider the schematic representation of milling shown in Figure 3.4(a). Here, a milling tool with multi cutting teeth is removing material from a workpiece. It should be highlighted that regenerative chatter can occur even in a linear one degree of freedom system due to the presence of a delay term in the forcing function; consequently a single degree freedom is considered here. However, it is straightforward to extend the

presented relationships to systems with many degrees-of-freedom, as would occur in many practical scenarios. Therefore, for simplicity the structure is assumed to be flexible in the y-direction, while the feed is parallel to the x-direction, the dynamic model is defined by the equation:

$$m_y \frac{\mathrm{d}^2 y}{\mathrm{d}t^2} + c_y \frac{\mathrm{d}y}{\mathrm{d}t} + k_y y = F_y \tag{4.5}$$

It should be re-iterated that the force F_y is a function of the current and delayed vibration y, along with the instantaneous angle of the tool. Consequently, equation (4.5) is a delay-differential equation with nonlinear and time-periodic coefficients.

In order to predict the time response of this system, a discretised model is formulated in the Simulink modelling environment that is shown in Figure 4.2. The model consists of three aspects, namely milling kinematics, milling forces, and system dynamics. These components were described with more details in the Chapter 3.

4.3.2 **Variable Speed Machining (VSM)**

Traditionally real-time is used as the independent variable for writing the solution of the equations of motion. This is particularly the case when simulating dynamic systems using the Simulink modelling environment. Here, physical time (with units of seconds) is assumed to be the independent variable, and a wide range of numerical integration routines are available for solving the equations of motion (e.g. the 4th order Runge Kutta method, etc).

However, a close inspection of the Simulink formulation described above reveals that the milling kinematics model requires a fixed number of time steps for each revolution of the tool. This means that a fixed-step solver (e.g. the Runga Kutta method) must be used, and the spindle speed must be fixed. In this section, this problem is overcome by using tool revolution as the independent variable in rewriting the system equation of motion. Consequently, 'Simulink time' is no longer equal to physical time, but rather the number of tool revolutions. With this approach, a fixed step solver will always involve a fixed number of time steps per tool revolution, even if the spindle speed is changed. This concept will now be derived more formally.

4.4 System Equation in Variable Speed Machining

With reference to equation (4.5), the relationship between physical time t and instantaneous spindle speed n is:

$$\frac{\mathrm{d}\tau_t}{\mathrm{d}t} = n \text{ (rev/sec)} \tag{4.6}$$

where τ_t is the number of tool revolutions, the velocity can then be rewritten using the chain rule as:

$$\frac{dy}{dt} = \frac{dy}{d\tau_t}\frac{d\tau_t}{dt} = \frac{dy}{d\tau_t}\, n \tag{4.7}$$

Moreover the system acceleration can be rewritten as:

$$\frac{d^2y}{dt^2} = \frac{d^2y}{d\tau_t^2}n^2 + \frac{dy}{d\tau_t}\frac{dn}{dt} \tag{4.8}$$

Here, the rate of change of spindle speed ω can be rewritten to give:

$$\frac{d^2y}{dt^2} = \frac{d^2y}{d\tau_t^2}n^2 + \frac{dy}{d\tau_t}\frac{dn}{d\tau_t}n \tag{4.9}$$

The equation of motion (4.5) can then be written in terms of the derivative expressions on the right-hand-side of equations (4.7) and (4.9)

$$F_y - k_y y(\tau_t) - c_y\frac{dy}{d\tau_t}n = m_y\left(\frac{d^2y}{d\tau_t^2}n^2 + \frac{dy}{d\tau_t}\frac{dn}{d\tau_t}n\right) \tag{4.10}$$

This can be rearranged to give:

$$\frac{d^2y}{d\tau_t^2} = \frac{F_y}{m_y\, n^2} - \frac{k_y y(\tau_t)}{m_y n^2} - \frac{c_y}{m_y n}\frac{dy}{d\tau_t} - \frac{1}{n}\frac{dy}{d\tau_t}\frac{dn}{d\tau_t} \tag{4.11}$$

The system dynamics which are represented by the equation of motion (4.11) give rise to the Simulink system shown in Figure 4.3.

4.5 Numerical Study

In order to demonstrate the implementation of the proposed model, a simple milling scenario with one degree of freedom is considered. The milling parameters were chosen to closely match those used in previous work by Seguy *et al* [89, 116], and are summarised Table 4-1.

To begin with, the milling spindle speed was assumed to be constant and the chatter stability was evaluated using the semi-discretisation method as implemented in reference [89, 116]. This served to check the validity of the time-domain model for the constant speed scenario. A variable spindle speed was then used in the time-domain model, with a triangular speed variation around a mean value. This was defined in accordance with reference [89, 116], with the parameters *RVA* and *RVF* fixed at 0.28 and 0.003 respectively.

For the time-domain simulations, the peak-to-peak displacement technique is used to determine the system displacement, since it is considered to be an effective method used for chatter detection. Previous studies [39, 40, 89, 116] have showed that the peak-to-peak approach provides a rapid means of identifying the stability boundary during time domain computation of the constant speed milling. However in the variable spindle speed case, it will be seen that the system displacement does not reach a steady state condition, making the peak-to-peak method difficult to use as a judgement of chatter stability.

It should be pointed out that the parameters chosen in the present study may not completely match those used in reference [89], since the tool helix angle, tool radial immersion; number of tool cycles, and number of simulation axial layers were not given.

4.6 **Results and Discussion**

Before presenting an analysis of the chatter stability, it is worth illustrating the time response of the system, and describing the implementation of the peak-to-peak displacement method for analysing the chatter stability as presented in Figure 4.4. A typical result of the case of constant speed machining (CSM=9100 rpm) is shown in Figure 4.4(a). As can be seen from the closed view (Figure 4.4(a)) the steady state is reached and the peak-to-peak displacement is used to evaluate the system stability. However Figure 4.4(b) and (d) demonstrate the case of variable speed machining. Here, the triangular waveform of the spindle speed is varying periodically about the mean value of the speed (ω_m=9100 rpm) as shown in Figure 4.4(d). Figure 4.4 (b) illustrates

the overall chatter level which is clearly stabilized at a level significantly lower compared to the constant speed machining case (Figure 4.4 (a)). Thereby the system here is considered to be stable. The comparison between the constant speed machining and variable speed machining is further illustrated in Figure 4.4(c). From this plot it can be clearly noticed that variable speed machining approach has lower and almost constant vibration which indicates significantly greater stability than for the constant spindle speed condition. However, close inspection of the closed view displacement signal shown in Figure 4.4(b) reveals a response that is no longer periodic with each tool revolution, due to the influence of the variable spindle speed. For consistency, the peak-to-peak measurements were therefore obtained from the data within the last period of the spindle speed waveform.

Now, in order to implement the peak-to-peak displacement approach, the maximum and minimum values of the displacement (Figure 4.4) is obtained. In the case of chatter instability, the displacement magnitude is expected to grow exponentially, so the value obtained depends entirely on the number of simulated tool revolutions (i.e. the length of the simulation time-span). Nevertheless, the magnitude obtained for completely stable cases depends only on the forced vibrations. Consequently, if the peak-to-peak values are plotted as a function of depth of cut b, then a clear transition is observed at the depth of cut corresponding to the stability boundary.

Next, a number of simulation tests at a constant speed have been conducted in order to verify the model. The results are shown in Figure 4.5. Stability of the constant speed machining is predicted using the semi-discretisation method. This method can be used to derive stability charts for constant spindle speed, and the variation of the delay arose due to the accurate modelling of the feed motion [34]. In order to verify the results obtained by semi-discretisation, the system's behaviour is determined as well by time domain simulations for some particular spindle speeds. The predicted behaviour of the system corresponds to the constant cutting speed is compared with the system behaviour when these speeds are continuously varied.

The stability lobe diagram for the constant spindle speed case is shown in Figure 4.5(a). Here, regions below the line indicate a prediction of stable, chatter-free machining, whilst regions above the line are associated with chatter. The individual markers at 4000 and 9100 rev/min correspond to milling conditions used in the time-domain simulations of the constant spindle speed.

As can be seen from the Figure 4.5(b), at 4000 rev/min the magnitudes of the peak-to-peak displacements increase proportionally with the axial depth of cut b. This case is related with a stable cutting process where the amplitudes of the forced vibrations are linearly increasing with the increased depth of cut. The use of a single axial discretised layer in the time domain model implies that the tool helix angle is 0 degrees, resulting in high forced vibration amplitudes that do not occur in practice. Figure 4.5(c) shows the peak-to-peak displacements at 9100 rev/min. A sharp transition occurs at $b = 0.6$mm, corresponding to the margin of stability indicated in Figure 4.5(a).

Figure 4.5(d) shows the peak-to-peak displacements acquired by time domain simulation for the variable spindle speed simulations at 9100 rpm. From this plot it can be seen that there appears to be a transition in the peak-to-peak amplitudes at $b = 2$mm, which indicates significantly greater stability than for the constant spindle speed condition (Figure 4.5(c)). This result is further illustrated in the Figure 4.5 (e) where the critical depth of cut at spindle speed 9100 rpm is increased from 0.6mm (constant speed machining) to about 2mm (variable speed machining).

These results agree reasonably well with those given in [89, 116], and the small differences could be attributed to the different parameters used in the simulations. Consequently these outcomes have validated the proposed variable spindle speed modelling procedure.

However, close inspection of the displacement signal shown in Figure 4.4 reveals that the transient behaviour of the signal that is arising due to the spindle speed alterations makes the peak-to-peak approach unable to provide an accurate measurement of chatter stability for variable spindle speed simulations, and that alternative methods are

required. Here the self-excited damping ratio approach (which is presented in reference [40]) is considered to be the more appropriate method for analyzing milling stability behaviour. This signal processing approach will be introduced in the next section.

4.7 **The Self-Excitation Damping Ratio**

Recently a number of time domain simulations and analytical approaches have been developed for chatter detection. However the problem arises of how to ascertain, based upon the computed data, whether the simulated cut was stable or unstable. For example the peak-to-peak (PTP) technique was used to identify the stability boundary during the constant cutting machining such as in [39, 40, 89]. However for the variable speed machining case it can be seen that the system displacement does not reach a steady state condition, making the peak-to-peak method difficult to use as a judgment of chatter stability. Therefore a signal processing method is considered as an effective method used to analyse chatter and the stability boundary of this case. Sims [40], implemented this approach for a constant speed machining case as well which provides more information on the behaviour of the self-excited vibrations.

In this section two scenarios of the variable speed mechanisms are considered, and the Matlab codes are used to identify these speed trajectories. In the first scenario, effects of a linear varying the spindle speed with different accelerations behaviours are investigated. With reference to Figure 4.6 the instantaneous spindle speed is determined according to the acceleration ratio (A_{sl}) which is calculated based on the start and ending spindle speeds (ω_{st} and ω_{en}) respectively, in addition to the total number of tool revolutions τ_t.

$$\omega = A_{sl}\tau_t \qquad \text{where} \quad A_{sl} = \frac{\omega_{en} - \omega_{st}}{\tau_t} \tag{4.12}$$

However, the second scenario is associated with the periodic triangular speed variation which has trajectory similar to that described in Section 4.2.

4.8 **Damping Ratio for the Chatter Criterion**

The theory of the free vibration has been well explained in a number of the vibration text books for example [119]. In this subject, it is well known that behaviour of the viscously damped system under the free vibration may take one of the vibration behaviours shown in Figure 4.7. With reference to equation (4.13) the damping ratio ζ can be estimated based upon the logarithmic decrement δ relationship, which it is measured by taking the logarithm between two amplitudes of two successive vibration cycles, x_1 and x_2.

$$\delta = log\frac{x_1}{x_2} \qquad \zeta = \frac{\delta}{2\pi} \tag{4.13}$$

With reference to Figure 4.7, there are three scenarios associated with linear viscously damped systems. In the first scenario (a) there is positive damping ($\zeta = +0.1$), this because the measured value of the logarithmic decrement δ is positive. This reveals that the amplitude of the advanced cycle x_2 is always smaller than the preceding cycle x_1, and this indicates that vibration amplitudes of this scenario are always decaying which finally leading the system to be stable. In the second scenario (b) there is zero damping ($\zeta = 0$). Here the logarithmic decrement δ is zero, because vibration amplitudes are always equal ($x_1 = x_2$), and this indicates the system is marginally stable. However in the third scenario (c) there is negative damping ($\zeta = -0.1$). Here the logarithmic decrement δ is negative; this can be attributed to the vibration amplitude of the advanced cycle x_2 being greater than the previous cycle x_1. Now, self-excited vibration is assumed to behave in the same fashion [40], and the logarithmic decrement was developed to measure the chatter stability through the constant milling speed. Consequently this concept will be extended to measure the milling stability due to the variable spindle milling.

It well known in milling processes particularly, that the obtained machined vibrations are usually dominated by the forced vibrations due to the tool rotation behaviour. Therefore, the self-excitations that give rise to chatter will be contaminated with the

force vibrations. This can be tackled by using a relevant signal processing technique which is briefly described in the next section.

4.9 **Methodology of the Signal Processing**

During the milling process, self-excited vibrations that cause chatter are usually contaminated by the forced vibrations (due to the rotation of the tool) which are dominating the response of the system. This is particularly the case at the region of marginal chatter instability, where the self-excited vibration will grow very slowly [40]. Consequently the signal process based upon the Fourier analysis is used as the most appropriated technique to separate the self-excited vibration from the forced vibration. This concept was widely used in milling experiments and simulations [40, 84], to analyse the stability of the steady-state response of the cutting process. It should be noted that, during the variable cutting speed a transient behaviour is mostly occurring at locations where the spindle speed are changing. In what follows, the Fourier analysis will be extended to consider these transient responses of the system, thereby allowing calculation of the damping ratio of the system even before the system reaches the steady state condition. The analysis approach used in the present study is an extension of original approach in [40] which is now summarised.

The flowchart in Figure 4.8 summarises the evaluation of the chatter criterion. The first stage (A) is to perform the time-domain simulation of the cutting process under given parameters (e.g., variable spindle speed, depth of cut, and cutting geometry). This leads to predicted vibration data y for single degree of freedom of the system in y-direction which possibly contained a transient behaviour. Before dividing this signal into f frames (B in Figure 4.8), it is important for this signal to be recorded at a sample rate at an integer multiple of the spindle speed rotation frequency. This allows each frame f to contain data n that represents one complete revolution $y(n, f)$ of the milling tool. In this case frames numbers will correspond with the spindle rotations.

After that the discrete Fourier transform is then applied for each frame, this is stage (C) in Figure 4.8. Here, each frame will contain a series of complex numbers which are

representing the magnitude and phase of the vibration at frequencies that are exactly corresponding with the tool rotational frequency ω. Since the used tool has uniform pitch teeth, frequencies of the forced vibrations will all lie on the spectral lines, which are multiple of the teeth passing frequency. This means, there is no spectral leakage of the forced vibrations, so they do not contaminate other regions of the Fourier transform. Therefore these spectral lines can be easily ignored (D in Figure 4.8) by setting their values to zero, so that the Fourier transform only contains information on the self-excited vibrations [40]. Now the frequencies of the data at each frame are studied to see whether the vibration frequencies grow or decay. However a large number of the spectral lines can be found in each frame, and in practice these may have only low magnitude [40], therefore they can be ignored (E in Figure 4.8) by selecting the spectral lines that have a maximum for each frame. These lines can then be plotted on a natural-logarithmic scale, thereby indicating the vibration behaviour per revolution of the tool (F in Figure 4.8).

Now in order to determine the damping ratio, the data are then fitted by a straight line where gradient represents the logarithmic δ_R decay per revolution. The maximum value of the logarithmic decay per revolution $\delta_{R,kpmax}$ that can define the least stable self excited oscillations is resulted from selecting the index $k_{p,max}$ that corresponds to the steepest gradient. It should be noted that there will be a number of these oscillations per revolution of the tool, so the value of $\delta_{R,kpmax}$ does not represent the logarithmic decrement per vibration cycle. Since the Fourier transform operation is averaging the magnitude of these oscillations within each frame so the number of the self-excited oscillations $k_{p,max}$ per tool revolution can be determined. Then the damping ratio ζ can be estimated by [40]:

$$\zeta = \frac{\delta_{R,kpmax}}{(2\, k_{p,max}\, \pi)} \tag{4.14}$$

Some Matlab codes in Appendix D2 demonstrate the procedure of how the damping ratio can be estimated.

4.10 **Stability Analysis**

In the present contribution, the time domain modelling approach is combined with the signal processing method in order to illustrate the stability of the VSM. A simple milling scenario with one degree of freedom is considered. The techniques and the procedures that are used in the current model can be applied to systems with multiple modes of vibration, and involving interrupted cutting with multiple teeth engaged in the cut simultaneously. It is also straightforward to include a nonlinear relationship between cutting force and chip thickness, and the periodic excitation force is inherently modelled.

To begin, model validation is presented by repeating some of the analysis presented in [89, 116]. The milling parameters were chosen to closely match those used in previous work by [89, 116] and are summarized in Table 4-1. A variable spindle speed was then used in the time-domain model, with a triangular speed variation around a mean value. This was defined in accordance with reference [89, 116], with fixed parameters of *RVA* and *RVF*.

To begin with demonstrating the difference in the chatter behaviour for constant speed machining and variable speed machining, a small selection of the results is considered. In addition the stability lobe diagram for the constant spindle speed case is produced. The self- excited damping ratio technique is then used for stability investigation. Here chatter was analysed by considering two cases of the milling speed variation. In the first case, at a constant depth of cut of ($b = 1\text{mm}$), milling speed was accelerated from 7500 to 10000 rpm. This procedure was performed for different scenarios of the spindle accelerations. In the second case, the milling speed was assumed to be variable with a periodic triangular speed variation around a mean value $\omega_m = 9100$ rpm. For the time-domain simulations, the signal processing technique is used to analyze the data signal of the simulated chatter and to determine so called self-excited damping ratio of each case of the simulation. It should be pointed out that the parameters are chosen in the present study may not completely match those used in reference [89, 116] since the tool helix angle; tool radial immersion; number of tool cycles, and number of simulation axial layers were not given.

4.11 **Results and Discussion**

4.11.1 **Stability Analysis for Accelerating Spindle Speed**

As can be seen in Figure 4.4 chatter levels are significantly reduced when the spindle speed varies periodically with triangular waveform. Now in this section, effects of linearly varying the spindle speed with different acceleration behaviours are investigated. Figure 4.9 shows the overall results of changing the spindle acceleration on the milling stability behaviour. Figure 4.9(a) shows the stability lobe with markers (*) *A* and (◁) *B* are corresponding to the start and end of the milling speed variation. In this case, simulation starts from an unstable region at 7500 rpm (associated with a secondary Hopf bifurcation) and ends by the stable region at 10000 rpm, while markers at (○) *C*, (□) *D* and (×) *E* correspond to the boundary of the stability at that defined milling speeds at the same depth of cut 1mm.

Figure 4.9(b) shows the variation of the milling speed from 7500 to 10000 rpm with accelerations 12.5, 25, 50 and 125 rpm/rev, while Figure 4.9 (c), (d), (e) and (f) of show the evaluation of the chatter obtained by the time domain simulation, at these variable milling speeds and the depth of cut 1mm, the maximum amplitude (X_{es}) for each frame was plotted in logarithmic scale to show whether the vibration amplitudes are growing or decaying. As can be seen from the Figure 4.9(c) the stages of the cutting stability are changing along the milling speed variation with a low acceleration of 12.5 rpm/rev. Here milling machining starts from unstable region where the chatter grows steadily between points A and C. Then the signal of the self-excited vibration is decaying between the points *C* to *D* and beyond the point E, these are corresponding to stable cutting regions. However chatter vibrations are steeply growing between points *D'* (star) and E.

However the stable region between points *D* and *D'* in plot (c) is inspected and can be attributed to the acceleration of the spindle. Figure 4.9(d), (e) and (f) demonstrate the stages of the chatter behaviour obtained from accelerating the spindle speed faster at 25, 50 and 125 rpm/rev respectively. Here the result obtained from the time domain

simulation is clearly demonstrating that, stability region (C to D) was reduced by increasing the milling speed acceleration through all the cases.

However there is a positive point of this approach which is that the sharp growth of the chatter (*D'* to *E*) through the flip bifurcation region is reduced by increasing the spindle acceleration. This result is considered as worthy of more investigations for high speed machining.

4.11.2 **Stability Analysis for Triangular Speed Variation**

For the same range of the spindle speed variation that is highlighted on plot (a) of (Figure 4.9) the depth of cut was now changed, and the chatter is analysed as shown in Figure 4.10. Plot (a) shows the triangular speed variation around the mean value $\omega_m = 9100$ rpm in a periodic fashion, with a fundamental period 6 tool revolutions per one tool cycle, while plot (b) shows the results of the chatter analysis obtained from simulating this speed with the given frequency ratio *RVF* and amplitude ratio *RVA*.

In this section, the analysis frames have been overlapped to three frames per two cycles of the tool revolutions ($3f: 2\tau_t$), so as to increase the number of data points available. As can be seen from the plot (b) for depth of cuts 0.2 and 0.8 mm the data of the self-excited vibrations (fitted by straight lines) declining with each tool rotation, and the patterns of the signal are in a periodic fashion, giving a positive damping ratio of ζ=0.00024 and .00023 respectively. Increasing depth of cut results is decreasing of the damping ratio values ($\zeta \to 0$). This indicates that the system is approaching the stability boundary where the values of the damping ration $\zeta = 0$. This can be clearly realised from the case of the depth of cut $b = 2$ mm, here the signal of the chatter is almost periodic with less slope inclination of the vibration data, giving a positive damping ratio value $\zeta = 0.00019$. This means at this depth of cut the system is approximately reaching the stability boundary, which this case gives a more stability than the constant speed machining case. However increasing the depth of cut to $b = 2.6$ mm the system becomes unstable. The self-excited vibrations now grow with each cycle, and the signal is start losing its periodicity, giving a negative $\zeta = -0.0031$. Increasing depth of cut

3mm causes the instability to worsen, the vibrations grow rapidly at a higher rate, and the signal is clearly losing the periodicity behaviour, giving $\zeta = -0.015$.

These outcomes are clearly agreed with results in [89, 116], were the margin stability of this milling scenario is defined at the depth of cut $b = 2\text{mm}$. However small differences could be attributed to the different parameters used in the simulations. Consequently these outcomes have validated the proposed variable spindle speed modelling procedure.

4.12 **Summary**

In this chapter, a comprehensive milling simulation model has been modified to account for milling scenarios that involve a variable spindle speed. The model is formulated in a Simulink environment, and in order to accommodate variable spindle speeds the system equation of motion has been reformulated in non-dimensional time. As a result, the simulation time used as the independent variable in Simulink becomes the tool revolution, rather than the simulated time in seconds.

The model results have been validated by comparing a small selection of simulation results with the work presented in reference [89, 116]. Reasonable agreement was observed, but the present study has re-enforced the issue of analyzing chatter stability for variable spindle speed simulations.

Chatter amplitude can be significantly reduced by using a periodic triangular speed variation approach. In addition, accelerating the spindle speed linearly shows some positive results of reducing the sharp growth of the chatter through the flip bifurcation region. This promise is considered as worthy of more investigations for high speed machining.

It is clear that peak to peak approach is unable to provide a formal and accurate interpretation of chatter stability for variable speed machining, whereas signal processing approach has provided some formal interpretation of chatter stability for variable spindle speed simulations.

However, with reference to Figure 4.10 it can be seen that self-excited damping ratio did not provide a comprehensive interpretation of the stability behaviour. This can be observed particularly for the stable cases where the lines that are fitting the maximum amplitudes (X_{es}) of each frame almost horizontal and straight, whereas, due to the proposed theory these lines are expected to be in decaying style since they were representing the stable behaviour as shown in constant speed machining case [40]. This can be attributed to the effect of the speed variation behaviour on the spectral lines approach, thereby the influence of varying chatter frequency can be not fully considered. Other nonlinearities such as process damping are also likely to cause such the variations in the chatter frequency. Therefore self-excited damping ratio is suggested to be unsatisfactory approach to offer comprehensive insight.

Consequently, an alternative approach for chatter analysis will be developed. The new developed approach is using an energy based method. In the next chapter a comprehensive analysis approach will be developed to be suitable for investigating the stability of all types of machining.

Sample	Parameter	Values
D	tool diameter	25 mm
N_t	number of teeth	3
λ	flute helix	00
r_e	radial immersion	2 mm
f_t	feed per tooth	1 mm
m	mass	1.637 kg
fn	natural frequency	222.5 Hz
ζ	damping ratio	0.005
RVA	amplitude ratio	0.28
RVF	frequency ratio	0.003

Table 4-1 Input Simulation Parameters

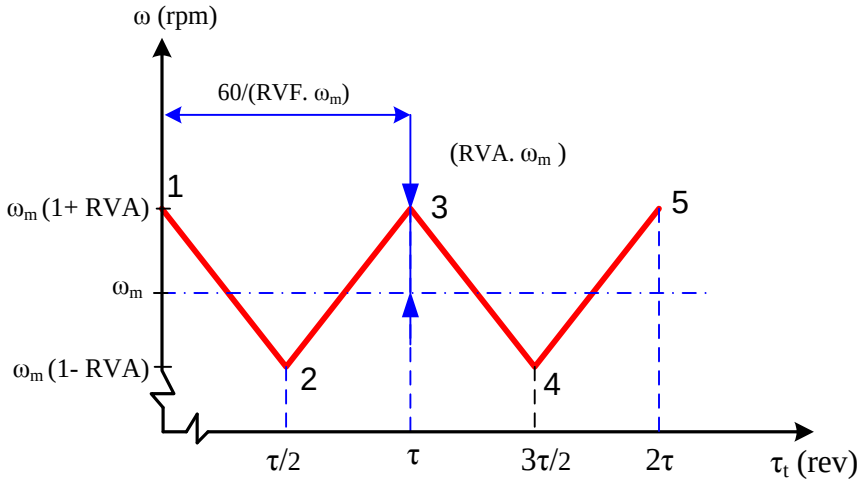

Figure 4.1 Typical triangular shape variation

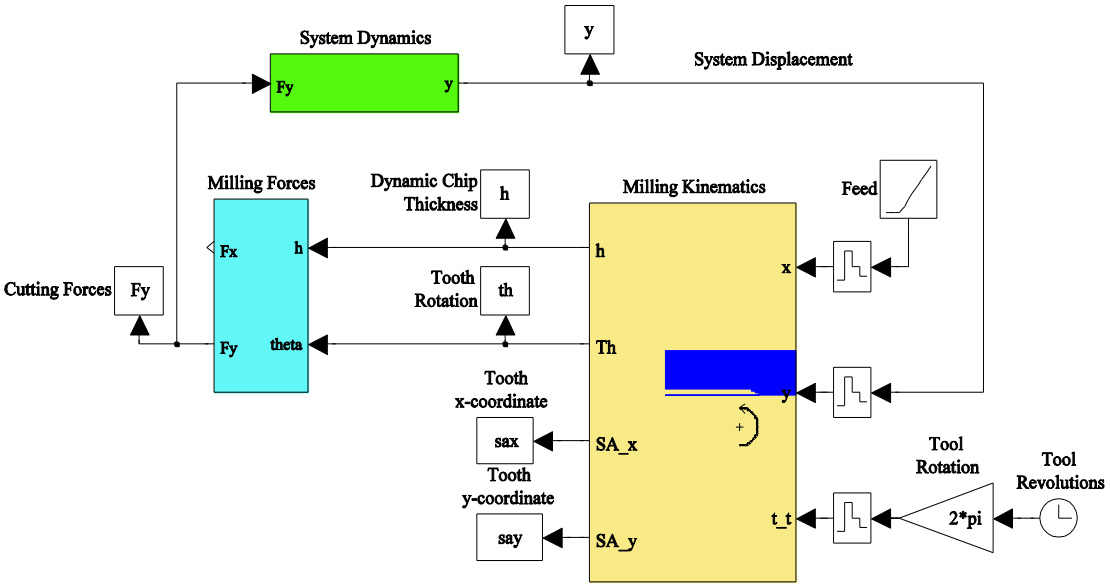

Figure 4.2: Simulink model of milling vibrations.

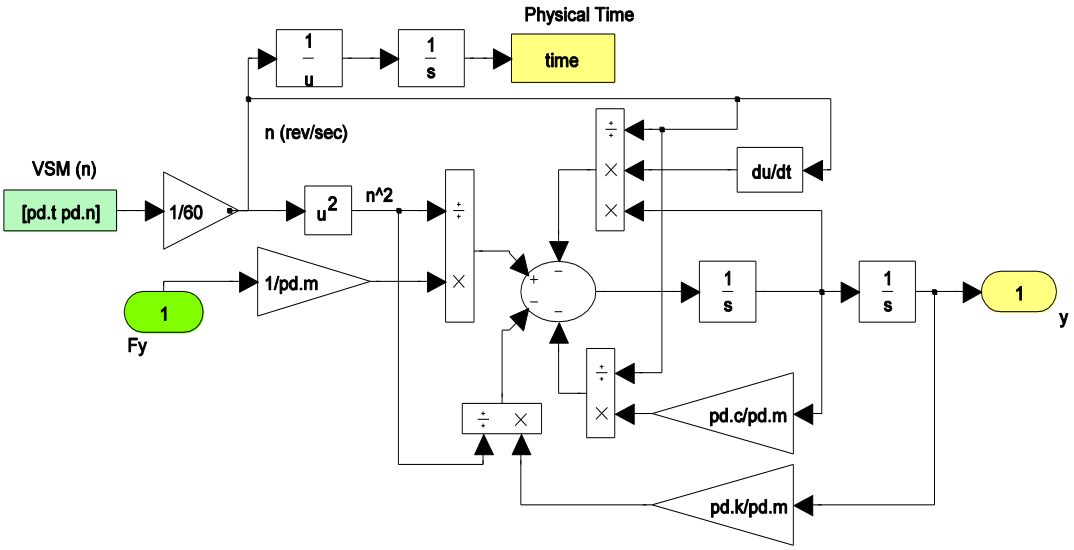

Figure 4.3: Simulink model structure in non-dimensional time

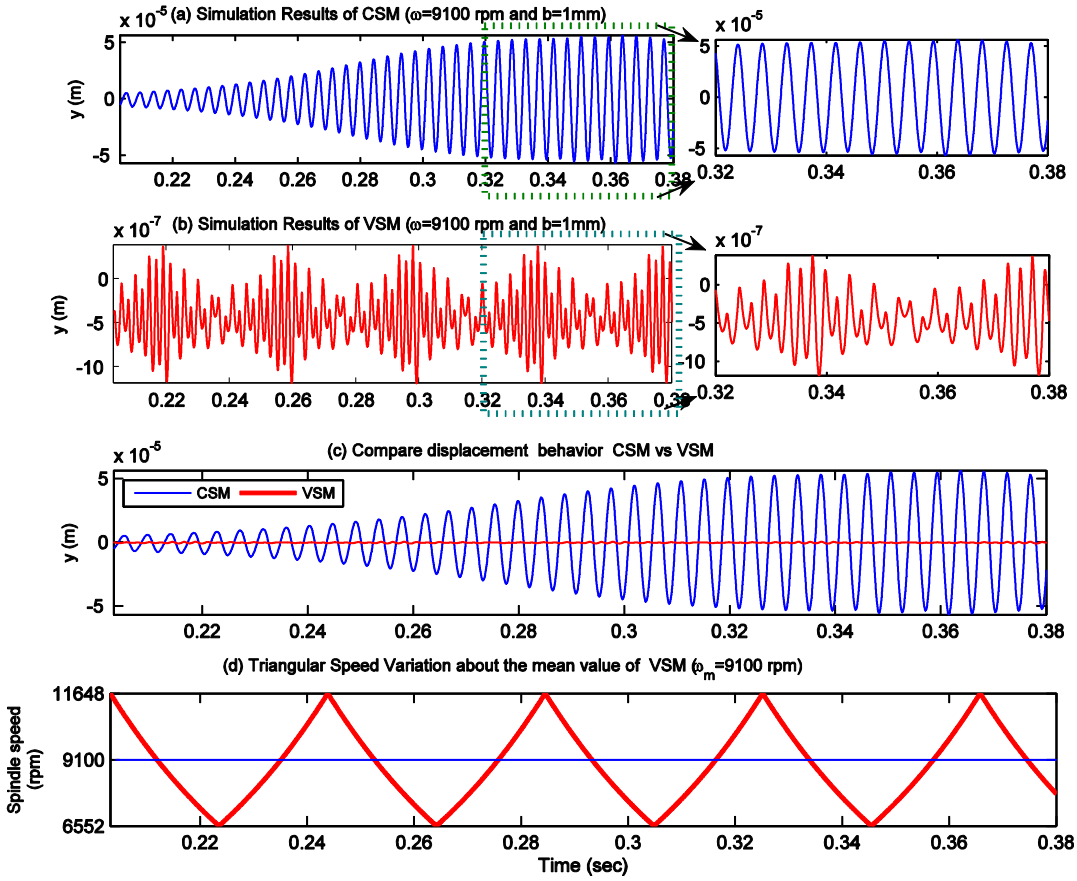

Figure 4.4 Unsteady simulation outputs for VSM

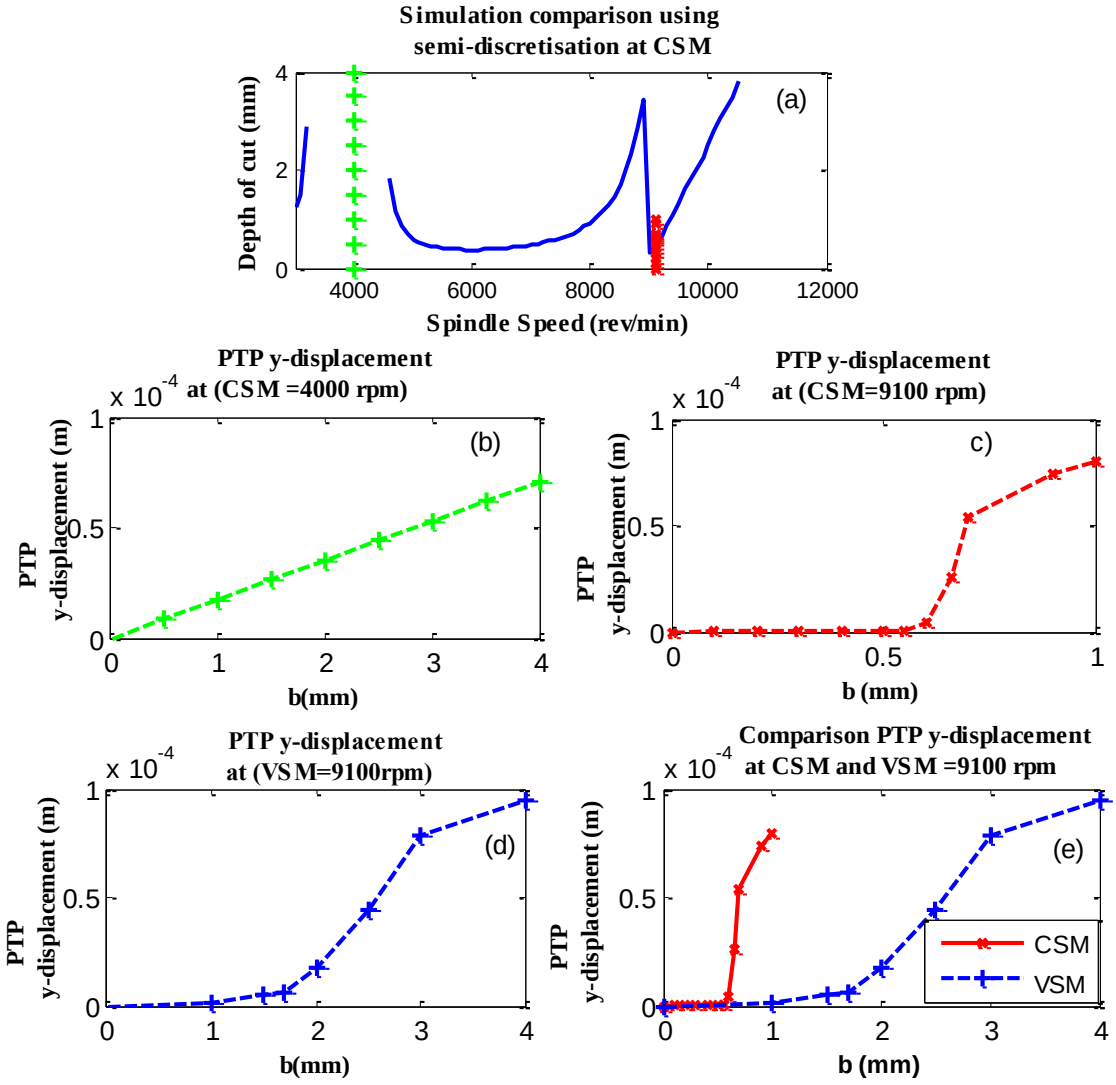

Figure 4.5 Model Simulation Results

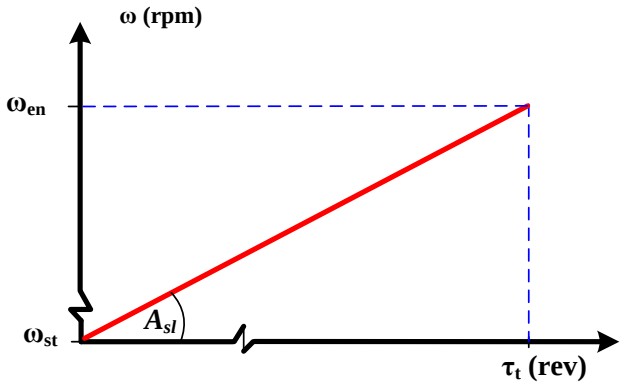

Figure 4.6 Typical linear Spindle Acceleration

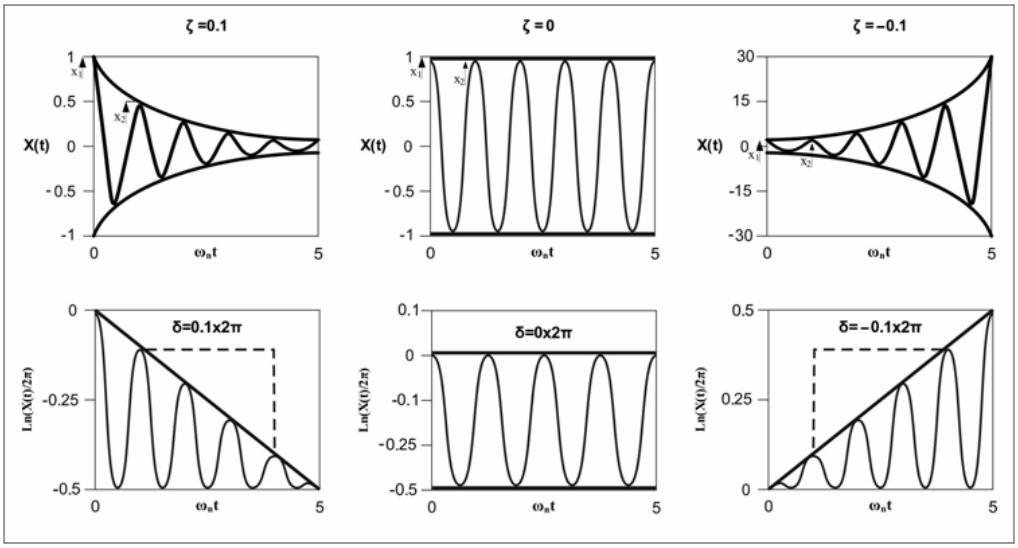

Figure 4.7 Free vibrations of a linear, viscously damped system with positive (ζ=0.1) zero (ζ=0) and negative (ζ=−0.1) damping, corresponding to stable, marginally stable, and unstable self-excited vibration systems, source [40].

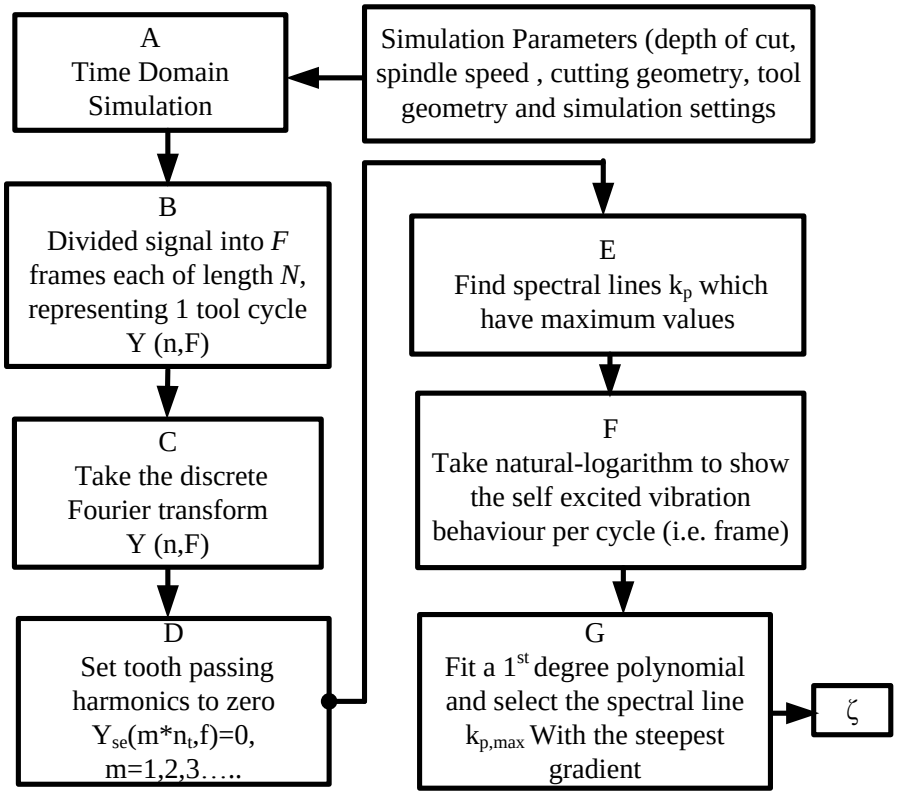

Figure 4.8 Flow chart to illustrate evaluation of the chatter criterion [40].

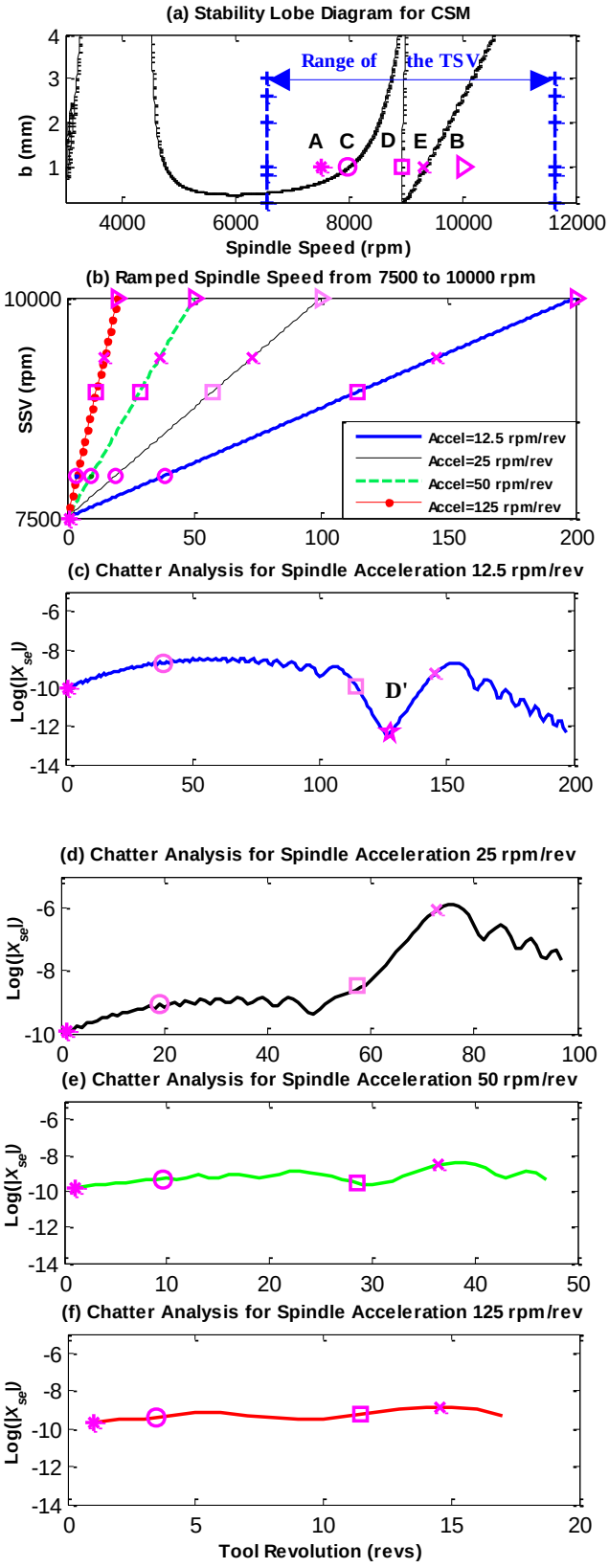

Figure 4.9 Effect of the changing spindle acceleration in milling stability.

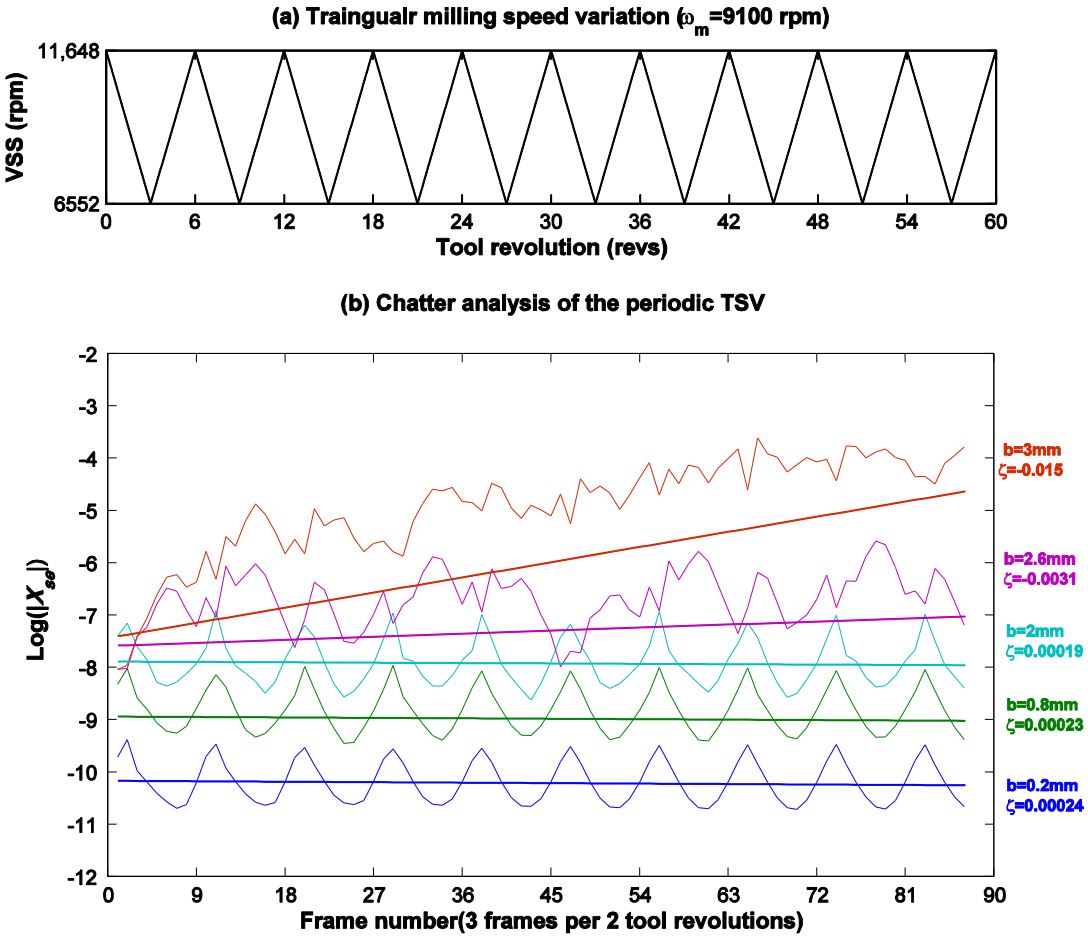

Figure 4.10 Model simulation results, (a) Triangular spindle speed variation, (b) Chatter analysis due to the periodic milling speed.

CHAPTER 5 ENERGY BALANCE FOR CHATTER ANALYSIS

5.1 Introduction

In recent years, different energy balance methods have been proposed by a small number of researchers to invstigate the effectivenss of some techniques used for chatter supression. Al-Regib, *et al* [29] for example introduced the concept of minimum cutting energy input to study chatter suppression based on varying the spindle speed. Budak and Tunk [11] presented a practical and modelling method for determining the process damping coefficient based on balancing the internal damping energy. More recently, Ahmadi and Ismail [106] used the same approach to develop the stability lobes analytically taking into account the effect of the process damping.

In this chapter, a new energy balance approach is used for studying chatter stability behaviour. This is based on balancing all the energies crossing the system boundary. For the machining operations the main energy balance is taken between the transmitted energy due to the total cutting forces and the dissipated energy due to structural and process damping mechanisms and loss of contact behaviour. This approach has been validated by selecting some milling scenarios where the results have been previously published.

5.2 System Boundary for System Dynamics

In a thermodynamic system, or simply a system, the system boundary is defined as the quantity of matter or region in space chosen for study. The region outside the system is called the surroundings. The real or imaginary surface that separates the system from its surroundings is called the boundary [120]. Physically, any system consists of a well-defined set of bodies that are interacting by means of forces. Any bodies that lie outside the boundary of the system reside in the surroundings. The state of the system is a set of measurable physical quantities that completely characterise the system. Therefore the system boundary is known as the boundary that separates the internal components of a system from the external entities. These entities can also be called effectors. Energy

balance for a dynamic milling system with a single mode is presented in the current chapter. Multi degree of freedom system will be presented in the next chapter.

5.3 **Energy Balance in Single Degree of Freedom Systems**

The diagram shown in Figure 5.1(a) represents a simple machining system. Machining dynamics are represented as lumped parameters in the y-direction with a single degree of freedom system. In fact this analysis can be easily extended to multi degree systems as can be seen in the next chapter. Now with reference to the same diagram, the equation of motion can be expressed as:

$$m\ddot{y} = F_y - c\dot{y} - ky \tag{5.1}$$

where m, c and k are the system equivalent mass, system viscous damping coefficient, and the system stiffness respectively, whereas $y, \dot{y}\ \ddot{y}$ are the mass, displacement, relative velocity and the acceleration respectively, F_y are the total forces acting on the mass.

The boundary defined by the dashed line, separates the internal components from the system's surrounding (outside effectors). With reference to Figure 5.1(b) the internal components are consisting of the inertia force ($m\ddot{y}$) due to the structural mass movement which possess a kinetic energy, and the spring force (ky) due to the spring deflection which generates a potential energy. In this system the potential energy and kinetic energy are the two types of mechanical energy, and are conservative. Whereas, the system's surrounding (Figure 5.1(b)) is represented by the structural damping forces ($c\dot{y}$) which cause energy to flow out of the system, and the total cutting forces F_y which normally do a positive work on the system. However, when the process damping forces are included, then the total cutting forces (F_y) will include theses process damping forces (F_{pd}) along with shear cutting forces (F_c). Including the process damping forces could reduce the work done on the system, due to the energy dissipative nature of these forces.

It should be known that, through the milling kinematics computation the positive and the negative values of the chip thickness could be measured which are called idealised chip thickness (h_{idl}). The positive values of the chip thickness are called cutting chip

thickness (h_c) whereas the negative values are called loss of contact chip thickness (h_{loc}). The idealised chip thickness is associated with calculating the idealised forces F_{idl}, whereas the loss of contact chip thickness is associated with calculating forces will be called loss of contact forces F_{loc}. Now, as show Figure 5.1(b), cutting force F_c is equal to the idealised force F_{idl} but after removing loss of contact forces F_{loc}. However the procedure of how this force modelled is explained in the next section.

Now, the total cutting force is expressed as follows:

$$F_y = F_c - F_{pd} = F_{idl} - F_{loc} - F_{pd} \tag{5.2}$$

By substituting equation (5.2) in equation (5.1), then the system equation of motion includes all forces becomes as follows:

$$m\ddot{y} + c\dot{y} + ky = F_{idl} - F_{loc} - F_{pd} \tag{5.3}$$

The forces in Equation (5.3) have direct effects on the energy behaviour. Idealised forces F_{idl} cause energy to flow into the system, whereas structural and process damping and loss of contact forces all causes the energy flow out of the system.

Effects of these forces are further illustrated in Figure 5.1(c) which shows the boundary of the system with the corresponding work done by each force in Equation (5.3). Here the sign convention is chosen so that positive values correspond to work done on the system, i.e. power is flowing into the system, whereas the negative sign corresponds with power flows out of the system. Therefore the energy balance theory for this system can be now developed. The instantaneous power corresponding to each force which is highlighted in Equation (5.3) calculated as (force multipied by the vibration velocity). Then these powers are integrated with respect to the time, to obtain the instantaneous work done. The balance of the total work done on the system as follows:

$$\begin{aligned} \int_{t_1}^{t_2} m\ddot{y}\ \dot{y}dt + \int_{t_1}^{t_2} c\,\dot{y}^2 dt + \int_{t_1}^{t_2} ky\,\dot{y}dt \\ = \int_{t_1}^{t_2} F_{idl}\,\dot{y}dt\ - \int_{t_1}^{t_2} F_{loc}\,\dot{y}dt - \int_{t_1}^{t_2} F_{pd}\,\dot{y}dt \end{aligned} \tag{5.4}$$

where t_1 and t_2 are the starts and exit cutting time respectively.

According to the conservation of energy theory, energy cannot be created or destroyed, just transformed from one form to another. Therefore any created kinetic energy is converted to the potential energy. The boundary of this conservative system (Figure 5.1) is defined as the system of mass and the spring. Consequently the kinetic energy and the potential energy are conservative at any instant of time and hence, they are not considered.

$$W_m = W_k = \int_{t_1}^{t_2} m\ddot{y}\ \dot{y}dt = \int_{t_1}^{t_2} ky\,\dot{y}dt \tag{5.5}$$

Therefore, the work done on this conservative system only due to the following forces

1- The idealised forces F_{idl} (i.e. forces that include cutting and loss-of contact forces) due to the positive and negative values of the chip thickness.
2- The loss-of contact forces F_{loc} which are associated with the negative values of the chip thickness due to the vibration behaviour.
3- The structure damping forces F_s which are associated with the system structural behaviour.
4- The process damping forces F_{pd} which are associated with the rubbing behaviour. Effects of this force are considered in Chapter 6.

Generally, at the steady state limit cycle behaviour, the energy balance equation can be expressed:

$$\int_{t_1}^{t_2} F_{idl}\,\dot{y}dt - \int_{t_1}^{t_2} F_{loc}\,\dot{y}dt = \int_{t_1}^{t_2} c\,\dot{y}^2dt + \int_{t_1}^{t_2} F_{pd}\,\dot{y}dt \tag{5.6}$$

Or in general can be written in the form:

$$W_{idl} - W_{loc} = W_s + W_{pd} \tag{5.7}$$

where W_{idl} is the idealised work don by the idealised forces F_{idl}, W_s work done by the structural damping forces F_s, W_{loc} loss of contact work resulted from the loss of contact forces F_{loc} and W_{pd} process damping work due to the rubbing forces F_{pd}.

It should be known that, the instantaneous work obtained directly from the model is accumulative work with units in Joules (J). However, energy can be also measured in rates by dividing the instantaneous work done over the instantaneous tool revolutions which units become in joules/revolutions (J/rev). Therefore energy rates can be useful indicator used to investigate the system stability behaviours through comparing the transmitted and the dissipated energy per tool revolution.

Before analysing the results of the energy balance approach it is worth while to recap the methodology of calculating the work done on the system during this chapter. In this chapter the process damping effects are not considered. The instantaneous power corresponding to other forces F_{idl}, F_{loc} and F_s is calculated directly in the model. Then these powers are integrated with respect to the instantaneous cutting time to respectively obtain the accumulative work done on the system W_{idl}, W_{loc} and W_s. The energy behaviour of this system along the steady state limit cycle behaviour can be defined as:

$$W_{idl} - W_{loc} = W_s \tag{5.8}$$

Again the sign convention is chosen so that the positive sign corresponds to work being done on the system, i.e. energy flows (transmitted) into the system, whereas negative sign corresponds with the energy flows out (dissipated) of the system.

5.4 **Example for Turning Operations**

To begin, a simple turning scenario is considered, with one degree of freedom, to illustrate how the energy behaves in the system during the single point machining process. A simple Simulink model as shown in Figure 5.2 is developed to adopt the block diagram of vibration in regenerative cutting with a simplified turning problem described in [68]. The work done by the cutting forces, loss of contact forces and structural damping forces are directly calculated among the Simulink blocks.

Simulation parameters of the simplified chatter in turning are chosen from the example 9.13 in [68]. Table 5-1 shows full details of the set up system parameters with two scenarios, a high depth of cut (b=2.5mm), and a low depth of cut (b=1mm).

5.5 Results and Discussion

5.5.1 First Scenario at Depth of Cut *b*=2.5mm.

Figure 5.3 shows results of the work done and chip thickness behaviours of the turning operation. Simulation is performed according to the first cutting scenario at the depth of cut b=2.5mm and the constant cutting speed ω= 800 rpm. As can be seen in Figure 5.3(a) the work done by the idealised forces is always positive and increasing. This can be attributed to the fact that the instantaneous idealised power is always positive. Here the average rate of change in the flow of the work is the slope of the work done (with respect to time) curve. From the same Figure 5.3(a) the vibration level is exponentially growing until the tool starts jumping out of the cut. Consequently a loss of contact behaviour now can be measured. Since these energy values are negative, this means loss of contact energy is always flowing out of the system, which can be attributed to the nonlinear behaviour of the system. Moreover since the damping energy is always flowing out of the system so the damping power is also negative. Basically this dissipated energy is converted to heat energy.

Figure 5.3 (b) shows the net work done on the system due to the total cutting forces. Here the work is positive and increases until the steady-state limit cycle oscillation is reached. Since the stead state limit cycle behaviour is reached the net work done on the system remains a constant. This can be attributed to the dissipated energy rates becoming equal to that transmitted energy rate. Consequently the average net power flow into the system is zero. The slope of the net work done on the system curve is horizontal. There is a flow of the power in and out of the system, but the average net power flow is zero.

This phenomenon is further observed in the Figure 5.3(c) which shows the chip thickness behaviour. Chip thickness grows until the loss-of-contact occurs, thereby increasing the nonlinearity of the system. As a result loss of contact mechanism has caused the chip thickness levels to stabilise after about 50 revolutions of the tool. General analysis of this cutting scenario: the response of the system is unstable. The

vibration level grows here to limit where loss of contact occurs, therefore the steady state of the limit cycle oscillation is observed.

5.5.2 **Second Scenario at Low Depth of Cut *b*=1mm.**

Figure 5.4 exhibits the energy and chip thickness behaviours for the second simulation scenario with depth of cut b=1 mm. It is very obvious here the response of the system is stable along the simulation period. Since the tool/workpiece are always in the contact (i.e. no loss-of-contact), thus loss-of-contact energy is always zero as shown in Figure 5.4(a). In addition, as the system is stable, chip thickness behaviour remains constant as shown in the Figure 5.4(c), there is no more change in the vibration and the damper power (the rate of energy dissipation) becomes zero. Therefore the net work done on the system Figure 5.4(b) remains a constant corresponding to the work done in compressing the structural spring, under the action of constant chip thickness.

5.6 **Milling Operations**

In this section a confirmed milling scenario is considered for validating both the energy analysis approach and the model performance. Here the energy balance approach is applied for investigating the chatter stability in up milling without considering the process damping effects. For this milling scenario, model details and simulation parameters can be found in [40]. Table 5-2 shows full details of the set up system parameters with four different depths of cut scenarios. It should be noted that process damping effects are not considered in this cutting scenario, thus the part of the model that related to the process damping simulation was deactivated.

Before demonstrating how the energy behaves in the milling system, it is worth to briefly highlight the main aspects of the model used in this work. The milling model used in this study is single degree of freedom model in y-direction as shown in Figure 5.8. Here, the energy calculation is also shown.

In addition, for the interrupting cut, limits of the cutting segment need to be carefully defined since it has a great effect in computing the chip thickness, which in turn plays a major role in estimating the cutting force behaviour and the energy associated with loss

of contact. The procedure of how the limits of the cutting segment can be carefully defined will be discussed in the next Section.

5.6.1 **Loss of Contact Energy Analysis**

For the interrupted cutting, chip thickness (formation along the cutting segment AB as shown in Figure 5.5) is not constant. When the tool rotates outside this region (tool loss contact with the workpiece) the chip thickness and cutting become zero. Now, in order to determine an accurate loss-of-contact energy, limits of the cutting segment need to be carefully defined. With reference to Figure 5.5 (a) and (b) tool rotation angles and the dimensions are measured relative to the feed direction (x-direction), now as can be seen from the same figures the tooth N_{t1} starts cutting at the point A and exits at the point B, so this milling segment is defined by the start θ_{st} and exit θ_{ex} cutting angles and indeed on the radial immersion dimension r_i, which can be mathematically expressed as follows:

$$\begin{aligned} \theta_{st} &= -90^o \\ \theta_{ex} &= -\sin^{-1}\left(\frac{r_t - r_i}{r_t}\right) \qquad \text{up} - \text{milling} \\ \theta_{st} &= \sin^{-1}\left(\frac{r_t - r_i}{r_t}\right) \\ \theta_{ex} &= 90^o \qquad \text{down} - \text{milling} \end{aligned} \tag{5.9}$$

where the r_t tool radius and r_i is the radial immersion.

However, feed motion has a vital effect on the cutting duration and the static entry and exit cutting angles. Balachandran and Zhao [121] and Long *et al* [122] presented the influence of the feed motion on the entry and exit cutting angles in the milling operation. They also found that the changes are occurred in the cutting zone and the immersion with respect to the workpiece and tool motion. At any instant, the relative motion of the tool/workpiece system is responding in x or y direction (which is appropriate) will either enhance or weaken the tooth engagement in the radial directions depending upon the angular positions. At some locations (start or exit of the cut), the tooth may rotate out of the cut; that is, the tooth may lose contact with the workpiece, thus changing the cutting immersion angle. In addition, the change in the static cutting zone to the dynamic cutting zone can cause some other issues such as in some cases the

machined material may not be completely removed from the entire cutting region, and during the modelling process an overlapping surfaces issues are mostly occurring. For further information about how the immersion of the tool changes due to the dynamic cutting zone, readers can be referred to [121].

Therefore in order to overcome these issues it was suggested to modify the start and exit cutting angles. Balachandran and Zhao [121] and Long *et al* [122] assumed a small angle $\Delta\theta$ in which one either advances the cutting start angle for up milling or delays the exit angle for down milling. The angular deviation for this static cutting zone has been approximated by:

$$\Delta\theta = \sin^{-1}\frac{T_d f_d}{2r_t} \tag{5.10}$$

where the delay T_d along the feed direction is constant in [121], f_d is the feed motion and r_t is the tool radius. Generally, $\Delta\theta$ was assumed to be a small angle taking a value at least 1^o under typical milling conditions. However in this work $\Delta\theta = 5^o$ is assumed to advance the entry angle or delay the exit angle.

Therefore, with reference to Figure 5.6 during the chip thickness calculation, the cutting tooth will enter and leave the new cutting region at the points C and D for both milling modes (up-milling Figure 5.6a and down-milling Figure 5.6b), limits of these cutting segments are now defined as follows:

$$\begin{aligned} &\theta_{st} = -90^o - \Delta\theta \\ &\theta_{ex} = -\sin^{-1}\left(\frac{r_t - r_{imm}}{r_t}\right) \quad \text{for up} - \text{milling} \\ &\theta_{st} = \sin^{-1}\left(\frac{r_t - r_{imm}}{r_t}\right) \quad \text{for down} - \text{milling} \\ &\theta_{ex} = 90^o + \Delta\theta \end{aligned} \tag{5.11}$$

However, when the loss contact response that depends on the loss of contact chip thickness h_{loc} is determined a careful consideration should be considered here, the small added angle $\Delta\theta$ to the main cutting sector (*AB*) is generating an extra distance (*AC*) and (*BD*). This allows the simulation algorithm to produce an extra negative chip thickness called rotation chip thickness h_{rot} which are associated with the distance *AC* (Figure 5.6a) or *BD* (Figure 5.6b).This scenario produces an additional force called rotation loss-of-contact force (F_{rot}). However such this force is not associated with the

cutting process, therefore this value should be eliminated from the main force calculation. Consequently the rotation chip thickness h_{rot} along the cutting distance (*CD*) should be excluded from the loss of contact chip thickness h_{loc}. Therefore, angles θ_{st} (up-milling) and θ_{ex} (down-milling) are both reduced by the same value of the added angle $\Delta\theta = 5^o$.

Now, the loss of contact chip thickness h_{loc} and the idealised chip thickness h_{idl} are both measured from the main cutting segment (*AB*) (Figure 5.6(a) and (b)). However when there is no loss of contact between the tool and the workpiece, the value of the loss of contact chip thickness is simply zero ($h_{loc} = 0$), and the idealised chip thickness (h_{idl}) involves only on the positive values of the cutting chip thickness (h_c).

The above scenario of how to model the chip thicknesses (h_{loc}), (h_c) and (h_{idl}) can be summarised in the following mathematical expressions:

First of all define the cutting region

$$(\theta_{ex} \geq \theta_u \geq \theta_{st}) \tag{5.12}$$

Remove rotation loss of contact h_{rot}

$$\begin{array}{ll} (\theta_{ex} \geq \theta_u \geq \theta_{st} - \Delta\theta) & \text{for up} - \text{milling} \\ (\theta_{ex} - \Delta\theta \geq \theta_u \geq \theta_{st}) & \text{for down} - \text{milling} \end{array} \tag{5.13}$$

Measure chip thicknesses

$$\begin{array}{ll} h_{loc} = h & if \quad h < 0 \\ h_c = h & if \quad h > 0 \\ h_{idl} = h_{loc} + h_c & \end{array} \tag{5.14}$$

where θ_u is the instantaneous tool immersion angle, h is the instantaneous chip thickness value and $\Delta\theta = 5^o$ in this work. These mathematical expressions are then interpreted to a Simulink blocks as shown in Figure 5.7. The calculated chip thickness is classified for the idealised h_{idl} and loss of contact h_{loc} chip thickness to respectively correspond with the idealised forces F_{idl} and the loss of contact forces F_{loc} forces calculation. Finally these Simulink blocks are added to the main milling model shown in Figure 5.8 to calculate all the corresponding energies during the machining process.

Once the model is finalized, a model convergence is performed along different numbers of iterations (samples/revolution), different number of the axial layers and different numbers of tool revolutions. In addition, the model results are validated by comparing the current model outputs in terms of total cutting forces F_y and the chip thickness h with the original model outputs [40].

5.6.2 **Results and Discussion**

In this milling scenario, for a single spindle speed, the depth of cut is changed incrementally, and the work done on the system is calculated for each cutting scenario as shown in Figure 5.9. The plots in Figure 5.9(a) compare the behaviour of the accumulative work (W_{idl}, W_{loc} and W_s) done on the system caused by the idealised forces, loss of contact and structural damping behaviours respectively, whereas plots in Figure 5.9(b) shows the behaviour of the net work ($W_{idl} + W_{loc} + W_s$) done on the system. Plots in Figure 5.9(c) and Figure 5.9(d) respectively show the behaviour of the chip thickness and the total cutting forces at the last tool revolution.

For the depth of cuts b=10mm and 12mm, there is no loss of contact work ($W_{loc} = 0$) (Figure 5.9 (a)). It can be seen also in Figure 5.9(b), the net power flow into the system is constant, and thereby the rate change of the net energy is zero. This can be attributed to the stable cut, where the tool/workpiece is always in contact causing, and there is not variations in the cutting forces as shown in Figure 5.9 (d) (cutting forces signal is more smoother). Therefore the vibration level is decaying here to a level that is barely discernable on the chip thickness (Figure 5.9 (c)). Here, the chip thickness settles at a constant level with the periodic change in the thicknesses that are attributed to each tooth entering and leaving the cut. Structural damping is still dissipating the energy of the forced vibration due to the period cutting forces. This is in contrast with the pervious turning example.

Increasing depth of cut to 14 mm results in system instability. Vibrations start to grow exponentially, and loss-of-contact energy is observed with each cycle (Figure 5.9 (a)). Loss of contact energy has negative values as this corresponds to the energy dissipation due to the nonlinear behaviour. The behaviour of the loss of contact can be clearly

discernable from the chip thickness behaviour at the last tool revolution (Figure 5.9 (c)). Despite the energy dissipation by the structural damping and the loss of contact behaviour, the net energy that flows into the system due to the cutting forces still exhibits an exponential growth (Figure 5.9 (b)). Increasing depth of cut to 16 mm causes the instability to worsen since the vibration amplitudes are severely increased causing a considerable increase in the loss-of-contact energy as shown in Figure 5.9(a). Here the net work done on the system also increases at higher rates causing the energy to flow into the system, (Figure 5.9 (b)). However, towards the final few revolutions the energy flows into the system becomes equivalent to that flows out of the system, this leads to stabilise the net work done at a certain level as in shown in Figure 5.9 (b).

This can be further explained with reference to Figure 5.9 (c), which shows the teeth are losing contact with the workpiece due to the high force variations as shown in Figure 5.9 (d). This means the system has dissipated more energy as the loss of contact behaviour increases. This phenomenon is more pronounced for 18 mm depth of cut. In this scenario, the dissipated energy by the loss-of-contact behaviour and the structural damping have caused the level of the net energy stabilises after about 10 revolutions (Figure 5.9(b)). Here the curve of the net work done on the system is horizontal. This behaviour is associated with the steady-state limit cycle oscillations.

Figure 5.10 compares the forces behaviour at the last tool revolution. Here the highest variations in the cutting forces can be clearly seen at the depth of cut b=18mm. This can be attributed to the vibration levels become so severe here causing high rates of the loss of contact which leads the system to become unstable. However, force's variations are considerably decreased at the low depths of cut. Therefore the vibration level is decaying here. This can be clearly realised from the loss of contact levels are vanishing at b=10mm, therefore the system becomes stable.

In general, the behaviour of the energy flow in or out of the system is found proportional with the depth of cut. As the depth of cut increases, the cutting energy that flows into the system increases. Despite of the dissipated energy by both loss of contact and structural damping, in some cases the net energy flow in the system increases to

limit where the system reach the limit cycle behaviour. In fact at that level, there is a flow of the power in and out of the system, but the average change in the power flow is zero.

5.7 **Summary**

In this chapter, a new technique for modelling machining stability in time-domain simulations has been proposed. The method is based on balancing all the energy rates that are crossing the system boundary. In this chapter this method is only applied for tools with regular pitch teeth and constant cutting speed, with no process damping effects. Further work is needed to adapt the energy analysis approach for the case of variable tool geometry and for variable cutting speed.

Compared to existing chatter analysis methods, the method has the following advantages:

1. The stability behaviour is predicted to be similar to that in [40].
2. The nonlinearity behaviour (loss of the contact) due to the vibration behaviour can be clearly illustrated.
3. The model is capable to compute the imposed energy due to the cutting forces and the dissipated energy due to structural damping and loss of contact behaviour.
4. Energy analysis approach has shown a realistic interpretation and quantifiable investigation for machining stability.
5. In addition, energy based analysis builds upon the usefulness of the damping analysis in Chapter 4, and is more applicable to nonlinear systems.

In the next chapter, energy analysis approach will be applied to consider effects of the process damping mechanism.

Turning Operation	
Cutting Speed	800 (rpm)
Iteration per revolution	500 (iters)
Number of revolutions	60 cycles
Mass	100 (kg)
Stiffness	$4x10^7$ (N/m)
Damping	5320 (N sec/m)
Cutting stiffness	$2x10^9$ (N/m^2)
Width of cut (first scenario)	$2.5x10^{-3}$ (m)
Width of cut (second scenario)	$1x10^{-3}$ (m)

Table 5-1 Turning System Parameters

Milling without process damping	
Cutting Speed	3000 (rpm)
Iteration per revolution	256 (iters)
Number of revolutions	50 cycles
frequency	700 (Hz)
Stiffness	$8x10^7$ (N/m)
Damping ratio	0.3%
$\boldsymbol{K_{tc}}$	796.1 (N/mm^2)
$\boldsymbol{K_{rc}}$	168.8 (N/mm^2)
Width of cuts (b)	12,14,16 &18 (mm)
Tool diameter	20 (mm)
Number of teeth	4
Flute helix	0^o(axial flute)
Milling Mode	up-milling
Radial immersion	8(mm)
Feed per tooth	0.05 (mm)

Table 5-2 Up milling process without process damping

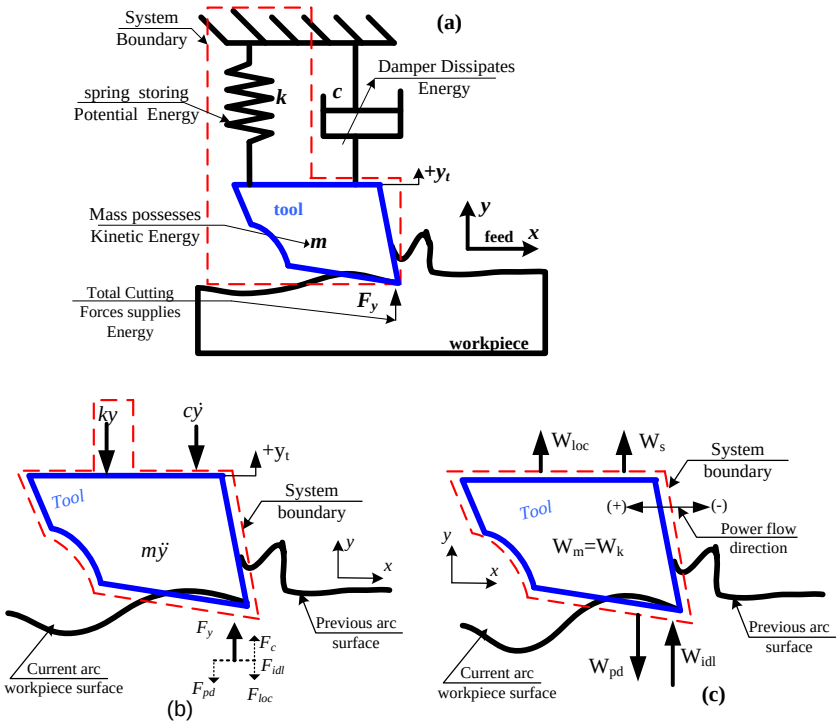

Figure 5.1(a) A simple machining dynamic boundary, (b) Diagram shows all the forces acting on the mass, (c) diagram shows all the energies crossing the system boundary

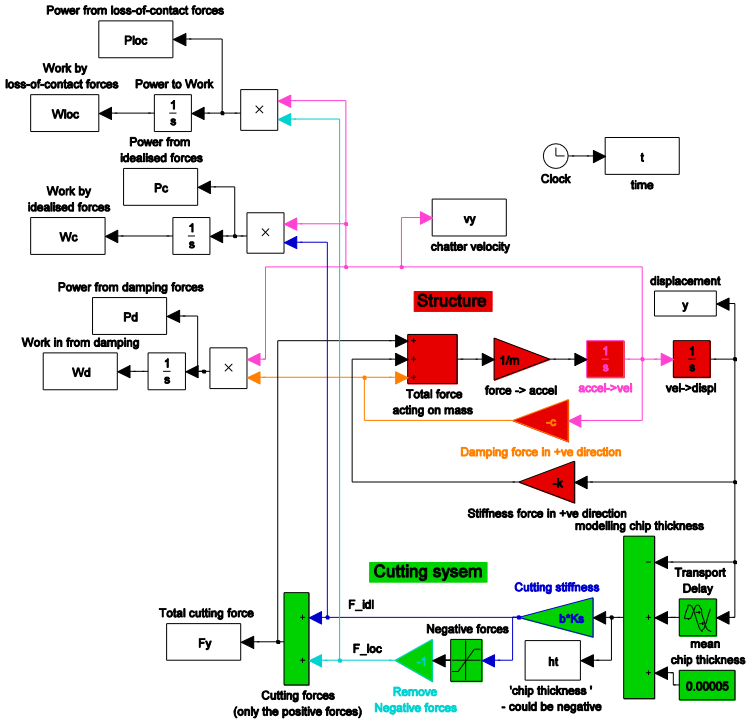

Figure 5.2 Simulink Model for Turning Simulation

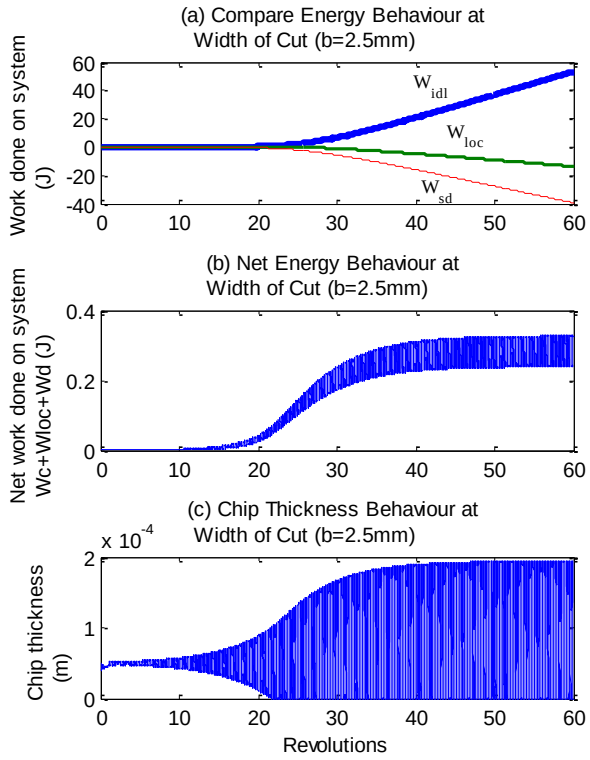

Figure 5.3 Simulation results of the first machining scenario

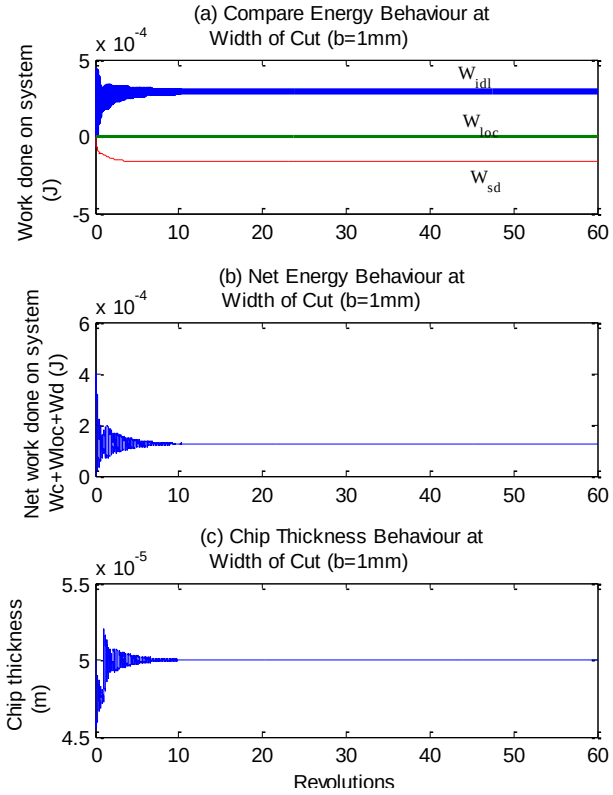

Figure 5.4 Simulation results of the second machining scenario

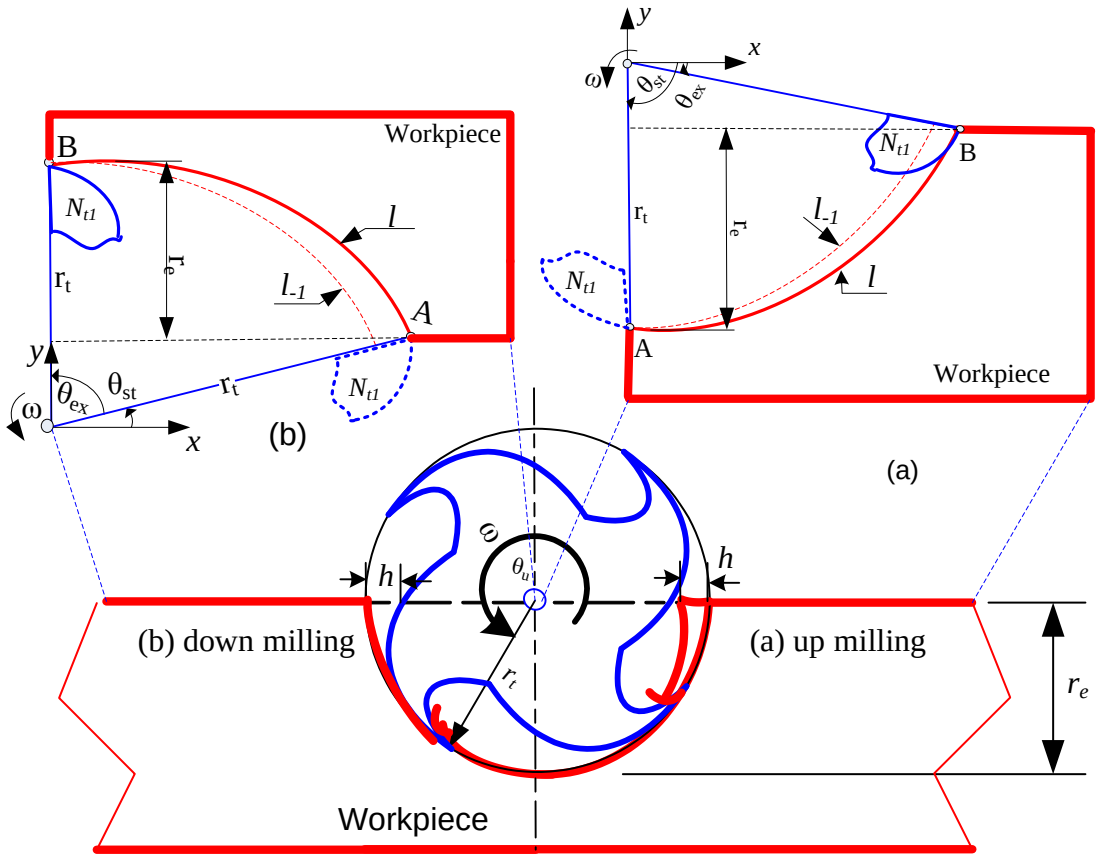

Figure 5.5 Milling Operation (a) Up-milling and (b) Down-milling

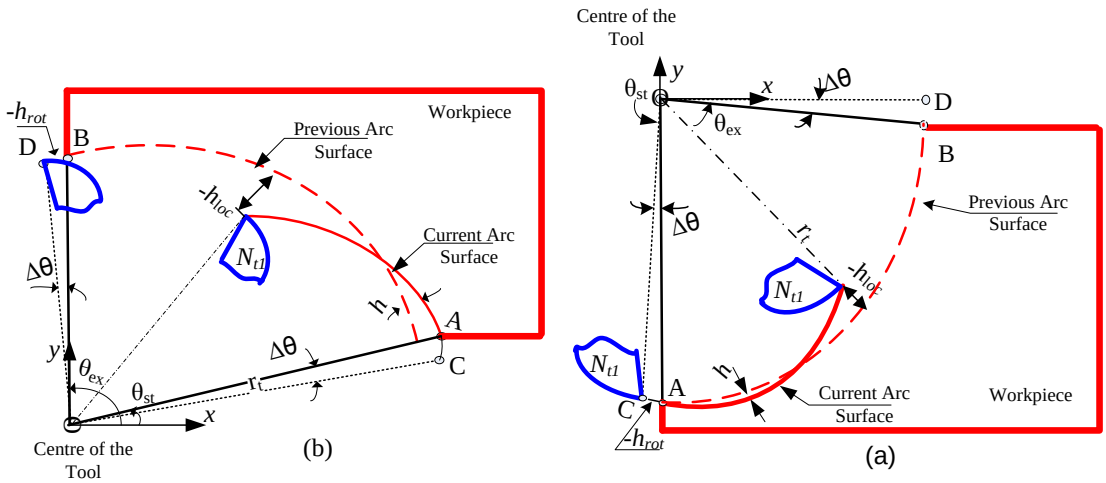

Figure 5.6 Loss of contact behaviour along the milling sector,
(a) up-milling mode and (b) down-milling mode

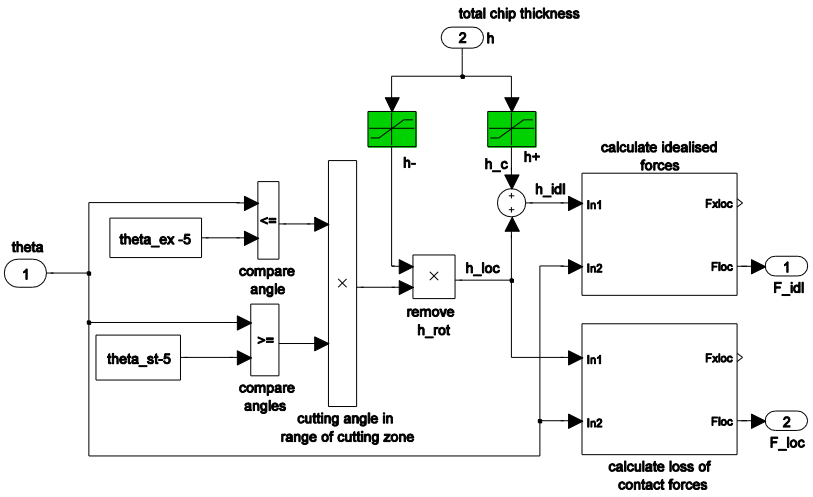

Figure 5.7 Simulink Blocks for calculating the idealised and loss of contact forces

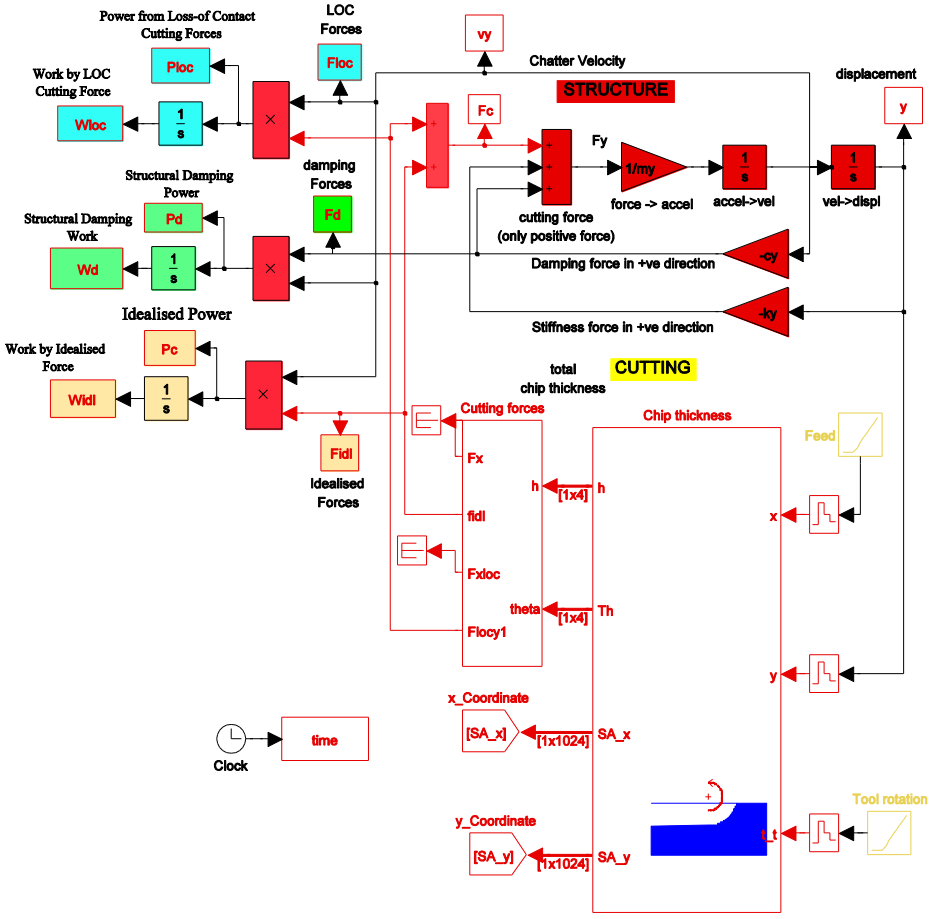

Figure 5.8 Simulink Model for Milling Operations

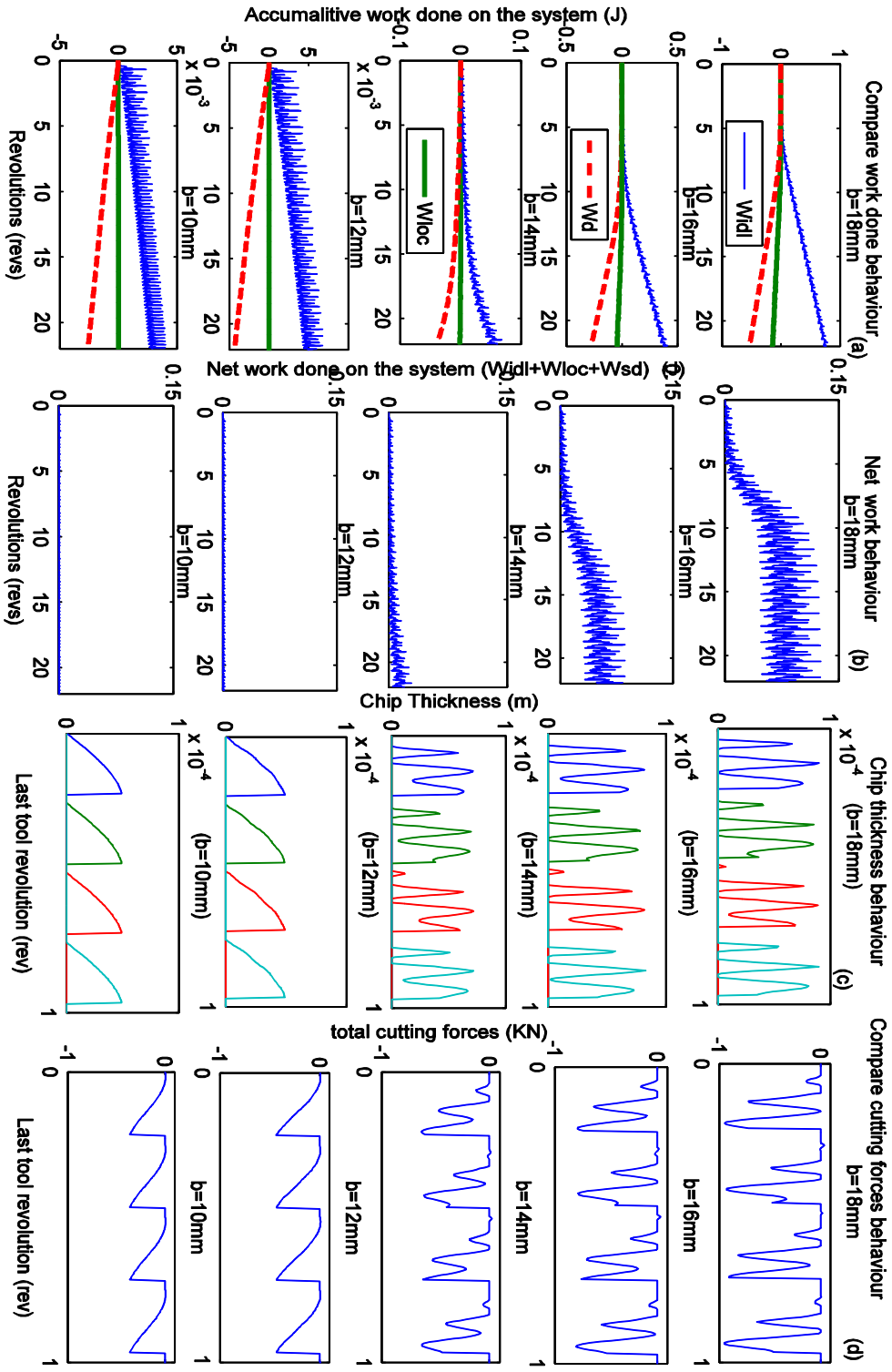

Figure 5.9 simulation results for up-milling operation

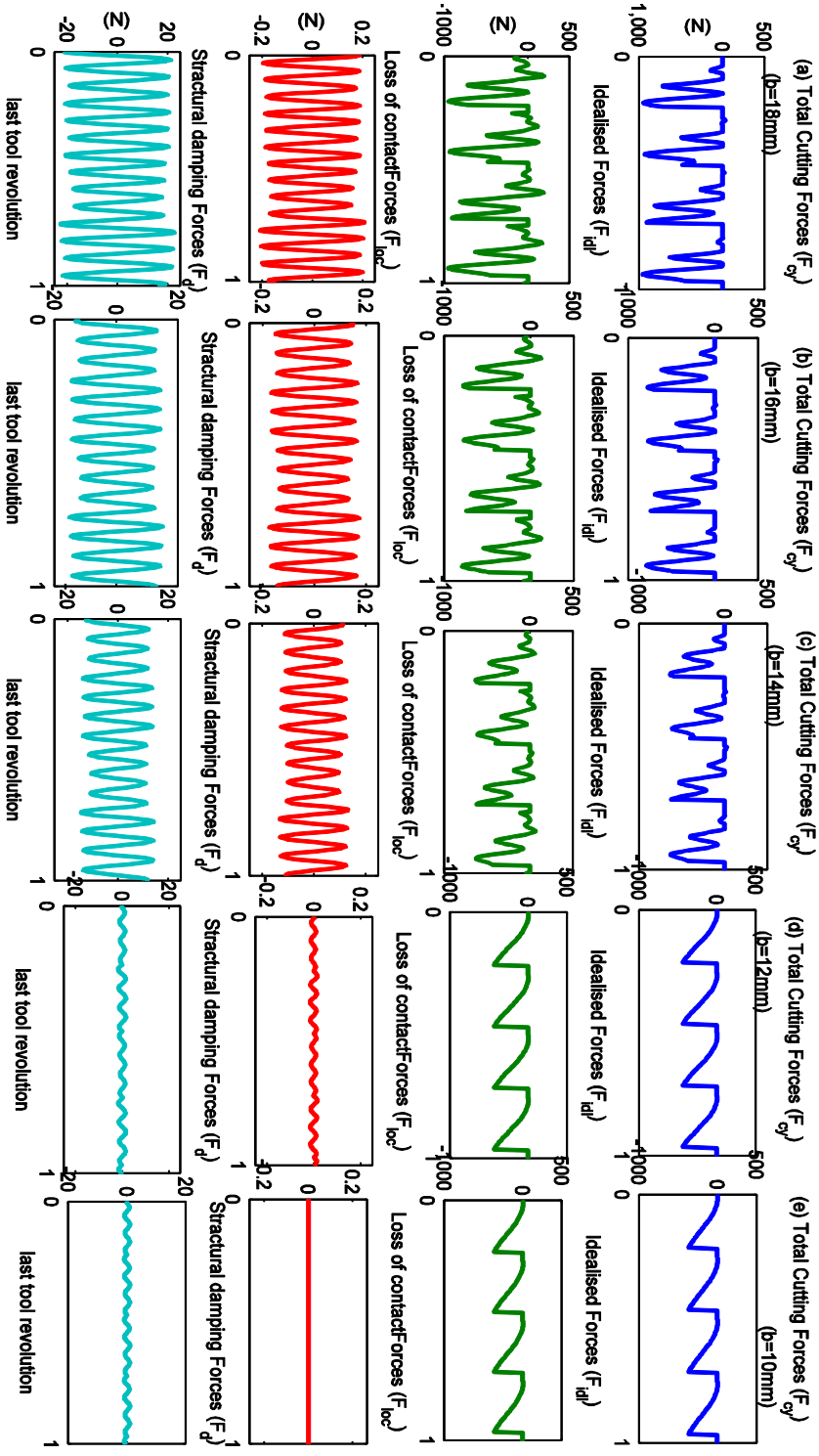

Figure 5.10 Compare forces behaviour at the last tool revolution

CHAPTER 6 ENERGY BALANCE FOR PROCESS DAMPING

6.1 Introduction

The mechanism of process damping due to the tool and workpiece interference is a commonly used strategy for machining chatter suppression, particularly at low cutting speeds. Whilst this phenomenon has been extensively discussed in the literature [2, 11-13, 17, 19, 20, 47, 107], there is no agreement as to the full physical mechanisms that lead to increasing the stability. Finding a mathematical model to represent this behaviour has been researched significantly, and several theories have been created to explain it in a physical sense. Nevertheless, there is still not a straightforward technique which can be used to measure and illustrate how these forces are quantifiably affecting the stability.

Consequently, in this chapter, by using the newly developed energy balance approach, it is straightforward to measure the amount of dissipated energy due to the work done by process damping forces. This allows the performance of the process damping "flank interference mechanism" to be explored through the simulation of the milling process. Furthermore, the performance of the process damping under different cutting conditions and the tool geometry effects will be investigated.

6.2 Tool/Workpiece Interference Mechanism

It is accepted that process damping depends on the contact pressure and the volume of the deformed material under the tool relief face. Therefore the concept of the process damping mechanism is defined as the interaction between the relief face of the cutting tool and the waveform traced by the cutting edge [13, 92, 107]. The commonly proposed mechanism of process damping is shown schematically in Figure 6.1. Here in the presence of the straight flank face, as the tooth penetrates the workpiece, the material approaching the cutting edge is separated into two parts. For the upper part, the material is removed as a part of the chip, whereas for the lower part, the material that cannot move upward is compressed under the flank face of the tooth. The volume of the

displaced material is dependent on the tool/workpiece geometry and also on the instantaneous cutting conditions. The elastic-plastic deformation creates a pressure under the flank face which results in more process damping force, particularly when the tool travels downwards (point 'B' Figure 6.1), whereas the interference is minimised when the tool travels upwards on the wave (position 'D' in Figure 6.1) due to the positive slope of the machined surface.

With reference to the same Figure 6.1, this type of process damping mechanism is considered in the current model. As explained in Section0 process damping forces are modelled based on the ploughing force F_{npt} acting on each tooth and in the direction of the normal to the flank surface. This is usually proportional to the indentation volume V_t. However frictional force F_{fpt} is acting in a direction parallel with the tool flank face and proportional with the frictional coefficient μ_p.

It is well known that the process damping forces that arise due to the flank interference concept are not linear, therefore modelling of process damping is still complicated and the basic subject matter has not been fully understood. Therefore in this chapter, simulated process damping effects are investigated by using the new analysis approach that was developed in the previous chapter. Energy analysis provides a reasonable quantifiable measurement for the process damping performance.

6.3 **Modelling System Boundary in Two Dimensions**

Before analysing the results, the system dynamics and the system boundary need to be defined and reviewed. In this chapter, process damping effects are studied in two different milling scenarios. In the first scenario, the milling dynamics are considered just in one direction normal to the feed direction and represented with a single degree of freedom. The system boundary and the energy calculation of this scenario were previously discussed in Chapter 5. However for the second milling scenario, the system dynamics are also represented with a single degree of freedom, however in two orthogonal directions x and y. Therefore the system boundary and energy calculation of this milling scenario will now be briefly reviewed.

The equations of motion for this system are expressed as follows:

$$m_x\ddot{x} + c_x\dot{x} + k_x x = F_x \quad (6.1)$$
$$m_y\ddot{y} + c_y\dot{y} + k_y y = F_y$$

The system equations of motion are interpreted using simple Simulink blocks to represent the system dynamics behaviour in x and y directions as shown in Figure 6.4(a) and (b). In addition, a set of a simple Simulink blocks for the energy calculation in x and y directions respectively can also be seen in same figure.

As described in the previous chapter, the system boundary should define all the internal and external components that are affecting the system in any direction. Now, Figure 6.2 shows the case of the milling scenario with system dynamics in x and y directions. This means any energy that crosses the system boundary will be defined and measured. With reference to Figure 6.2(b), here there are two types of energies which are crossing the system boundary. Firstly, energy flowing into the system in x and y directions is known as the idealised energy (W_{idlx} and W_{idly}). Secondly, energy flowing out of the system in x and y directions is known as dissipated energy. The dissipated energy includes the process damping energy (W_{pdx} and W_{pdy}), the structural damping (W_{sx} and W_{sy}) and loss of contact energy (W_{locx} and W_{locy}).

In summary, the model shown in Figure 6.3 will be used in this chapter to quantifiably investigate the performance of the process damping due to the flank interference mechanism. For a comprehensive investigation, stability behaviour of two scenarios is investigated based on analysing the behaviour of the process damping and the loss of contact energy rates in both x and y directions, which are calculated as follows:

$$W_{rpd} = (W_{rpdx} + W_{rpdy}) \quad (6.2)$$
$$W_{rloc} = (W_{rlocx} + W_{rlocy})$$

In addition, energy dissipation can also be computed in percentage terms. This provides a clear comparison measurement between the process damping and loss of contact mechanisms:

For loss of contact: $$W_{loc}(\%) = \frac{W_{loc}}{W_{loc} + W_{pd} + W_s} \times 100$$ (6.3)

For process damping: $$W_{pd}(\%) = \frac{W_{pd}}{W_{loc} + W_{pd} + W_s} \times 100$$

These values are then plotted in contour plots or with reference to the variable parameters. This part of the calculation is performed by using Matlab codes stored in a Matlab script file, using the simulated data generated by Simulink.

6.4 **Simulation Conditions**

In summary, the main aim of this study is to demonstrate how the milling stability behaviour is affected by dissipating more energy from the system due to the process damping mechanism. Therefore a small selection of the results previously confirmed are listed in Table 6-1, to replicate a previous study [19]. Then in the second milling scenario, the simulation is carried out to investigate the influence of the process damping in two x and y directions based on the influence of the depth of cuts, clearance angles, radial immersion and the natural frequency. The stability degree was distinguished based on the behaviour of the energy rates per tool revolution. Simulation parameters are summarised in

Table 6-2 and Table 6-3 which are chosen from the work published in [11, 123]. Model results are validated based on a small selection; however a small difference is observed which could be attributed to the lack of information provided in the literature. Despite this, the model shows almost the same behaviour.

6.5 **Results and Discussion**

6.5.1 **System Dynamics with One Mode in One Direction**

Figure 6.5 shows behaviours of the work done on the system caused by the following forces: idealized forces (F_{idl}), loss of contact forces (F_{loc}), structural damping forces (F_s) and process damping forces (F_{pd}), at a depth of cut b=20 mm and spindle speed ω=290

rpm. Here the work done by the idealized forces F_{idl} is positive which means these forces are always causing energy to flow into the system. However the work done by the other forces (F_{loc}, F_s and F_{pd}) is negative which means all these forces are causing energy to flow out of the system (dissipating energy).

The effects of the process damping on the degree of stability are investigated by analyzing the energy behaviour in the system. As can be seen in Figure 6.5(a), the highest dissipated energy was due to the work done by the process damping forces (W_{pd}). In addition, the work done (W_s) by the structural damping forces is also visible. However loss of contact energy behaviour (W_{loc}) is negligible. This can be attributed to the process damping effects which had played a major role in suppressing the chatter.

However Figure 6.5(b) shows almost the opposite scenario, since the effects of the process damping are not included, therefore the amount of dissipated energy from the system is significantly reduced, whereas the amount of transmitted energy (W_{idl}) to the system is considerably increased by almost 3 times, particularly at the last tool cycle compared to Figure 6.5(a). It was also evident that loss of contact energy has a sharp increase after 23 tool revolutions. This can be attributed to the vibration amplitudes severely growing here which causes more loss of contact behaviour. Therefore the structure damping was provoked to dissipate the imposed energy. As a result, the dissipated energy by the structural damping behaviour is markedly higher compared to that in Figure 6.5(a). Furthermore, it can also be noticed that, towards the last tool cycles, the total dissipated energy from the system is almost equivalent to the total energy supplied to the system as shown in Figure 6.5(a) and (b) particularly. This behaviour can be attributed to the onset of steady state limit cycle oscillations.

Figure 6.6 compares the behaviour of the net cutting energy $(W_{rc} = W_{ridl} + W_{rloc})_{\mp pd}$ per revolution and the total damping energy $(W_{rD} = W_{rs} + W_{rpd})_{\mp pd}$ per tool revolution. Here the behaviour of the energy was evaluated based on the presence (+*pd*) and absence (-*pd*) the process damping effects. These results are chosen particularly to demonstrate the effects of the process damping on chatter suppression. Without the process damping effect, the rates of the total cutting energy per tool revolution

($W_{rc_{-pd}}$) are clearly higher compared to that ($W_{rc_{+pd}}$) obtained from the milling scenario which includes the process damping effect. In addition, the same behaviour can be seen for the dissipated energy rates. The total dissipated energy rates ($W_{rD_{-pd}}$) without including process damping are considerably greater than that ($W_{D_{+pd}}$) obtained from the milling scenario considering the process damping.

Next, the process damping performance was further investigated using five depths of cut (10, 15, 20, 25 and 30 mm) for the maximum chip thicknesses of 75μm to emulate the experimental data in [19]. For each depth of cut, the simulation is performed for spindle speeds ω=200 to 560rpm. Here for each simulated scenario, the energy rates of the process damping per tool revolution W_{rpd} were calculated, and the results are presented in Figure 6.7. It is very clear particularly at low cutting speeds, that process damping energy rates are increasing by increasing the depth of cut. In other words, more rubbing behaviour is occurring for higher depth of cuts particularly at low spindle speeds. However at the high cutting speeds, process damping effects for dissipating the energy per tool revolution vanishes. This can be attributed to the surface speed increase, and the increased wavelength of the wavy surface generated by the chatter. Consequently the interference behaviour between the tool flank face and the workpiece surface never occurs, so that process damping forces do not exist, and thereby there is no work done by these forces. With reference to Figure 6.7, the dissipated energy rates at the depth of cut b=30mm are severely fluctuating along the cutting speeds up to ω=440 rpm. After this cutting speed, process damping is not dissipating energy anymore, which caused a catastrophic simulation failure.

Figure 6.8 further demonstrates and compares the energy behaviour for process damping and loss of contact in contour representation. It is very that clear process damping energy rates are increased as the depth of cut is increased, particularly at low cutting speeds. In these cutting conditions the process damping rates are sufficient to dissipate the vibration energy (Figure 6.8(a)). Consequently the loss of contact energy was not significant and is not shown in Figure 6.8(b).

6.5.2 System Dynamics with One Mode in Two Directions

Simulation verification for time domain milling was performed through selecting a confirmed data set previously published in [11]. Energies that are crossing the system boundary in all directions are calculated for each revolution. For each milling scenario the average rate of the dissipated energy was calculated from the last tool revolutions. This means these energy rates are measured after the system is reaching the steady state limit cycle behaviour.

1- Effect of Depth of Cut

Figure 6.9, presents loss of contact energy rates without including the process damping effects. As can be seen in plots (a), (b) and (c), energy rates were respectively measured at the selected cutting speeds ω=2083 rpm, 2290 rpm and 3750 rpm at depths of cut b=0.2 to 1.6 mm. According to these results, loss of contact energy rates were sharply increased just from the depth of cut b=0.4mm. This means beyond this cutting limit, the rates of the vibration energy that are imposed onto the system are sharply increased, leading to instability.

In order to demonstrate process damping effects on stability improvement, the simulations including the process damping effects are repeated for the same cutting conditions. Then the results of the process damping and loss of contact energy rates are both presented in Figure 6.10. At the cutting speed ω=2083 rpm (Figure 6.10(a)), the process damping energy rates increase along the depths of cut. It is very obvious here that the process damping effects are sufficient to dissipate the imposed vibration energy leading to more stability. Consequently energy rates of the loss of contact were invisible along all these cutting conditions.

For the cutting speed ω=2290 rpm (Figure 6.10 (b)), loss of contact energy rates were not emerging along the depths of cut up to b=1.4mm, because the process damping effects are still dominant here to dissipate the vibration energy. However beyond these depths of cut vibration amplitudes are clearly growing causing the system to lose stability.

However for the cutting speed ω=3750 rpm, Figure 6.10(c), loss of contact energy rates are clearly higher and dominate compared to the process damping energy rates. For this cutting speed process, the damping effects cannot dissipate the vibration energy even at the lower depth of cut *b*=0.4mm. As a result, energy rates of the loss of contact become significant. These outcomes agree reasonably with the results in [11].

Process damping and loss of contact energy rates are further compared through the contour plot shown in Figure 6.11. It is very obvious here that at low cutting speeds process damping is dominant in dissipating the vibration energy. For instance at the cutting speed ω=1800 rpm process damping was efficiently dissipating the vibration energy up to a depth of cut *b*=2mm, whereas loss of contact energy is negligible. However process damping energy rates are decreased at the high cutting speeds. This can clearly be seen along the cutting speeds ω=2400 to 3200 rpm, where the process damping effects become insufficient to dissipate the imposed vibration energy along the depths of cut greater than *b*=1 mm. This allows the vibration energy to significantly increase, which in turn provokes loss of contact energy to rise at high rates.

2- Effect of Clearance Angle

Effects of the flank clearance angles on the process damping performance and thereby on the stability limits can be investigated through the energy behaviour. Results of the process damping and loss of contact energy rates are presented in Figure 6.12. Here for each flank relief angle ($\gamma = 3^o, 5^o, 7^o$ and 10^o), the simulation is performed to calculate these energy rates along the cutting speeds $\omega = 1000$ to 1800 rpm. For the flank relief angle $\gamma = 3^o$ the results are shown in Figure 6.12(a). It can be seen here that the process damping effects are significant and sufficient to dissipate the vibration energy and prevent the loss of contact energy to emerge along all the cutting speeds. For the flank angle $\gamma = 5^o$ (Figure 6.12(b)) at the low cutting speeds, almost the same behaviour can be seen. However, loss of contact energy becomes visible at the cutting speeds greater than $\omega = 1300$ rpm. For the angle $\gamma = 7^o$, results are presented in Figure 6.12(c). Here the process damping effects are clearly decreased since the loss of contact energy rates are steadily increased to become almost similar to the process damping energy rates,

particularly along the high cutting speeds. However for the clearance angle $\gamma = 10^{o}$ (Figure 6.12(d)), it is very obvious that loss of contact energy rate is dominant and the process damping has become absolutely ineffective to dissipate the imposed vibration energy.

3- Effect of Natural Frequency

The influence of natural frequency on the process damping energy behaviour is demonstrated in Figure 6.14. Here the amount of dissipated energy by the process damping mechanism is measured as a percentage. This percentage measurement is based on the total dissipated energy from the system calculated from equation (6.3). For the natural frequency $f_{nx,y}$ = 343 Hz the dissipated energy is stabilised at 3%, whereas 18.4% for $f_{nx,y}$=681Hz, and 39.9% for the $f_{nx,y}$=1195Hz. To summarise, the process damping performance increases for higher natural frequencies. This is because the high frequency generates small wave lengths thereby more tool/workpiece interference, which leads to more process damping forces.

4- Effect of Radial Immersion

The effects of radial immersion on the process damping performance are also investigated, and the results are presented in Figure 6.14. The dissipated energy by the process damping energy mechanism is measured in rates (J/rev) as shown in Figure 6.14(a) and as a percentage as shown in Figure 6.14(b). According to these results, high immersion rates provide high dissipated energy rates of the process damping. This can be attributed to the increase in the interference contact between the tool flank face and the workpiece surface. For the redial immersion r_e =35%, the dissipated energy rates by the process damping after the steady state limit cycle behaviour is reached are 0.024 J/rev; this rate accounts for about 15% of the total dissipated energy from the system. However for the radial immersions r_e= 50%, 70% and 100%, the energy rates are respectively recorded at 0.055J/rev, 0.121 J/rev and 0.91 J/rev, whereas the percentages respectively are 22 %, 28% and 54%.

6.6 **Summary**

A new analysis methodology based on the energy analysis has been implemented for process damping simulations. The effect of the process damping mechanism in vibration suppression is illustrated and the relative importance of different energy dissipation mechanisms is observed and quantified. Here influence of cutting parameters including tool geometry, on the process damping due to the flank interference mechanism is quantifiably investigated. In milling, increasing the contact length between the tool flank face and the work surface results in higher process damping, thus higher energy dissipation. This means that decreasing the clearance angle increases the energy dissipation. This is well-known in practice, but this chapter has provided a new visualised interpretation based upon the proposed energy analysis.

It is also demonstrated that an increased radial depth of cut leads to a significant increase in the stability behaviours, unlike the case for high cutting speeds where the effect of process damping vanishes. Natural frequency is another important parameter affecting the stability; higher frequency leads to increase in the tool/workpiece contact behaviour and thereby an increase in the rates of the process damping energy dissipation. The steady-state limit cycle behaviour under the process damping effects is investigated.

In this work, the amount of the energy dissipation due to the rubbing behaviour was quantifiably measured. This provides a clear representation about how the process damping performance is affected by the cutting parameters and tools the geometry, and thereby on the machining stability behaviour. These outcomes become quite important in selecting the appropriate tool in practice.

With reference to the previous results, energy analysis has been considered as a reasonable approach which can be used for assessing the relative contribution of the process damping for stability improvement. Consequently implementation of this approach will be extended to analyse the interaction between the variable helix and process damping on the chatter mitigation. This will be the main subject of the next chapter.

Parameter	Value
Number of cycles	40
Iterations per cycle	12000
Number of axial layers (n_l)	30
Stiffness	$40x10^6$ (N/m)
Damping ratio	0.01%
Natural frequency	600 (Hz)
$\boldsymbol{K_{tc}}$	1676 (N/mm^2)
$\boldsymbol{K_{rc}}$	503 (N/mm^2)
Width of cuts (b)	10,15,20,25&30 (mm)
Tool diameter	16 (mm)
Number of teeth	4
Flute helix	30^o(axial flute)
Milling Mode	down-milling
Radial immersion	1(mm)
Feed per tooth	0.155(mm/tooth)
Process damping friction coefficient (μ)	0.25
Process damping normal forces coefficient (K_{np})	80 (Nmm^{-2})
Tooth flank length (l_{flank})	0.3mm
Tooth relief angle ($\boldsymbol{\gamma}$)	5^o

Table 6-1 Simulation parameters of the milling including process damping

case	($\boldsymbol{\gamma}^o$)	r_i (%)	k_x (N/μm)	f_{nx} (Hz)	ζ_x (%)	k_y (N/μm)	f_{ny} (Hz)	ζ_y (%)	*Ref.*
1	3	50	9.73	3110	1.43	10.35	3106	1.68	[11]
2	3,5,7,10	50	15.9	1267	2.62	15.9	1267	2.62	[11]
3	3	50	16	1195	1.49	16	1195	1.49	
			15.6	681	1.25	15.6	681	1.25	[11]
			15	343	1.04	15	343	1.04	
4	3	35,50, 70,100	8.1	1370	1.9	7.7	1330	1.9	[123]

Table 6-2 simulation parameters for second scenario

case	Spindle speeds (rpm)	K_p (N/mm^3)	K_{tc} (N/mm^2)	K_{rc} (N/mm^2)	*Ref.*
1	2083, 2290, 3750	40000	900	270	[11]
2	1390	40000	900	270	27]
3	1390	70000	900	270	27]
4	900	1.5x10^4	1150	345	[123]

Table 6-3 Spindle speeds and cutting forces coefficients

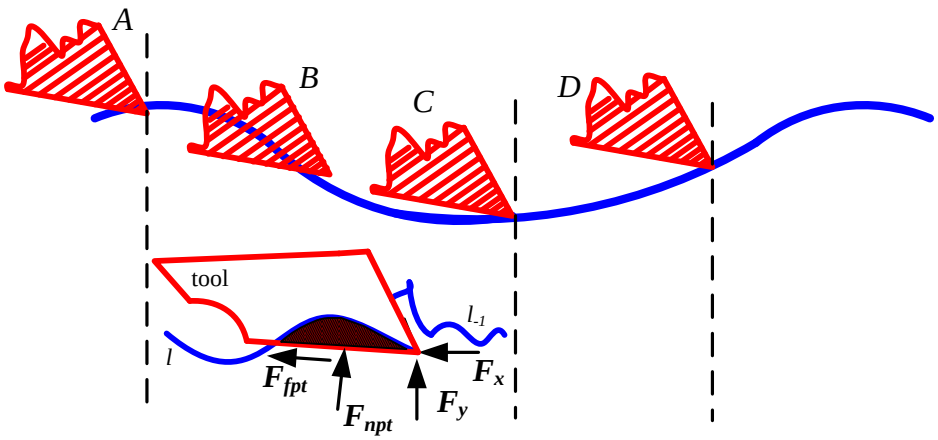

Figure 6.1 tool clearance face and the arc surface interference

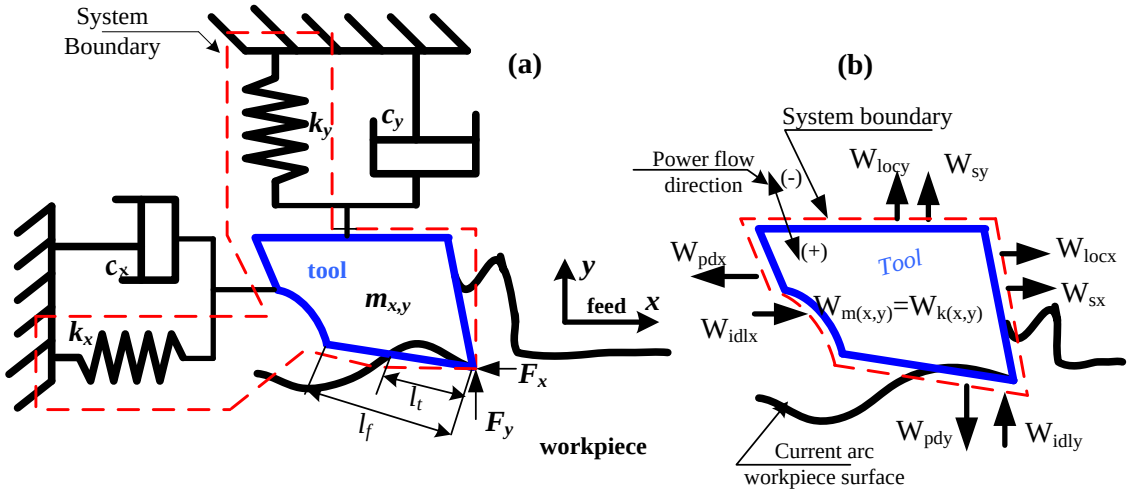

Figure 6.2 Schematic diagram of a: (a) 2D system dynamics with boundary, and (b) Energy behaviour

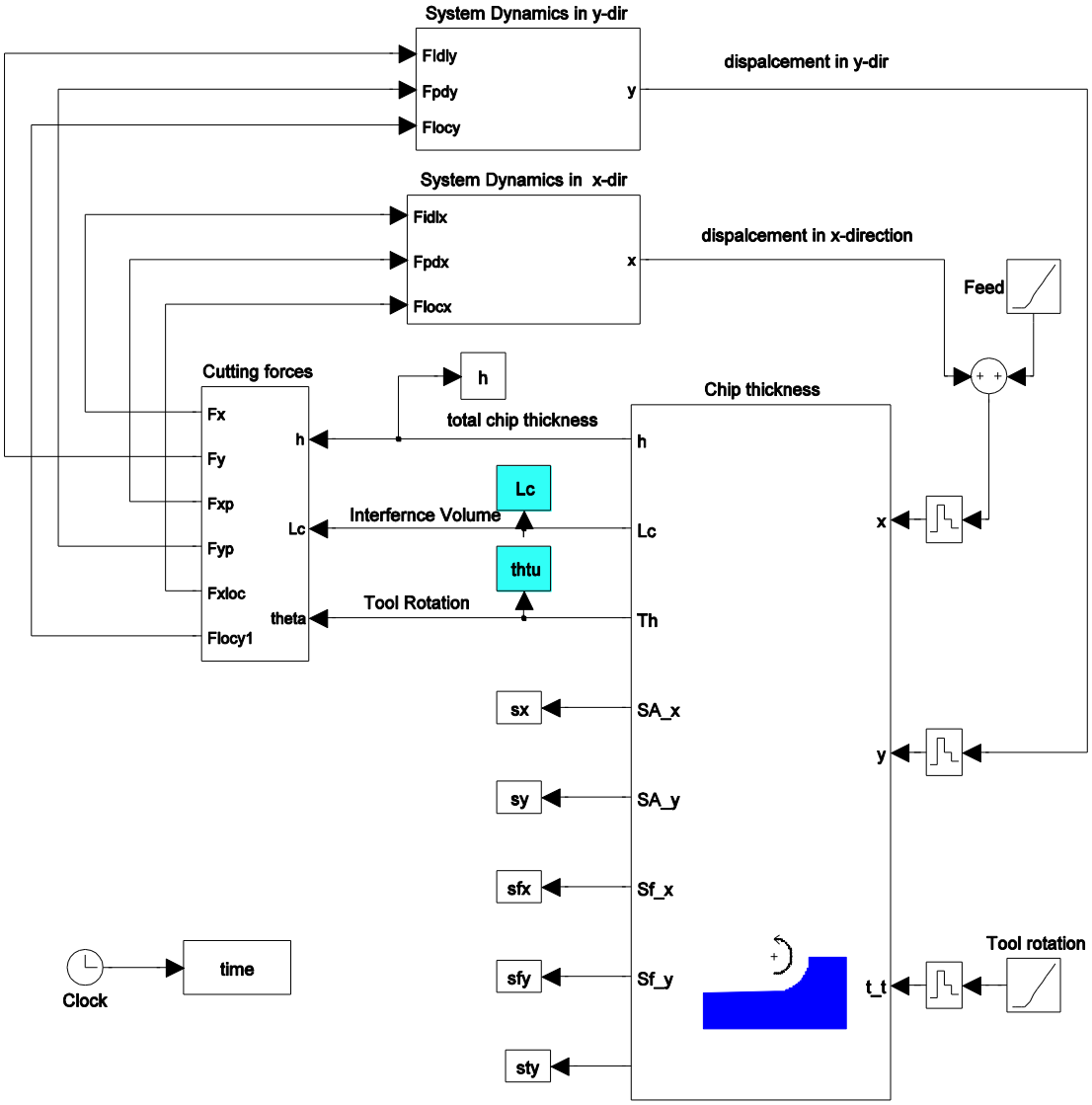

Figure 6.3 Simulink Milling Model including Chip thickness transfer function

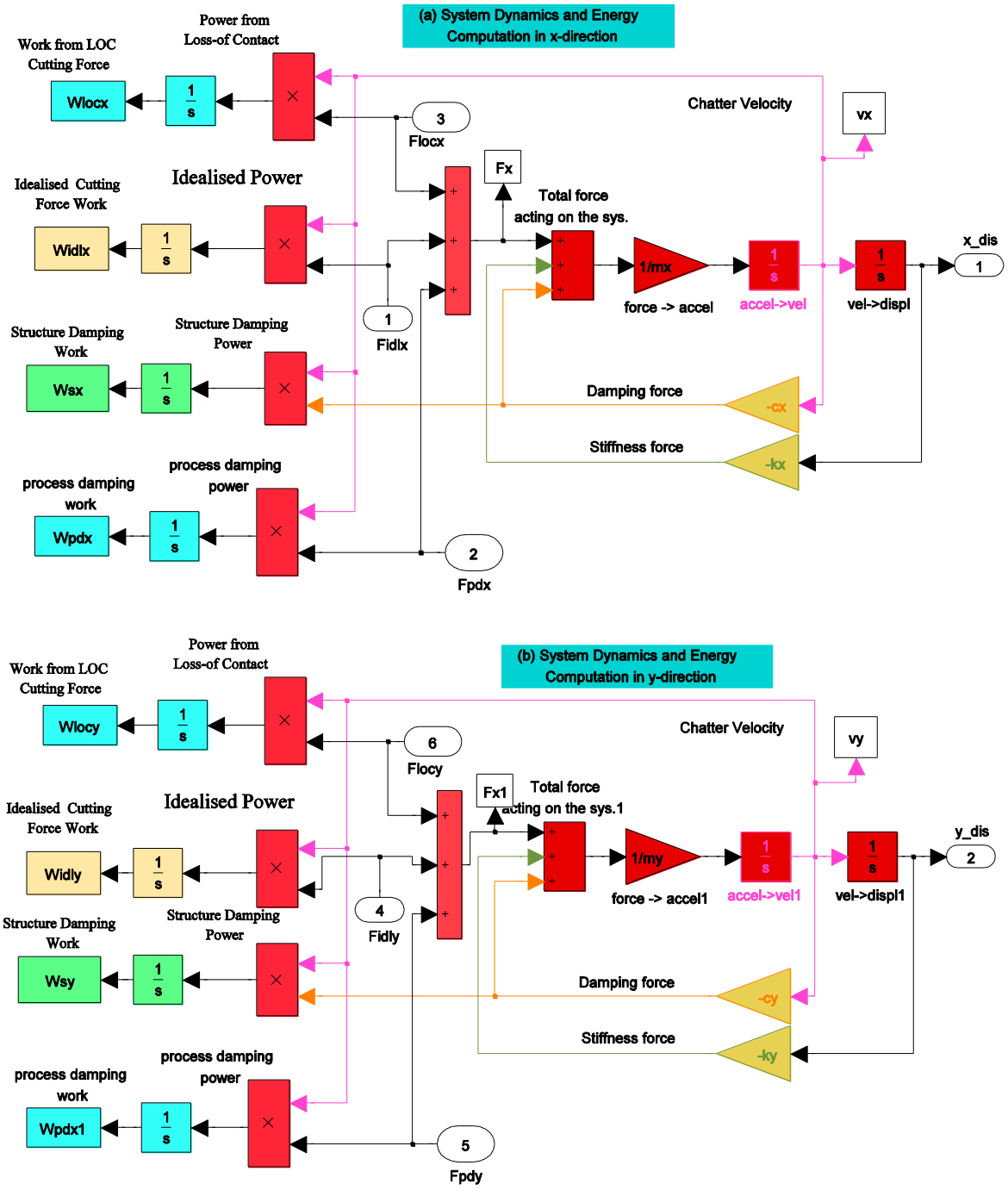

Figure 6.4 Simulink Blocks: (a) System dynamics and energy calculation in x-directions. (b) System dynamics and energy calculation in y-direction

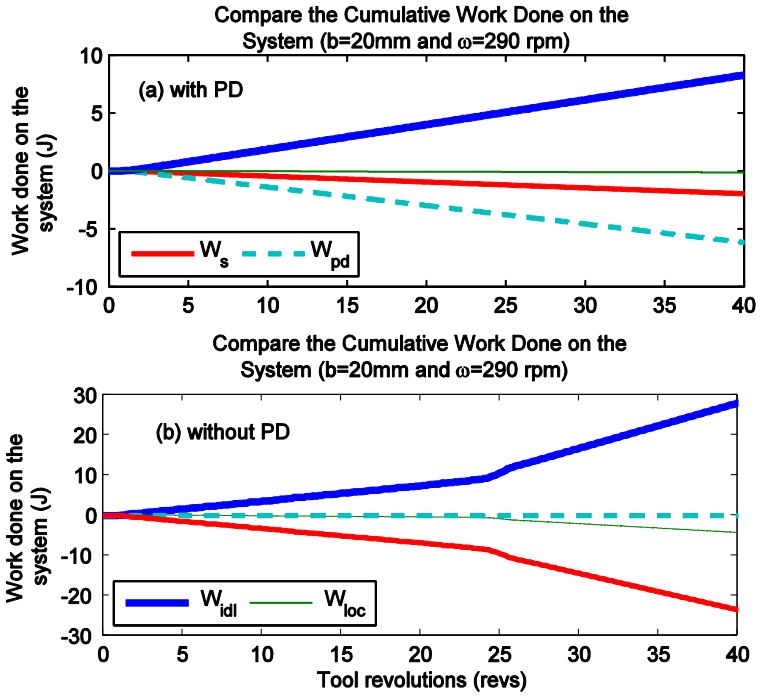

Figure 6.5 compare the cumulative work done on the system (a) with process damping (b) without process damping .

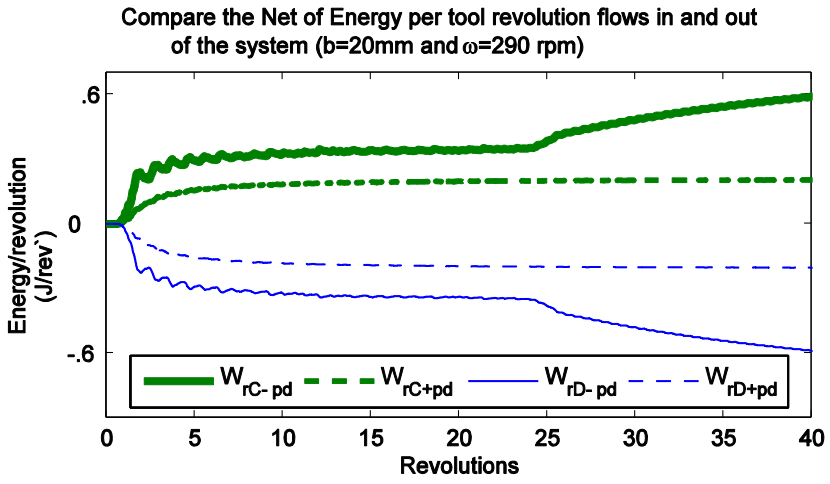

Figure 6.6 compare the net energy behaviour per tool revolution

– – – – – (+pd) with process damping , ———— (-pd) without process damping

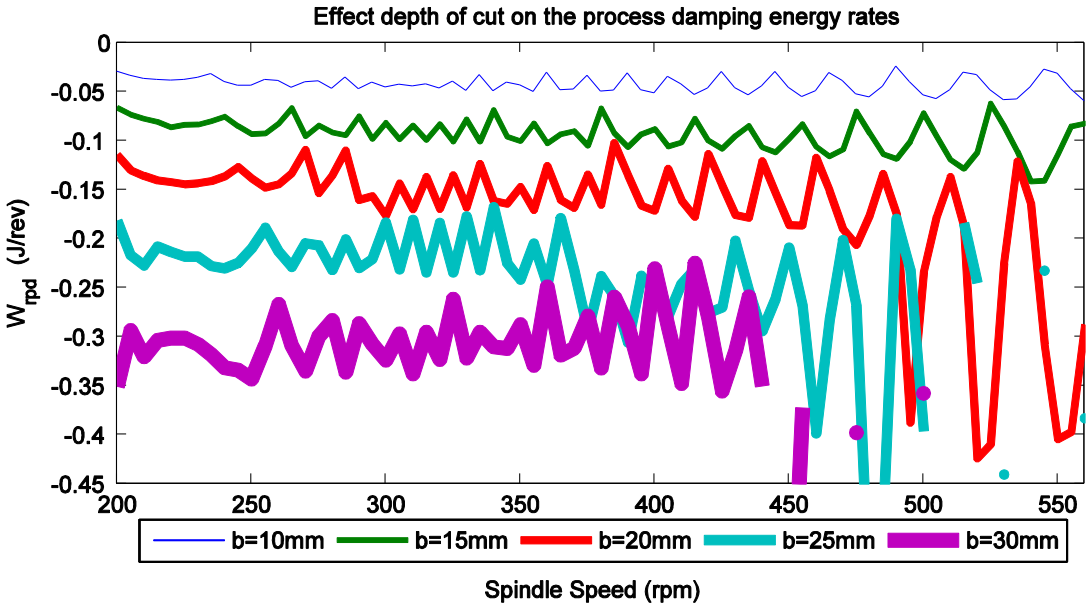

Figure 6.7 Effect depth of cut on process damping energy rates

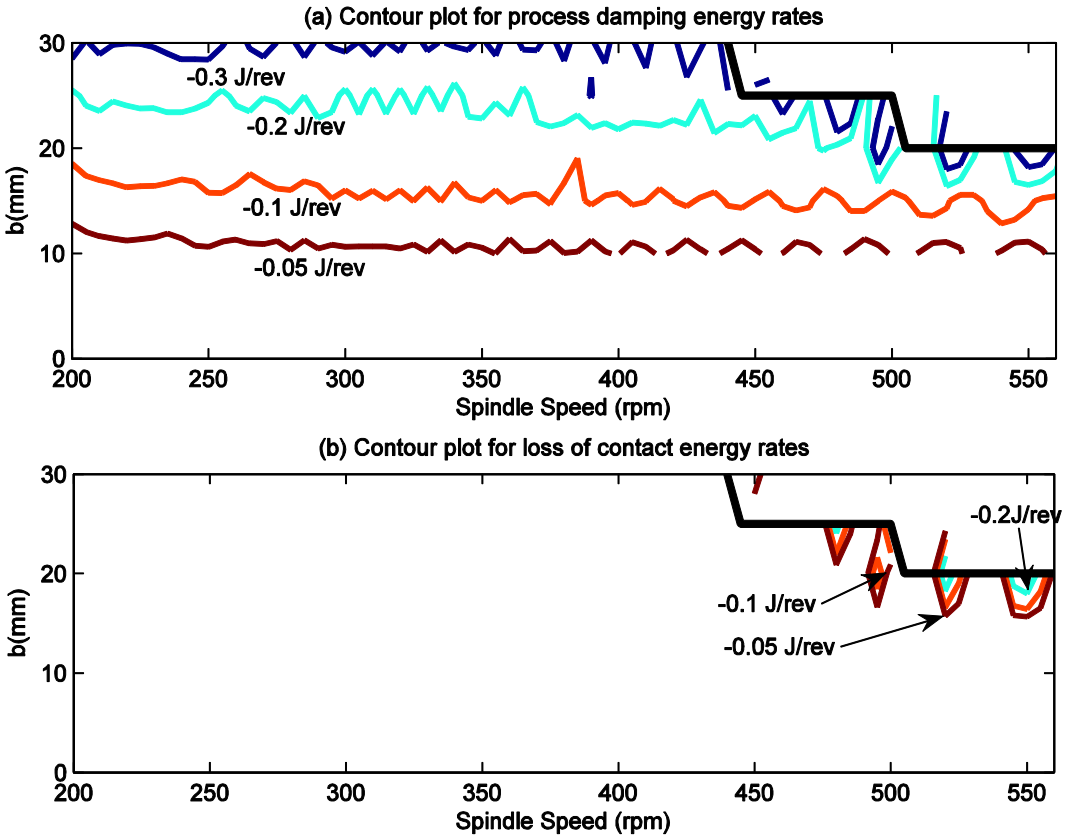

Figure 6.8 Contour plot for the energy dissipation

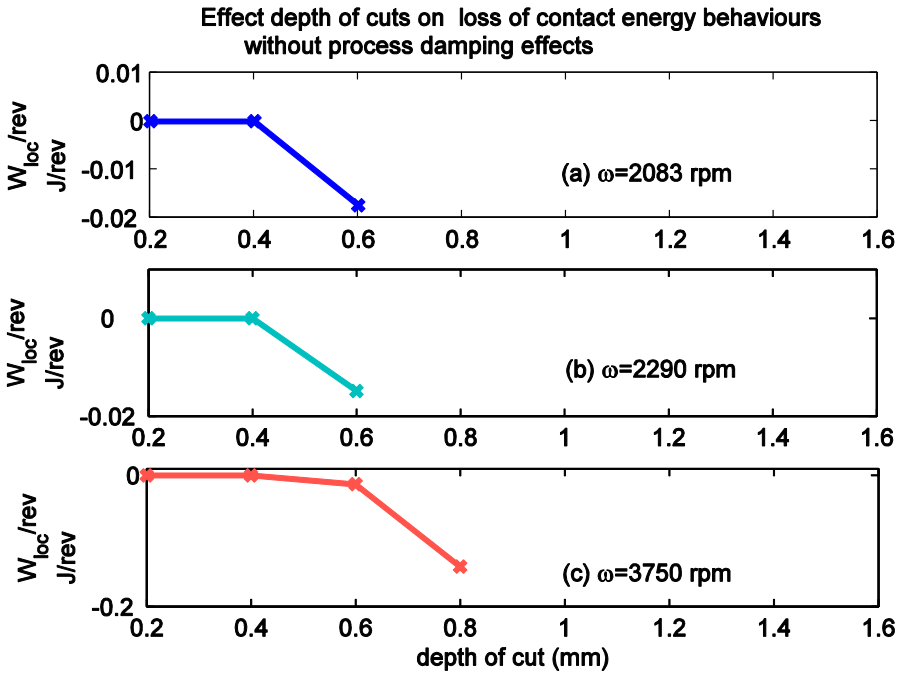

Figure 6.9 effect depth of cuts on loss of contact energy behaviour without process damping effects

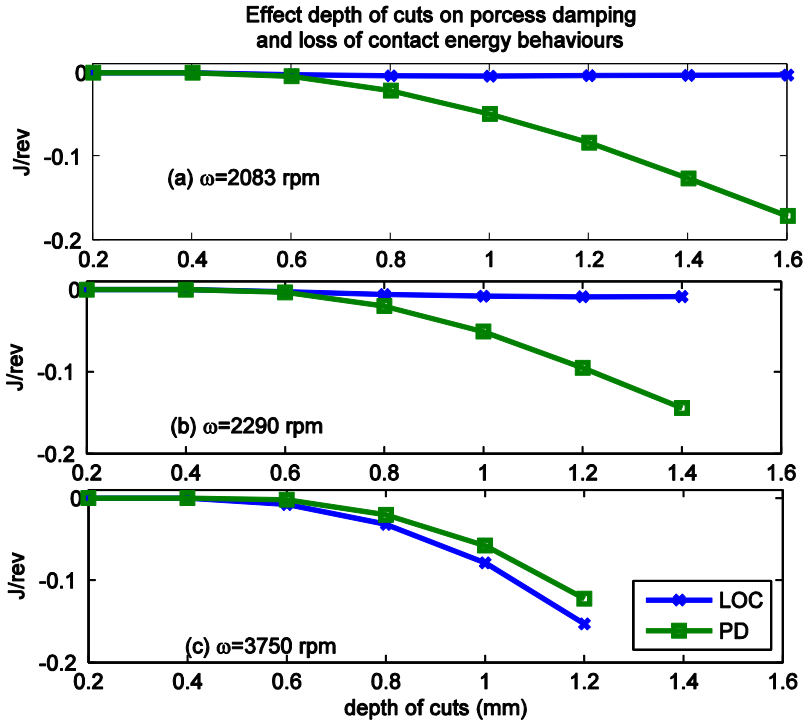

Figure 6.10 effect depth of cut on process damping and loss of contact energy behaviour

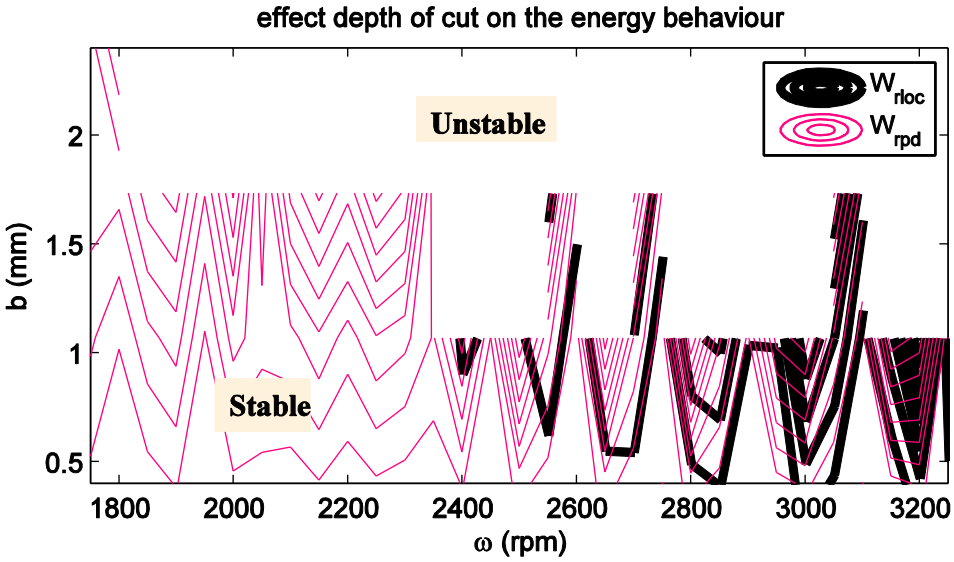

Figure 6.11 compare process damping and loss of contact energy behaviours

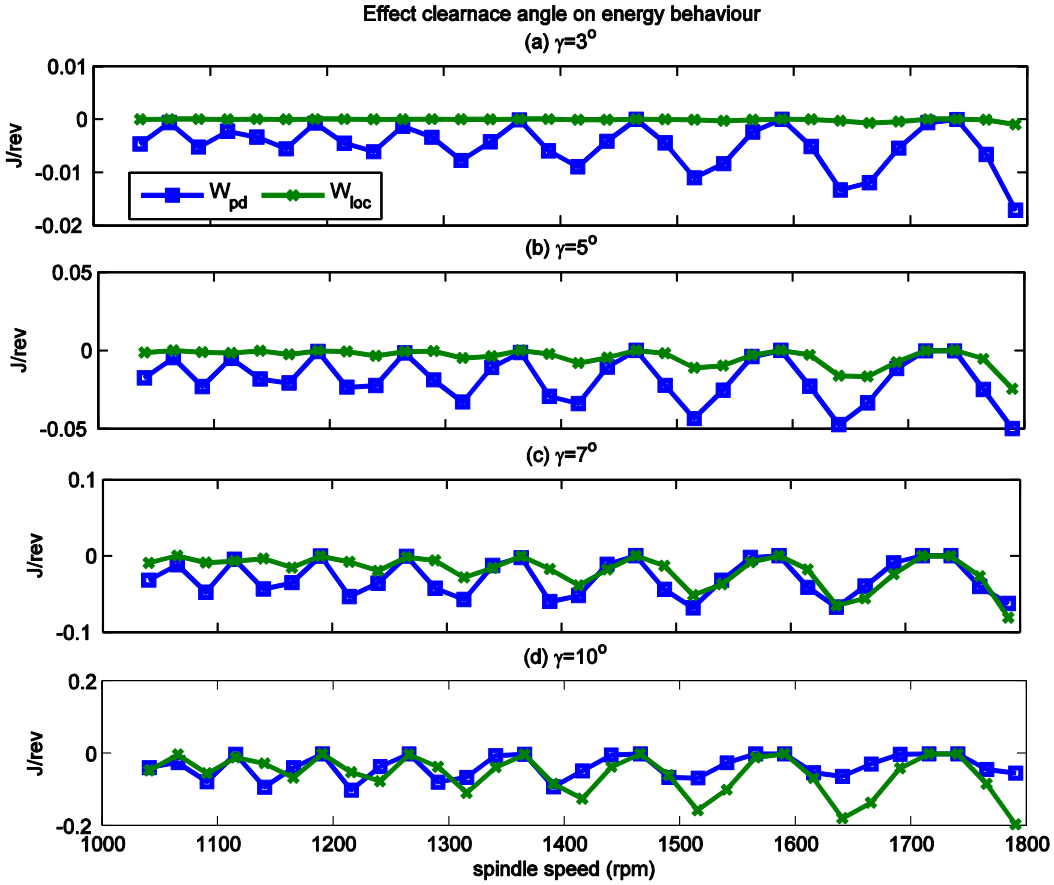

Figure 6.12 Effect flank relief angles on the energy behaviour

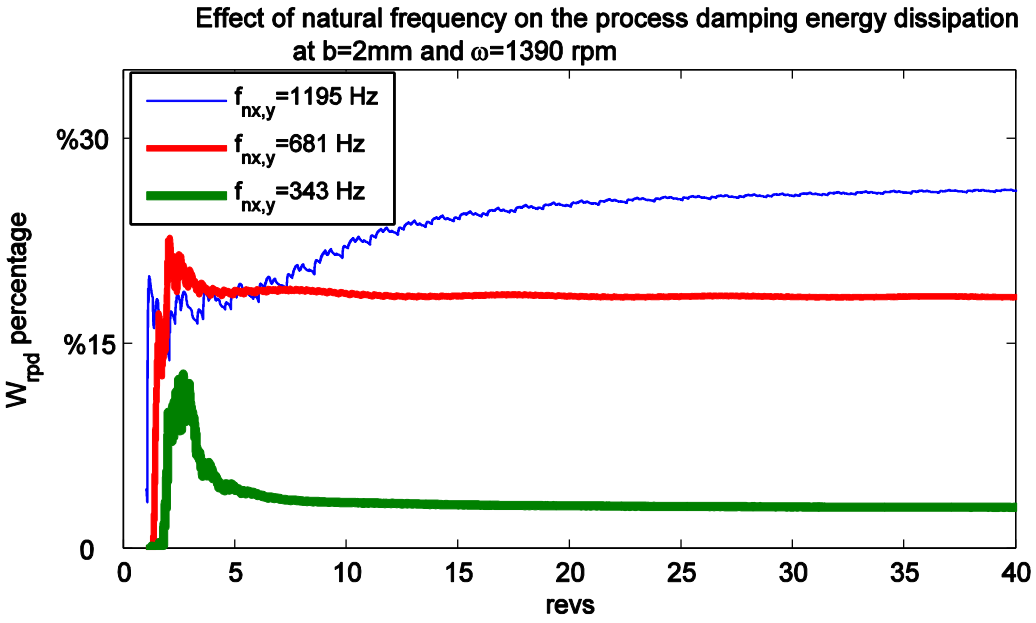

Figure 6.13 effect natural frequency on the process damping energy behaviour

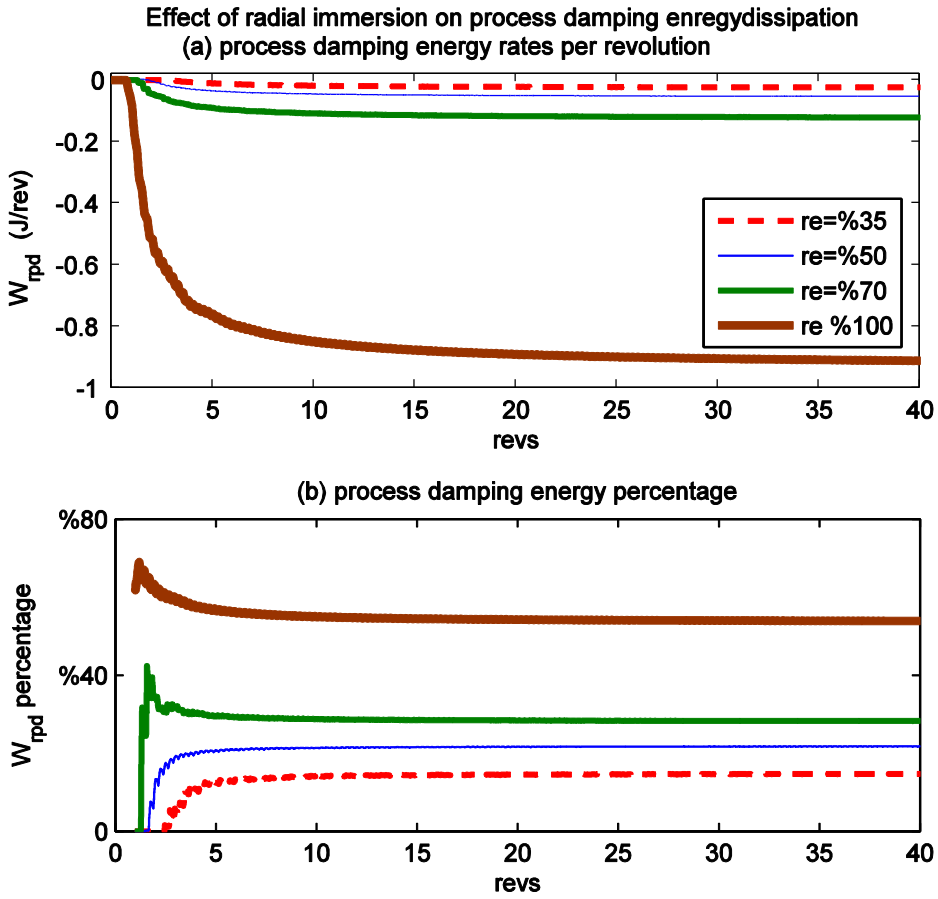

Figure 6.14 effect of radial depth of cut on the energy behaviour

CHAPTER 7 ENERGY ANALYSIS FOR PROCESS DAMPING AND VARIABLE HELIX MILLING

7.1 Introduction

Variable helix/pitch tools have been proposed as a vital method to improve stability during milling. Most of the research done for the variable helix/pitch tools such as in [20, 26, 90, 124, 125] was on predicting the chatter stability. In the context of this work, a variable helix tool is defined as one where the helix angle changes from one flute to the next but is a constant along a single flute, also referred to as an alternate helix cutter.

The phase delay between the inner and the outer waves has a fundamental effect on the stability of cutting. Figure 7.1 shows different angular positions of teeth on the tool circumference. For instance diagram (a) shows an end mill with equal pitch, diagram (b) shows an end mill with a variable helix and an equal pitch angle, diagram (c) demonstrates a uniform helix variable end-teeth pitch angle, and diagram (d) shows an end mill with both a variable helix and end-teeth angles, which is adopted in this study.

Turner [90] studied the influence of variable helix/pitch end-mill on machining stability, using analytical and time domain methods. In some cases neither model accurately predicted the stability, for example the stability of the variable helix tool (VH4 Fig1[90]) was much greater than the standard helix equivalent. Turner attributed this to the process damping effects, and the stable phases along the flute length inhibiting the onset of regenerative chatter. This proposition is very difficult to test experimentally. However a time domain model could offer a comprehensive representation of the kinematics of milling, and process damping can be included. The model could therefore offer a reasonable explanation for the observed empirical results. Furthermore the energy analysis approach that has been described in the previous chapters provides a useful analysis for such a complex system.

The procedure of this work is summarised as follows:

1. Extend the energy analysis approach to a multi degree of freedom system.
2. Reconsider the scenarios published in [90] and in [20] to study how variable helix/pitch tools affect the machining stability .
3. Include the process damping mechanism to determine if it has an effect on the machining stability, according to Turner's argument [90].

7.2 **Modelling System Dynamics in 3-DOF System**

In Chapter 6, the system boundary with the energy balance approach for the single degree of freedom system is explained. Moreover the procedure of defining the cutting segments and loss of contact forces computation are described. However in this section, milling dynamics for the multi degree of freedom system will be explained.

Therefore, this section only considers the system dynamics with 3-DOF modes in two orthogonal x and y directions. Here the structural damping energies will be defined with each damping element at each mode. In this model, the state-space formulation shown in (7.1) is considered:

$$\dot{\bar{x}} = A\bar{x} + Bu \tag{7.1}$$
$$\bar{y} = C\bar{x} + Du$$

The state space formula is used as Simulink blocks to predict the vibration displacements and velocities in *x* and *y* directions as shown in Figure 7.2. The input and output of the state space function are carefully defined, particularly for this model because the vibration velocity of each mode needs to be defined for the energy calculation. Therefore, as shown in Figure 7.2, the input of the state space function is the net cutting forces $F_{c(x \text{ and } y)}$, whereas the outputs are the system displacements (x and y) and velocities ($\dot{x}$ and $\dot{y}$).

Generally, the state space matrices A, B, C and D (Equation (7.1)) are defined based on the uncoupled system equations of motion as shown in Appendix C. The Matlab codes in Appendix D3 are used to define the system dynamics. Now, having defined all the

parameters of the system dynamics in both directions, then state space matrices for both directions can be defined:

State matrix A

$$A_{[x,y]} = \begin{bmatrix} 0 & 0 & 0 & 1 & 0 & 0 \\ 0 & 0 & 0 & 0 & 1 & 0 \\ 0 & 0 & 0 & 0 & 0 & 1 \\ -\hat{m}_1^{-1}\hat{k}_1 & 0 & 0 & -\hat{m}_1^{-1}\hat{c}_1 & 0 & 0 \\ 0 & -\hat{m}_2^{-1}\hat{k}_2 & 0 & 0 & -\hat{m}_2^{-1}\hat{c}_2 & 0 \\ 0 & 0 & -\hat{m}_3^{-1}\hat{k}_3 & 0 & 0 & -\hat{m}_3^{-1}\hat{c}_3 \end{bmatrix}_{[x,y]} \quad (7.2)$$

Input matrix B

$$B_{[x,y]} = \begin{bmatrix} 0 \\ 0 \\ 0 \\ \hat{m}_1^{-1} \\ \hat{m}_2^{-1} \\ \hat{m}_3^{-1} \end{bmatrix}_{[x,y]} \quad (7.3)$$

Output matrix C

$$C_{[x,y]} = \begin{bmatrix} 1 & 1 & 1 & 0 & 0 & 0 \\ 0 & 0 & 0 & 1 & 0 & 0 \\ 0 & 0 & 0 & 0 & 1 & 0 \\ 0 & 0 & 0 & 0 & 0 & 1 \end{bmatrix} \quad (7.4)$$

Feed through matrix D

$$D_{[x,y]} = [0] \quad (7.5)$$

From the output matrix C, the output can be set to be the displacement, velocity or both. Here for this case the first row of the output matrix C is referring to the total displacement; whereas the second, third and forth rows are related to the velocities in model coordinates.

7.3 **Energy Analysis for 3-Dof System**

In Section 5.3 (Chapter 5), the system boundary was defined for a single degree of freedom system in two directions. However, in this Section the system dynamics are represented with three-degree of freedom, the system was described by a coupled a

three equations of motion in two directions x and y, as shown in Figure 7.3(a). After decoupling the system equations of motion, the system dynamics can be represented by an equivalent uncoupled mass, stiffness and damper as shown in Figure 7.3(b) (see Appendix C2). This allows the system equations of motion to be solved as a single degree freedom procedure. Then the system boundary is defined as internal components and the surrounding effecters in both directions as shown in Figure 7.4(a). Briefly, as shown in Figure 7.4(b), the equivalent internal and external components that are acting on the system boundary in *x* and *y* directions are: inertia forces ($\widehat{\mathrm{M}}_{\mathrm{x}}\ddot{\mathrm{x}}$) and$\left(\widehat{\mathrm{M}}_{\mathrm{y}}\ddot{\mathrm{y}}\right)$, spring forces ($\widehat{\mathrm{K}}_{\mathrm{x}}\mathrm{x}$) and ($\widehat{\mathrm{K}}_{\mathrm{y}}\mathrm{y}$), structural damping forces ($\hat{\mathrm{C}}_{\mathrm{x}}\dot{\mathrm{x}}$) and ($\hat{\mathrm{C}}_{\mathrm{y}}\dot{\mathrm{y}}$) and the total cutting forces F_x and F_y. It should be pointed out that these cutting forces are composed of the idealised forces (F_{idl}), process damping forces (F_{pd}), and loss of contact forces (F_{loc}). The relationship between these forces has been explained previously in chapter 5.

Now, having defined all these forces, the corresponding work done on the system can be determined. Figure 7.4(c) shows the direction of the work done on the system; a positive sign means the work will be done on the system so the energy will flow into the system, whereas a negative sign means the work will be done to flow the energy out of the system. Briefly here, idealised work done $W_{idl_{(x,y)}}$ has a positive direction in x and y. This means this energy is always transmitted into the system. However, the work done by the structural damping $W_{s_{(x,y)}}$, loss of contact $W_{loc_{(x,y)}}$ and the process damping $W_{pd_{(x,y)}}$ for x and y directions are negative. This means the work done here is always for dissipating the energy from the system. It should be noted that all these energies are directly calculated in the model using the simple Simulink blocks shown in Figure 7.5 .

With reference to the same Figure 7.5, the state-space function is represented by a Simulink block to evaluate the system dynamics and determine the total system displacement and three detached velocities in model coordinates. These detached velocities are corresponding with each mode. Now, each velocity is used to determine the corresponding mode's structural energy. The velocity of the first mode v_1 is used to calculate the energy from the first structural damping mode$\hat{\mathrm{c}}_1$, whereas the second and

third mode's velocities v_2 and v_3 are used for computing the energies of the second and third structural damping modes $\hat{c}_2$ and $\hat{c}_3$ respectively. Then these energies are summed together to produce the total structural damping energy of the system (W_s).

However, the loss of contact energy (W_{loc}), process damping energy (W_{pd}) and the idealised energy (W_{idl}) are calculated from the total system velocity ($\dot{z}$) which is determined by summing together all the mode velocities after they have been scaled by their eigenvectors ($\emptyset$) (see Appendix C2). This means, each mode velocity is multiplied by its eigenvector as following:

First mode: $\dot{z}_1 = v_1 . \emptyset_1$

Second mode: $\dot{z}_2 = v_2 . \emptyset_2$ (7.6)

Third mode: $\dot{z}_3 = v_3 . \emptyset_3$

Total scaled velocity : $\dot{z} = \dot{z}_1 + \dot{z}_2 + \dot{z}_3$

The procedures of calculating the energy behaviour are expressed by the equation (7.7).

$$W_{s[x,y]} = \int_{t_1}^{t_2} \hat{c}_1 . v_1^2 dt_{[x,y]} + \int_{t_1}^{t_2} \hat{c}_2 . v_2^2 dt_{[x,y]} + \int_{t_1}^{t_2} \hat{c}_3 . v_3^2 dt_{[x,y]}$$

$$W_{loc[x,y]} = \int_{t_1}^{t_2} F_{loc} . \dot{z}\, dt_{[x,y]}$$

$$W_{pd[x,y]} = \int_{t_1}^{t_2} F_{pd} . \dot{z}\, dt_{[x,y]} \quad (7.7)$$

$$W_{idl[x,y]} = \int_{t_1}^{t_2} F_{idl} . \dot{z}\, dt_{[x,y]}$$

All these energies are calculated in both directions x and y. In order to measure the system stability through the energy balance approach, these energies which are crossing the system boundary are summed.

$$W_{idl[x,y]} = W_{loc[x,y]} + W_{pd[x,y]} + W_{s[x,y]} \quad (7.8)$$

It should be reiterated that the instantaneous determined energies shown in Equation (7.8) are accumulative energies with units in Joules (J). However, in this chapter, energy

rates in joule/revolution (J/rev) are also used to investigate the degree of stability due to the variable helix tools and the process damping phenomenon effects.

7.4 **Simulation Approach**

In the Simulink model, a non-uniform helix introduces a different pitch angle at each axial segment of the cutter. In this Chapter, variable helix angles are defined by the Matlab codes (Appendix D4). The variable angles are defined according to the total tool teeth number N_t and along the discretised axial layers l (Figure 7.6), then the values of the helix angles are stored in an array with size $[l, N_t]$.

$$\lambda = \begin{bmatrix} \lambda_{h[1\ 1]} & \cdots & \lambda_{h[1\ N_t]} \\ \vdots & \ddots & \vdots \\ \lambda_{h[l\ 1]} & \cdots & \lambda_{h[l\ N_t]} \end{bmatrix} \tag{7.9}$$

Experimental data from two confirmed studies are considered to analyse the chatter stability due to the influence of variable helix tools and the process damping mechanism. For the scenario of the one degree of freedom system, the experimental data at the low radial immersion (summarised in Table 7-1) was selected from [20] to represent the dynamics parameters of the tool and the workpiece. However, for the second milling scenario the investigation is carried out along the simulation parameters listed in Table 7-2 which represents a small selection from the experimental work in [90].

Having finalized all the simulation parameters, Matlab codes are used to define the values of the helix angles and store them in an array (Equation 7.9). Then the simulation is carried out along the selected parameters to calculate the cutting forces which are composed of the idealised, loss of contact and process damping forces. Next, along with the total cutting forces, the system dynamics are modelled as a spring-mass-damper (Figure 7.7) for a one degree of freedom system, whereas it is modelled in a state-space formulation (Figure 7.5) for a 3-DOF system to determine the system displacements and velocities. The obtained system velocities are then multiplied by the related forces to determine the instantaneous power that corresponds with each force. Then each of the instantaneous powers is directly integrated in the model with respect to the time to

calculate the cumulative energy. The cumulative energies obtained directly from the model are: the idealised energy (W_{idl}), loss of contact energy (W_{loc}), structural damping energy (W_s), and the process damping energy (W_{pd}). Then the energy rates per revolution are calculated by dividing the instantaneous cumulative energies by the instantaneous tool revolutions which are W_{ridl}, W_{rloc}, W_{rpd} and W_{rs}. Now, after all the energies are defined, the degree of stability along the regular and variable helix tools are measured and compared. In addition, the performance of the process damping along the regular and variable helix tools is measured and compared to the loss of contact behaviour.

In addition, arc surfaces including rubbing behaviour due to the variable and the regular helix tools effects are also investigated. The components of the arc surface data in *x* and *y* directions are extracted from the model at the last data point of the tool revolution. Here one step time contains a full revolution of data points to define the arc surface for all of the axial layers l and the number of the cutting teeth N_t. These data are then stored in an array with dimensions $[l \times N_t]$. Rubbing data are also extracted from the last tool revolution.

Arc's surfaces including the rubbing behaviour were firstly defined along the Cartesian coordinates *x* and *y*. However, these plots did not offer a clear representation for the arc surface behaviour. Therefore polar coordinates were proposed to be an alternative way to demonstrate the machined arc surface behaviour. Consequently all the Cartesian data are converted to polar coordinates after the linear trends and feed rate displacement are removed. This means each data point is defined by the radius (r_p) and its angle (θ_p). This procedure is performed through Matlab codes (see Appendix D5).

7.5 Results and Discussion

7.5.1 Variable Helix Tool in SDOF System

Yusoff et al [20] investigated the stability of a regular and variable helix tool under process damping conditions. Their work was purely experimental, with no modelling of the system. They used a custom-built flexible workpiece to provide a tightly controlled single degree of freedom system. The experimental procedure involved increasing the spindle speed for a given depth of cut, until severe chatter occurred. This spindle speed was then rewritten as a chatter wavelength (process damping wavelength) based on the cutting conditions. They found that the regular helix tool become unstable at spindle speeds above 255 rpm ($\lambda_c \cong 1.06\text{mm}$, Fig11,[20]), whereas the variable helix tool remained stable until at least 600 rpm. The aim of this section is to compare Yusoff's experimental results with that from the Simulink model, and to use the energy analysis method to explore the process damping provided by each tool.

Figure 7.8 compares the behaviour of the chip thickness variations for both regular and variable helix tools. This comparison is made at the last tool revolution and with the same cutting conditions. In general, when the system is stable the output chip thickness is a smooth shape, whereas it becomes jagged when the system loses stability. For the regular tool (Figure 7.8 (a)) the behaviour of the chips' thickness obtained by three cutting teeth results in equal spaces and the same amplitudes. It is quite obvious here that chatter is very severe which makes the teeth lose their contact to zero. This behaviour makes the output shape of the chips' thickness spiky. However, for the variable helix tool (Figure 7.8 (b)), it is very clear the behaviour of the obtained chips' thickness results in irregular spaces and different amplitudes. In addition, the chatter is not severe here compared to the regular helix tool (Figure 7.8 (a)).

Now from this comparison it can be concluded that a regular tool provides higher chip variation compared to that obtained from the variable helix tool in Figure 7.8 (b). Consequently loss of contact energy rates for the regular tool become higher than the variable helix tools. On other words, a variable helix tool is more stable compared to a regular tool.

Figure 7.9 shows the behaviour of the process damping and loss of contact energy rates due to the regular tool. As can be seen in Figure 7.9(a), along the first 9 tool revolutions the idealised W_{ridl} and the process damping W_{rpd} energy rates have a sharp increase. However, the idealised energy rates W_{ridl} are then changed to have a steady increase and record about 0.125J/rev at the last tool revolution, whereas the energy rates from the process damping W_{rpd} and loss of contact W_{rloc} are respectively stabilised at 0.077 J/rev and 0.022 J/rev.

The performance of the process damping is compared to loss of contact behaviour as shown in Figure 7.9(b). Here the process damping and the loss of contact energy are measured in percentage using equation (6.3). It is very obvious here that after the first 9 revolutions the energy dissipated by the process damping mechanism remains almost constant at 61.5%, whereas the energy dissipated by the loss of contact behaviour remains at 17.5%. The most interesting result that can be drawn here is that at the beginning of the cut the process damping performance was significantly higher in dissipating the vibration energy, which effectively inhibits the loss of contact energy.

Now, the regular cutting tool is replaced by a variable helix tool and the simulation is repeated along the same cutting conditions. Behaviours of the transmitted and dissipated energy rates are significantly changed as shown in Figure 7.10. From Figure 7.10(a), it can be seen that the rates of the transmitted energy are stabilised at $W_{ridl} = 0.0065$ J/rev, whereas process damping dissipates the vibration energy at $W_{rpd} = 0.005$ J/rev. However loss of contact energy W_{rloc} has almost vanished here. This can be attributed to the process damping effects which become sufficient to dissipate the imposed vibration energy. This can be clearly observed in Figure 7.10(b) which shows that process damping dissipates almost 73.7 % of the total energy. However there is no loss of contact energy recorded, and as a consequence the vibration energy here is totally dissipated by both the process damping and structural damping.

Figure 7.11 demonstrates the predicted behaviour for both tools across a range of spindle speeds. Here, the loss of contact energy rate is compared to the process damping energy rate. It can be seen that for the regular pitch/helix tool, the two energy

dissipation mechanisms have similar magnitudes once the speed is more than 270 rpm. In contrast, the variable helix tool has very small levels of loss of contact energy dissipation rate for the majority of spindle speeds. Meanwhile, the process damping energy dissipation rate is considerably higher. This suggested that for some reason the variable helix tool is able to reach a steady-state limit cycle with much lower energy dissipation rates than the regular tool. Furthermore, for many of spindle speeds, the energy rate associated with loss of contact is very small.

The results in Figure 7.11 show repeating patterns that are consistent with the stability lobes for each of the two tools. This is further illustrated in Figure 7.12. Here, the semi-discretisation method [126] is used to obtain stability lobe diagrams (Figure 7.12 (a)). The stability boundary is defined by the depth of cut where the semi-discretisation method predicts a characteristic multiplier (*CM*) greater than or equal to 1. Consequently, Figure 7.12 compares the energy dissipation for the regular (Figure 7.12(b)) and variable helix (Figure 7.12(c)) tools to the magnitude of the *CMs* (Figure 7.12(d)), at the depth of cut is 2mm.

At low spindle speeds, the variable helix tool appears to have much higher *CMs* than the regular tool, which suggests that the tool should have been more unstable. This makes it more surprising that the variable helix tool was deemed ‘chatter free’ or ‘process damping’ in both the corresponding experiments [20] and the simulation analysis (Figure 7.12(c)).

In order to explore this further, the rubbing and loss of contact mechanisms on the arc surface behaviour are investigated further. Small results are presented in Figure 7.13 which are selected at the cutting condition spindle speed ω=255 rpm and depth of cut *b*=2mm. Here the behaviour of the arc’s surfaces at the axial layer number *l*=10 with rubbing effects are presented in the polar coordinates. Each data point here is represented by the radius r_p and its inclination angle θ_p is measured from the tool centre. Now a clear representation for the arc surfaces including the loss of contact and rubbing behaviour effects are presented in Figure 7.13. Results of the regular tool are shown in Figure 7.13(a); it is very clear to see here that amplitudes of the arc’s surfaces and the

phase difference are almost similar along the cutting passes. Moreover, it can be seen that rubbing and loss of contact are both occurring as illustrated respectively by the "■" and "●" markers. Here more loss of contact happens compared to rubbing.

Now, results of the variable helix tool are shown in Figure 7.13 (b). It is quite clear here that waveform's amplitudes and the phase delay are irregular. It can also be noticed that at some stages of the cut, some teeth are cutting with same phase. In addition, rubbing behaviour is clearly higher here as highlighted by "■" markers in Figure 7.13(b). It seems process damping effects are sufficient enough here to dissipate the vibration energy which prevents loss of contact from arising.

7.5.2 **Variable Helix Tool in 3-DOF System**

In this section investigations are carried out to consider the influence of the variable helix tools on the system stability with a three degree of freedom. The aims here are to consider cutting conditions that are similar to those used experimentally by Turner et al [90], when they first proposed that variable helix tools offer enhanced process damping. This also allows more validation for the energy approach in analysing the machining stability with more complex system dynamics.

Now, for the regular and the variable helix tools, results of the process damping and loss of contact energy rates are presented in contour plots, as shown respectively in Figure 7.14 and Figure 7.15. These contour plots are performed along the cutting speeds $\omega = 3500$ to 5000 rpm for different depths of cut up to b=3mm. Here it can be seen that energy dissipation levels are increasing as the depth of cut becomes greater. However, beyond the depth of cut b=2.5 mm process damping energy rates become clearly lower than the loss of contact for the regular tool (Figure 7.14), whereas in contrast for variable helix tool (Figure 7.15).This can clearly be observed in Figure 7.16 which compares the process damping and loss of contact energy rates for a variable helix tool in plot (a) and the regular tool in plot (b). It is very clear that for the variable helix tool, process damping becomes effective in dissipating the energy just after the depth of cut b=1mm, with energy rates that are higher than the loss of contact along all the depths of the cut (plot (a)). Almost the same behaviour for the regular tool is also

shown (plot (b)), however loss of contact energy rates become dominant at the depth of cut at almost b=2.5mm.

Further comparisons between the regular and variable helix tool's performance are presented in Figure 7.17. Along these cutting conditions, the produced process damping energy rates from both tools are linearly increased with almost the same levels (plot (a)). However, the obtained loss-of-contact energy rates from both tools are exponentially increased and are much higher for the regular tool (plot (b)).

Further investigations of the regular and variable helix tool's effects on the stability behaviour are performed at greater depths of cut. For the variable helix tool, the behaviour of the loss of contact and the process damping energy rates are also presented in contour plots as shown respectively in Figure 7.18(a) and Figure 7.18(b). It is very obvious beyond the depth of cut b=3.25mm, energy rates of the process damping are clearly lower than that obtained from the loss of contact behaviour. This can be attributed to chatter levels become so severe here causing more loss of contact which in turn leads to more reduction in the rubbing behaviour. For the regular tool, results of the loss of contact and process damping energy rates are also presented in contour plots as shown respectively in Figure 7.19(a) and Figure 7.19(b). It is quite clear here loss of contact energy rates are considerably higher compared to the process damping energy rates. This can be attributed to the vibration amplitudes were grown more severely here compared to that of variable helix tool (Figure 7.18). In addition, energy rates of the loss of contact become significantly high at the depth of cut b=4.5mm where the system becomes completely instable causing a simulation failure.

In summary, compared to a regular tool, the degree of stability of a variable helix tool is higher due to more rubbing which occurs and which leads to more energy dissipation.

7.6 **Summary**

In this chapter, a comparison of the milling stability for the regular and variable helix end mills is presented using a new analysis approach. The energy approach has analysed the effects of the variable helix tools on machining stability through the time domain simulation. In addition, this approach has enhanced the possibility of investigating the variable helix and pitch tools under the process damping effects.

Stability behaviour of the regular and variable helix tools was investigated by comparing behaviours of the loss of contact and the process damping energy rates, which showed a reasonable correspondence with the stability lobes and the characteristic multiplier's behaviours. Variable helix tools showed greatly enhanced stability compared to a regular tool, especially at low speeds.

Rubbing behaviour and loss of contact effects are presented on the workpiece surface. The phase delay between any subsequent arc's surfaces was disrupted along the variable helix tool, whereas it remains uniform for a regular tool. In addition, a regular tool provides high chip thickness variation compared to the variable helix tool behaviour.

Process damping performance has been investigated along with the variable helix tool's effects. The time domain model has offered a comprehensive representation of the kinematics of milling, including the process damping phenomena. However it does not offer a reasonable explanation for the case observed from the empirical results in (VH4 Fig1) [90], which did not match with the model's results.

The developed energy analysis is considered as a capable approach for measuring and investigating the interaction between the variable helix tool's performance under the process damping effects that can be utilized both in designing new milling cutters and in identifying cutting parameter regions of extremely high material removal rates.

Now, this approach will be further implemented to investigate the performance of the short regenerative effect on the milling stability compared to the process damping due to the flank interference mechanism. This subject will be presented in the next chapter.

Simulation parameters of 1-DOF system	
Iterations per cycle (–)	1280
Number of axial layers l (–)	30
Radial cutting force coefficient $\boldsymbol{K_{rc}}$ (N/mm^2)	187.5
Tangential cutting force coefficient $\boldsymbol{K_{tc}}$ (N/mm^2)	1250
Process damping friction coefficient (–)	0.3
Process damping normal force coefficient $\boldsymbol{K_{np}}$ (N/mm^3)	40
Number of teeth N_t (–)	3
Tool diameter D (mm)	16
Tooth flank length l_f (mm)	0.2
Tool relief angle $\boldsymbol{\gamma}$ (deg)	6
Tool helix angle $\boldsymbol{\lambda_h}$(deg)	30
Tool variable helix angles $\boldsymbol{\lambda_{hv}}$(deg)	48,44,43
Tool variable pitch angle $\boldsymbol{\varphi_{pv}}$(deg)	84, 220, 55
Depth of cut b (mm)	2
Radial immersion re (mm)	1
y-direction natural frequency (Hz)	200
mass (kg)	1.41
y-direction damping ratio (–)	0.0078

Table 7-1 simulation parameters for one degree system dynamics

Simulation parameters for 3-DOF system	
Iterations per cycle (–)	1280
Number of axial layers l (–)	40
Radial cutting force coefficient K_{rc} (N/mm^2)	160
Tangential cutting force coefficient K_{tc} (N/mm^2)	400
Radial cutting edge force coefficient K_{re} (N/mm^2)	30
Tangential cutting edge force coefficient K_{te} (N/mm^2)	26
Process damping friction coefficient _ (–)	0.3
Process damping normal force coefficient K_{np} (N/mm^3)	40
Number of teeth N_t (–)	4
Tool diameter D (mm)	16
Tooth flank length l_f (mm)	0.5
Tool relief angle γ (deg)	7
Tool helix angle λ_h(deg)	35
Tool variable helix angles λ_{vh}(deg)	35, 40, 35, 40
Tool variable pitch angle φ_{vp}(deg)	107, 73, 107, 73
Depth of cut b (mm)	(Vary)
Radial immersion r_e (mm)	16
Spindle Speed ω *(rpm)*	4000
***Modal parameters in x-direction*:**	
Natural frequency f_{nx} (Hz)	2061, 2609, 3032
Stiffness K_x (N/m)	1.932e7,5.192e7, 4.433e8
damping ratio ζ_x (–)	0.0162, 0.0541, 0.0129
***Modal parameters in y-direction*:**	
Natural frequency f_{ny} (Hz)	2058, 2444, 2992
Stiffness K_y (N/m)	1.886e7, 9.190e7, 1.902e8
damping ratio ζ_y (–)	0.0227, 0.0224, 0.0164

Table 7-2 simulation parameters for 3-degree of freedom system

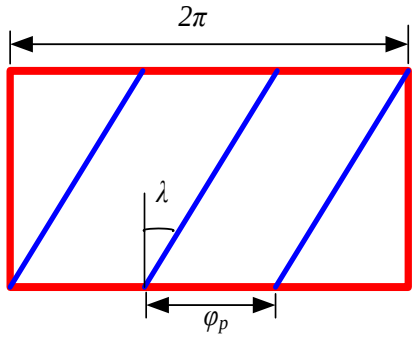

(a) Uniform helix with equal pitch

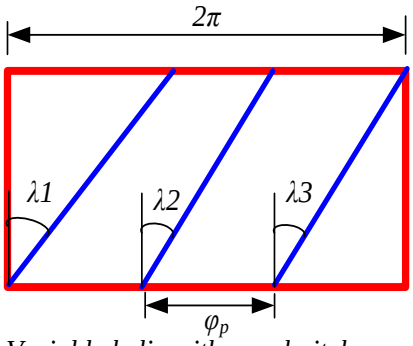

(b) Variable helix with equal pitch

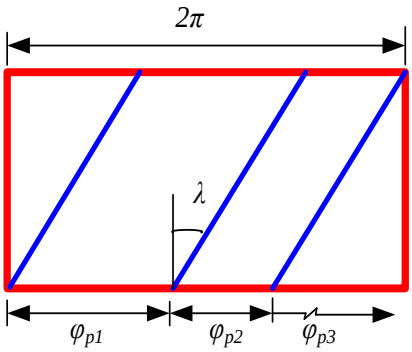

(c) Uniform helix with variable pitch

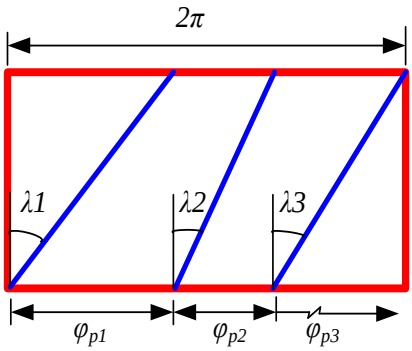

(c)Variable helix with variable pitch

Figure 7.1 Angular position of edges for end mills on tool circumference (a) End mill with equal pitch. (b) End mill with variable helix angle and equal pitch. (c) End mill with uniform helix and variable pitch angle. (d) End mill with both variable helix and variable helix angles.

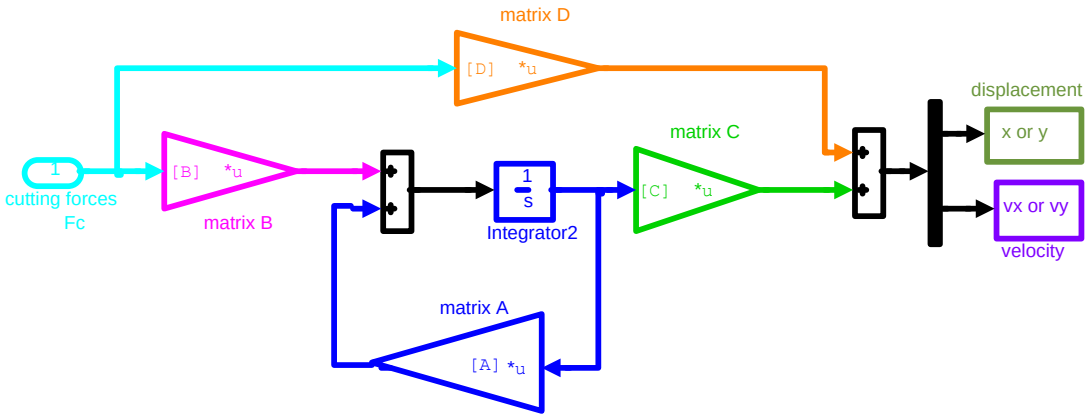

Figure 7.2 State Space in Simulink blocks form.

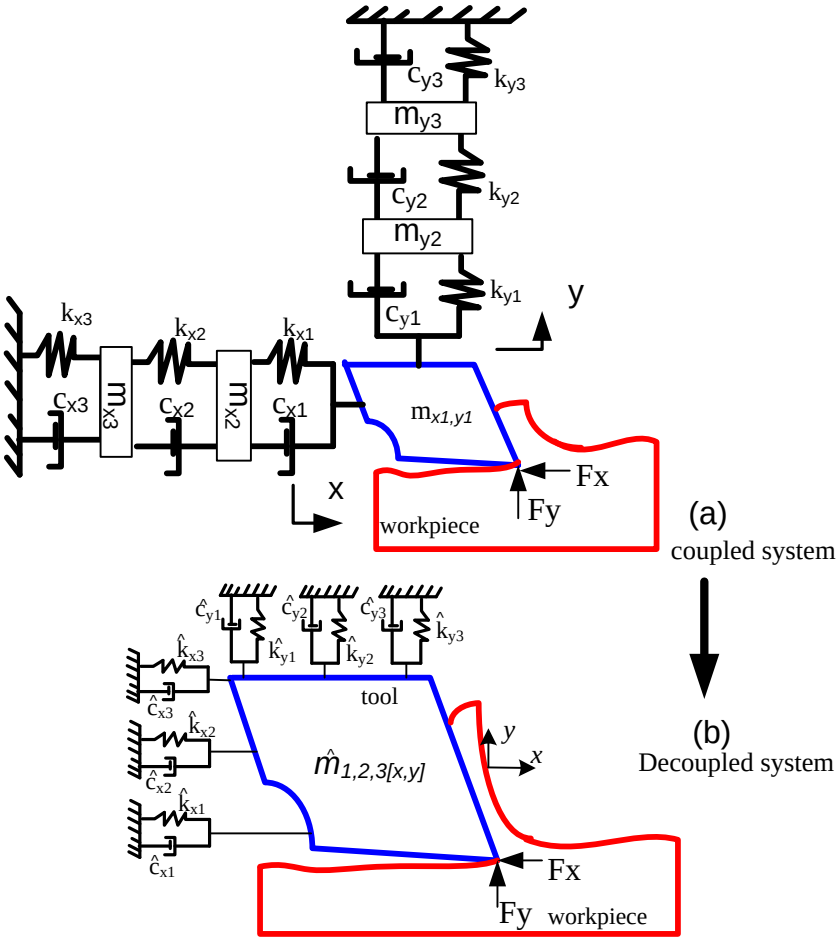

Figure 7.3 Two directional milling with 3DOF system

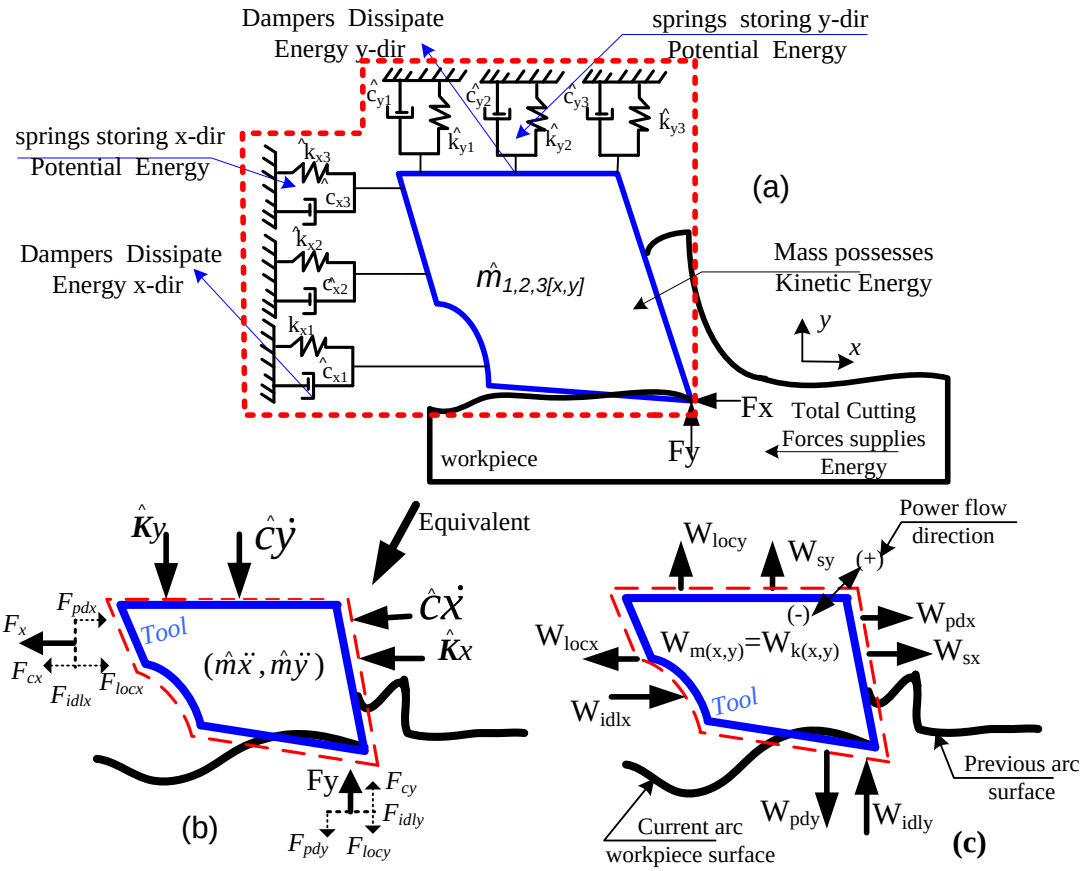

Figure 7.4 (a) system dynamics with equivalent mass, damper and spring, (b) forces acting on the system boundary, (c) energy behaviour acting on the system boundary

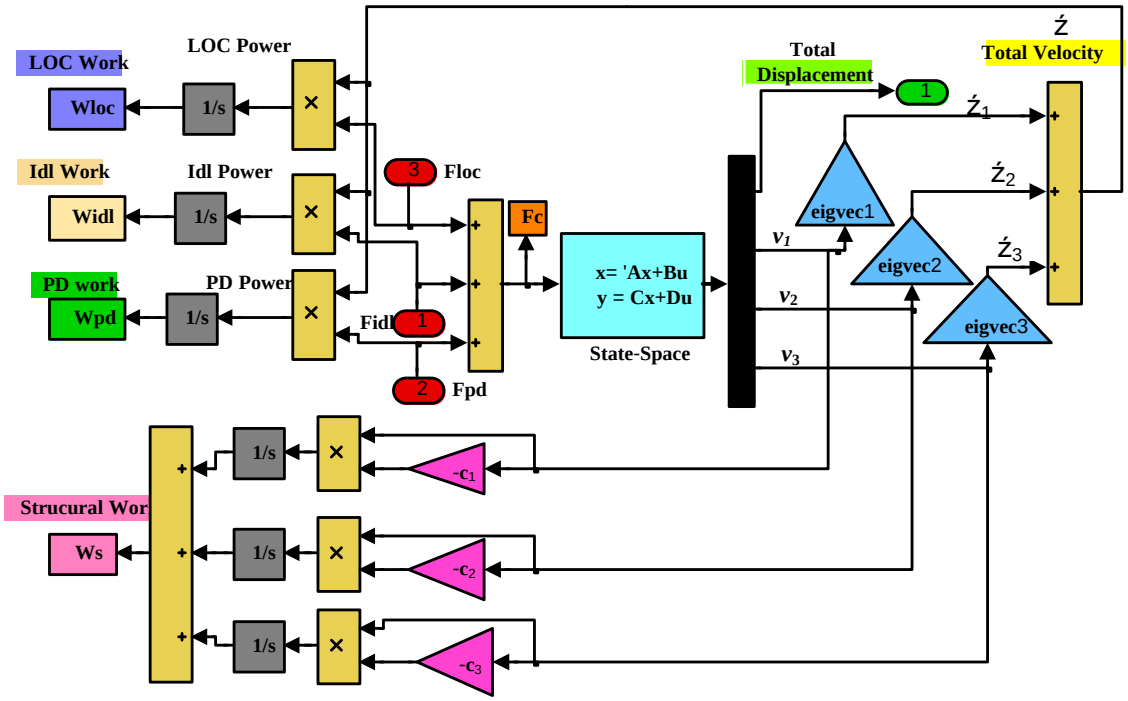

Figure 7.5 System dynamics in Simulink blocks

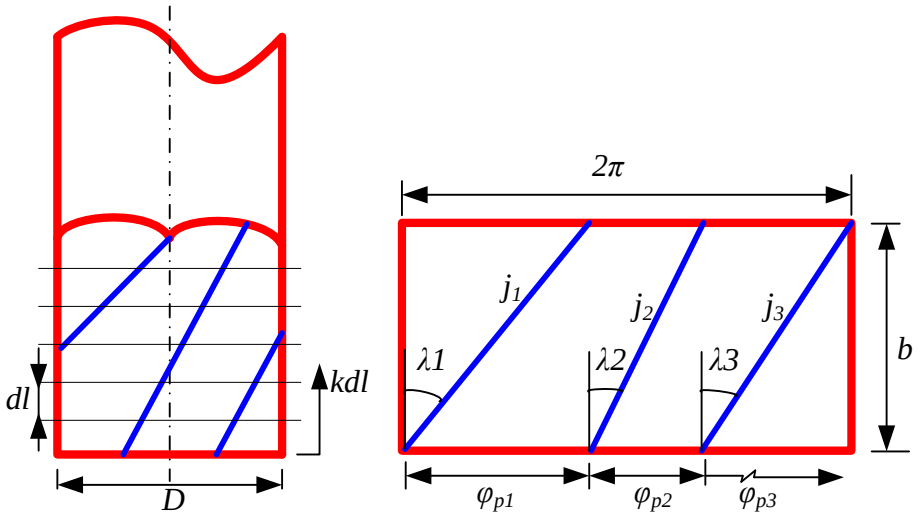

Figure 7.6 Discretisation of tool into axial slices

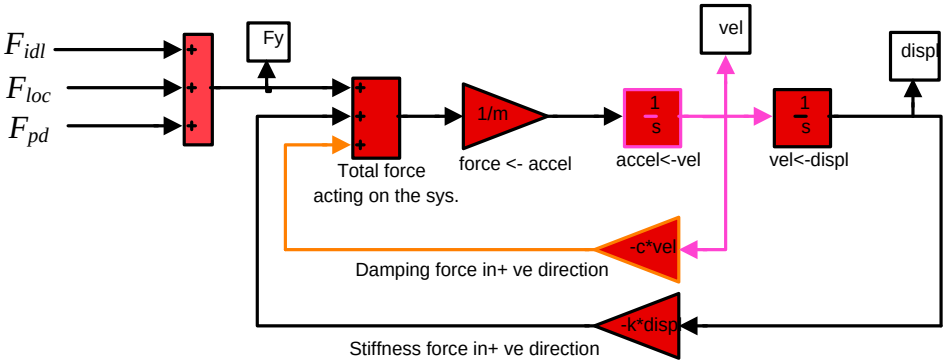

Figure 7.7 system dynamics are modelled as spring-mass-damper

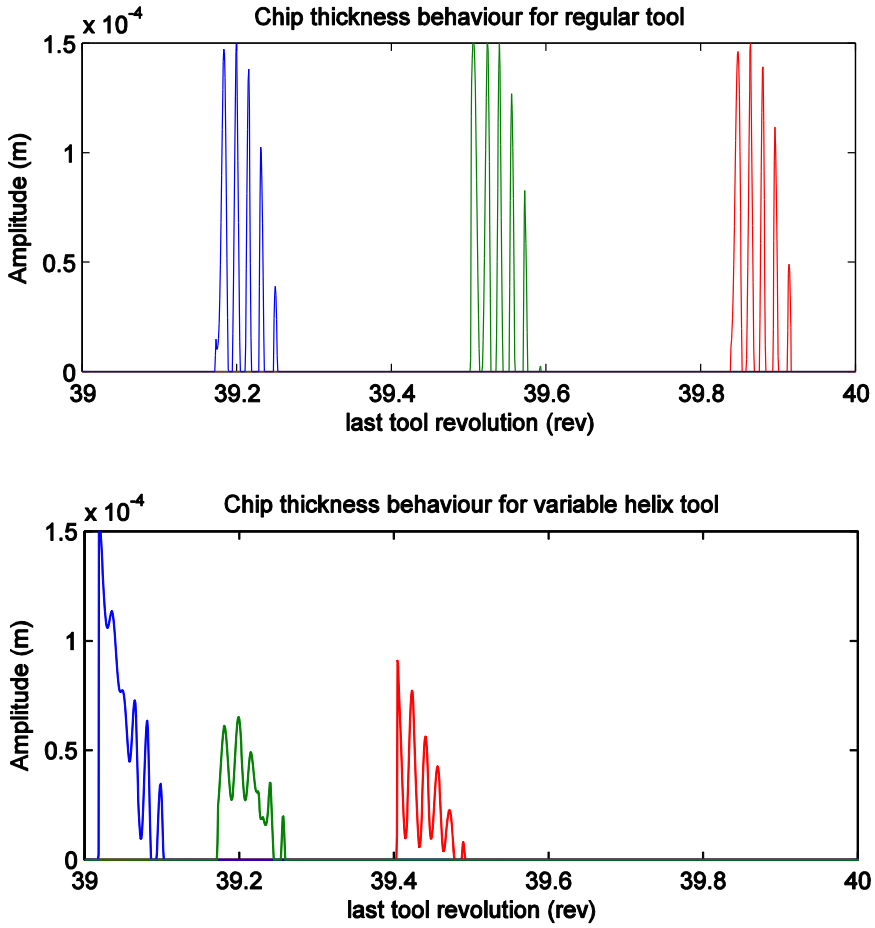

Figure 7.8 chip thickness variation at the last tool revolution, (a) regular tool, (b) variable helix tool.

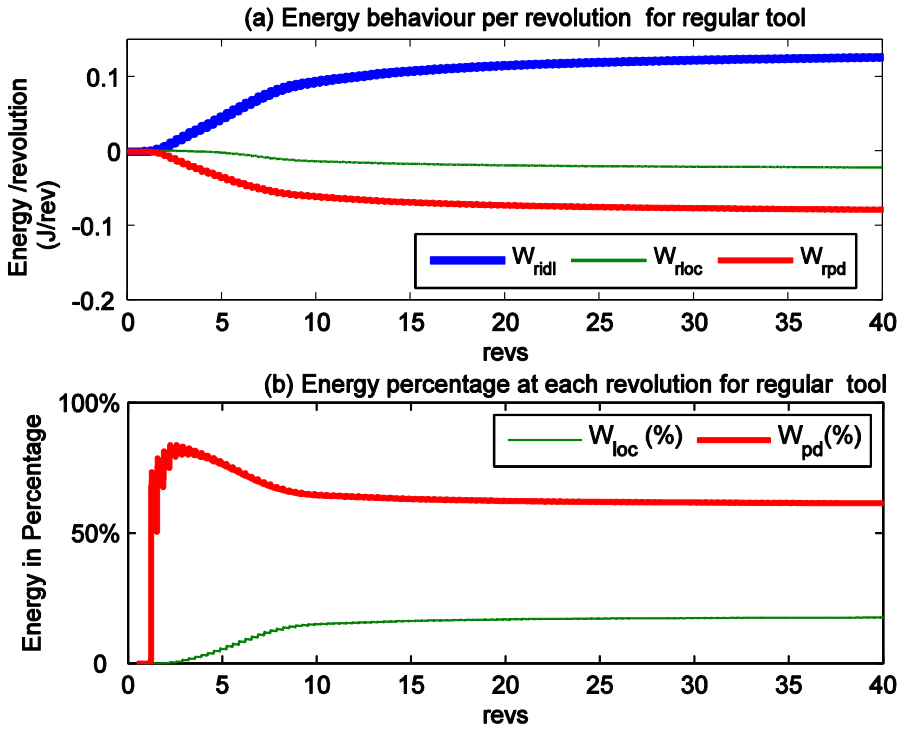

Figure 7.9 Energy behaviour for the regular tool

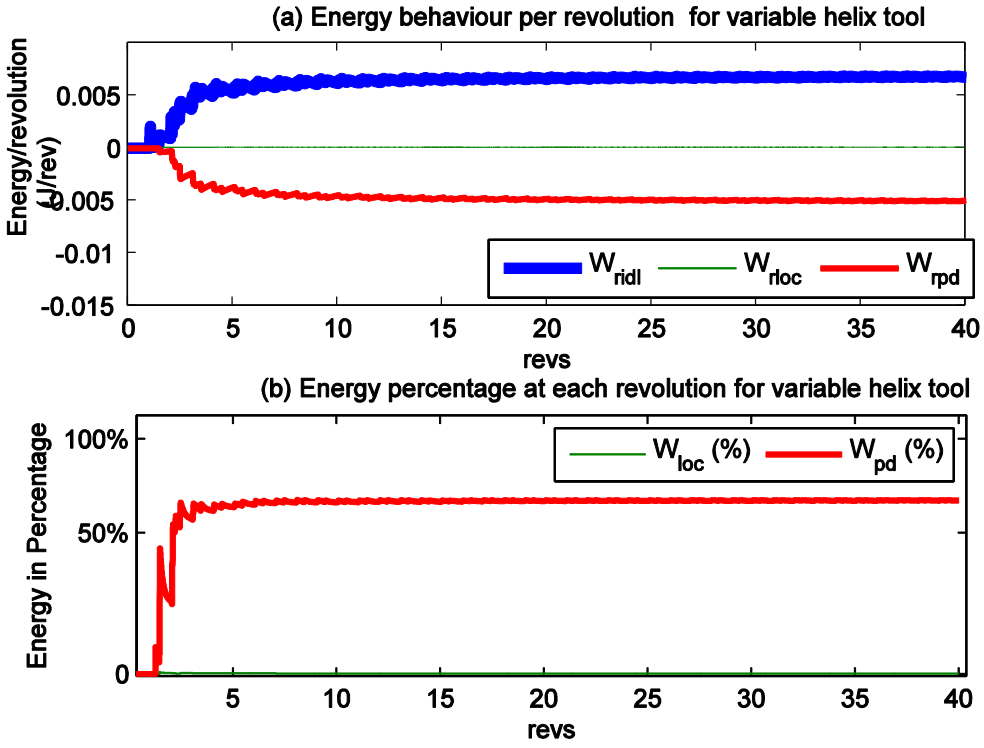

Figure 7.10 Energy behaviour due to the variable helix tool

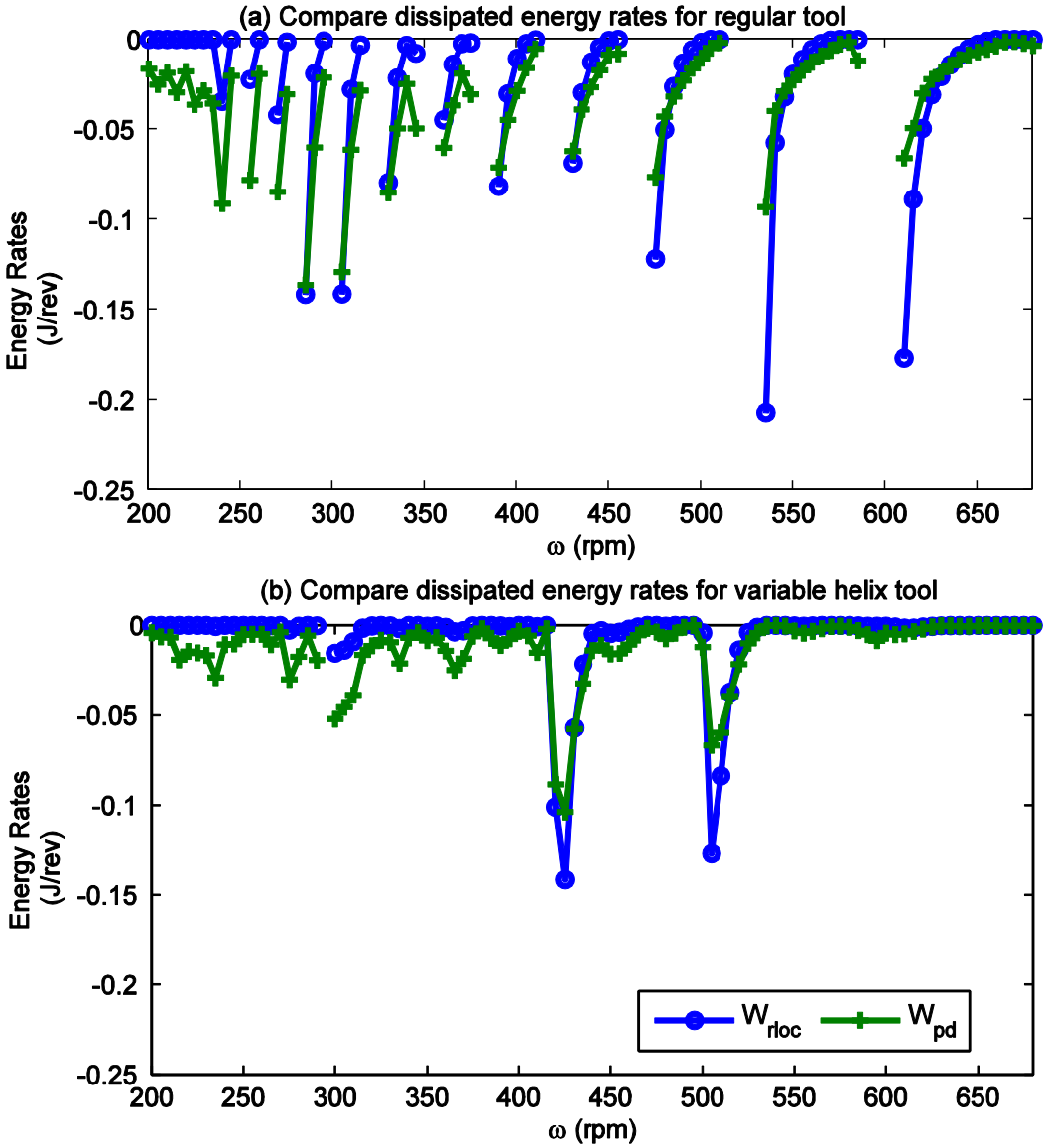

Figure 7.11 comparison of the process damping and loss of contact energy dissipation for different cutting speeds, (a) regular tool at *b*=2mm, (b) variable helix tool at *b*=2mm.

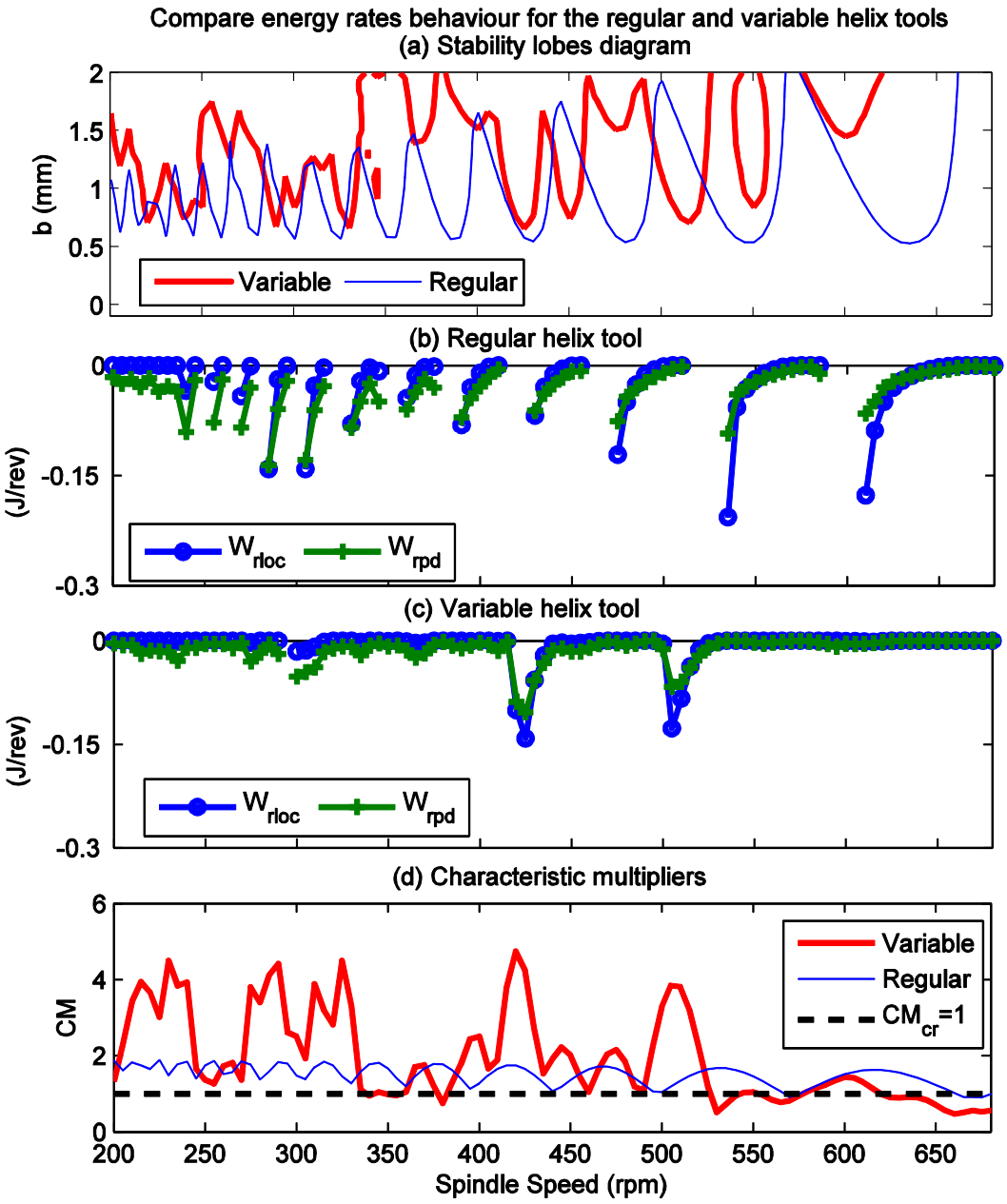

Figure 7.12 compare behaviours of (a) stability lobes diagram, (b) loss of contact energy rates at *b*=2mm, (c) process damping energy rates at *b*=2mm and (d) characteristic multipliers at *b*=2mm.

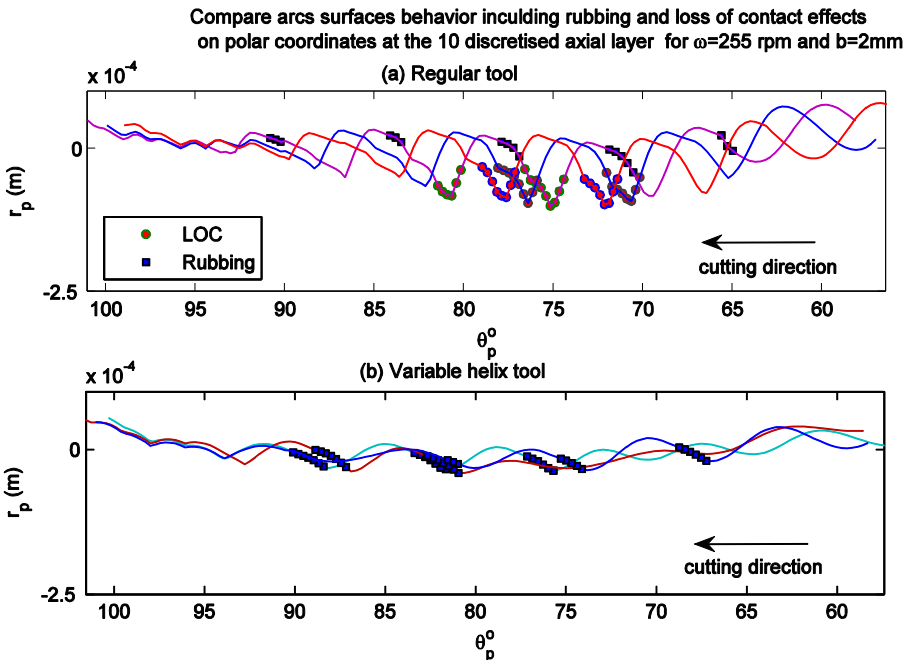

Figure 7.13 Arc surfaces, loss of contact and rubbing behaviours

(a) regular tool (b) variable helix tool

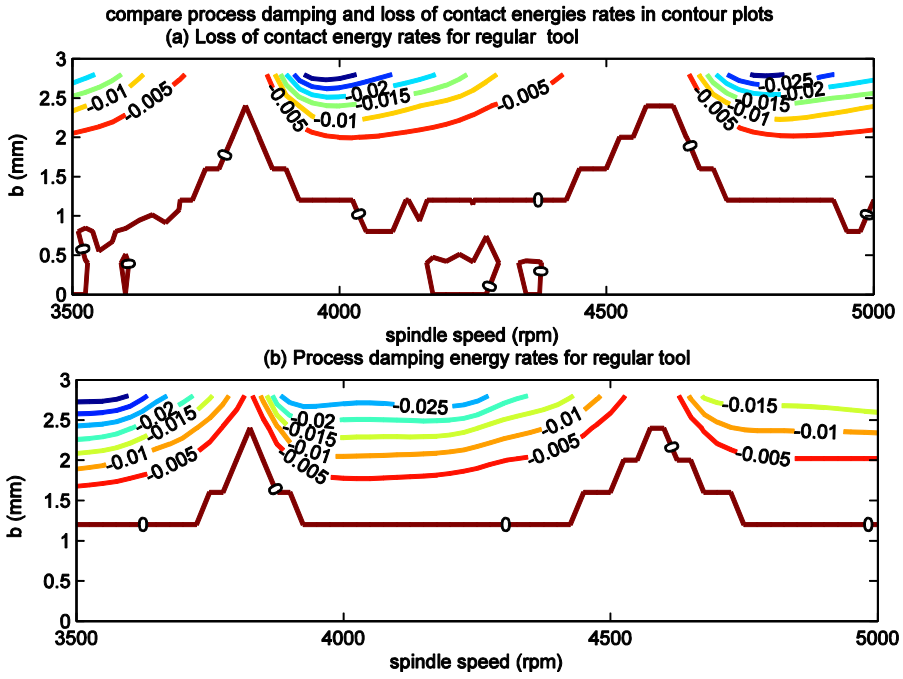

Figure 7.14 compare energy behaviour when regular tools are used

(a) loss of contact (b) process damping

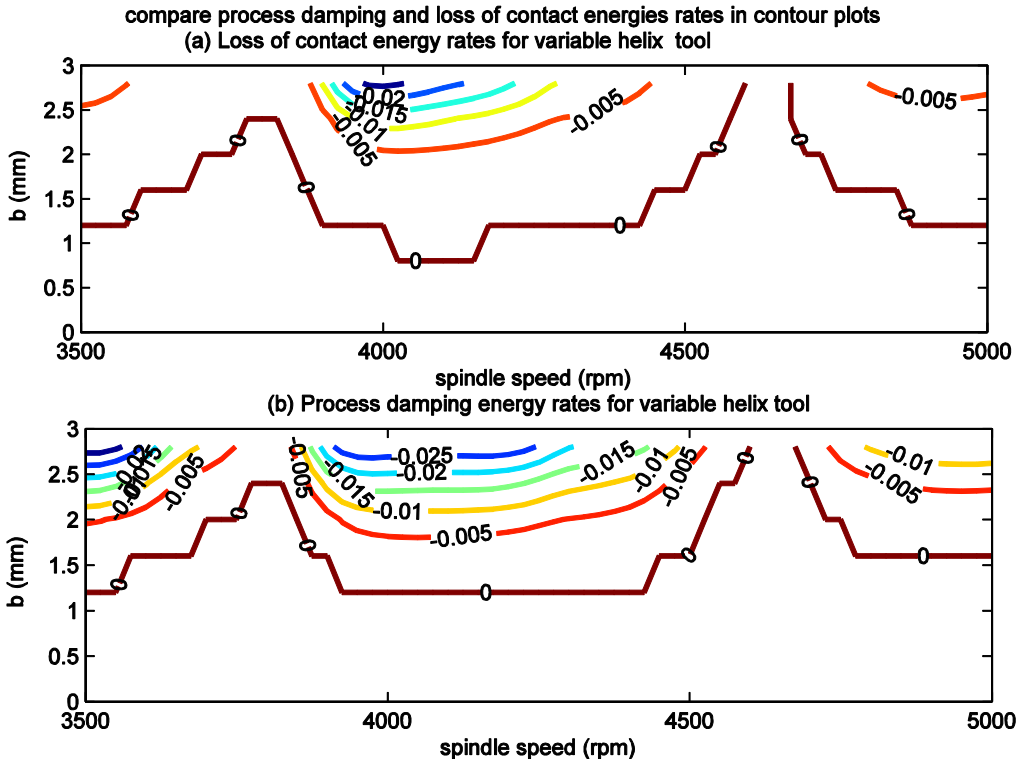

Figure 7.15 compare energy behaviour when the variable helix tools are used (a) loss of contact (b) process damping

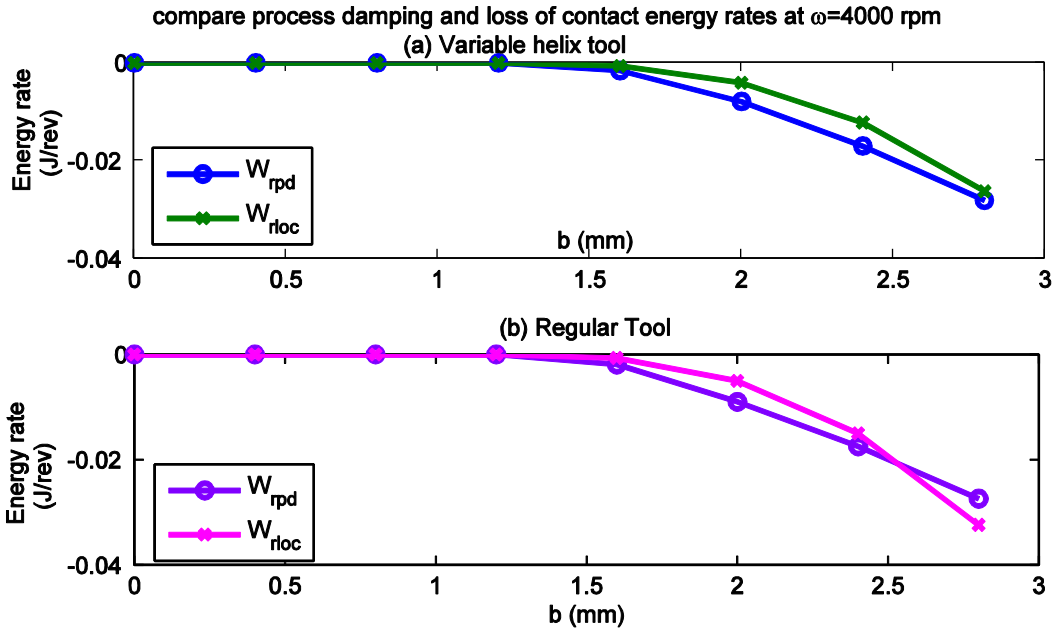

Figure 7.16 compare energy behaviour (a) variable helix tool (b) regular tool

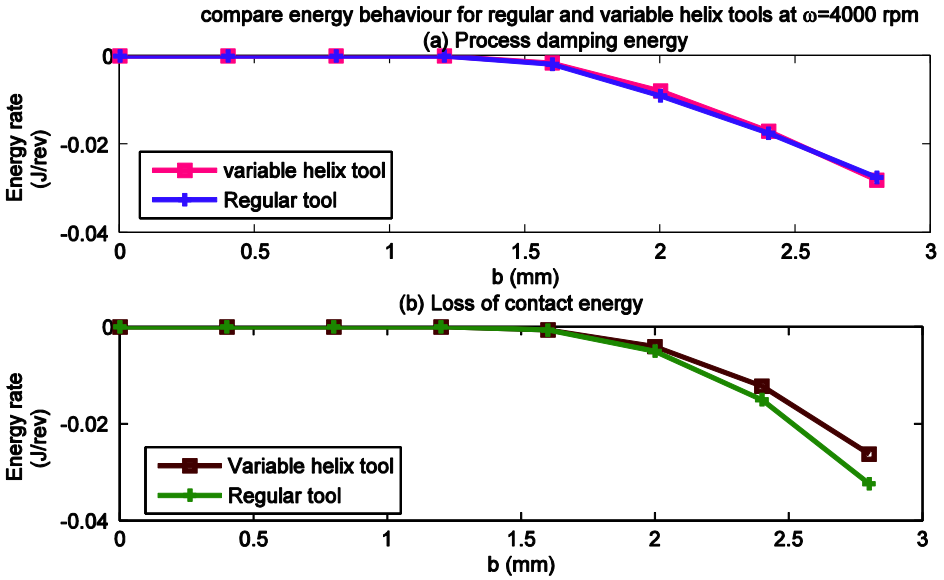

Figure 7.17 compare regular and variable helix tools performance

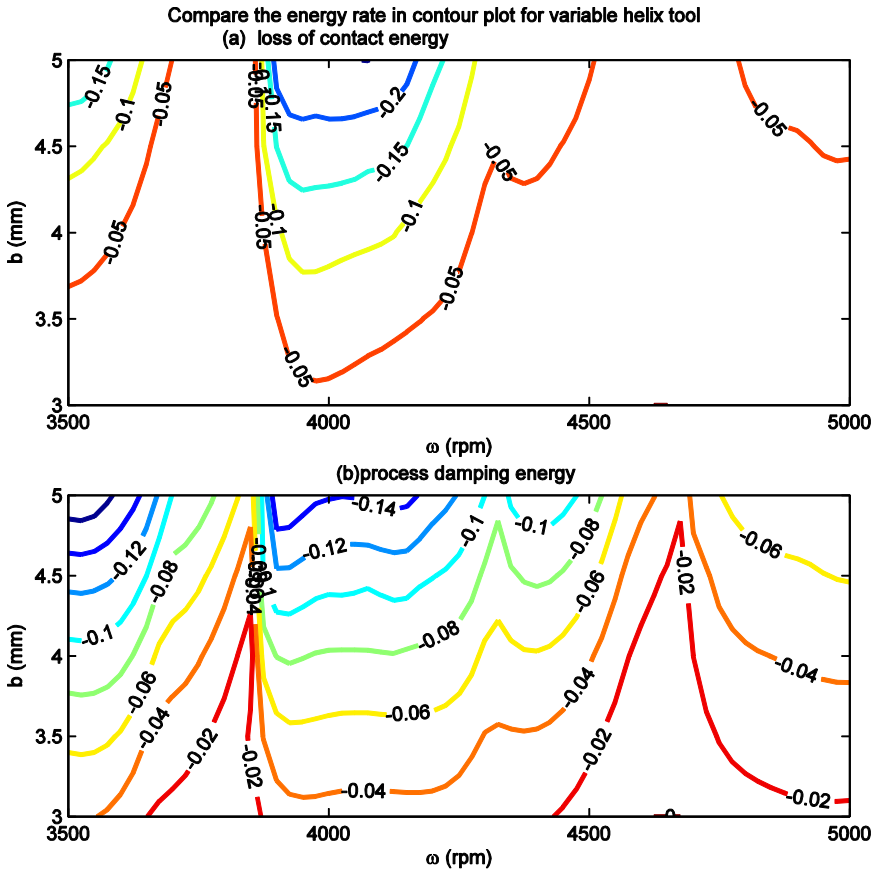

Figure 7.18 compare energy rates in contour plots for variable helix tool (a) loss of contact energy (b) process damping

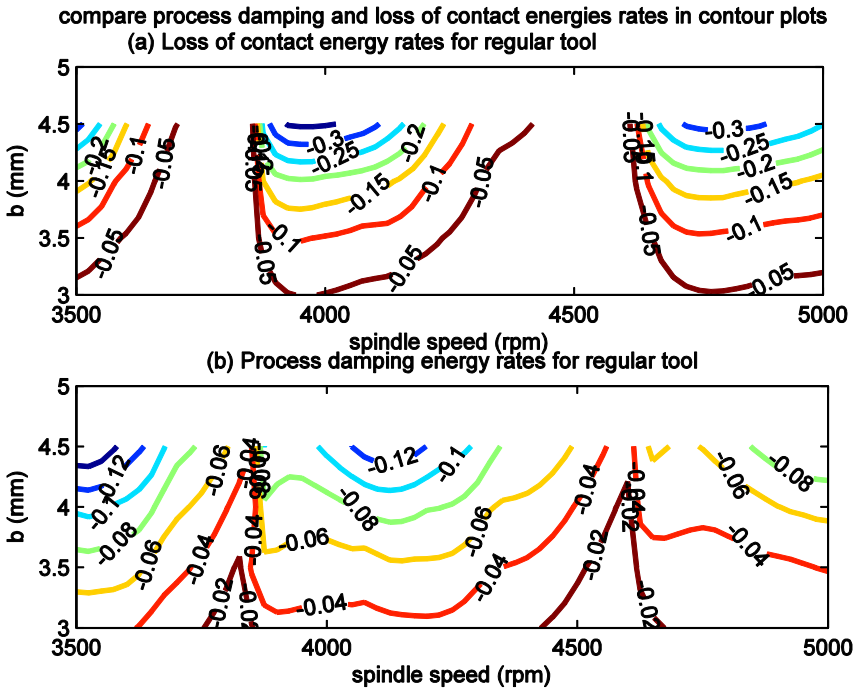

Figure 7.19 compare energy rates in contour plots for the regular tool
(a) loss of contact energy (b) process damping

CHAPTER 8 PROCESS DAMPING AND SHORT REGENERATIVE EFFECT

8.1 Introduction

The short regenerative effect is an alternative mechanism to explain increased stability at lower speeds. It was initially introduced by Stépán [22], who proposed that instead of modelling the cutting forces as a single point force, it could be assumed that the contact between the chip and the tool can be seen to be distributed along the rake face of the tool along a contact length l_c shown in Figure 8.1. Khasawneh *et al*. [21] theoretically showed that in turning, the distributed cutting forces along the tooth face causes a short delay term in the governing equation of motion. This distributed delay was proved to increase the stability limit at low speeds. However, they did not carry out any experiments to check if this kind of force distribution needs to be considered when explaining low speed stability.

More recently, Taylor *et al*.[23], developed a signal processing approach to analyse the behaviour of the two process damping mechanisms 'flank interference concept' and 'short regenerative effect' in turning. For the short regenerative effect, they conclude that this mechanism relies on an estimation of the chip contact time on the tool rake face, along with knowledge of a weighting function that distributes the cutting force along the tool rake face as a function of the chip thickness along the rake face. They also revealed that none of these weighting functions can provide sufficient increases in stability for their model to match the experimental observed data.

It should be noted that to date there is no literature that has proposed to model or investigate the influence of the short regenerative effect mechanism in milling. This could be because this mechanism is quite complicated and the basic subject matter has not fully been recognised. Moreover there is not a straightforward technique which can be used to measure and illustrate how this mechanism affects the stability behaviour.

However, since the model used in this thesis has the ability to consider the process damping due to the tool/workpiece interferences mechanism, it will also be developed here to consider the concept of the short regenerative effect.

In addition, the new proposed technique based upon energy analysis will be implemented to investigate the influence of this phenomenon on the milling stability. Moreover, the obtained results from the short regenerative effect concept will be compared with other results including process damping due to the flank interference mechanism.

8.2 **The Short Regenerative Effect**

It is well known that increased stability behaviour is commonly observed at low speed machining due to the phenomenon known as process damping. In the past, this phenomenon was attributed to the rubbing behaviour that occurs by the interference mechanism between the tool flank face and the work surface. However, another representation known as the short regenerative effect has recently been introduced for stability improvement at lower turning speeds [21-23, 91].

Now, following Taylor *et al*. [23], the theory of the short regenerative effect concept with some mathematical expressions will be briefly reviewed and described. With reference to Figure 8.1(b), the contact between the chip and the tool is assumed to be distributed along the rake face of the tool along the face length l_c. The distributed force along this contact length is assumed to be proportional to the instantaneous chip thickness that is in contact with the tool rake face, and not the uncut chip thickness at the tool tip. This assumption leads to an additional delay term which was introduced to the block diagram as a transfer function filter $G_h(s)$, as shown in Figure 8.2 [23]. Taylor has listed some weighting functions that were first proposed by Stépán [91]. According to this hypothesis, the cutting force can be estimated as follows [23] :

$$F_c(t) = bk_b \int_0^{\tau_{ch}} w(\tau_s) h(t - \tau_s) d\tau_s \qquad (8.1)$$

Here, τ_s is the short time delay, τ_{ch} represents the time taken for the chip to pass along the contact length l_c and $w(\tau)$ is a weighting function.

The proposed weighting functions were converted to transfer functions to represent the relationship between this short time delayed chip thickness and the total cutting force. This was obtained by taking the Laplace transforms for the equation (8.1) and performing the integration along the time τ_{ch} the chip needs to pass along the tool rake length. The obtained transfer function in Equation (8.2) is based on the cutting force and instantaneous chip thickness. This means that this transfer function becomes a filter to connect the chip thickness and the cutting forces as shown in the cutting process diagram Figure 8.2.

$$G_h(s) = \frac{F_c(s)}{H(s)bk_b} \tag{8.2}$$

Table 8-1 shows a list of the weighting functions and corresponding transfer functions as proposed by Taylor et al [23] .

The short time delayed chip thickness τ_{ch} is basically determined from the chip surface velocity $\mathrm{v_s}$ and the chip contact length l_c. It is well known that during the chip formation, the angle of the primary shear plane leads to compression of the chip before it travels up the rake face [21, 23]. Consequently, the chip velocity v_c is determined based upon the surface velocity v_s (m/min) the chip compression ratio λ_r ($\lambda_r = \frac{v_c}{v_s}$). Therefore the total chip contact time τ_{ch} can be determined by [23]:

$$\tau_{ch} = \frac{60\lambda_r}{v_c} l_c \tag{8.3}$$

Here the material considered in this work is Al7075 and the average chip/rake face contact length $l_c = 0.75$ mm was selected according to experimental work done by César [127]. However, the compression ratio $\lambda_r = 2$ was also taken from the experimental work done by Chee [128].

It should be stated that this model involves a number of assumptions regarding the form of the stress distribution and its relationship with the short-delayed chip thickness. The

present contribution does not intend to investigate these assumptions in any detail. Instead, some of the selection of weighting functions listed in Table 8-1(proposed in [23]) will be investigated, so that their influence on improving the milling stability can be ascertained.

8.3 **Numerical Study**

The influence of the short regenerative effect will be investigated using an energy analysis approach. The stability degree will be measured based on the behaviour of the loss of contact energy rates for each tool revolution. Simulation parameters are summarised in Table 8-2 chosen from the work published in [129].

However before analysing the results, the system dynamics and the system boundary need to be reviewed briefly. In this chapter the system dynamics are represented with a single degree of freedom system with mass, spring and damper in two directions x and y. However model formulation, the system boundary and energy calculations have been explained previously in earlier chapters. In addition, the transfer functions developed are then interpreted into simple Simulink blocks as can be seen for example in the exponential transfer function G_{h_exp} presented in Figure 8.3. Then these transfer function blocks are added to the main milling model as a subsystem Simulink block connecting the chip thickness block with the cutting forces block as shown in Figure 8.4.

Again this work does not aim to validate or calibrate these model parameters, but published data has been used to obtain realistic values of the chip contact length and some potential weighting functions have been considered to measure milling stability behaviour.

8.4 **Results and Discussion**

As can be seen in Figure 8.5, loss of contact energy rates are used to investigate the stability behaviour under the influence of the short regenerative effect concept and the flank interference mechanism when compared to the normal system behaviour.

Figure 8.5(a) shows energy rates of the normal model without including the process damping effects. Here energy rates are considerably higher even at the low cutting speeds. The rates are also increased along the depths of cut up to b=1.5mm. Beyond this depth of cut, the vibration energy increases significantly causing a simulation failure.

Figure 8.5(b) presents the energy behaviour of the loss of contact when the rubbing effects due to flank interference mechanism are included. It can be seen here that there is more improvement in the stability, particularly at the low cutting speeds. Loss of contact energy remains almost constant at 0.002 J/rev. However, these energy rates are slightly increased at the high cutting speeds. For example at the cutting speed 1500 rpm, the loss of contact energy starts at the depth of cut b=2mm with energy rate W_{rloc} =0.002J/rev to reach the maximum rate with 0.008 J/rev at b=3mm.

However plots (c), (d) and (e) in Figure 8.5 present the behaviour of the loss of contact energy rates that are obtained by the short regenerative effect, due to the influence of the following weighting functions: exponential $G_{h\text{-}exp}$, constant $G_{h\text{-}con}$ and linear $G_{h\text{-}lin}$ respectively. It should be known that process damping (flank interference mechanism) effects are not included here. Now from these plots it can be seen that these functions have different effects on the degree of the stability since the energy rates of the loss of contact are different. In general these weighting functions have shown a considerable improvement in the stability behaviour compared to the normal model in plot(a); however they did not offer a better performance compared to the process damping mechanism shown in plot (b).

Now the effects of the weighting function including the process damping mechanism (flank interference mechanism) on the stability behaviour are investigated and illustrated in Figure 8.6. Here energy rates of the loss of contact are used to demonstrate the results as contour plots. Plots (a), (b) and (c) show the loss of contact energy rates respectively for the systems: exponential weighting function with the process damping effects ($G_{h\text{-}exp}$), constant weighting function with the process damping effects ($G_{h\text{-}con}$) and linear weighting function with the process damping effects ($G_{h\text{-}lin}$), are much decreased compared to the system just including the process damping effects in plot (d).

In general, the stability behaviour is clearly improved since the rates of the loss of contact energy are decreased through all these systems. However the degree of stability was slightly different from one system to another. Here the exponential $G_{h\text{-}exp}$ and the constant $G_{h\text{-}con}$ weighting functions almost have the same performance although it is slightly higher for the $G_{h\text{-}con,}$ particularly at high spindle speeds. However the linear weighting function $G_{h\text{-}lin}$ showed the lowest stability degree since the obtained energy rates are quite high compared to the other functions. Despite of the machining process being different, the main trends of these outcomes are almost in agreement with that observed in [23].

8.5 **Summary**

A specific contribution of the current chapter is the introduction of a new phenomenon of the process damping in milling where a distributed cutting force model is used.

The new analysis approach based upon the energy analysis has been applied to investigate the physical explanation for the process damping effects. Process damping due to the tool/workpiece interference mechanism has been combined with the short regenerative effect. The model is validated by selecting a confirmed simulation data previously published. The main conclusive remarks are:

1. The energy approach can be used to investigate the chatter stability behaviour due to the process damping effects by both the flank interference mechanism and short regenerative effect.
2. The distributed force model also provides an alternative explanation for the improved stability of milling while still allowing more investigation.
3. Different shape functions for the force distribution have shown an improvement in the stability behaviour through the reduction in the loss of contact energy rates compared to the normal system (system without process damping or weighting functions effects). However, it has been shown that none of these

functions can provide a sufficient increase in stability for the model to match the process damping effects.

4. The loss-of-contact energy rates are much decreased when the flank interference mechanism is combined with the short regenerative effect. This reveals that stability could be increased by considering both process damping mechanisms.
5. This study has not aimed to validate or calibrate the model parameters, but published data has been used to obtain realistic values of the chip contact length and a range of potential weighting functions have been considered.

Possible tasks for future research include experimental verification and/or a comparison study with historical models of process damping. This will avert the complications of previous works which either uses the damping term which is inversely proportional to spindle speed or a displaced volume relationship which must be numerically and experimentally calibrated.

Description	Weighting Functions $(\boldsymbol{w(\tau_s)})$	Transfer Functions $(\boldsymbol{G_h})$
Exponential	$\frac{ae^{-\frac{a\tau_s}{\tau_{ch}}}}{\tau_{ch}(1-e^{-a})}$	$\left(\frac{a}{(e^a-1)}\right)\left(\frac{1}{(a+s\tau_{ch})}\right)(e^a-e^{-s\tau_{ch}})$
Constant	$\frac{1}{\tau_{ch}}$	$\frac{(1-e^{-s\tau_{ch}})}{s\tau_c}$
Linear	$\frac{2}{\tau_{ch}}\left(1-\frac{\tau_s}{\tau_{ch}}\right)$	$\frac{2(s\tau_{ch}-1+e^{-s\tau_{ch}})}{\tau_c^2 s^2}$

Table 8-1 Weighting Functions and the Corresponding Chip Transfer Functions [23]

Simulation parameters	
Stiffness	K_x=5.6x10^6 (N/m) K_y=5.7x10^6 (N/m)
Structural damping	C_x=115.29Ns/m C_y=95.35Ns/m
Natural frequency	f_x=603 (Hz) f_y=666 (Hz)
$\boldsymbol{K_{tc}}$	700 (N/mm^2)
$\boldsymbol{K_r}$	0.07
Tool diameter	25.4 (mm)
Number of teeth	3
Flute helix	0^o(axial flute)
Milling Mode	up-milling
Radial immersion	50%
Feed per tooth	0.07(mm/tooth)
Process damping friction coefficient (μ)	0.3
Process damping normal forces coefficient (K_{np})	1.5x10^5 (Nmm^{-3})

Table 8-2 simulation parameters

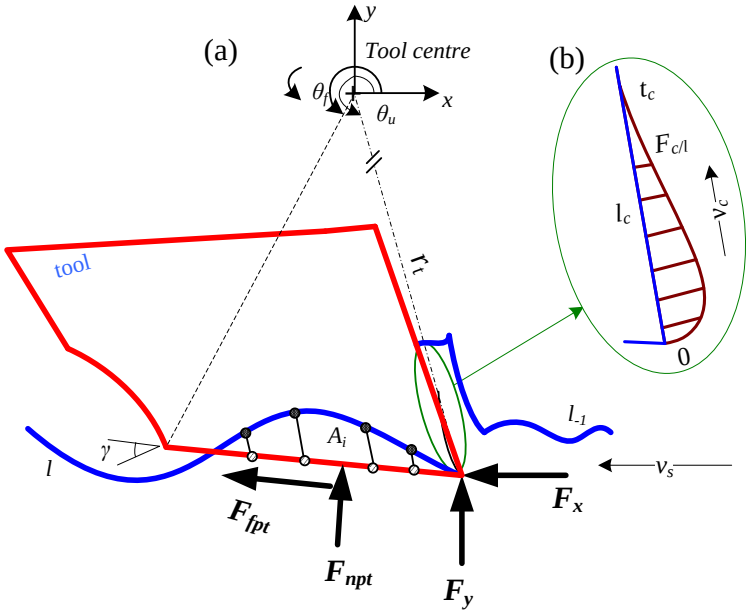

Figure 8.1 (a) the interference contact region, and (b) distributed force on the rake tool face

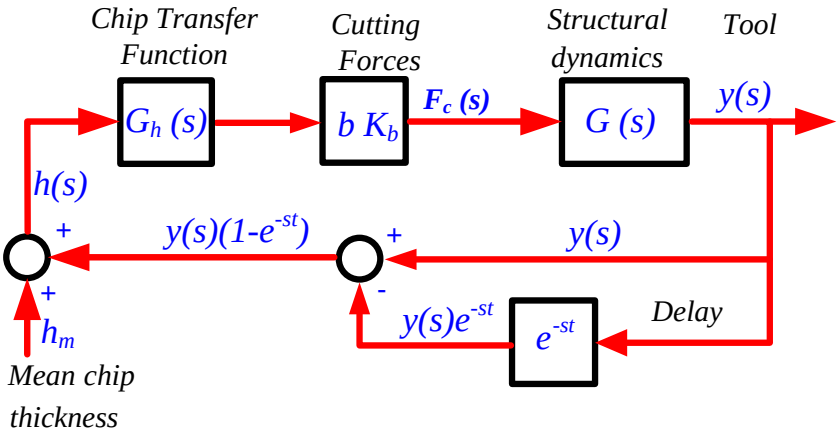

Figure 8.2 Block diagram of cutting process in the traditional stability model,[23]

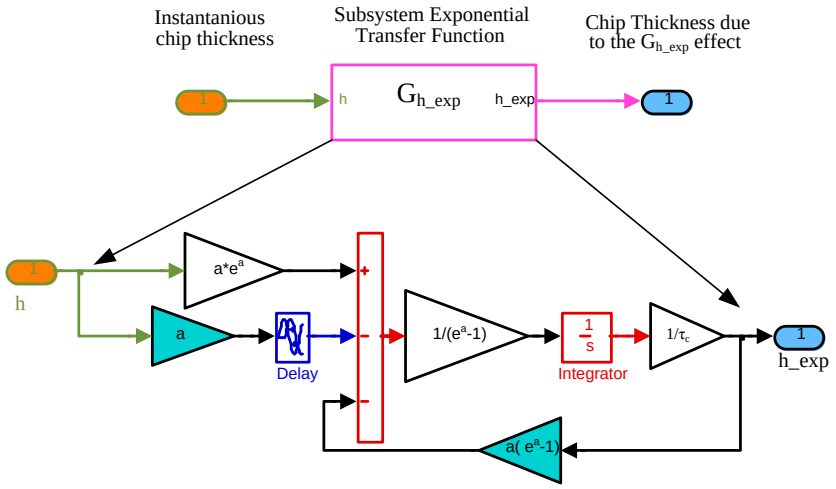

Figure 8.3 Exponential Transfer Function G_{h_exp}

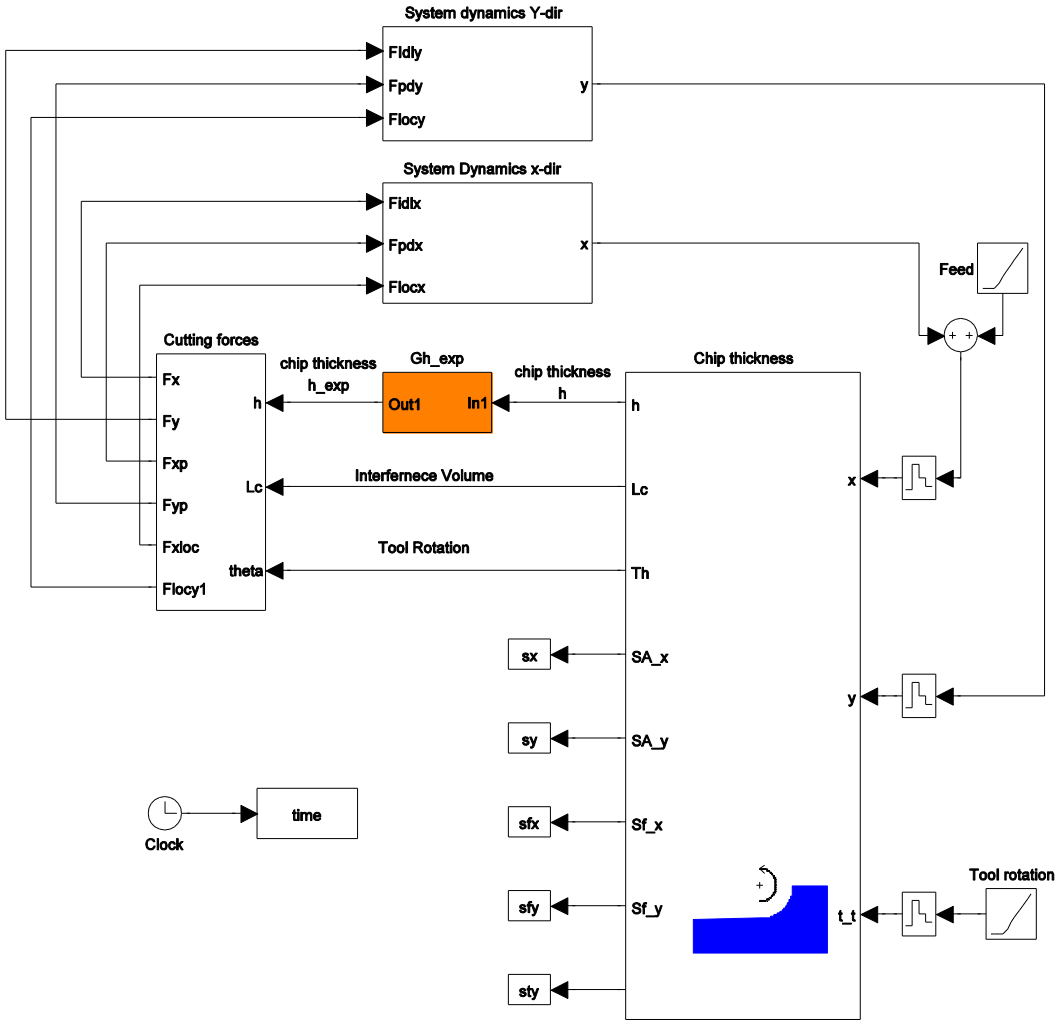

Figure 8.4 Simulink Milling Model including Chip thickness transfer function

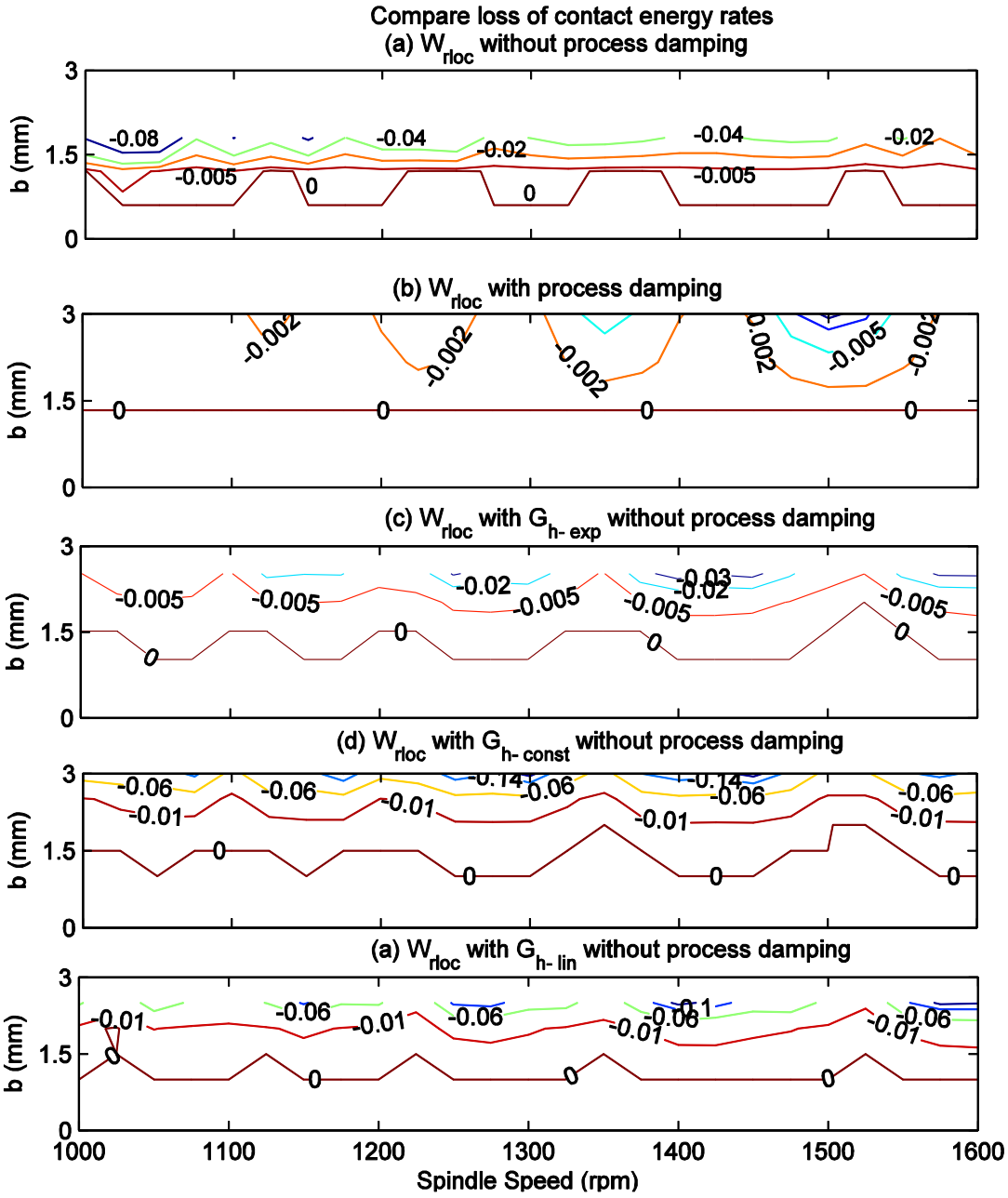

Figure 8.5 compare behaviour of the loss of contact energy rates due to the normal weighting functions and process damping mechanism

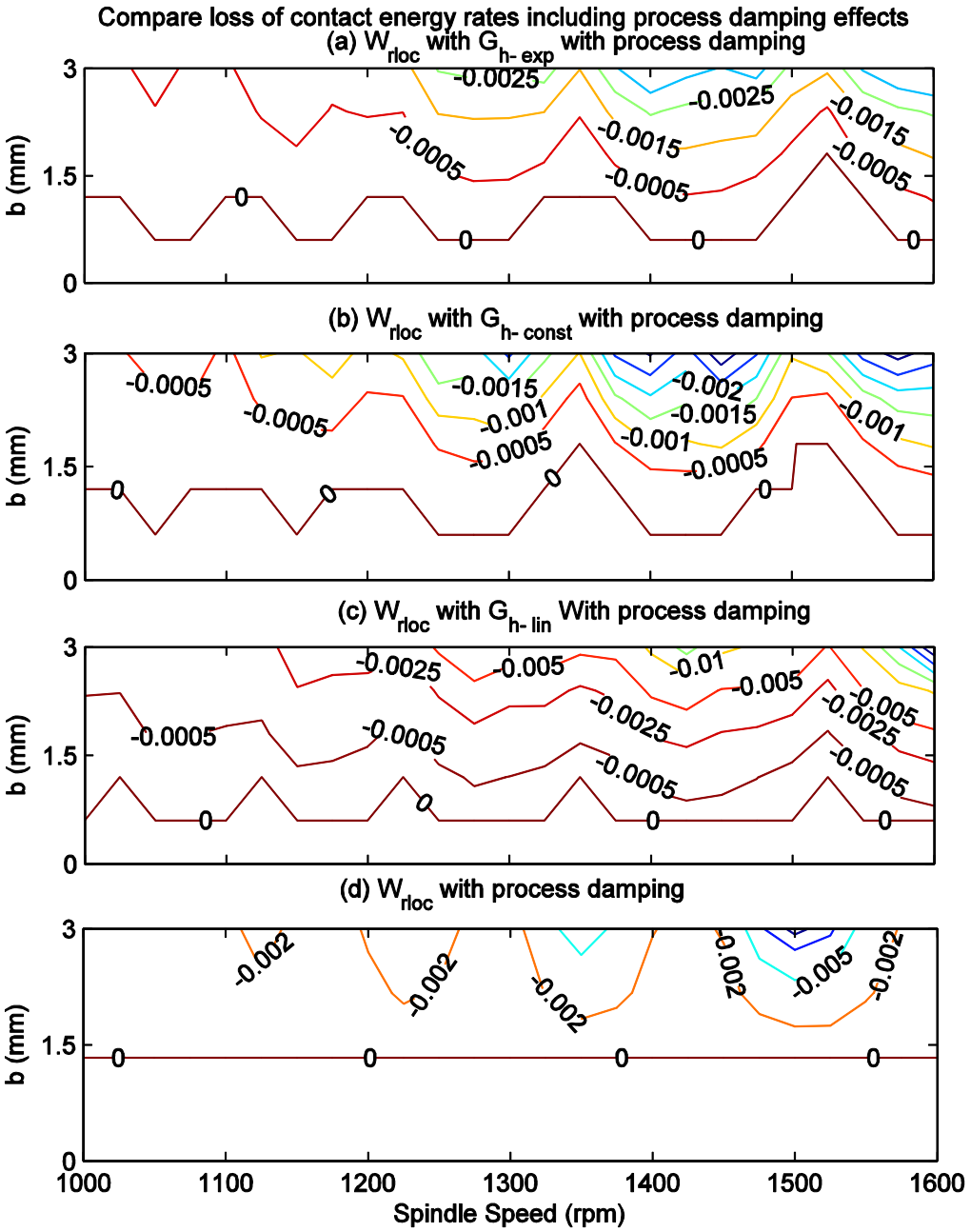

Figure 8.6 compare behaviour of the loss of contact energy rates due to the weighting functions including process damping effects

CHAPTER 9 CONCLUSION AND FURTHER WORK

9.1 Summary of Thesis

In Chapter 4 of this research, a comprehensive milling simulation model has been modified to involve a variable spindle speed mechanism. The model was formulated in a Simulink environment, and in order to consider variable spindle speeds the system equations of motion have been rewritten in non-dimensional time. This was achieved by using tool revolutions as independent variable instead of time in seconds. The peak-to-peak (PTP) approach was used for analysing the simulation results. However this approach was unable to provide a formal and accurate interpretation of chatter stability for variable spindle speed simulations, consequently the self-excited damping ratio was used as the alternative method for this investigation.

In Chapter 5, a new analysis method was introduced. This method is based on balancing the cutting energies and the damping energies that are crossing the system boundary. The new analysis approach has been used to describe and investigate the stability behaviour for both turning and milling.

In Chapter 6 new analysis method was used to investigate the process damping phenomenon based upon the flank interference contact. The influence of several cutting conditions and tool geometry parameters was investigated through simulation. The new analysis approach proposed in this research has enabled a physical explanation for the process damping mechanism. Process damping performance on chatter suppression was quantifiably measured and investigated.

In Chapter 7, the simulation and analysis was extended to also consider the special case of variable helix tools. The energy analysis was further developed to consider multi degree of freedom system dynamics. To the author's knowledge this is the first study that has modelled the process damping of variable helix tools. Enhanced process damping was observed for these tools, in approximate agreement with previous experimental results in literature.

In Chapter 8 an alternative mechanism for the process damping phenomenon based upon the short regenerative effect has been investigated, using the energy balance. To the authors knowledge this is the first study that has simultaneously modelled the short regenerative effect and tool flank interference in milling. The study showed that the short regenerative effect can add further damping behaviour over and above that caused by tool flank interference.

The conclusions and contributions will now be listed and recommendations for future works suggested.

9.2 **Conclusions**

1- The self excited damping ratio can provide a formal interpretation of instability for variable spindle speed milling simulations, but it cannot interpret stable behaviour. This can be observed particularly for the stable cases where the lines that are fitting the maximum amplitudes (X_{es}) of each frame almost horizontal and straight, whereas, due to the proposed theory these lines are expected to be in decaying style since they were representing the stable behaviour as shown in constant speed machining [40]. The reason of that can be attributed to the effect of the speed variation behaviour on the spectral lines approach, in addition to the time-variant dominant frequencies is the stable response of the system, thereby the influence of varying chatter frequency can be not fully considered. Other nonlinearities such as process damping are also likely to cause such the variations in the chatter frequency. Therefore self-excited damping ratio is suggested to be unsatisfactory approach to offer comprehensive insight.

2- An energy balance approach has been developed as an alternative method of exploring the system stability from time domain simulation data. The approach has been shown to provide a useful and quantifiable interpretation that can be applied to various nonlinearities including the fundamental loss of contact that occurs under high vibration levels.

3- The energy balance approach has been used to explore the simulated behaviour when tool flank interference is modelled. This allows an accurate interpretation of the energy dissipation associated with the interference effects. Furthermore, the magnitude of this energy dissipation can be compared to that observed from the simulated tool losing contact with the workpiece. This provides some new insight into how these two nonlinearities act to limit the amplitude of unstable chatter vibrations in practice.

4- For the special case of simulated variable helix tools, it has been observed that process damping appears to have an even more beneficial effect at low spindle speeds. Although the energy analysis method has provided some useful visualisation of this enhanced stability. The underlining mechanisms require further investigation. Furthermore, the literature provides experimental evidence that enhanced stability occurs at higher spindle speeds range than that found in the present modelling work.

5- Finally, the combination of tool flank interference and the short regenerative effect have been modelled and analysed using energy method. The simulations suggest that the combined phenomena provide even greater energy dissipation.

9.3 **Contributions from Current Work**

The main contributions of this work are:

- A milling model has been developed to consider variable speeds by considering non dimensional time. This technique was not considered before; however Tsao et al [3] presented a method for a simplified situation of continuous cutting with only one tooth in cut at any point of time. The work described in this thesis was presented at an international conference (RASD 2010) see Appendix A1.

- The self-excited damping ratio technique was applied for the first time to variable speed machining (VSM). For this case it was seen that the system displacement does not reach a steady state condition, making the common techniques such as peak-to-peak method difficult to use as a judgement of

chatter stability. The result of this work was a published in conference paper see (WCE2012) Appendix A2.

- The main contribution of this research is the introduction of a new comprehensive method for chatter stability analysis that allows more realistic and detailed investigation for chatter stability in time domain simulation. The idealised cutting energy, loss of contact energy, process damping energy and the structural damping energy of the milling system are directly measured in the milling model.
- The new analysis method has been applied to simulations that consider three topical methods for mitigation of chatter: variable helix tools, tool flank interference, and the short regenerative effect. This has provided new insight into the relation performance of these phenomena.
- Finally, it is worth reiterating that this study has focussed on a method based approach. However, wherever possible the simulation scenarios have been based upon conditions used for experimental testing in the literature

9.4 **Suggestions for Future Work**

A number of areas are suggested for further work.

- First, time constraints meant that the energy balance approach was not applied for the case of variable speed machining. With hindsight, this would have been on obvious step in the research. However, at the time the main focus of the research topic was the process damping phenomenon.
- Second, it is clear that variable helix tools do provide an interesting process damping behaviour that appears to offer enhance stability. Further experimental work is needed to explore this.
- Finally the short regenerative effect has received very little attention. Measurement of this phenomenon is likely to be extremely challenging, but such experiments could provide useful new insight.

REFERENCES

[1] Quintana, G. And J. Ciurana, *Chatter in machining processes: A review.* International Journal of Machine Tools & Manufacture, 2011. 51(5): p. 363-376.

[2] Tobias.S. A and W. Fishwick, *Theory of Regenerative Machine Tool Chatter.* The Enginee, 1958. 205: p. 199-203.

[3] Ema, S. And E. Marui, *Suppression of chatter vibration of boring tools using impact dampers.* International Journal of Machine Tools & Manufacture, 2000. 40(8): p. 1141-1156.

[4] Liu, K.J. and K.E. Rouch, *Optimal passive vibration control of cutting process stability in milling.* Journal of Materials Processing Technology, 1991. 28(1-2): p. 285-294.

[5] Sims, N.D., *Vibration absorbers for chatter suppression: A new analytical tuning methodology.* Journal of Sound and Vibration, 2007. 301(3-5): p. 592-607.

[6] Tobias, S.A., ed. *Machine Tool Vibration* 1965, Blackie & Son Limited.

[7] Chung, B., *et al.*, *Active damping of structural modes in high-speed machine tools.* Journal of Vibration and Control, 1997. 3(3): p. 279-295.

[8] Huyanan, S. And N.D. Sims, *Active vibration absorbers for chatter mitigation during milling*, in *Ninth International Conference on Vibrations in Rotating Machinery 2008*. 2008.

[9] Tewani, S.G., *et al.*, *A study of cutting process stability of a boring bar with active dynamic absorber.* International Journal of Machine Tools & Manufacture, 1995. 35(1): p. 91-108.

[10] Zhang, Y.M. and N.D. Sims, *Milling workpiece chatter avoidance using piezoelectric active damping: a feasibility study.* Smart Materials & Structures, 2005. 14(6): p. N65-N70.

[11] Budak, E. And L.T. Tunc, *Identification and modeling of process damping in turning and milling using a new approach.* Cirp Annals-Manufacturing Technology. 59(1): p. 403-408.

[12] Delio, T., *et al.*, *Stiffness, stability, and loss of process damping in high speed machining : Fundamental issues in machining.* 43, 1991. 3: p. 171-191.

[13] Elbestawi, M.A., Ismail, F., Du, R., and Ullagaddi, B. C., *Modeling Machining Dynamics Including Damping in the Tool-Workpiece Interface.* ASME J. Eng. Ind, 1994. 116: p. 435–439.

[14] Fontaine, M., *et al., Modelling of cutting forces in ball-end milling with tool-surface inclination Part II. Influence of cutting conditions, run-out, ploughing and inclination angle.* Journal of Materials Processing Technology, 2007. 189(1-3): p. 85-96.

[15] Huang, C.Y. and J.J.J. Wang, *Mechanistic modeling of process damping in peripheral milling.* Journal of Manufacturing Science and Engineering-Transactions of the Asme, 2007. 129(1): p. 12-20.

[16] Lee, B.Y., *et al., Modeling of the process damping force in chatter vibration.* International Journal of Machine Tools & Manufacture, 1995. 35(7): p. 951-962.

[17] Montgomery, D. And Y. Altintas, *Mechanism of cutting force and surface generation in dynamic milling.* Journal of Engineering for Industry-Transactions of the Asme, 1991. 113(2): p. 160-168.

[18] Ranganath, S., *et al., A comprehensive model for the flank face interference mechanism in peripheral milling.* Transactions of the North American Manufacturing Research Institution of Sme, Vol Xxvi, 1998, 1998: p. 249-254.

[19] Sims.Neil. D and S. Turner, *The influence of feed rate on process damping in milling: Modelling and experiments.* Engineering Manufacture, 2010.

[20] Yusoff, A.R., *et al., The role of tool geometry in process damped milling.* International Journal of Advanced Manufacturing Technology. 50(9-12): p. 883-895.

[21] Khasawneh, F.A., *et al., Increased Stability of Low-Speed Turning Through a Distributed Force and Continuous Delay Model.* Journal of Computational and Nonlinear Dynamics, 2009. 4(4).

[22] Stepan, G., *Modelling nonlinear regenerative effects in metal cutting.* Philosophical Transactions of the Royal Society of London Series a-Mathematical Physical and Engineering Sciences, 2001. 359(1781): p. 739-757.

[23] Taylor, C.M., *et al., Chatter, process damping, and chip segmentation in turning: A signal processing approach.* Journal of Sound and Vibration, 2010. 329(23): p. 4922-4935.

[24] Altintas, Y., *et al., Analytical stability prediction and design of variable pitch cutters.* Journal of Manufacturing Science and Engineering, Transactions of the ASME, 1999. 121(2): p. 173-178.

[25] Budak, E., *An analytical design method for milling cutters with nonconstant pitch to increase stability, part 2: Application.* Journal of Manufacturing Science and Engineering-Transactions of the Asme, 2003. 125(1): p. 35-38.

[26] Sims, N.D., *et al., Analytical prediction of chatter stability for variable pitch and variable helix milling tools.* Journal of Sound and Vibration, 2008. 317(3-5): p. 664-686.

[27] Slavicek, J., *The effect of irregular tooth pitch on stability of milling.*, in *Proceedings of the 6th MTDR Conference*. 1965.

[28] Yusoff, A., *Optimisation of variable helix end milling tools*, in *Mechanical Engineering*. 2010, The university of Sheffield.

[29] Al-Regib, E., *et al., Programming spindle speed variation for machine tool chatter suppression.* International Journal of Machine Tools and Manufacture, 2003. 43(12): p. 1229-1240.

[30] Altintas, Y. And P.K. Chan, *In-process detection and suppression of chatter in milling.* International Journal of Machine Tools & Manufacture, 1992. 32(3): p. 329-347.

[31] Ismail, F. And E.G. Kubica, *Active suppression of chatter in peripheral milling .1. a statistical indicator to evaluate the spindle speed modulation method.* international Journal of Advanced Manufacturing Technology, 1995. 10(5): p. 299-310.

[32] Liao, Y.S. and Y.C. Young, *A new on-line spindle speed regulation strategy for chatter control.* International Journal of Machine Tools & Manufacture, 1996. 36(5): p. 651-660.

[33] Lin, S.C., *et al., The effects of variable speed cutting on vibration control in face milling.* Journal of Engineering for Industry-Transactions of the Asme, 1990. 112(1): p. 1-11.

[34] Seguy, S., *et al., Control of chatter by spindle speed variation in high-speed milling*, in *Advances in Structural Analysis of Advanced Materials*. P. 179-186.

[35] Seguy, S., *et al., Suppression of period doubling chatter in high-speed milling by spindle speed variation.* Machining Science and Technology. 15(2): p. 153-171.

[36] Sri, N.N. and R. Beddini, *Spindle speed variation for the suppression of regenerative chatter.* Journal of Nonlinear Science, 2003. 13(3): p. 265-288.

[37] Sridhar, R., *et al., A general fomulation of the milling process equation, contribution to machine-tool chatter research.* Transaction ASME Journal of Engineering Industry, 1968. 90(2): p. 317-324.

[38] Tsao, T.C., *et al., A new approach to stability analysis of variable-speed machining systems.* International Journal of Machine Tools & Manufacture, 1993. 33(6): p. 791-808.

[39] Smith, S. And J. Tlusty, *Update on high-speed milling dynamics.* Journal of Engineering for Industry-Transactions of the Asme, 1990. 112(2): p. 142-149.

[40] Sims, N.D., *The self-excitation damping ratio: A chatter criterion for time-domain milling simulations.* Journal of Manufacturing Science and Engineering-Transactions of the Asme, 2005. 127(3): p. 433-445.

[41] F.W.Taylor, *On the art of cutting metals.* Transactions of ASME, 1907. 28: p. 31–248404.

[42] S.A.Tobias, ed. *Machine Tool Vibration* 1965, Blackie & Son Limited.

[43] Wang, Z., *Chatter Analysis of Machine Tool Systems in Turning Processes*, in *Department of Mechanical and Industrial Engineering*. 2001, University of Toronto.

[44] Cheng, K., ed. *Machine Dynamics Fundamental applications and Prectice*. 2010.

[45] Shah, V., *Experimental investigations of chatter and critical cutting conditions in turning*, in *Department of Mechanical, Aerospace and Industrial Engineering* 2003, Ryerson University.

[46] Hanna, N.H. and S.A. Tobias, *Theory of nonlinear regenerative chatter.* Journal of Engineering for Industry-Transactions of the Asme, 1974. 96(1): p. 247-255.

[47] Ahmadi, K. And F. Ismail, *Machining chatter in flank milling.* International Journal of Machine Tools & Manufacture. 50(1): p. 75-85.

[48] Budak, E. And Y. Altintas, *Analytical prediction of chatter stability in milling - Part 1: General formulation.* Journal of Dynamic Systems Measurement and Control-Transactions of the Asme, 1998. 120(1): p. 22-30.

[49] Budak, E. And Y. Altintas, *Analytical prediction of chatter stability in milling - Part II: Application of the general formulation to common milling systems.* Journal of Dynamic Systems Measurement and Control-Transactions of the Asme, 1998. 120(1): p. 31-36.

[50] Dombovari, Z., *et al., The effect of serration on mechanics and stability of milling cutters.* International Journal of Machine Tools & Manufacture. 50(6): p. 511-520.

[51] Hashimoto, M., *et al., Experimental research on cutting force variation during regenerative chatter vibration in a plain milling operation.* International Journal of Machine Tools & Manufacture, 1996. 36(10): p. 1073-1092.

[52] Minis, *et al., Analysis of linear and nonlinear chatter in milling.* CIRP Annals Manufacturing Technology, 1990. 39(1): p. 459–462.

[53] Baker, J.R. and K.E. Rouch, *Use of finite element structural models in analyzing machine tool chatter.* Finite Elements in Analysis and Design, 2002. 38(11): p. 1029-1046.

[54] Chiou, R.Y. and S.Y. Liang, *Chatter stability of a slender cutting tool in turning with tool wear effect.* International Journal of Machine Tools & Manufacture, 1998. 38(4): p. 315-327.

[55] Chiou, R.Y. and S.Y. Liang, *Analysis of acoustic emission in chatter vibration with tool wear effect in turning.* International Journal of Machine Tools & Manufacture, 2000. 40(7): p. 927-941.

[56] Clancy, B.E. and Y.C. Shin, *A comprehensive chatter prediction model for face turning operation including tool wear effect.* International Journal of Machine Tools & Manufacture, 2002. 42(9): p. 1035-1044.

[57] Deshpande, N. And M.S. Fofana, *Nonlinear regenerative chatter in turning.* Robotics and Computer-Integrated Manufacturing, 2001. 17(1-2): p. 107-112.

[58] Larue, A. And Y. Altintas, *Simulation of flank milling processes.* International Journal of Machine Tools & Manufacture, 2005. 45(4-5): p. 549-559.

[59] Lee, A.C. and C.S. Liu, *Analysis of chatter vibration in the end milling process.* International Journal of Machine Tools & Manufacture, 1991. 31(4): p. 471-479.

[60] Minis, I. And R. Yanushevsky, *A new theoretical approach for the prediction of machine-tool chatter in milling.* Journal of Engineering for Industry-Transactions of the Asme, 1993. 115(1): p. 1-8.

[61] Tarng, Y.S., *et al.*, *An analytical model of chatter vibration in metal-cutting.* International Journal of Machine Tools & Manufacture, 1994. 34(2): p. 183-197.

[62] Fofana, M.S., *Aspects of stable and unstable machining by Hopf bifurcation.* Applied Mathematical Modelling, 2002. 26(10): p. 953-973.

[63] Tarng, Y.S., *et al.*, *Chatter suppression in turning operations with a tuned vibration absorber.* Journal of Materials Processing Technology, 2000. 105(1-2): p. 55-60.

[64] Tlusty , J. And Macneil.P., *Dynamics of cutting forces in end milling.* Annals of the CIRP, 1975. 24: p. 21-25.

[65] Campomanes, M.L., *Dynamics of milling flexible structures* in *department of mechanical engineering* 1993, the university of Manitoba.

[66] Faassen, R.P.H., *et al.*, *Prediction of regenerative chatter by modelling and analysis of high-speed milling.* International Journal of Machine Tools & Manufacture, 2003. 43(14): p. 1437-1446.

[67] Tlusty, J., *A method of analysis of machine tool stability*. Proc 6th MTDR Conference, 1965: p. 5-14.

[68] Tlusty, J., ed. *Manufacturing processes and Equipment*. 2002, Prentice Hall, Upper Saddle River, NJ.

[69] Merritt, H.E., *Theory of self-excited machine-tool chatter-1*. Mechanical Engineering, 1965. 87(3): p. 86-&.

[70] Opitz, H., *et al. Improvement of the dynamics stability of the milling process by irregular tooth pitch.* In *Advances in Machine Tool Design and Research, Proc. of MTDR Conference*. 1966.

[71] Shi, H.M. and S.A. Tobias, *Theory of finite-amplitude machine-tool instability.* International Journal of Machine Tools & Manufacture, 1984. 24(1): p. 45-69.

[72] Altintas Y. And Budak E., *Analytical prediction of stability lobes in milling.* CIRP Annals - Manufacturing Technology, 1995. 44(1): p. 357-362.

[73] Huaizhong Li and X. Li, *Modelling and simulation of chatter in milling using a predictive force model.* International Journal of Machine Tools & Manufacture, 2000. 40: p. 2047–2071.

[74] Tlusty J and Ismail F, *Basic Non-Linearity in Machining Chatter.* Annals of the CLR, 1981. 31: p. 299-304.

[75] Altintas, Y., *Modeling approaches and software for predicting the performance of milling operations at MAL-UBC.* Machining Science and Technology, 2000. 4(3): p. 445-478.

[76] Tlusty. J and Ismail.F, *Special aspects of chatter in milling.* ASME Journal of Vibration, Acoustics, Stress and Reliability in Design, 1983. 105: p. 24-32.

[77] J.Tlusty, *Dynamics of high-speed milling.* Journal of Engineering for Industry-Transactions of the Asme, 1986. 108(2): p. 59-67.

[78] Altintas, Y. And P. Lee, *Mechanics and dynamics of ball end milling.* Journal of Manufacturing Science and Engineering-Transactions of the Asme, 1998. 120(4): p. 684-692.

[79] Campomanes, M.L. and Y. Altintas, *An improved time domain simulation for dynamic milling at small radial immersions.* Journal of Manufacturing Science and Engineering-Transactions of the Asme, 2003. 125(3): p. 416-422.

[80] Li, H.Z., *et al., A novel chatter stability criterion for the modelling and simulation of the dynamic milling process in the time domain.* International Journal of Advanced Manufacturing Technology, 2003. 22(9-10): p. 619-625.

[81] Schmitz, T.L., *Chatter recognition by a statistical evaluation of the synchronously sampled audio signal.* Journal of sound and vibration, 2003. 262(3): p. 721.

[82] Kurdi, M.H., *et al., Simultaneous Optimization of Removal Rate and Part Accuracy in High-Speed Milling.* ASME International mechanical engineering congress and exposition (IMECE), Anaheim, 2004.

[83] Tarng, Y.S. and E.C. Lee, *A critical investigation of the phase shift between the inner and outer modulation for the control of machine tool chatter.* International Journal of Machine Tools & Manufacture, 1997. 37(12): p. 1661-1672.

[84] Delio, T., *et al., Use of audio signals for chatter detection and control.* Journal of Engineering for Industry-Transactions of the Asme, 1992. 114(2): p. 146-157.

[85] Sim, W., *et al., An integrated approach to the highspeed machining of moulds and dies involving both a knowledge-based system and a chatter detection and control system.* Proceedings of the Institution of Mechanical Engineers Part B-Journal of Engineering Manufacture, 2002. 216(12): p. 1635-1646.

[86] Sastry, S., *et al., Chatter stability analysis of the variable speed face-milling process.* Journal of Manufacturing Science and Engineering-Transactions of the Asme, 2001. 123(4): p. 753-756.

[87] Yilmaz, A., *et al., Machine tool chatter suppression by multi-level random spindle speed variation.* Journal of Manufacturing Science and Engineering-Transactions of the Asme, 2002. 124(2): p. 208-216.

[88] Pakdemirli, M. And A.G. Ulsoy, *Perturbation analysis of spindle speed vibration in machine tool chatter.* JVC/Journal of Vibration and Control, 1997. 3(3): p. 261-278.

[89] S. Seguy, T.I., L. Arnaud, G. Dessein, G. Peigné, *Chatter Suppression in Milling Processes Using Periodic Spindle Speed Variation*, in *12th Cirp Conference on Modelling of Machining Operations*. 2009: Donostia-San Sebastián, Spain.

[90] Turner, S., *et al., Modelling of the stability of variable helix end mills.* International Journal of Machine Tools & Manufacture, 2007. 47(9): p. 1410-1416.

[91] Stepan, G., *Retarded Dynamical Systems:Stability and Characteristic Functions*. Pitman Research Notes in Mathematics, Long man Scientific and Technical. 1989.

[92] Tlusty, J., *Dynamics of high-speed milling.* Journal of Engineering for Industry-Transactions of the Asme, 1986. 108(2): p. 59-67.

[93] Kline, W.A. and R.E. Devor, *The effect of run out on cutting geometry and forces in end milling.* International Journal of Machine Tools & Manufacture, 1983. 23(2-3): p. 123-140.

[94] Merritt, H.E., *Theory of Self-excited machine tool chatter, contribution to machine-tool chatter research-I.* Trans. ASME Journal of Engineering Industry, 1965. 87(4): p. 447-454.

[95] Ganguli, A., *Chatter reduction through active vibration damping*, in *Department of Mechanical Engineering & Robotics*. 2005, Universite Libre de Bruxelles.

[96] Sims N.D., *et al. A model of milling dynamics using Matlab and Simulink*. In *I Grabec and E Govekar, Bled, Slovenia*

International workshop on modeling of machining operations, 2006. University of Ljublijana.

[97] Budak, E., Altintas, Y., and Armarego, E. J. A, *Prediction of Milling Force Coefficients from orthogonal Cutting Data.* ASME J. Eng. Ind, 1996. 118: p. 216–224.

[98] Matlab, *Writing s-functions.* 2004.

[99] Peigne, G., *et al., A model of milled surface generation for time domain simulation of high-speed cutting.* Proceedings of the Institution of Mechanical Engineers Part B-Journal of Engineering Manufacture, 2003. 217(7): p. 919-930.

[100] PHILIP, P.K., *Built-up edge phenomenon in machining steel With carbide.* Int. J. Mach. Tool Des. Res., 1970. 11: p. 121-132.

[101] Sisson T. R and Kecg R. L, *An Explanation of Low-speed Chatter Effects.* Trans. ASME J. Engngjor Indust, 1969. 91: p. 951-955.

[102] Lau W. S and Rubens'rein C, *"[he influence of flank wear, cutting speed and cutting fluid on the surface and sub-surface workhardening produced in an orthogonal planing operation.* Int. J. Mach. Tool Des. Res., 1972. 12: p. 311-323.

[103] Wu, D.W., *Application of a comprehensive dynamic cutting force model to orthogonal wave-generating processes.* International Journal of Mechanical Sciences, 1988. 30(8): p. 581-600.

[104] Albrecht P, *Mechanics of the cutting process.* ASME Int. Res. In Prod. Engng, 1963: p. 32 41.

[105] Thomsen e.G., *et al., Flank friction studies with carbide tools reveal sublayer plastic flow.* Trans ASME J. Engng for lndust., 1962. 84: p. 53 62.

[106] Ahmadi, K. And F. Ismail, *Analytical stability lobes including nonlinear process damping effect on machining chatter*. International Journal of Machine Tools & Manufacture. 51(4): p. 296-308.

[107] Ranganath, S., Narayanan, K., and Sutherland, J. W., *The Role of Flank Face Interference in Improving the Accuracy of Dynamic Force Predictions in Peripheral Milling.* ASME J. Manuf. Sci. Eng., 1999. 121: p. 593–599.

[108] Wu, D.W., *A new approach of formulating the transfer-function for dynamic cutting processes.* Journal of Engineering for Industry-Transactions of the Asme, 1989. 111(1): p. 37-47.

[109] Abrari, F., *et al., On the dynamics of ball end milling: Modeling of cutting forces and stability analysis.* International Journal of Machine Tools & Manufacture, 1998. 38(3): p. 215-237.

[110] Armarego, E.J. and C.J. Epp, *An investigation of zero helix peripheral up-milling.* International Journal of Machine Tool Design and Research, 1970. 10(2): p. 273-&.

[111] Joenigsberger, F. And Sabberwal. A.J.P, *An investigation into the cutting force pulstations during milling operations.* International Journal of Machine Tool Design and Research, 1961. 1: p. 15-33.

[112] Turner, S., *Process Damping Parameters,* in *Trends in Aerospace Manufacturing 2009 International Conference*. 2011.

[113] Tlusty, J., *Analysis of the State of Research in Cutting Dynamics.* CIRP Annals - Manufacturing Technology, 1978. 27(2): p. 582-589.

[114] Jemielniak, K. And A. Widota, *Numerical-simulation of non-linear chatter vibration in turning.* International Journal of Machine Tools & Manufacture, 1989. 29(2): p. 239-247.

[115] R. L. Kecg, *Cutting Dynamics in Machine Tool Chatter, contribution to machine tool chatter research.* Trans. ASME J. Engng for Indust., 1965. 87: p. 464-470.

[116] Sébastien Seguy, G.D., Lionel Arnaud, Tamás Insperger, *On the stability of high-speed milling with spindle speed variation.*The International Journal of Advanced Manufacturing Technology, 2009: p. 2336-9.

[117] Jayaram, S., *et al., Analytical stability analysis of variable spindle speed machining.* Journal of Manufacturing Science and Engineering-Transactions of the Asme, 2000. 122(3): p. 391-397.

[118] Insperger, T. And G. Stepan, *Stability analysis of turning with periodic spindle speed modulation via semidiscretization.* Journal of Vibration and Control, 2004. 10(12): p. 1835-1855.

[119] Rao, S.S., ed. *Mechanical Vibrations, Prentice*. 2004, Hall, Englewood Cliffs, NJ.

[120] Çengel., Y.A. and M.A. Boles., eds. *Thermodynamics: An Engineering Approach*. 1989.

[121] Balachandran, B. And M.X. Zhao, *A mechanics based model for study of dynamics of milling operations.* Meccanica, 2000. 35(2): p. 89-109.

[122] Long, X.H., *et al.*, *Dynamics of milling processes with variable time delays.* Nonlinear Dynamics, 2007. 47(1-3): p. 49-63.

[123] Elbestawi, M.A., *et al.*, *Modeling machining dynamics including damping in the tool-workpiece interface.* Journal of Engineering for Industry-Transactions of the Asme, 1994. 116(4): p. 435-439.

[124] Yusoff, A.R. and N.D. Sims, *Optimisation of variable helix end millings tools by minimising self excited vibration*, in *7th International Conference on Modern Practice in Stress and Vibration Analysis*. 2009.

[125] Yusoff, A.R., *et al.*, *Experimental validation of chatter stability for variable helix milling tools*, in *Trends in Aerospace Manufacturing 2009 International Conference*.

[126] Insperger, T. And G. Stepan, *Semi-discretization method for delayed systems.* International Journal for Numerical Methods in Engineering, 2002. 55(5): p. 503-518.

[127] César, M.R.M., *FEM Analysis in Machining and Experimental Validation*, in *Departamento de Engenharia Mecânica*. 2008, Universidade de Aveiro

[128] Chee, K., Ng, *Experimental Study of Micro-/Nano-Scale Cutting of Aluminum 7075 and P20 Mold Steel*, in *Woodruff School of Mechanical Engineering*. 2005, Georgia Institute of Technology.

[129] Ahmadi, K. And F. Ismail, *Stability lobes in milling including process damping and utilizing Multi-Frequency and Semi-Discretization Methods.* International Journal of Machine Tools & Manufacture. 54-55: p. 46-54.

APPENDIX A: ABSTRACTS OF CONFERENCE PUBLICATIONS

APPENDIX A1

A NEW APPROACH TO TIME DOMAIN SIMULATION OF VARIABLE SPINDLE SPEED MILLING

ABSTRACT

During metal machining, unstable self-excited vibrations (known as regenerative chatter) can occur, leading to poor surface finish, excessive tool wear, and damage to the machine. Consequently there has been a great deal of research (experiments and numerical simulations) to understand the mechanisms of regenerative chatter so that productivity can be enhanced.

Spindle speed variation is one technique for improving regenerative chatter stability that has received some attention in the research literature. However, this approach results in stability boundaries that are defined by delay-differential equations with periodic coefficients and variable time delays. Consequently from a practical standpoint it seems very difficult to determine the theoretical stability boundary, let along the acceptable stability boundary in practical scenarios.

In the present study, a Simulink model that can predict regenerative chatter in milling is modified to enable its use under variable spindle speed conditions. This is achieved by rewriting the equations of motion in non-dimensional time, where the non-dimensional time is equal to the number of simulated revolutions of the tool. In this way, the relationship between non-dimensional time and physical time can be altered to achieve a variable spindle speed. Results from the model are compared to previous publications predicting variable spindle speed chatter stability.

APPENDIX A2

(WCE2012)

The Self-Excitation Damping Ratio in Time-Domain Variable Speed Milling

ABSTRACT

During metal machining, unstable self-excited vibrations (known as regenerative chatter) can occur, leading to poor surface finish, excessive tool wear, and damage to the machine. Consequently there has been a great deal of research (experiments and numerical simulations) to understand the mechanisms of regenerative chatter so that productivity can be enhanced.

A chatter suppression method that has received attention recently is the spindle speed variation technique whereby greater depth of cut can be achieved by continuous by varying the spindle speed. However, this approach results in stability boundaries that are defined by delay-differential equations with periodic coefficients and variable time delays. Consequently from a practical standpoint it seems very difficult to determine the theoretical stability boundary, let alone the acceptable stability boundary in practical scenarios.

In the present study, a Simulink model which is designed for milling chatter simulation is modified to enable its use under variable spindle speed circumstances. This is achieved by rewriting the equations of motion in non-dimensional time where the non-dimensional is representative of the number of simulated tool revolutions. In this way, the relationship between non-dimensional time and physical time can be altered to achieve a variable spindle speed. A signal processing technique is then adopted for analysing the chatter stability of time-domain variable speed milling. This method relies on signal periodicity of the predicted vibrations of the tool and workpiece, to calculate the so-called self-excitation damping ratio. Results from the model are compared to previous publications predicting variable spindle speed chatter stability.

APPENDIX B: AN EXAMPLE FOR THE 4TH RUNGE-KUTTA TO

For the x-coordinate of the equation (3.32) can be written as:

$$\ddot{x} = \frac{1}{m_x}[F_x(t) - c_x\dot{x} - k_x x] \qquad \text{B-I}$$

The initial conditions x_o and $\dot{x}_o$ are assumed to be know as

$$\begin{cases} x_o = x(0) = 0 \\ \dot{x}_o = \dot{x}_o(0) = 0 \end{cases} \qquad \text{B-II}$$

By letting $\dot{x} = q$, this equation is reduced to the following two first order equation

$$\begin{cases} \dot{x} = q \\ \dot{q} = f(x, q, t) \end{cases} \qquad \text{B-III}$$

The basis of the method can be developed from the Taylor expansion of x_{i+1} and q_{i+1} about the previous time step i, with the time interval being $dt = \Delta t$. Subtracting and ignoring higher order terms, the following recurrence formula are obtained,

$$\begin{aligned} x_{i+1} &= x_i + \frac{dt}{6}(K_1 + 2K_2 + 2K_3 + K_4) \\ q_{i+1} &= q_i + \frac{dt}{6}(L_1 + 2L_2 + 2L_3 + L_4) \end{aligned} \qquad \text{B-IV}$$

where $t_i = i \cdot dt$, and,

$$\begin{aligned} K_1 &= q_i \\ L_1 &= f(t_i, x_i, q_i) \\ K_2 &= q_i + \frac{dt}{2} L_1 \\ L_2 &= f\left(t_i + \frac{dt}{2}, x_i + \frac{dt}{2}K_1, q_i + \frac{dt}{2}L_1\right) \\ K_3 &= q_i + \frac{dt}{2} L_2 \\ L_3 &= f\left(t_i + \frac{dt}{2}, x_i + \frac{dt}{2}K_2, q_i + \frac{dt}{2}L_2\right) \\ K_4 &= q_i + dt\, L_3 \\ L_4 &= f(t_i + dt, x_i + dtK_3, q_i + dtL_3) \end{aligned} \qquad \text{B-V}$$

The differential equation for the y-coordinate can be solved in the same way.

APPENDIX C: MILLING DYANAMICS IN 3-DOF SYSTEM

APPENDIX C1: SYSTEM EQUATIONS OF MOTION

With the reference to Figure C.1the system equations of motion are determined in x and y directions as follows:

$$\begin{aligned} &m_{x1}\ddot{x}_1 + c_{x1}\ddot{x}_1 - c_{x1}\dot{x}_2 + k_{x1}x_1 - k_{x1}x_2 = F_x \\ &m_{x2}\ddot{x}_2 + (c_{x1} + c_{x2})\dot{x}_2 - c_{x1}\dot{x}_1 - c_{x2}\dot{x}_3 \\ &\qquad + (k_{x1} + k_{x2})x_2 - k_{x1}x_1 - k_{x2}x_3 = 0 \\ &m_{x3}\ddot{x}_3 + (c_{x2} + c_{x3})\dot{x}_3 - c_{x2}\dot{x}_2 + (k_{x2} + k_{x3})x_3 - k_{x2}x_2 = 0 \end{aligned} \tag{C-1}$$

$$\begin{aligned} &m_{y1}\ddot{y}_1 + c_{y1}\dot{y}_1 - c_{y1}\dot{y}_2 + k_{y1}y_1 - k_{y1}y_2 = F_y \\ &m_{y2}\ddot{y}_2 + \left(c_{y1} + c_{y2}\right)\dot{y}_2 - c_{y1}\dot{y}_1 - c_{y2}\dot{y}_3 + \left(k_{y1} + k_{y2}\right)y_2 - k_{y1}y_1 \\ &\qquad - k_{y2}y_3 = 0 \\ &m_{y3}\ddot{y}_3 + \left(c_{y2} + c_{y3}\right)\dot{y}_3 - c_{y2}\dot{y}_2 + \left(k_{y2} + k_{y3}\right)y_3 - k_{y2}y_2 = 0 \end{aligned} \tag{C-2}$$

These equations (C-1) and (C-2) can be represented in matrices forms as follows:

$$\begin{bmatrix} m_{x1} & 0 & 0 \\ 0 & m_{x2} & 0 \\ 0 & 0 & m_{x3} \end{bmatrix}\begin{bmatrix} \ddot{x}_1 \\ \ddot{x}_2 \\ \ddot{x}_3 \end{bmatrix} + \begin{bmatrix} c_{x1} & -c_{x1} & 0 \\ -c_{x1} & c_{x1} + c_{x2} & -c_{x2} \\ 0 & -c_{x2} & c_{x2} + c_{x3} \end{bmatrix}\begin{bmatrix} \dot{x}_1 \\ \dot{x}_2 \\ \dot{x}_3 \end{bmatrix} + \begin{bmatrix} k_{x1} & -k_{x1} & 0 \\ -k_{x1} & k_{x1} + k_{x2} & -k_{x2} \\ 0 & -k_{x2} & k_{x2} + k_{x3} \end{bmatrix}\begin{bmatrix} x_1 \\ x_2 \\ x_3 \end{bmatrix} = \begin{bmatrix} F_x \\ 0 \\ 0 \end{bmatrix} \tag{C-3}$$

$$\begin{bmatrix} m_{y1} & 0 & 0 \\ 0 & m_{y2} & 0 \\ 0 & 0 & m_{y3} \end{bmatrix}\begin{bmatrix} \ddot{y}_1 \\ \ddot{y}_2 \\ \ddot{y}_3 \end{bmatrix} + \begin{bmatrix} c_{y1} & -c_{y1} & 0 \\ -c_{y1} & c_{y1} + c_{y2} & -c_{y2} \\ 0 & -c_{y2} & c_{y2} + c_{y3} \end{bmatrix}\begin{bmatrix} \dot{y}_1 \\ \dot{y}_2 \\ \dot{y}_3 \end{bmatrix} + \begin{bmatrix} k_{y1} & -k_{y1} & 0 \\ -k_{y1} & k_{y1} + k_{y2} & -k_{y2} \\ 0 & -k_{y2} & k_{y2} + k_{y3} \end{bmatrix}\begin{bmatrix} y_1 \\ y_2 \\ y_3 \end{bmatrix} = \begin{bmatrix} F_y \\ 0 \\ 0 \end{bmatrix} \tag{C-4}$$

Define mass, stiffness and structural damping matrices according to the x and y system directions:

$$M_{x,y} = \begin{bmatrix} m_1 & 0 & 0 \\ 0 & m_2 & 0 \\ 0 & 0 & m_3 \end{bmatrix}_{[x,y]}$$

$$K_{x,y} = \begin{bmatrix} k_1 & -k_1 & 0 \\ -k_1 & k_1 + k_2 & -k_2 \\ 0 & -k_2 & k_2 + k_3 \end{bmatrix}_{[x,y]} \quad \text{(C-5)}$$

$$C_{x,y} = \begin{bmatrix} c_1 & -c_1 & 0 \\ -c_1 & c_1 + c_2 & -c_2 \\ 0 & -c_2 & c_2 + c_3 \end{bmatrix}_{[x,y]}$$

Since the state-space model represents the relationship between the inputs and the outputs of the system, so the state vector can be coordinate independent by decoupling the equations (C-3) and (C-4) as can be seen in next section.

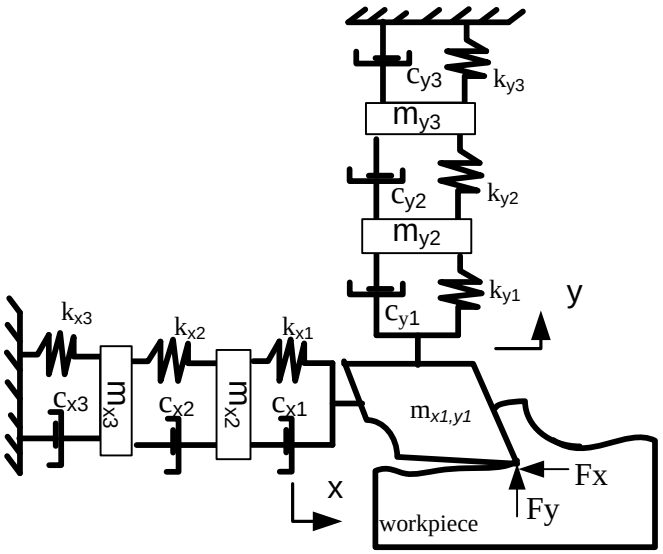

Figure C1 Two directional milling with 3-DOF coupled system

APPENDIX C 2 : Modal Analysis for Decupling the Equations of Motion

Firstly the system is assumed to be under free vibration behaviour for the un-damped system to calculate the eigenvalues and eigenvectors of the system.

$$[M]\ddot{\vec{z}} + [K]\vec{z} = 0 \tag{C-6}$$

Assume a harmonic solution:$\{z(t)\} = \{Z\}e^{j\omega_r t}$, $\{\dot{z}\} = j\omega_r\{Z\}e^{j\omega_r t}$ and $\{\ddot{z}\} = -{\omega_r}^2\{Z\}e^{j\omega_r t}$ substitute these equations in matrix equation we can obtain the eigenvalues and eigenvector solutions:

$$([K] - {\omega_r}^2[M])\{Z\}e^{j\omega_r t} = \{0\} \tag{C-7}$$

Pre-multiplied by $[k^{-1}]$

$$([I] - {\omega_r}^2[K^{-1}][M])\{Z\}e^{j\omega_r t} = \{0\} \tag{C-8}$$
$$\left([I]\lambda_g - \quad [K^{-1}][M]\right)\{Z\}e^{j\omega_r t} = \{0\}$$

where $\lambda_g = \frac{1}{{\omega_r}^2}$

Matlab codes (see Appendix D2) are used to determine matrices of the system eigenvalues λ_g and eigenvectors $\emptyset$. Now having determined the natural frequencies and modes for the un-damped case, the generalised mass, stiffness and damping ($\emptyset' M\emptyset =$ [M], $\emptyset' K\emptyset =$ [K]and $\emptyset C\emptyset =$ [C]respectively) are then determined. However the system damping here is approximated proportional, i.e proportional to the stiffness *K* of the system:

$$C = \beta\, K \tag{C-9}$$

where β is a constant (This constant has physical unit, β in [sec]) and can be approximated as follows:

$$\begin{bmatrix} c_1 & -c_1 & 0 \\ -c_1 & c_1 + c_2 & -c_2 \\ 0 & -c_2 & c_2 + c_3 \end{bmatrix}_{[x,y]} = \beta \begin{bmatrix} k_1 & -k_1 & 0 \\ -k_1 & k_1 + k_2 & -k_2 \\ 0 & -k_2 & k_2 + k_3 \end{bmatrix}_{[x,y]} \tag{C-10}$$

Then $\beta = \frac{c_1}{k_1}$

Now the new values of the damping coefficients C_1, C_2 and C_3 are defined according to the assumption ($C_2 = \beta\, k_2$ and $C_3 = \beta\, k_3$). So the damping matrix is determined by substitute matrix (C-5) in matrix (C-9) as follows:

$$C_{x,y} = \begin{bmatrix} \beta\, k_1 & -\beta\, k_1 & 0 \\ -\beta\, k_1 & \beta\,(k_1 + k_2) & -\beta\, k_2 \\ 0 & -\beta\, k_2 & \beta\,(k_2 + k_3) \end{bmatrix}_{[x,y]} \tag{C-11}$$

Similar to the undamped modal analysis, it is considered the modal transformation takes the form: $\hat{z} = \emptyset\, q$, $\dot{z} = \emptyset\, \dot{q}$ and $\ddot{z} = \emptyset\, \ddot{q}$. The equation of motion becomes:

$$\mathrm{M}_{[x,y]}\emptyset\ddot{q} + \mathrm{C}_{[x,y]}\emptyset\dot{q} + \mathrm{K}_{[x,y]}\emptyset q = \mathrm{F}_t \tag{C-12}$$

Pre-multiply the equation above by$\emptyset$' and substitute matrices ($\mathrm{M}_{x,y}$ and $\mathrm{K}_{x,y}$ in (C-)) and ($\mathrm{C}_{x,y}$in (C-12)) to obtain uncoupled equation of motion:

$$\left(\emptyset'\mathrm{M}_{[x,y]}\emptyset\right)\ddot{q} + \left(\emptyset'\mathrm{C}_{[x,y]}\emptyset\right)\dot{q} + \left(\emptyset'\mathrm{K}_{[x,y]}\emptyset\right)q = \emptyset'\mathrm{F}_{[x,y]} \tag{C-13}$$

Now the system become uncoupled and can be represented as shown in Figure C2. This is the uncoupled diagonal system equation in matrix form for x and y directions.

$$\begin{bmatrix} \hat{m}_1 & 0 & 0 \\ 0 & \hat{m}_2 & 0 \\ 0 & 0 & \hat{m}_3 \end{bmatrix}_{[x,y]} \begin{bmatrix} \ddot{q}_1 \\ \ddot{q}_2 \\ \ddot{q}_3 \end{bmatrix} + \begin{bmatrix} \hat{c}_1 & 0 & 0 \\ 0 & \hat{c}_2 & 0 \\ 0 & 0 & \hat{c}_3 \end{bmatrix}_{[x,y]} \begin{bmatrix} \dot{q}_1 \\ \dot{q}_2 \\ \dot{q}_3 \end{bmatrix} + \begin{bmatrix} \hat{k}_1 & 0 & 0 \\ 0 & \hat{k}_2 & 0 \\ 0 & 0 & \hat{k}_3 \end{bmatrix}_{[x,y]} \begin{bmatrix} q_1 \\ q_2 \\ q_3 \end{bmatrix} = \begin{bmatrix} f_1 \\ f_2 \\ f_3 \end{bmatrix}_{[x,y]} \tag{C-14}$$

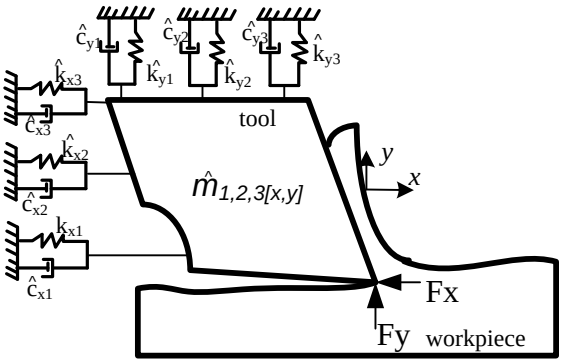

Figure C2 Two directional milling with 3-DOF decoupled system

APPENDIX D: MATLAB PROGRAM CODES

APPENDIX D1

```
%A sample of the Matlab codes for the triangular milling
speed trajectory
%input parameters
pd.cycles;   %number of revolutions
pd.omega_m;  % mean spindle speed
pd.RVA;      % amplitude ratio
pd.RVF;      % frequency ratio
pd.Tv=60/(pd.RVF*pd.omega_m);% determine signal periodicity

pd.Na=pd.RVA*pd.omega_m;
pd.t=(0:pd.Tv/2:pd.cycles); %define speed signal length

%define speed signal upper limits
pd.n(1:2:length(pd.t))=pd.omega_m+pd.Na;

%define speed signal lower limits
pd.n(2:2:length(pd.t))=pd.omega_m-pd.Na;

pd.omega=[pd.n]';   %speed signal
pd.time=[pd.t]';    %speed period signal
```

APPENDIX D2

% Sample of the Matlab codes for calculating damping ratio

```
nt                          % define number of teeth
iters                       %define number of iteration per revolution
y                           % define vibration signal
x=y(3:end);                 %strip the first 3 data points
x=buffer(x,iters,iters-iters);  %buffer the rest divided to frames
X=fft(x);                   %take the fft
nanind=1:nt:size(X,1);      %tooth passing indexes
X(nanind,:)=nan;            %set to nan (remove forced vibration)
X=X(2:end/2,:);             %use only first half, and not DC value
X=X(:,nt+1:end);            %don't use first cycle+1
[dummy,kps]=max(abs(X))     %find spectral indexes which have a local maximum
kps=unique(kps);            %select those indexes
for n=1:length(kps);        %for each useful spectral index, kp
```

```
Xkp=log(abs(X(kps(n),:)));
polycoeff=polyfit(1:length(Xkp),Xkp,1);  % curve fit
DeltaRkp(n)=-polycoeff(1);                % evaluate log decrement
end
[DeltaRm, kpm]=min (DeltaRkp);            %DeltaR for this observation and corresponding index kpm
Kpm= kps (kpm);
[DeltaR, kpmax  kpmaxm]=min(DeltaRm);     %DeltaR is lowest decay per rev
kpmax=Kpm (kpmaxm);                       %Get corresponding spectral index
zeta=DeltaR, kpmax  /2/pi/kpmax*nt;       %Evaluate corresponding damping ratio.
```

APPENDIX D3

```
% Sample of the Matlab codes for determining the system dynamics parameters.
%Define input parameters
% stiffness, natural frequency and damping ratio in x-directions
kx=[kx1 kx2 kx3];
fnx=[fnx1 fnx2 fnx3];
zx=[zx1 zx2 zx3];
% Stiffness, natural frequency and damping ratio in y-directions
ky=[ky1 ky2 ky3];
fny=[fny1 fny2 fny3];
zy=[zy1 zy2 zy3];
%Determine Mass matrix and stiffness matrix in x and y directions
Mx=[kx(1)/(fnx(1)*2*pi).^2 0 0;0 kx(2)/(fnx(2)*2*pi).^2 0;0 0
kx(3)/(fnx(3)*2*pi).^2];
Kx=[kx(1) -kx(1) 0;-kx(1) kx(1)+kx(2) -kx(2);0 -kx(2) kx(2)+kx(3)];
My=[ky(1)/(fny(1)*2*pi).^2 0 0;0 ky(2)/(fny(2)*2*pi).^2 0;0 0
ky(3)/(fny(3)*2*pi).^2];
Ky=[ky(1) -ky(1) 0;-ky(1) ky(1)+ky(2) -ky(2);0 -ky(2) ky(2)+ky(3)];
%Equation of motions
P=eye(3);     % identity matrix
Sx=Kx\Mx;
Sy=Ky\My;
```

```
% the modal model:
[Vx,Lx]=eig(P,Sx);
[Vy,Ly]=eig(P,Sy);
Lx=diag(Lx);              %the natural frequencies squared
Ly=diag(Ly);
% sorts the eigenvalues and eigenvectors:
[Lx,indx]=sort (Lx);
Vx=-Vx(:,indx);
[Ly,indy]=sort(Ly);
Vy=-Vy(:,indy);
%define modal mass, damping and stiffness
mrx=diag(diag(Vx'*Mx*Vx));
krx=diag(diag(Vx'*Kx*Vx));
cx1=Mx(1)*(zx(1).*2.*(fnx(1)*2*pi));
mry=diag(diag(Vy'*My*Vy));
kry=diag(diag(Vy'*Ky*Vy));
cy1=My(1)*(zy(1).*2.*(fny(1)*2*pi));
% define proportional damping coefficient.(damping proportional with stiffness)
%define the new damping coefficient
betax=(cx1/kx(1));
cx2=betax*kx(2);
cx3=betax*kx(3);
cx=[cx1 -cx1 0;-cx1 cx1+cx2 -cx2;0 -cx2 cx2+cx3];
crx=diag(diag(Vx'*cx*Vx));
betay=(cy1/ky(1));
cy2=betay*ky(2);
cy3=betay*ky(3);
cy=[cy1 -cy1 0;-cy1 cy1+cy2 -cy2;0 -cy2 cy2+cy3];
cry=diag(diag(Vy'*cy*Vy));
% define the state space matrices
Tx=length(krx);
```

```
pd.Ax=[zeros(Tx)            eye(Tx)
-(krx*inv(mrx))   -(crx*inv(mrx))];
    pd.Bx=[zeros(Tx,1);  1/mrx(1,1); 1/mrx(2,2); 1/mrx(3,3)]
pd.Cx=[1 1 1 0 0 0;0 0 0 1 0 0;0 0 0 0 1 0;0 0 0 0 0 1];
pd.Dx(1:min(size(pd.Cx)),:)=0;
Ty=length (kry);
pd.Ay=[zeros(Ty)            eye(Ty)
-(kry*inv(mry))   -(cry*inv(mry))];
pd.By=[zeros(Ty,1); 1/mry(1,1); 1/mrx=y(2,2); 1/mry(3,3)];
pd.Cy=[1 1 1 0 0 0;0 0 0 1 0 0;0 0 0 0 1 0;0 0 0 0 0 1];
pd.Dy(1:min(size(pd.Cy)),:)=0;
```

APPENDIX D4

```
% Sample of the Matlab codes for defining the variable helix angle
pd.helix1=[hel1 hel2 hel3 hel4] *pi/180; % converts angles to radians
pd.numlayers=la                          %define number of axial layers
pd.numteeth =Nt                          %define number of cutter teeth
for j=1:pd.numlayers
pd.helix(j,:)=pd.helix1(:,1:pd.numteeth)
end
```

APPENDIX D5

```
% Sample of the Matlab codes for plotting the arc surface and rubbing behaviour.
    %Calculate the displacement due the feed rate
    xf=pd.feed*pd.numteeth*pd.omega/2/pi*time (end);
    %Select the rubbing data from the process damping mechanism at the last tool
    revolution
    Fpd1                    %process damping forces data
    nt= numteeth;         % Number of teeth (arc surfaces)
    for n=1:nt              % For each arc surfaces
    l=l1;                 % each layer
    fdd=Fpd1(l1,n,:)~=0;    % Select the indices for rubbing 1 when occur and 0
    when not.
```

```
ssx=sx(l1,1+iters*(n-1):iters*n);    % Define arc surfaces data (x and y components)
ssy=sy(l1,1+iters*(n-1):iters*n);    % for the current tooth n_t at the last revolution
% Removes feed rate displacement effect and converts arc surface data points to the
polar coordinates
[th,r]=cart2pol(ssx-xf,ssy);
indr=((~isnan(r)));         % remove what is not a number
indr=indr(1:iters);
rubind=(fdd(indr));   % Index number to define the rubbing data points
rd=detrend(r(indr)); % remove any linear trends
thd=th(indr);
%plot polar arc surface with rubbing behaviour after removing a linear trends
figure;
hold all
plot((thd/pi*180),rd)
plot(thd(rubind)/pi*180,(rd(rubind)),'d')
ha=gca;
set(ha, 'xdir', 'reverse');     % reverse the axis to be from right to left
end
```